Dynamical Scaling Behavior in Non-Equilibrium Quantum Phase Transitions

A Thesis

Submitted to the Faculty

in partial fulfillment of the requirements for the

degree of

Doctor of Philosophy

in

Physics and Astronomy

by

Shusa Deng

DARTMOUTH COLLEGE

Hanover, New Hampshire

24 June 2011

Examining Committee:

Lorenza Viola

Marcelo Gleiser

Chandrasekhar Ramanathan

Gerardo Ortiz

Brian W. Pogue
Dean of Graduate Studies

Abstract

This thesis focuses on the emergence of universal dynamical scaling in quantum critical spin systems driven out of equilibrium, with emphasis on quench dynamics which involves isolated standard critical points, multi-critical points, and non-isolated critical points (that is, critical regions). One of our main conclusions is that the so-called Kibble-Zurek scaling holds for a large class of physical observables throughout the whole quench process when isolated standard critical points are involved, irrespective of the quench path. However, for both isolated multi-critical points and non-isolated critical points, the knowledge of equilibrium critical exponents is not enough to predict non-equilibrium dynamical scaling. Instead, our analysis shows that the resulting power-law scaling *depends sensitively on the control path*, and that anomalous critical exponents may emerge depending on the universality class. In particular, we argue that for a multi-critical point the observed anomalous behavior originates in the fact that the dynamical excitation process takes place asymmetrically with respect to the static multi-critical point, requiring the introduction of genuinely *non-static* exponents.

We further explore the robustness of universal dynamical scaling behavior with respect to *initialization* in a large class of states with finite energy above the ground state, including thermal mixtures. We find that the critical exponents of the ground-state quantum phase transition can be encoded in the dynamical scaling exponents despite the finite energy of the initial state. In particular, we identify conditions on the initial distribution of quasi-particle excitation which ensure the Kibble-Zurek scaling to persist.

The emergence of *effective thermal equilibrium behavior* following a sudden quench towards criticality is also investigated, with focus on the long-time expectation value of the quasi-particle number operator. We find that effective thermalization fails to occur in quenches towards a multi-critical point, in contrast to quenches to a standard critical point. We argue that the observed lack of thermalization originates in this case in the asymmetry of the impulse region that is also responsible for anomalous multi-critical dynamical scaling.

Acknowledgements

Acknowledgement! I finally reached this part of my Thesis. When I look back to my past six years at Dartmouth as a Ph.D student, my heart is full of thanksgiving. I would like to express my gratitude to all those who gave me the possibility to complete this Thesis.

First, I would like to thank my dear advisor Lorenza! You have provided me extraordinary guidance throughout my entire study: not only you have provided me with the big picture behind research ideas, but also went through many details of calculations hand by hand. You are also the one who challenges me to go deep into my research thoughts. Sometimes your comments might be tough, but I am glad that you were strict on me. Just like this verse in the Bible—"No discipline seems pleasant at the time, but painful. Later on, however, it produces a harvest of righteousness and peace for those who have been trained by it." (Hebrew 12:11). I have benefited greatly from your insights on personal life, as well as on research. You are always here to support me, and encourage me when I feel confused about my future steps. In particular, I would like to thank you for your support and understanding after my daughter Teresa was born. I really feel lucky to have you as my advisor, somebody who really cares for the students.

Also, I am deeply indebted to my collaborator Gerardo Ortiz from Indiana University, whose stimulating suggestions and encouragement helped me throughout my Thesis research. I am always inspired by your passion for Physics. The (almost) weekly visual meetings between you and us (Lorenza and I) have been one of the most fun and enjoyable parts of my Ph.D life.

I would like to express my thanks to Winton for the stimulating discussions on Physics, and for your patient help on my oral English. It is a pity I did not study English more seriously earlier in the past six years. Also, to Winton, Becky, and Jeremy, for the warm and fun office atmosphere you created!

Special thanks go to my Thesis committee members. To Marcelo and Sekhar, who are willing to be my committee members in spite of the short notice. I am sure I will benefit greatly from your intelligent comments. Also thanks to Jay and Yeong-Ah, who were part of my proposal committee but unfortunately could not join my Thesis committee, thanks for your helpful discussion and suggestions in the initial stages of my research.

Last, but certainly not least, I would like to thank my heavenly Father. You always encourage me to finish my Thesis research by various signs and wonders. In fact, some of my research ideas and physical understandings are inspired by your whispers. Thank you for your acceptance for who I am. I also want to thank the brothers and sisters from the Chinese-English Livingwater Fellowship and the elder Kent, who greatly supported me through prayers. I must also thank you my dear husband Peng for your strong arms for me to cling to, and my sweet daughter Teresa for being my little sunshine, when I was stressed; finally thanks to my parents and parents-in-law, who helped me greatly in taking care of Teresa. I would like to thank all my friends at Dartmouth, who made my stay here a fond memory!

Shusa Deng

24th June, 2011

Contents

List of Figures

Chapter 1

Introduction and Motivation

1.1 Equilibrium Quantum Phase Transitions

Understanding quantum phases of matter is one of the primary goals in condensed-matter physics and quantum statistical mechanics. Unlike classical phase transitions, which are associated with a non-analytical behavior of the free energy driven by thermal fluctuation, *quantum phase transitions* (QPTs) are driven solely by quantum fluctuations at zero temperature, and are associated with a non-analyticity of the many-body ground state energy [1, 2]. If the ground-state energy is discontinuous in its first derivative, the QPT is called a first-order QPT, which involves sudden jumps of certain physical properties. For instance, in the itinerant ferromagnet $ZrZn_2$, there is a sudden change of the ferromagnetic moment in a ferromagnetic first-order QPT [3]. The more common and interesting QPTs in Nature are *continuous* QPTs, where the ground state energy is discontinuous in its second-order (or even higher-order) derivatives. Typically, such a non-analyticity of the ground-state energy is induced when a temperature-independent control parameter λ in the system Hamiltonian $H(\lambda)$ is varied across the point at which a transition occurs from one quantum phase to a different one, the so-called *quantum critical point* (QCP). QPTs are usually accompanied by a qualitative change in the nature of the quantum correlations in the ground state. In addition to the ground-state energy, often we can find some other physical observables, including an order parameter (a quantity which

is zero in one phase and nonzero in the other)[1], that exhibit singular behavior in the vicinity of a QCP.

Remarkably, striking similarities exist in the behavior close to a QCP among systems that are very different in nature. The numerical values of the critical exponent describing the quantitative nature of the singularities are identical for large groups of apparently diverse physical systems [5]. In a continuous QPT, the energy gap Δ between the ground state energy and the first-excited state energy closes in the thermodynamic limit. In most cases, it turns out that when the parameter λ approaches the critical value λ_c, the characteristic vanishing energy scale Δ scales as:

$$\Delta \sim |\lambda - \lambda_c|^{z\nu}, \tag{1.1}$$

where z and ν are critical exponents, whose physical meaning shall become clearer soon. Generally speaking, continuous QPTs are also accompanied with a divergence of the correlation length ξ, which is the characteristic length scale above which the (two-body) correlation function is negligibly small. Suppose that we define the (single-time) correlation function as follows:

$$C(r) \equiv \langle \Psi_{GS}|A_i A_{i+r}|\Psi_{GS}\rangle - \langle \Psi_{GS}|A_i|\Psi_{GS}\rangle\langle \Psi_{GS}|A_{i+r}|\Psi_{GS}\rangle,$$

where A_i is some observable, r is the distance between two lattice sites, and $|\Psi_{GS}\rangle$ is the ground state, respectively. Then the correlation length can be thought as the characteristic length scale entering into the exponential decay of $C(r)$ at long distance, that is,

$$\lim_{r\to\infty} |C(r)| \sim e^{-r/\xi}.$$

Typically, in a continuous QPT the correlation length ξ diverges as

$$\xi \sim |\lambda - \lambda_c|^{-\nu}, \tag{1.2}$$

[1] According to Landau's symmetry-breaking theory, different order parameters correspond to different symmetries. However, two different *topological orders* may share the same symmetry (for instance, the fractional quantum Hall system [8]), which is beyond Landau's paradigm. Notice that addressing systems exhibiting topological order is beyond the scope of this Thesis.

where ν is called the *correlation length critical exponent* [1]. On the other hand, the vanishing characteristic energy scale also leads to the so-called *critical slowing down*, that is, the divergence of the relaxation time $\tau_{rel} \sim \Delta^{-1}$, which characterizes the minimum time the system needs to reach a new thermal equilibrium state after a small perturbation. Based on the scaling assumptions in Eq. (1.1) and Eq. (1.2), we also obtain the following relations:

$$\Delta \sim \xi^{-z}, \qquad \tau_{rel} \sim \xi^{z}, \tag{1.3}$$

where z is called *dynamical critical exponent*. The fact that two apparently different physical systems share the same set of critical exponents is known as *universality*, which is also one of the hallmarks of classical critical phenomena. Phenomena with the same set of critical exponents are said to form a *universality class*. Usually, members of the same universality class have at least two things in common: the symmetry group of the Hamiltonian and the dimensionality.

Among the critical points, there is a special class of critical points, so-called *multi-critical points*. A multi-critical point (MCP) may be defined phenomenologically as a point of sudden change of behavior on an otherwise smooth, universal line of critical points [17]. There are different types of MCPs: some are characterized as the meeting of two separate critical lines corresponding to two, distinct, competing order parameters; some are characterized by the coexistence of at least three different phases. The most commonly known MCP in classical phase transitions is the triple point of water (critical temperature around 273K, critical vapor pressure around 0.006atm), at which solid ice, liquid water, and water vapor coexist. In our model system, we will encounter a number of quantum MCPs. Remarkably, they are not just special from the point of view of static QPTs, but they also exhibit highly-nontrivial dynamical scaling behavior.

In real world, absolute zero temperature is unaccessible. However, it is well known that the influence of a QCP can extend well into the finite temperature regime, the so-called *quantum-critical region* [1], which provides the theoretical foundation for the observation of QPTs in laboratory experiments. For instance, in the pioneer work by Greiner *et al.* [7], the QPT from a superfluid to a Mott insulator phase was realized experimentally in a Bose-Einstein condensate at low temperature with the increase of repulsive interactions.

1.2 Non-equilibrium Quantum Phase Transitions and the Kibble-Zurek Scaling

When a system is close to a critical point, besides the static properties discussed in Section 1.1, singular behavior may also occur in a wide variety of dynamical properties, such as the multi-time correlation functions, *e.g.* the time-dependent two-point correlation function defined as:

$$C(r, t - t') \equiv \langle A_i(t) A_{i+r}(t') \rangle - \langle A_i(t) \rangle \langle A_{i+r}(t') \rangle.$$

These dynamical properties are determined by the equations of motion, rather than by the equilibrium distribution for static equilibrium properties [11]. Typically, the term "dynamical scaling" refers to the universal scaling theory of multi-time correlation functions and response functions close to a QPT perturbed by a time-dependent change of control parameter, which results into a "non-equilibrium QPT".

While studies of QPTs have primarily focused on equilibrium scaling properties in the vicinity of QCPs, the investigation of dynamics in non-equilibrium QPTs presents new challenges of practical relevance. In particular, understanding and manipulating the dynamics of QPTs in matter has a broad significance across fields as diverse as quantum statistical mechanics, material science, quantum information science (QIS), and cosmology. Back to 1976, Kibble proposed a theory to predict the topological defect formation in the cosmological (finite-temperature) phase transition of the early Universe [20]: In the hot Big-Bang model of the Universe, initially the temperature is believed to be well above the critical temperature (T_c) of a symmetry-breaking phase transition, and the Universe is in the "normal" phase. As it expands and cools, and the temperature drops below T_c, a domain structure of "cosmic strings" might arise. These cosmic strings are important since if they exist, they can survive for a long time, and may help to understand what the Universe was like when it was formed [21]. In the early 80's, in analogy to the defect formation during a cosmological phase transition, Zurek proposed that formation of topological defects might also be found in small-scale condensed-matter phase transitions [22, 23], leading to a prediction for the scaling behavior of "defect density", the so-called *Kibble-Zurek scaling* (KZS). Over the last two decades, the KZS

was numerically confirmed and experimentally tested in a variety of classical phase transitions, see [24, 25, 26, 27, 28, 29, 30, 31, 32, 33, 34] for representative literature. However, the application of KZS to QPTs remained largely unexplored until the recent studies in Refs. [57, 58, 59, 60, 61].

Basically, the KZ argument is rooted in the intuition that, irrespective of how slowly a system is driven across a continuous phase transition, adiabaticity is necessarily lost in the thermodynamic limit due to the vanishing energy gap at the critical point. Thus, it is assumed that the system will first go through an adiabatic regime (far away from the critical point), and then an approximately impulse regime (close to the critical point), and finally back to an adiabatic regime (see the top panel of Fig. 1.1). Qualitatively, the typical time and length scales, $\hat{t}$ and $\hat{\xi}$ respectively, characterize the adiabatic-to-impulse crossover. The fact that "order" cannot be established on distances larger than $\hat{\xi}$, results in the formation of a domain structure and the generation of a *finite* density of topological defects in the system. Quantitatively, consider the simplest quench scheme that a time-dependent Hamiltonian $H(t)$ is driven across its QCP by changing a control parameter $\lambda(t)$ (*e.g.*, the magnetic field along the z-axis) in time with constant quench rate $\tau > 0$, that is:

$$\lambda(t) - \lambda_c = \frac{t - t_c}{\tau}, \quad \tau > 0, \tag{1.4}$$

where t_c is the time at which $\lambda(t_c) = \lambda_c$ ($t_c = 0$ without loss of generality). The time-scale of adiabaticity breaking ($\hat{t}$) can be obtained when the relaxation time scale matches with the quench time scale, that is:

$$\tau_{rel} \equiv \Big| \frac{(\lambda(t) - \lambda_c)}{\dot{\lambda}(t)} \Big|, \tag{1.5}$$

associated with the scaling assumption of τ_{rel} in Eq. (1.3) and the other two scaling assumptions in Eq. (1.1)–(1.2), leading to the scaling result:

$$\hat{t} \sim \tau^{\nu z/(\nu z+1)}. \tag{1.6}$$

Thus, the typical gap $\hat{\Delta} \sim \hat{t}^{-1}$. Correspondingly, the typical correlation length $\hat{\xi} \sim \xi(\hat{t}) \sim \hat{\Delta}^{-z}$ also

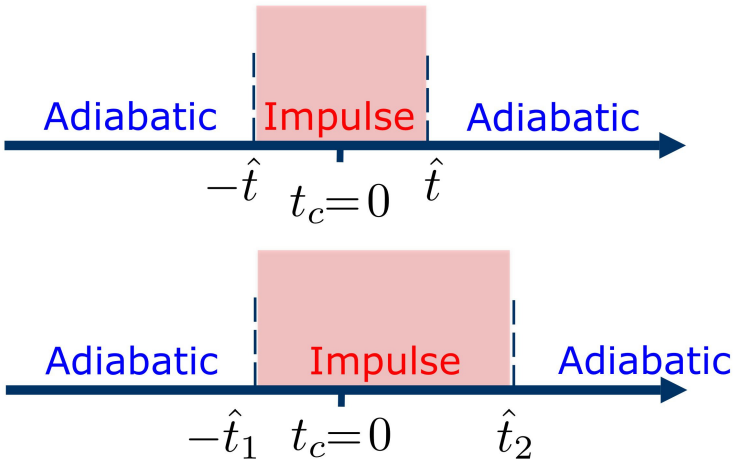

Figure 1.1: Qualitative sketch of the adiabatic-impulse-adiabatic sequence of regimes relevant to dynamical scaling arguments. Top: Symmetric impulse region, as assumed by the standard KZS scenario. Bottom: Asymmetric impulse region, as resulting from the existence of quasicritical path-dependent energy states, see Ref. [112].

scales with the quench rate τ:

$$\hat{\xi} \sim \tau^{\nu/(\nu z+1)}. \tag{1.7}$$

Since $\hat{\xi}$ is the universal length scale near criticality, it determines the scaling of the final ($t = t_f$) density of defects and, more generally, the density of excitations, $n_{\rm ex}(t_f)$, created in the system. If d denotes the spatial dimension, the KZS result then follows:

$$n_{\rm ex}(t_f) \sim \hat{\xi}^{-d} \sim \tau^{-d\nu/(\nu z+1)}. \tag{1.8}$$

Thus, in the current context, "non-equilibrium dynamical scaling" will be taken to refer to the *scaling of the excitation density or other physical observables that quantify adiabaticity loss*, which might be a different notion than dynamical scaling as defined in *e.g.* Ref. [11] in the context of dynamical critical phenomena.

Interestingly, in a seemingly totally different line of research, Barouch *et al.* studied the time-dependent zero-temperature magnetization of the anisotropic XY spin chain [12], and showed that equilibrium is not reached in the long-time limit ($t_f \mapsto \infty$), back to 1970. The fact that the final

magnetization sensitively depends on the initial magnetic field is a manifestation of *non-ergodic* behavior. The possible emergence of non-equilibrium scaling, however, was not anticipated. While it is suggestive to realize that defect formation in the KZ paradigm is also a manifestation of broken ergodicity in Barouch's sense [12], fascinating experimental progress in systems ranging from ultracold atomic gases to quantum magnets [7, 9, 10] demand the above KZS to be carefully scrutinized.

The main goal of my Thesis research has been to explore the universality of KZS within the framework of exactly solvable quantum spin chains, by focusing in particular on the following problems:

• The validity of KZS for different universality classes, observables [Chapter 3], and initial conditions [Chapter 4];

• The modification to dynamical scaling behavior that are needed in complex quench scenarios, for instance, when non-isolated QPTs (critical regions) are involved and/or when the qualitative picture of Fig. 1.1 (top) no longer holds (see bottom panel of Fig. 1.1);

• The extent to which KZS can manifest in decoherence dynamics, for instance using the decoherence of a central qubit as a probe to monitor the dynamical QPT of the environment Hamiltonian [Chapter 5].

1.3 Entanglement and Quantum Phase Transitions

Traditionally, the study of many-body condensed-matter systems has focused on characterizing various order parameters, the system response to external perturbations, the excitation spectrum, and so on. Beginning in the early 90's, QIS has become a fascinating and naturally cross-disciplinary research area. Since then, there has been a growing body of research at the interface between condensed-matter theory, quantum statistical mechanics, and QIS. Can QIS concepts and tools contribute to advance our understanding of many-body quantum systems? Methods developed in QIS have contribute to unveil new properties of many-body quantum system. In particular, entanglement theory has emerged as a natural and powerful bridging testbed for tackling this broad question from an information physics perspective.

Entanglement, a property which has no classical counterpart, refers to the existence of purely quantum-mechanical correlations in a composite quantum system. It has been a subject of intense study in recent years due to the key role it plays across QIS [4]. By its own nature, entanglement is a property inherent to quantum states and intimately related to many-body quantum correlations. Therefore, on the one hand, one may expect that entanglement undergoes a significant change across a QCP. On the other hand, by appropriately quantifying entanglement, one may use entanglement to identify and characterize a QPT. As a result, the study of entanglement may shed new light on QPTs. The intriguing issue of the relation between entanglement and QPTs has been intensively investigated recently, *e.g.*, see a recent review by Amico *et al.* [35]. Such investigations mostly focused on exploring standard notions (and measures) of entanglement, that are based on partitioning the system of interest into subsystems. For instance, in the work of Ref. [15], the so-called concurrence [18] was used to quantify the entanglement of arbitrary mixed states of a bipartite spin system. It was shown, in particular, that the derivative of concurrence displays singular behavior as a function of the control parameter at a QCP. Likewise, in Ref. [16], the block entropy of entanglement S_L was used to quantify the entanglement between a block of spins (of size L) and the rest in a pure state. It was proved that at a QCP, S_L shows logarithmic divergence as a function of the block size, whereas, away from the QCP, S_L either vanishes for all L or grows monotonically as a function of L until it reaches a saturation value for a certain block size L_0. While these two examples focused on QCPs in spin systems, the works in Ref. [54, 55] showed that block entropy of entanglement can be used to identify QPTs in fermionic systems as well. In spite of the success of subsystem-based entanglement measures, however, it became clear that this approach has intrinsic limitations. As we will discuss in more detail in the next Chapter, this prompted the introduction of an "observable-based" entanglement concept, so-called *Generalized Entanglement* [45, 46].

In my work, I have also addressed the problem of characterizing quantum-critical models from a GE perspective [50, 51], by continuing the earlier exploration with a twofold objective in mind:

• To further test the usefulness of GE-based criticality indicators in characterizing static quantum phase diagrams with a higher degree of complexity than in Ref. [50] (including multiple competing phases and various universality classes);

• To start analyzing time-dependent behavior of GE, with the goal of establishing the emergence

and validity of universal scaling laws (in particular, KZS) for non-equilibrium quantum correlations in QIS [Chapter 3].

The main results of my Thesis research have been published to date in the following papers:

• S. Deng, L. Viola, and G. Ortiz, "Generalized entanglement in static and dynamic quantum phase transition", *Recent Progress in Many-Body Theories*, Vol. **11** (World Scientific, Singapore, 2008), p. 387, arXiv:0802.3941 [Appendix B];

• S. Deng, G. Ortiz, and L. Viola, "Dynamical non-ergodic scaling in continuous finite-order quantum phase transitions", Europhys. Lett. **84**, 67008 (2008) [Appendix C];

• S. Deng, G. Ortiz, and L. Viola, "Anomalous nonergodic scaling in adiabatic multicritical quantum quenches", Phys. Rev. B **80**, 241109(R) (2009) [Appendix D];

• S. Deng, G. Ortiz, and L. Viola, "Dynamical critical scaling and effective thermalization in quantum quenches: Role of the initial state", Phys. Rev. B **83**, 094304 (2011) [Appendix E];

An additional paper is currently in preparation on critical decoherence dynamics, jointly with H. T. Quan from University of Maryland and L. Viola.

Chapter 2

Equilibrium Critical Properties of the Alternating XY Chain

2.1 Exact Equilibrium Phase Diagram

One of the most important and pedagogical models to study quantum critical phenomena is the one-dimensional spin-1/2 anisotropic XY model introduced by Lieb *et al.* [37]. Its importance mainly comes from the fact that it is exactly solvable, and thus can provide an excellent ground for a rigorous study of different properties of quantum magnetic systems, and their quantum-critical behavior. Moreover, this model is not just interesting to theoretical physicists. From an experimental point of view, many compounds can be described as (quasi) one-dimensional, for instance, $(VO)_2P_2O_7$ and $CuGeO_3$ studied in Ref. [38] and Ref. [39] respectively were found to form one-dimensional spin ladder configurations. Furthermore, it was reported in Ref. [40] that in cobalt niobate, $CoNb_2O_6$, which has a coupling between zigzag chains in the crystal, so that the spins prefer to parallel to each other when these is no external magnetic field, provides a good testbed for quantum criticality of the quantum Ising chain—a particular case of the anisotropic XY spin chain. Theoretically, after the equilibrium properties of the XY spin chain in a transverse field were analyzed, various modifications were introduced into the model, and the effects of these changes were explored. In

particular, Derzhko *et al.* studied the ground-state and thermodynamic properties of the spin-1/2 anisotropic XY chain in a regularly alternating transverse magnetic field [41]. Remarkably, a new universality class $\nu = 2, z = 1$ was found.

Motivated by the new critical behavior pointed out in Ref. [41], we focused on a class of spin-1/2 one-dimensional models described by the following Hamiltonian:

$$H = -\sum_{i=1}^{N} \left[\frac{(1+\gamma)}{2} \sigma_x^i \sigma_x^{i+1} + \frac{(1-\gamma)}{2} \sigma_y^i \sigma_y^{i+1} \right] + \sum_{i=1}^{N} \Big(h - (-1)^i \delta \Big) \sigma_z^i, \tag{2.1}$$

where periodic boundary conditions (PBCs) are assumed, that is, $\sigma_\alpha^i \equiv \sigma_\alpha^{i+N}$, $\alpha = x, y, z$. Here, $\gamma \in [-\infty, \infty]$ is the anisotropy, $h \in [-\infty, \infty]$ is the magnetic field strength, and $\delta \in [-\infty, \infty]$ is the alternation strength. Without loss of generality, we will assume that N is an even number. The above Hamiltonian includes several relevant cases in special limits:

- $\delta = 0$: Anisotropic XY model in a transverse field;
- $\delta > 0$, $\gamma = 1$: Ising model in an alternating transverse field;
- $\gamma = 0$: Isotropic XX limit.

For generic values of the parameters, the Hamiltonian Eq. (2.1) has a global discrete $\mathbb{Z}_2^z$-symmetry ($\mathbb{Z}_2^z = \prod_{j=1}^{N} \sigma_z^j$), which can be spontaneously broken in the thermodynamic limit. For specific values of the parameters, the Hamiltonian may develop additional symmetries, which will be discussed in detail later (see Sec. 2.1.1). An exact solution for the energy spectrum of this Hamiltonian may be obtained by generalizing the basic steps carried out in the standard Ising case to account for the existence of a two-dimensional periodic cell introduced by the alternation. After using a generalized Jordan-Wigner transformation [42]:

$$a_{2j-1}^\dagger = \prod_{l=1}^{2j-2} (-\sigma_z^l) \sigma_{2j-1}^\dagger, \quad b_{2j}^\dagger = \prod_{l=1}^{2j-1} (-\sigma_z^l) \sigma_{2j}^\dagger \ ,$$

where $a_{2j-1}^\dagger$ ($b_{2j}^\dagger$) are canonical fermionic operators that create a spinless fermion at site $2j-1$ ($2j$),

the Hamiltonian Eq. (2.1) rewrites as a quadratic form in the fermionic operators:

$$\begin{aligned} H &= -\sum_{j=1}^{M}(a_{2j-1}^{\dagger}b_{2j}+\gamma a_{2j-1}^{\dagger}b_{2j}^{\dagger}+\text{h.c.})+\sum_{j=1}^{M-1}b_{2j}^{\dagger}a_{2j+1}+\gamma b_{2j}^{\dagger}a_{2j+1}^{\dagger}+\text{h.c.}) \\ &+ \sum_{j=1}^{M}[(h+\delta)a_{2j-1}^{\dagger}a_{2j-1}+(h-\delta)b_{2j}^{\dagger}b_{2j}-h]+\mathcal{P}\,(b_{N}^{\dagger}a_{1}+\gamma b_{N}^{\dagger}a_{1}^{\dagger}+\text{h.c.}), \end{aligned} \tag{2.2}$$

where $M = N/2$, the last term originates from the spin periodic boundary conditions and the parity operator:

$$\mathcal{P}\equiv\prod_{j=1}^{N}(-\sigma_{z}^{j})=e^{i\pi/2\sum_{j=1}^{N}\sigma_{z}^{j}}=e^{i\pi\sum_{j=1}^{N/2}\left(a_{2j-1}^{\dagger}a_{2j-1}+b_{2j}^{\dagger}b_{2j}\right)}, \tag{2.3}$$

which is equal to $+1(-1)$ depending on whether the eigenvalue of the total fermionic number operator is even (odd), respectively. Physically, $\mathcal{P}$ corresponds to a global $\mathbb{Z}_2^z$-symmetry which, for finite N, allows the even and odd subspaces to be exactly decoupled, $H \equiv H^{(+)} + H^{(-)}$, and the diagonalization to be carried out separately in each symmetry sector.

In finite systems, the eigenstates with an even number of fermions belong to the $\mathcal{P} = +1$ sector. From Eq. (2.2), $\mathcal{P} = +1$ provides a positive sign for the hopping term $b_N^{\dagger}a_1$, while the nearest neighbor hopping term is negative, *e.g.* $-b_N^{\dagger}a_{N+1}$, leading to anti-periodic boundary condition in the fermionic language for $\mathcal{P} = +1$, that is, $a_{2j-1+N} = -a_{2j-1}, b_{2j+N} = -b_{2j}$. By exploiting the translational invariance of the Hamiltonian, we can apply a Fourier transformation to momentum modes:

$$\begin{cases} a_{k}^{\dagger}=\frac{1}{\sqrt{M}}\sum_{j=1}^{M}e^{ik(2j-1)}a_{2j-1}^{\dagger}, \\ \\ b_{k}^{\dagger}=\frac{1}{\sqrt{M}}\sum_{j=1}^{M}e^{ik(2j)}b_{2j}^{\dagger}, \end{cases}$$

where $M = N/2$, $k \in K \equiv K_+ + K_- = \{\pm\frac{\pi}{N}, \pm\frac{3\pi}{N}, \cdots \pm(\frac{\pi}{2} - \frac{\pi}{N})\}$ for the anti-periodic boundary conditions (APBs). Eq. (2.2) can then be expressed as:

$$H=\sum_{k\in K_{+}}H_{k}=\sum_{k\in K_{+}}\hat{A}_{k}^{\dagger}\hat{H}_{k}\hat{A}_{k},$$

where $\hat{A}_k$ is a vector operator:

$$\hat{A}_k^\dagger = (a_k^\dagger, a_{-k}, b_k^\dagger, b_{-k}),$$

and $\hat{H}_k$ is the following 4×4 Hermitian matrix:

$$\hat{H}_k = \begin{pmatrix} 2(h+\delta) & 0 & J_k & \Gamma_k \\ 0 & -2(h+\delta) & -\Gamma_k & J_k \\ J_k^* & -\Gamma_k^* & 2(h-\delta) & 0 \\ \Gamma_k^* & J_k^* & 0 & -2(h-\delta) \end{pmatrix} \begin{array}{l} J_k = -2\cos(k), \\ \Gamma_k = -2i\gamma\sin(k). \end{array} \tag{2.4}$$

Therefore, the problem reduces to the diagonalization of the matrices $\hat{H}_k$ for each $k \in K_+$. Let the eigenvalues of $\hat{H}_k$ be denoted by $\epsilon_{k,1}, \epsilon_{k,2}, \epsilon_{k,3}, \epsilon_{k,4}$, with $\epsilon_{k,1} \leq \epsilon_{k,2} \leq 0 \leq \epsilon_{k,3} \leq \epsilon_{k,4}$. Then H_k can be expressed as

$$H_k = \sum_{n=1,\ldots 4} \epsilon_{k,n} \gamma_{k,n}^\dagger \gamma_{k,n}, \tag{2.5}$$

where $\gamma_{k,n}^\dagger$ is the quasi-particle creation operator with respect to mode k at energy level n. So at $T = 0$ (zero temperature), only the $\epsilon_{k,1}$ and $\epsilon_{k,2}$ bands are occupied, whereas $\epsilon_{k,3}$ and $\epsilon_{k,4}$ are empty. Hence, the many-body ground state energy is $E_g = \sum_{k \in K_+} (\epsilon_{k,1} + \epsilon_{k,2})$. Accordingly, an excitation gap in the $\mathcal{P} = +1$ sector for each momentum k can be defined as $\Delta_k = \epsilon_{k,3} - \epsilon_{k,2}$, yielding

$$\Delta_k(\gamma, h, \delta) = 4\Big[\, h^2 + \delta^2 + \cos^2 k + \gamma^2 \sin^2 k - 2\sqrt{h^2 \cos^2 k + \delta^2 (h^2 + \gamma^2 \sin^2 k)}\,\Big]^{1/2}. \tag{2.6}$$

In finite systems, eigenstates with an odd number of fermions belong to the $\mathcal{P} = -1$ sector, which implies PBCs on the fermions for the same reason as $\mathcal{P} = 1$ corresponds to APBs for fermions, that is, $a_{2j-1+N} = a_{2j-1}, b_{2j+N} = b_{2j}$, and a different set $\bar{K}$ of allowed momentum modes, $\bar{K} \equiv \bar{K}_+ + \bar{K}_- + 0$, where $\bar{K}_\pm = \Big\{ \pm\frac{2\pi}{N}, \pm\frac{4\pi}{N}, \ldots, \pm\Big(\frac{\pi}{2} - \frac{2\pi}{N}\Big), \pm\frac{\pi}{2} \Big\}$. The reduced matrices $\hat{H}_k$ for all the modes are the same as the ones with anti-periodic boundary condition, except for $k = 0$. One may show that for

this mode:

$$\hat{H}_{k=0} = 2\begin{pmatrix} (h+\delta) & 0 & -1 & 0 \\ 0 & -(h+\delta) & 0 & -1 \\ -1 & 0 & (h-\delta) & 0 \\ 0 & -1 & 0 & -(h-\delta) \end{pmatrix},$$

such that the creation operators $a_0^\dagger, b_0^\dagger$ and the annihilation operators a_0, b_0 are decoupled. This implies that the number operator $\mathcal{N}_0 = a_0^\dagger a_0 + b_0^\dagger b_0$ is conserved. The two branches from $\mathcal{N}_0 = 1$ have energy spectrums $\epsilon_0 = h \pm \sqrt{\delta^2+1}$, whereas the two branches from $\mathcal{N}_0 = 0$ have energy spectrums $\epsilon_0 = -h \pm \sqrt{\delta^2+1}$. Notice that the solution should obey the boundary condition. Thus in fermionic language, we need to require an odd number of total fermion particles for the APBs. It can be verified through numerical calculation that the ground state in $\mathcal{P} = -1$ sector has the following property: the $k = 0$ mode contributes an odd number of particles, whereas all other modes contribute an even number of particles, such that the boundary condition would be satisfied. Thus, the occupied two bands for $k = 0$ are one from the lower energy branch of $\mathcal{N}_0 = 1$ (say $\epsilon_{0,1}$) and one from the lower energy branch of $\mathcal{N}_0 = 0$ (say $\epsilon_{0,2}$). Suppose that $\epsilon_{k,1}$ and $\epsilon_{k,2}$ are the two negative bands for mode k (except that $k = 0$, as we explained, should be treated separately). Then the ground state energy in the $\mathcal{P} = -1$ sector is $E_g = \sum_{k\in\bar{K}_+,0}(\epsilon_{k,1} + \epsilon_{k,2})$.

It can be shown numerically that the ground state of the Hamiltonian Eq. (2.1) in a finite system (with N even) is in the even sector, $\mathcal{P} = 1$. An alternative way to diagonalize H_k is to expand it in the basis given by the following fermionic operators:

$$\mathcal{B}_k = \{|\mathtt{vac}\rangle, a_k^\dagger a_{-k}^\dagger|\mathtt{vac}\rangle, b_k^\dagger b_{-k}^\dagger|\mathtt{vac}\rangle, a_k^\dagger b_{-k}^\dagger|\mathtt{vac}\rangle, a_{-k}^\dagger b_k^\dagger|\mathtt{vac}\rangle, a_k^\dagger a_{-k}^\dagger b_k^\dagger b_{-k}^\dagger|\mathtt{vac}\rangle\},$$

by exploiting the symmetry of the Hamiltonian (here, $|\mathtt{vac}\rangle$ stands for the fermionic vacuum, that

is, no fermion particles). Accordingly, H_k can be expressed as:

$$H_k = \begin{pmatrix} -4h & 0 & 0 & \Gamma_k^* & \Gamma_k & 0 \\ 0 & 4\delta & 0 & J_k^* & -J_k & 0 \\ 0 & 0 & -4\delta & J_k^* & -J_k & 0 \\ \Gamma_k & J_k & J_k & 0 & 0 & \Gamma_k \\ \Gamma_k^* & -J_k^* & -J_k^* & 0 & 0 & \Gamma_k^* \\ 0 & 0 & 0 & \Gamma_k^* & \Gamma_k & 4h \end{pmatrix} \tag{2.7}$$

Once we get the lowest eigenvalue, we can find the corresponding ground state with respect to mode k:

$$|\Psi_k\rangle = \left(u_k^{(1)} + u_k^{(2)} a_k^\dagger a_{-k}^\dagger + u_k^{(3)} b_k^\dagger b_{-k}^\dagger + u_k^{(4)} a_k^\dagger b_{-k}^\dagger + u_k^{(5)} a_{-k}^\dagger b_k^\dagger + u_k^{(6)} a_k^\dagger a_{-k}^\dagger b_k^\dagger b_{-k}^\dagger\right)|\mathtt{vac}\rangle, \tag{2.8}$$

for complex coefficients determined by diagonalizing H_k, with $\sum_{a=1}^6 |u_k^{(a)}|^2 = 1$. Thus, the many-body ground state may be expressed in the form $|\Psi_{GS}\rangle = \prod_{k\in K^+} |\Psi_k\rangle$. In fact, by exploiting the fact that $\gamma_{k,3}|\Psi_k\rangle = 0, \gamma_{k,4}|\Psi_k\rangle = 0$, we can relate the coefficients $u_k^{(a)}$ and the expression of $\gamma_{k,3}$, $\gamma_{k,4}$ in the basis of $\hat{A}_k$. Let

$$\gamma_{k,3} = v_{k,1}a_k + v_{k,2}a_{-k}^\dagger + v_{k,3}b_k + v_{k,4}b_{-k}^\dagger, \quad \gamma_{k,4} = w_{k,1}a_k + w_{k,2}a_{-k}^\dagger + w_{k,3}b_k + w_{k,4}b_{-k}^\dagger. \tag{2.9}$$

Then,

$$\begin{cases} u_k^{(1)} = v_{k,3}w_{k,1} - v_{k,1}w_{k,3}, & u_k^{(2)} = v_{k,2}w_{k,3} - v_{k,3}w_{k,2}, \\ u_k^{(3)} = v_{k,1}w_{k,4} - v_{k,4}w_{k,1}, & u_k^{(4)} = v_{k,4}w_{k,3} - v_{k,3}w_{k,4}, \\ u_k^{(5)} = v_{k,2}w_{k,1} - v_{k,1}w_{k,2}, & u_k^{(6)} = v_{k,4}w_{k,2} - v_{k,2}w_{k,4}. \end{cases}$$

Similarly, the many-body ground state in the $\mathcal{P} = -1$ sector can be expressed in the form $|\tilde{\Psi}_{GS}\rangle = |\tilde{\Psi}_0\rangle \prod_{k\in\tilde{K}^+} |\tilde{\Psi}_k\rangle$, where $|\tilde{\Psi}_k\rangle$ has the same form as $|\Psi_k\rangle$ in Eq. (2.8):

$$|\tilde{\Psi}_k\rangle = \left(\tilde{u}_k^{(1)} + \tilde{u}_k^{(2)} a_k^\dagger a_{-k}^\dagger + \tilde{u}_k^{(3)} b_k^\dagger b_{-k}^\dagger + \tilde{u}_k^{(4)} a_k^\dagger b_{-k}^\dagger + \tilde{u}_k^{(5)} a_{-k}^\dagger b_k^\dagger + \tilde{u}_k^{(6)} a_k^\dagger a_{-k}^\dagger b_k^\dagger b_{-k}^\dagger\right)|\mathtt{vac}\rangle, \tag{2.10}$$

and $|\tilde{\Psi}_0\rangle = \tilde{u}_0^{(1)} a_0^\dagger|\mathtt{vac}\rangle + \tilde{u}_0^{(2)} b_0^\dagger|\mathtt{vac}\rangle$ such that the total number of fermions is odd.

2.1.1 Quantum Phase Transitions in the Alternating XY Chain

As we discussed in Chapter 1, QPTs are caused by non-analytical behavior of the ground state energy in the thermodynamic limit. However, thanks to the free-fermion picture the Hamiltonian Eq. (2.1) exhibits, the non-analytical behavior of the many-body ground state coincides with the zeroes of $\epsilon_2(k)$ in the thermodynamic limit. Thus, the QCPs are determined by the zeroes $(h_c, \delta_c, \gamma_c)$ of $\epsilon_2(k)$. Analytically, the boundary lines of the phase diagram are determined by the following two equations:

$$\begin{cases} h^2 = \delta^2 + 1, \\ \delta^2 = h^2 + \gamma^2. \end{cases}$$

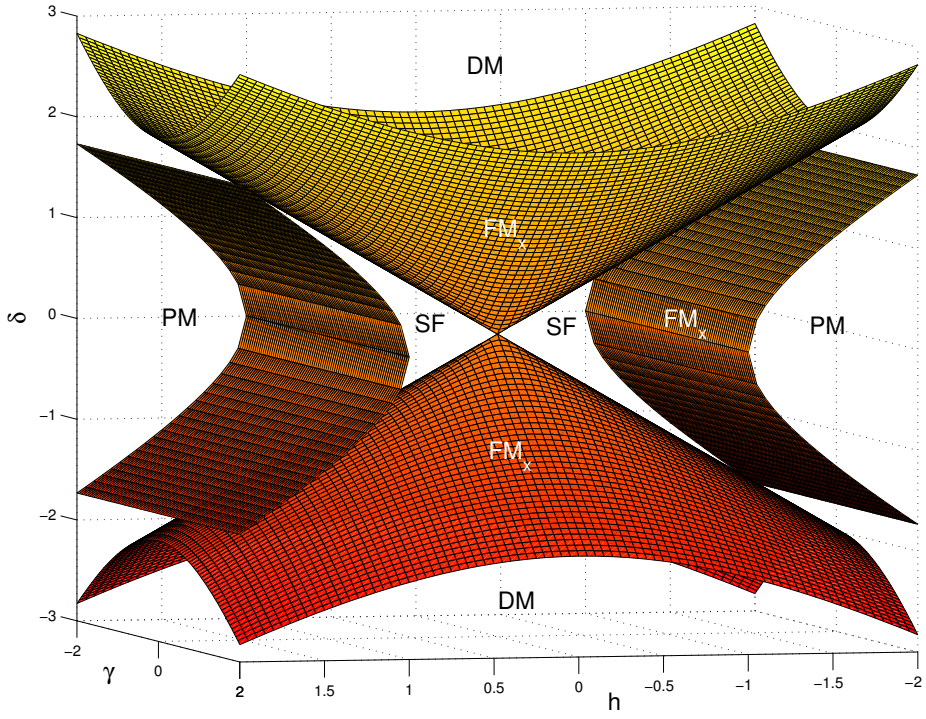

Figure 2.1: 3D phase diagram of the spin-1/2 XY alternating Hamiltonian given in Eq. (2.1).

The resulting phase diagram is depicted in Fig. 2.1. The different quantum phases can be understood by taking different limits of Hamiltonian Eq. (2.1). Let us first consider the anisotropic

cases, where $\gamma \neq 0$. Notice that the Hamiltonian Eq. (2.1) is invariant under the transformation that maps $(\sigma_x^i; \sigma_y^i; \sigma_z^i) \mapsto (-\sigma_x^i; -\sigma_y^i; \sigma_z^i)$ ($\mathbb{Z}_2^z$ symmetry), implying that $\langle \sigma_x^i \rangle = 0$ (similarly, $\langle \sigma_y^i \rangle = 0$) for all h and δ. However, since in the thermodynamic limit the ground state becomes two-fold degenerate in the center of the phase diagram, it is possible to build up a ground state where the discrete $\mathbb{Z}_2^z$ symmetry is broken, i.e., $\langle \sigma_x^i \rangle \neq 0$ (and, similarly, $\langle \sigma_y^i \rangle \neq 0$). We can understand this statement by considering the Ising limit $\gamma = 1(-1)$: when $\delta \to \infty, h = 0$, the spins tend to align in the opposite direction of the alternating magnetic field, with ground state $|g\rangle = |\downarrow, \uparrow, \cdots, \downarrow, \uparrow\rangle$, which we call Dimer Phase (DM); conversely, when $h \to \infty, \delta = 0$, the ground state corresponds to all spins pointing down in the z direction which gives a Paramagnetic Phase (PM). The ground state in both the DM and PM phases has no net magnetization in the $x(y)$ direction. On the other hand, for $h = 0, \delta = 0, \gamma = 1$, the states $|\psi_g^e\rangle = \frac{1}{\sqrt{2}}(|\rightarrow, ..., \rightarrow\rangle + |\leftarrow, ..., \leftarrow\rangle)$ (ground state of the $\mathcal{P} = 1$ sector) and $|\psi_g^o\rangle = \frac{1}{\sqrt{2}}(|\rightarrow, ..., \rightarrow\rangle - |\leftarrow, ..., \leftarrow\rangle)$ (ground state of the $\mathcal{P} = -1$ sector), with $|\rightarrow\rangle$ the positive eigenvalue for σ_x operator, and $|\leftarrow\rangle$ the negative eigenvalue for the σ_x operator, become degenerate in the thermodynamic limit. Thus, a ground state with $\langle \sigma_x^i \rangle \neq 0$ can be constructed from any superposition of the two. A similar conclusion for $\langle \sigma_y^i \rangle \neq 0$ can be reached for the limit $h = 0, \delta = 0, \gamma = -1$. Therefore, long-range order in the xy plane exist in the center of the phase diagram, leading to a Ferromagnetic Phase (FM) [43, 12]. More specifically, when $h = 0, \delta = 0, \gamma > 0$, spin-spin correlations in the x direction are established, leading to what we call the FM_x phase, while spin-spin correlations in the y direction are the dominant contribution to the Hamiltonian for $h = 0, \delta = 0, \gamma < 0$, leading to the FM_y phase.

In the isotropic limit ($\gamma = 0$), the Hamiltonian of Eq. (2.1) has a continuous $U(1)$-symmetry; that is, it is invariant under *any* $\hat{z}$ rotation of the form $e^{i\theta \sum_j \sigma_z^j}$ (not just $\theta = \pm\pi/2$). Since the model is one-dimensional, according to the Mermin–Wagner theorem, this symmetry cannot be spontaneously broken, regardless of the magnitude of the coupling constants [48]. Nevertheless, a simple calculation of the ground state energy indicates a divergence in its second (or higher order) derivative at the critical points on this plane, thus, continuous non-broken symmetry QPTs. In terms of the fermionic operators $(a_i^\dagger(b_i^\dagger), a_i(b_i))$, an insulator-to-metal- (or superfluid-) like second-order QPT occurs at (h_c, δ_c) for the isotropic case, with no symmetry order parameter (SF stands for superfluid phase). Thus, according to the definition of multi-criticality [17], the critical lines on

the $\gamma = 0$ plane, which describe the coexistence of at least three different phases (FM_x, FM_y, SF, PM/DM), consist entirely of MCPs.

Let us now have a clearer picture of the phase diagram for the Hamiltonian Eq. (2.1) by considering separately different physical limits.

2.1.1.1 The Anisotropic Limit

Without loss of generality, we can restrict to $\gamma > 0$ cases since there is a mirror symmetry in the 3D phase diagram with respect to the plane $\gamma = 0$. Furthermore, we can let $\gamma = 0.5$ without affecting the critical behavior. The corresponding quantum phase diagram is shown in Fig. 2.2.

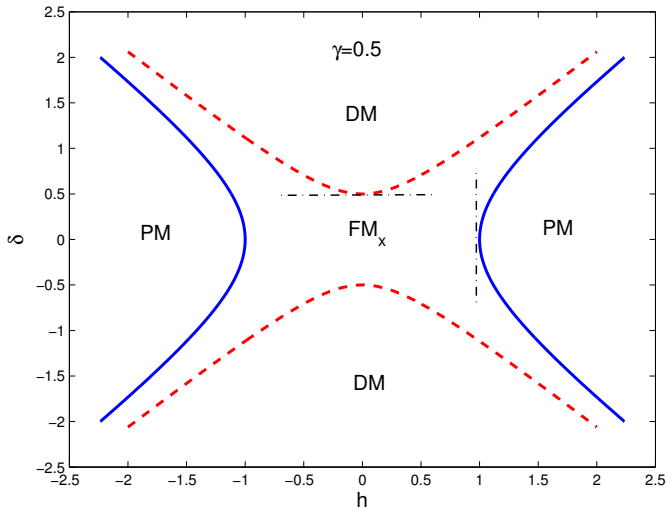

Figure 2.2: Phase diagram of the spin-1/2 XY alternating Hamiltonian given in Eq. (2.1) with $\gamma = 0.5$. The solid (blue) and dashed (red) lines are the phase boundaries. The dashed-dotted lines are the sample paths to approach the QCPs in a tangent way. Since $\gamma > 0$, the FM phase in the center correspond to ferromagnetic order in x direction.

In the generic case, the boundaries between FM and PM, as well as FM and DM are characterized by second order broken-symmetry QPTs. However, it is interesting to realize that the ground state

develops weaker singularities at the special points:

$$\begin{cases} (h_c, \delta_c, \gamma_c) = (h = 0, \delta = \pm\gamma), \\ (h_c, \delta_c, \gamma_c) = (h \pm 1, \delta = 0), \end{cases}$$

where fourth-order broken-symmetry QPTs occur along the paths approaching the QCPs (Fig. 2.2, dashed-dotted lines) [41].

In order to obtain the critical exponents ν and z of the QPTs in our system, let us first recall the scaling assumptions for general QPTs introduced in Chapter 1. Eq. (1.1) characterizes the scaling behavior of the gap with respect to the control parameter close to the QCP, and Eq. (1.3) characterizes the scaling behavior of the gap with respect to the correlation length at the QCP. The ground state in a finite system is the ground state of the $\mathcal{P} = 1$ sector, and the first-excited state in a finite system is the ground state of the $\mathcal{P} = -1$ sector. Thus, the many-body gap Δ in Eq. (1.1) and Eq. (1.3) is the gap between these two states. However, the error in the computation of the many-body gap (and also other observables) arising from identifying the two sets of modes K and $\bar{K}$ scales like $1/N$, which leads to the scaling behavior of the gap between the ground state and the first-excited state in the $\mathcal{P} = 1$ to be the same as Δ in Eq. (1.1) and Eq. (1.3) for large N. Thus, we can obtain the critical exponents by analyzing the gap between the ground state and the first-excited state in the $\mathcal{P} = 1$ sector, which corresponds to the smallest gap $\Delta_k(\gamma, h, \delta)$ (Eq. (2.6)) among all the modes $k \in K_+$ for fixed control parameters γ, h, δ.

We define a mode to be the *critical mode* (k_c) if the corresponding gap $\Delta_k(\gamma_c, h_c, \delta_c)$ closes in the thermodynamic limit. Thus, at $(\gamma_c, h_c, \delta_c) = (0.5, 1, 0)$, $k_c = 0$, whereas at $(\gamma_c, h_c, \delta_c) = (0.5, 0, 0.5)$, $k_c = \pi/2$. Let us analyze the critical exponents at QCP $(\gamma_c, h_c, \delta_c) = (0.5, 1, 0)$, for instance. Typically, we can have two paths approaching this QCP, one being the horizontal path at fixed δ, the other being the vertical path at fixed h. Along the horizontal path, for $k_c = 0$,

$$\Delta_0(0.5, h, 0) \sim (h - 1)^1,$$

indicating that $\nu z = 1$. On the other hand, by using a Taylor-expansion of $\Delta_k(0.5, 1, 0)$ for k around

k_c one obtains:

$$\Delta_k(0.5, 1, 0) \sim (k - k_c)^1 \sim \xi^{-1},$$

indicating that $z = 1$. Thus, we infer that $\nu = 1, z = 1$ along the horizontal path approaching $(\gamma_c, h_c, \delta_c) = (0.5, 1, 0)$, which then belongs to $d = 2$ *Ising universality class*. Similarly, for the vertical path, for $k_c = 0$,

$$\Delta_0(0.5, 1, \delta) \sim (\delta - 0)^2,$$

indicating that $\nu z = 2$. Then, a Taylor-expansion of $\Delta_k(0.5, 1, 0)$ for k around k_c yields:

$$\Delta_k(0.5, 1, 0) \sim (k - k_c)^1 \sim \xi^{-1},$$

indicating that $z = 1$. Thus, we know that $\nu = 2, z = 1$ along the vertical path approaching $(\gamma_c, h_c, \delta_c) = (0.5, 1, 0)$, which we call the *alternating universality class*. Actually, the analysis shown here makes it clear that following different paths approaching the same QCP might results in (two) different critical exponents ν, but the same z. Since z is determined by Taylor-expanding the gap with respect to k at the fixed control parameters at QCP, following different paths approaching the same QCP will not result in different z. In summary, there are two distinct universality classes for nonzero γ, one is the Ising universality class, with $\nu = 1, z = 1$; the other is the alternating universality class, with $\nu = 2, z = 1$ at the fourth-order broken-symmetry QCPs.

2.1.1.2 The Isotropic Limit

The phase diagram in the isotropic limit ($\gamma = 0$) is depicted in Fig. 2.4. Generic QCPs on the boundary lines belong to the so-called *Lifshitz universality class*, with critical exponents $\nu = 1/2, z = 2$. As explained in the previous subsection, different critical behavior still occurs at $(h = \pm 1, \delta \to 0)$ (see *e.g.* the dash-dotted line in Fig. 2.4), where now $\nu = 1, z = 2$. Furthermore, Ising critical exponents are recovered while approaching the point $(h = 0, \delta = 0) \equiv \mathtt{0}$ along every path other than $(\delta = 0, h \to 0)$ (when there is no QCP).

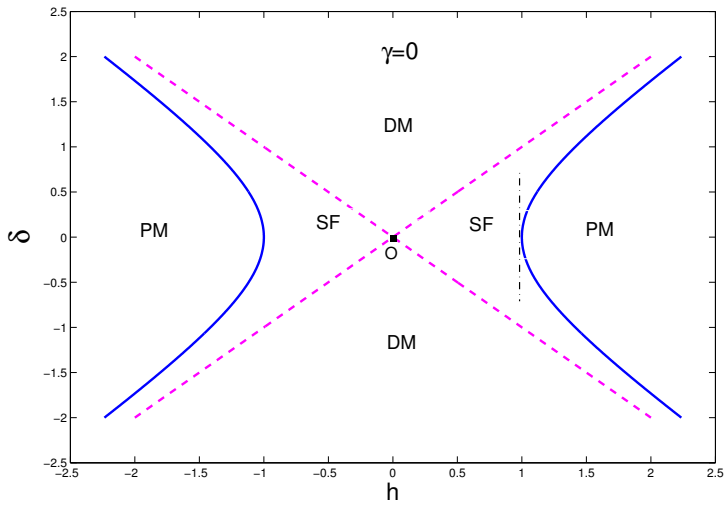

Figure 2.3: Phase diagram of the alternating spin chain, Eq. (2.1). Solid (blue) and dashed (magenta) lines define the phase boundaries for $\gamma = 0$. Point O at $(h = 0, \delta = 0)$ is marked.

2.1.1.3 The Variable-Isotropy Limit

The phase diagram in the region perpendicular to the $\gamma = 0$ plane is depicted in Fig. 2.4. Without loss of generality, we choose the phase diagram at $h = 1$ (top of Fig. 2.4) and $\delta = 0$ (bottom of Fig. 2.4) for further scrutiny. Regular QCPs in Fig. 2.4 belong to Ising universality class. As explained earlier, the critical lines on the plane $\gamma = 0$ consist of MCPs. Generally speaking, MCPs are associated with different universality classes. So we choose to study the critical behavior across MCP A and MCP B as marked on Fig. 2.4 by different approaching paths. The results may be summarized in the following table. Thus, there are two universality classes: the first one is the

Path	ν	z	Parameterization of the paths
1	1	2	change both γ and δ across MCP A ($\gamma = \delta$); $h = 1$
2	1	2	change γ across MCP B; $h = 1, \delta = 1$
3	1/2	2	change both γ and δ across MCP B ($\gamma = \delta - 1$); $h = 1$
4	1/2	2	change both γ and h across MCP A ($\gamma = h - 1$); $\delta = 0$

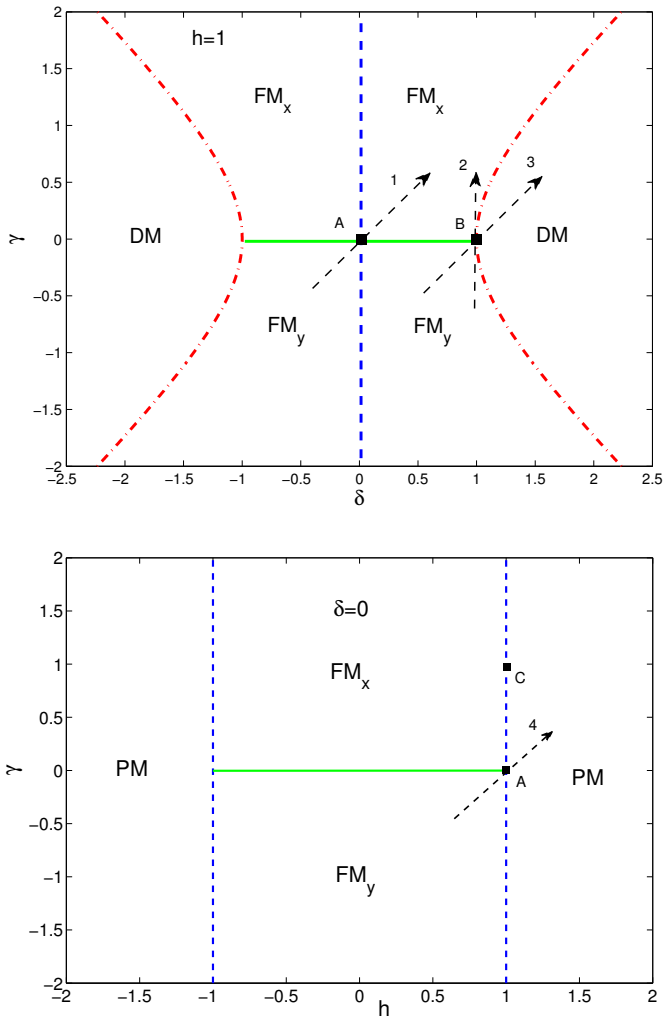

Figure 2.4: Phase diagram of the Hamiltonian in Eq. (2.1) when $h = 1$ (top) and $\delta = 0$ (bottom). The dashed (blue) line separates the FM and PM phases, the dashed-dotted (red) lines separate DM and FM, whereas the solid (green) line is the SF phase. The arrows indicate the control paths we choose to approach the MCPs `A` and `B`. The standard (non-multicritical) QCP `C` ($h_c = 1, \gamma_c = 1$) is marked as well for later reference.

Lifshitz universality class for paths 3 and 4; the second one is a new universality class for paths 1 and 2, which, to the best of our knowledge, has not been reported before.

2.2 Generalized Entanglement in the Alternating XY Chain

The term "Entanglement", introduced by Schrödinger in 1935, essentially captures the failure of classical intuition in describing the relationship between the "parts" and the "whole" of a composite system in the quantum world [44]: a (pure) state is entangled if knowledge of the whole state does not imply the 'maximal' knowledge of its parts. This definition implies that entanglement is a genuine quantum correlation between certain degrees of freedom of the parties of the whole system, and implies that (i) a preferred subsystem division is available for the whole system; and that (ii) the subsystems involved in the whole system are distinguishable. If we consider states of identical fermions or bosons, however, they possess intrinsic correlations due to the associated quantum statistics; still, the latter need not be useful from the viewpoint of QIS. Therefore, this standard view of entanglement, which is built upon the distinguishability of subsystems, has its own limitation. This limitation calls for a new definition of entanglement, that is, so-called generalized entanglement (GE) [45], which will be discussed in detail in this section.

2.2.1 Subsystem-Dependent Entanglement Measure

Before we describe the concept of GE, let us start by recalling some basic concepts from the standard framework of conventional (subsystem-based) entanglement. Let us first focus on bipartite systems, defined on Hilbert space $\mathcal{H} = \mathcal{H}_A \otimes \mathcal{H}_B$. A pure state of a bipartite quantum system is called entangled if it is unfactorizable, that is,

$$|\psi_{\mathrm{AB}}\rangle = |\Psi_A\rangle \otimes |\phi_B\rangle. \tag{2.11}$$

A mixed state ρ_{AB} is separable if and only it can be represented as a mixture of factorizable pure states, that is,

$$\rho_{\mathrm{AB}} = \sum_s p_s |\Psi^s\rangle_A\langle\Psi^s| \otimes |\phi^s\rangle_B\langle\phi^s|, \tag{2.12}$$

where p_s is the corresponding probability, satisfying $\sum_s p_s = 1$. In general, note that it is not easy to check whether it is possible to write a quantum state in a form like Eq. (2.12). Since we are only interested in entanglement at zero temperature, we will focus on pure states only. The Schmidt decomposition for a bipartite pure state is a valuable tool to analyze its separability [19]. Any bipartite pure state $|\psi_{\rm AB}\rangle$ can be expressed as

$$|\psi_{\rm AB}\rangle = \sum_{s=1}^{R} c_s |\Phi_A^s\rangle \otimes |\Phi_B^s\rangle, \tag{2.13}$$

where R is the Schemdt rank, equal to the number of nonzero coefficient c_s, Φ_A^s and Φ_B^s are orthonormal states of subsystem A and B respectively, with $\sum_{s=1}^{R} |c_s|^2 = 1$. When $R > 1$ in the decomposition, $|\psi_{\rm AB}\rangle$ is entangled; otherwise, it is separable. Or equivalently, if $|\psi_{\rm AB}\rangle$ is an entangled state, then the reduced density matrix of subsystem A(B) is a mixed state, since

$$\rho_A = {\rm Tr}_B(\rho_{AB}) = \sum_{s=1}^{R} |c_s|^2 |\Phi_A^s\rangle\langle\Phi_A^s|,$$

$R > 1$ leads to $|c_s|^2 < 1$. Notice that exactly the same spectrum would be obtained for ρ_B, leading to the same information about the separability of $|\psi_{\rm AB}\rangle$. Quantitatively, the von Neumann entropy of ρ_A (ρ_B) provides an effective way to measure the entanglement between subsystem A and B:

$$E \equiv S_{\rho_A} = -{\rm Tr}(\rho_A \log_2(\rho_A)) = -\sum_{s=1}^{R} |c_s|^2 \log_2 |c_s|^2, \tag{2.14}$$

where $E = 1$ correspond to maximally entangled states, and $E = 0$ to separable states, respectively. The most commonly used two-qubit maximally entangled states are the well-known *Bell states*:

$$|\psi^{\pm}\rangle = \frac{1}{\sqrt{2}}(|00\rangle \pm |11\rangle), \quad |\phi^{\pm}\rangle = \frac{1}{\sqrt{2}}(|01\rangle \pm |10\rangle). \tag{2.15}$$

It is easy to verify that the von Neumann entropy of all the Bell states is 1. On the other hand, if $|\psi\rangle_{AB} = |i\rangle_A \otimes |j\rangle_B$, the von Neumann entropy is zero.

While the Schmidt decomposition provides a successful characterization for the entanglement of bipartite pure states, problems arise for systems with more than two parties. Even in the simplest

extension of a bipartite systems of two qubits, that is, a three-qubit system, the characterization of entangled states is not an easy task [49]. The qualitative definition of separability and entanglement is much richer in multipartite systems than in the bipartite case. Besides the so-called full separability, which is the direct generalization of bipartite separability, there are many types of "partial separability" (see *e.g.* the recent review in Ref. [36]). The difficulty in characterizing multipartite entanglement mainly comes both from the fact that the tensor product decomposition is no longer unique, and the fact that different (inequivalent) types of entanglement can be found.

These difficulties become even more severe when states of indistinguishable particles are considered, as necessary in condensed-matter physics. The "decomposition" issue, in particular, also exists if we consider "mode entanglement", instead of particle entanglement in certain systems. For example, let us consider a single particle which can be either in site i or j. In second quantization, this state can be expressed as:

$$|\psi_s\rangle = \frac{1}{\sqrt{2}}(c_i^\dagger + c_j^\dagger)|\mathtt{vac}\rangle = \frac{1}{\sqrt{2}}(|1,0\rangle + |0,1\rangle), \tag{2.16}$$

where $c_i^\dagger$ is the creation operator at site i, $|\mathtt{vac}\rangle$ is the particle vacuum, and $|1\rangle$, $|0\rangle$ denote the presence or absence of the particle in a site, respectively. Thus, this single-particle state is one of the Bell states in the mode picture, hence maximally entangled. A paradox arises since there is clearly no way to decompose one particle into two subsystems, thus it is impossible to talk about entanglement from this point of view. Even in the mode entanglement realm, different mode pictures may give completely different conclusions about entanglement. Let us think about the exact solution of the XY model with alternating magnetic field discussed in Section 2.1. The reason why we can have a simple analytical solution is because in the fermionic language, there is no interaction between fermions with different momentum modes. However, in the position-mode picture, the fermions are not independent from each other, and thus they can be entangled. Furthermore, before using the generalized Jordan-Wigner transformation, in the spin language, entanglement would be completely different than in the fermionic language. Then how would one judge which language would be physically more appropriate to describe entanglement?

This serves to illustrate how the subsystem-dependent entanglement notion has intrinsic limi-

tations. The nontrivial quantum statistics, or other physical restrictions, can make the choice of preferred subsystem problematic. The generalized approach introduced in Ref. [45] can overcome such difficulties, by removing the need for a subsystem decomposition from the start, and by redefining entanglement in such a way that it depends *only* upon the choice of a preferred *set of observables*, irrespective of the choice of a particular operator language (*e.g.* spin, fermion,...) used to describe the system. This is the main motivation for the concept of GE.

2.2.2 Generalized Entanglement as an Observer-Dependent Concept

Physically, GE [45] is based on the idea that entanglement is an *observer*-dependent concept, whose properties are determined by the expectation values of a distinguished subspace of observables Ω, without reference to a preferred decomposition of the Hilbert space into subsystems. Notice that in the standard entanglement definition, entangled pure states of a composite quantum system look mixed relative to an observer whose knowledge is restricted only to local expectation values. Thus the GE definition generalizes the observable subspace, that is, it no longer restricts it to local observables. Let us consider the simplest case – two distinguishable spin-1/2 subsystems in a singlet state defined on a tensor-product state space $\mathcal{H} = \mathcal{H}_A \otimes \mathcal{H}_B$, that is $|\phi^-\rangle$ in Eq. (2.15). The statement that $|\psi^-\rangle$ is entangled is equivalent to the property that (either) reduced subsystem state, *e.g.*, $\rho_A = \mathrm{Tr}_B|\psi^-\rangle\langle\psi^-|$ is mixed, that is $\mathrm{Tr}\rho_A^2 = 1/2(1 + \sum_{\alpha=x,y,z}\langle\sigma_\alpha^A\rangle^2) < 1$, in terms of expectations of the local Pauli spin-1/2 matrices σ_α^A for subsystem A. To the purposes of defining GE, the key step is to realize that to construct a meaningful *reduced state* for any pure state $|\psi\rangle \in \mathcal{H}$, one may not need to invoking a partial trace. We can, for instance, specify a reduced "Ω-state" as a list of expectations of operators in the preferred set Ω, determined by the observer. The fact that the space of all Ω-states is *convex* then motivates the following definition [45, 46]:

Pure-state GE: A pure state $|\psi\rangle \in \mathcal{H}$ is *generalized unentangled relative to* Ω *if its reduced* Ω*-state is pure, generalized entangled otherwise.*

One can realize that there are at least two major advantages of GE comparing to the standard entanglement definition for the purpose of application to many-body physics: first, GE is directly applicable to both distinguishable and indistinguishable degrees of freedom, thus quantum-statistical

constraints can be incorporated naturally; second, the property of a many-body state $|\psi\rangle$ to be entangled or not is independent on both the choice of modes and the operator language used to describe the system, but depends only on the observables Ω, which is more meaningful physically.

For a large class of physical systems, the set of distinguished observables Ω may be identified with a *Lie algebra* (*i.e.*, an algebra closed under commutation) consisting of Hermitian operators, $\Omega \simeq \mathfrak{h}$, which is the generator of a corresponding unitary Lie group, that is, $\mathfrak{h} \mapsto \mathcal{G} = e^{i\mathfrak{h}}$. While the assumption of a Lie-algebraic structure is not necessary for the GE concept to be applicable [45, 46], it has the advantage of quantifying GE in a simple way. In particular, a geometric measure of GE can be constructed by taking the square length of the projection of $|\psi\rangle\langle\psi|$ onto $\mathfrak{h}$, that is:

Relative purity: Let $\mathfrak{h} = \{O_1, \ldots, O_M\}$ be a M-dimensional Hermitian Lie-algebra. The reduced $\mathfrak{h}$-state of a pure $|\psi\rangle$ state is defined to be a linear functional on the operators in $\mathfrak{h}$: $\langle\psi|O_\ell|\psi\rangle (\ell = 1, \ldots, M)$. Thus the *purity of* $|\psi\rangle$ *relative to* $\mathfrak{h}$ *is given by the square length of the* $\mathfrak{h}$-state:

$$P_{\mathfrak{h}}(|\psi\rangle) = \mathsf{K} \sum_{\ell=1}^{M} \langle\psi|O_\ell|\psi\rangle^2 \,, \tag{2.17}$$

where K is a *global* normalization factor chosen so that $0 \leq P_{\mathfrak{h}} \leq 1$, with $P_{\mathfrak{h}} = 0$ the generalized maximumally-entangled state, $P_{\mathfrak{h}} = 1$ the generalized unentangled state.

Notice that $P_{\mathfrak{h}}$ is invariant under group transformations, that is, $P_{\mathfrak{h}}(|\psi\rangle) = P_{\mathfrak{h}}(G|\psi\rangle)$, for all $G \in \mathcal{G}$, which is a desirable property physically. If, additionally, $\mathfrak{h}$ is a semi-simple Lie algebra *irreducibly* represented on $\mathcal{H}$, generalized unentangled states coincide [45] with *generalized coherent states* (GCSs) of $\mathcal{G}$, that is, they may be seen as "generalized displacements" of an appropriate reference state (or vacuum):

$$|\mathsf{GCS}(\{\eta_\ell\})\rangle = \exp(i \sum_{\ell} \eta_\ell O_\ell)|\mathsf{ref}\rangle. \tag{2.18}$$

Physically, GCSs can be shown to correspond to unique ground states of Hamiltonians in $\mathfrak{h}$: States of matter such as BCS superconductors (*e.g.* states of the form $\prod_k (u_k + i v_k c_k^\dagger c_{-k}^\dagger)|\mathsf{vac}\rangle$) or normal Fermi liquids ($\prod_k c_k^\dagger |\mathsf{vac}\rangle$) are typically described by GCSs. Here, we illustrate the GE notion by two examples that are relevant to the application of GE measure to our model Hamiltonian.

• **Example 1**: Standard entanglement revisited.

Suppose we have N local (distinguishable) parties separated in real space, with Hilbert space $\mathcal{H} = \mathcal{H}_1 \otimes \ldots \otimes \mathcal{H}_N$. The natural set of preferred observables can be the ones restricted to arbitrary local transformations, that is, $\mathfrak{h}_{loc} = \mathfrak{su}(\dim(\mathcal{H}_1)) \oplus \ldots \oplus \mathfrak{su}(\dim(\mathcal{H}_N))$, as the distinguished algebra in the GE approach. If, for example, each local Hilbert space is two-dimensional, then $\mathfrak{h}_{loc} = \text{span}\{\sigma_\alpha^\ell \,; \alpha = x, y, z, \ell = 1, \ldots, N\}$, and Eq. (2.17) yields

$$P_{\mathfrak{h}_{loc}}(|\psi\rangle) = \frac{1}{N} \sum_{\ell,\alpha} \langle \psi | \sigma_\alpha^\ell | \psi \rangle^2 = \frac{2}{N} \Big(\sum_\ell \text{Tr} \rho_\ell^2 \Big) \; - 1, \tag{2.19}$$

which is nothing but the average (normalized) subsystem purity. Thus, $P_{\mathfrak{h}_{loc}}$ quantifies multipartite subsystem entanglement in terms of the average bipartite entanglement between each spin and the rest. Maximum local purity, $P_{\mathfrak{h}} = 1$, is attained if and only if the underlying state is a pure product state, that is, a GCS of the local unitary group $\mathcal{G}_{loc} = SU(2)_1 \otimes \ldots \otimes SU(2)_N$. On the contrary, maximum GE is realized, *i.e.* $P_{\mathfrak{h}} = 0$, when each subsystem is maximally entangled ($\text{Tr}\rho_\ell^2 = 1/2$) in the standard sense.

• **Example 2**: Fermionic GE.

Consider a system of indistinguishable (spinless) fermions able to occupy N modes, which could for instance correspond to distinct lattice sites or momentum modes, and are described by canonical fermionic operators $c_j, c_j^\dagger$ on the 2^N-dimensional Fock space $\mathcal{H}_{Fock}$. The standard subsystem-based definition of entanglement associated with a given choice of modes may be applied if the indistinguishability condition can be relaxed. However, in the presence of many-body interactions, choosing a specific mode description may not be physically justified [52]. These difficulties are avoided in the GE approach by associating "generalized local" resources with *number-preserving* bilinear fermionic operators, which identifies the unitary Lie algebra $\mathfrak{u}(N) = \text{span}\{c_j^\dagger c_j \,; 1 \leq i, j \leq N\}$ as the distinguished observable algebra for fermionic GE. By re-expressing $\mathfrak{u}(N)$ in terms of an orthogonal Hermitian basis of generators, Eq. (2.17) yields

$$P_{\mathfrak{u}(N)}(|\psi\rangle) = \frac{2}{N} \sum_{j<k=1}^{N} \Big[\langle c_j^\dagger c_k + c_k^\dagger c_j \rangle^2 - \langle c_j^\dagger c_k - c_k^\dagger c_j \rangle^2 \Big] + \frac{4}{N} \sum_{j=1}^{N} \langle c_j^\dagger c_j - 1/2 \rangle^2 \, . \tag{2.20}$$

One may show that a many-fermion pure state is generalized unentangled relative to $\mathfrak{u}(N)$ ($P_{\mathfrak{u}(N)} =$

1) if and only if it is a *single Slater determinant* (with any number of fermions), whereas $P_{\mathfrak{u}(N)} < 1$ for any state containing fermionic GE [50]. For instance, for a product state (Slater determinant) of the form $|\psi\rangle = \prod_l c_l^\dagger |\mathtt{vac}\rangle$, $\langle\psi|c_j^\dagger c_k|\psi\rangle (j \neq k)$ vanishes, thus the only contributing term is $\langle\psi(|c_k^\dagger c_k - 1/2)|\psi\rangle = \pm 1/2$, which leads to $P_{\mathfrak{u}(N)}(|\psi\rangle) = \frac{4}{N}\sum_{j=1}^{N}\frac{1}{4} = 1$. Note that a pure single-particle Bell state $|\psi_s\rangle$ as defined in Eq. (2.16), which is maximally mode-entangled in the standard definition, is $\mathfrak{u}(N)$-*un*entangled, which is consistent with the fact that it is a one-particle state, thus the fermion number is conserved.

2.2.3 Generalized Entanglement as an Indicator of Quantum Criticality

By construction, if $\mathfrak{h}$ denotes all the linearly independent observables of the quantum system, the $\mathfrak{h}$-state fully determines the state of the system. In such a case, *any* pure state is generalized unentangled, thus this algebra carries no useful information about a QPT. If the correct sub-algebra is chosen, however, the relative purity can contain information about the relevant quantum correlations that uniquely identify and characterize the QCPs of the system. It has been demonstrated that GE can faithfully detect QCPs in the one-dimensional anisotropic XY model in a transverse magnetic field [50], when purity with respect to an appropriate sub-algebra is chosen. In particular, purity relative to the $\mathfrak{u}(N)$ algebra, generated by the set of bilinear fermionic operators $\{c_j^\dagger c_{j'}; 1 \leq j, j' \leq N\}$, has been used to identify QPTs belonging to $d = 2$ Ising universality class ($z = 1, \nu = 1$), whereas the first-order derivative of the purity relative to local algebra, $\mathfrak{h} = \bigoplus_{i=1}^{N} \mathfrak{su}(2)_i$, has been used to identify QPTs belonging to the Lifshitz universality class ($z = 2, \nu = 1/2$).

The key step toward applying GE as a QPT indicator is to identify a (Lie) algebra of observables whose expectations reflect the changes in the ground state as a function of the control parameters. The Hamiltonian in Eq. (2.1), once written in the fermionic language, is an element of the Lie algebra $\mathfrak{so}(2N)$, which includes *arbitrary* bilinear fermionic operators. As a result, the ground state is always a GCS of $\mathfrak{so}(2N)$, and GE relative to $\mathfrak{so}(2N)$ carries no information about QCPs. However, the ground state becomes a GCS of the number-conserving sub-algebra $\mathfrak{u}(N)$ in both the fully PM and DM limit. This still motivates the choice of the fermionic $\mathfrak{u}(N)$-algebra discussed as a natural candidate for this class of systems with general control parameters ($\gamma \neq 0$). In momentum space,

the Hermitian, orthonormal operator basis of the $\mathfrak{u}(N)$ algebra reads:

$$\begin{aligned}
&\sqrt{2}(a_k^\dagger a_k - 1/2), \qquad \sqrt{2}(b_k^\dagger b_k - 1/2),\\
&(a_k^\dagger a_{k'} + a_{k'}^\dagger a_k), \qquad i(a_k^\dagger a_{k'} - a_{k'}^\dagger a_k), \quad k \neq k',\\
&(b_k^\dagger b_{k'} + b_{k'}^\dagger b_k), \qquad i(b_k^\dagger b_{k'} - b_{k'}^\dagger b_k), \quad k \neq k',\\
&(a_k^\dagger b_{k'} + b_{k'}^\dagger a_k), \qquad i(a_k^\dagger b_{k'} - b_{k'}^\dagger a_k), \quad k \neq k',
\end{aligned} \tag{2.21}$$

where $k, k' \in K$. Taking advantage of the symmetries of the Hamiltonian Eq. (2.1), $P_{\mathfrak{u}(N)}$ for the ground state can be expressed as:

$$\begin{aligned}
P_{\mathfrak{u}(N)} = \frac{2}{N} \sum_{k \in K_+} & 2\left(\langle a_k^\dagger a_k - 1/2\rangle^2 + \langle a_{-k}^\dagger a_{-k} - 1/2\rangle^2 + \langle b_k^\dagger b_k - 1/2\rangle^2\right)\\
& + 2\left(\langle b_{-k}^\dagger b_{-k} - 1/2\rangle^2\right) + 4|\langle a_k^\dagger b_k\rangle|^2 + 4|\langle a_{-k}^\dagger b_{-k}\rangle|^2.
\end{aligned} \tag{2.22}$$

Analytical results of $P_{\mathfrak{u}(N)}$ are only available for $\delta = 0$, when GE can sharply detects PM-FM QPTs [50]. Remarkably, however, ground-state fermionic GE can still faithfully portrait the underlying quantum phases in the presence of alternation. We find that derivatives of GE develop singular behavior *only* at QCPs, as shown in Fig. 2.5. For weak singularities developed at $(\gamma_c, h_c, \delta_c) = (0.5, 0, 0.5)$, the second derivative of $P_{\mathfrak{u}(N)}$ is needed to identify the QPT. Moreover, the scaling properties of GE provide additional evidence that GE is a faithful QPT indicator. When $\delta = 0$, by taking a Taylor expansion of $P_{\mathfrak{u}(N)}$ in its analytical expression, one can find that the spin correlation length enters into the expression of $P_{\mathfrak{u}(N)}$ near the QCP, that is,

$$P_{\mathfrak{u}(N)}(h) - P_{\mathfrak{u}(N)}(h_c) \sim \frac{1}{\xi} \sim (h - h_c)^\nu. \tag{2.23}$$

where ξ is the spin correlation length. Therefore, we can extract the relevant critical exponent ν in a log-log plot of $P_{\mathfrak{u}(N)}$ [50]. Similarly here, with general control parameters, numerical results indicate that a Taylor-expansion of $P_{\mathfrak{u}(N)}$ can still be used to extract the critical exponent ν for both the Ising and the alternating universality class (see Fig. 2.6).

Interestingly, in Ref. [50], it was analytically proved that in the limit $\delta = 0$, the ground-state

$\mathfrak{u}(N)$-purity can be directly related to the *fluctuations* of the total fermion operator $\hat{N} = \sum_i c_i^\dagger c_i$:

$$P_{\mathfrak{u}(N)} = 1 - \frac{2}{N}\big(\langle \hat{N}^2 \rangle - \langle \hat{N} \rangle^2\big). \tag{2.24}$$

While the relative purity can always be related to a sum of variances of observables [45], it is remarkable that the $\mathfrak{u}(N)$-purity can be expressed in terms of the variance of a *single* observable. Physically, this explains why this purity measure carries information about QPTs, given the fact that QPTs are precisely driven by the quantum fluctuations of observables. Since $P_{\mathfrak{u}(N)}$ can successfully identify the QCPs and the critical exponents of *all* the QPTs in the anisotropic limit irrespective of the value of δ, we would expect $P_{\mathfrak{u}(N)}$ to be able to be expressed in terms of fluctuations of the total fermion operator as well. In fact, Eq. (2.24) still holds for the ground state of the Hamiltonian Eq. (2.1) with alternating magnetic field:

$$P_{\mathfrak{u}(N)} = 1 - \frac{2}{N}\Big[\langle\big(\sum_{k\in K} a_k^\dagger a_k + b_k^\dagger b_k\big)^2\rangle - \langle\sum_{k\in K} a_k^\dagger a_k + b_k^\dagger b_k\rangle^2\Big]. \tag{2.25}$$

The proof of this statement is shown in Appendix A, and relies on particle-hole symmetry.

2.3 Duality Transformation

It is interesting to observe that the alternating universality class ($\nu = 2, z = 1$) arises in a related class of model Hamiltonians, where alternation occurs in the spin coupling strengths, rather than in the strength of the applied magnetic field. That is, let

$$H' = -\sum_{i=1}^{N}\big(g - (-1)^i\delta\big)\Big[\frac{(1+\gamma)}{2}\sigma_x^i\sigma_x^{i+1} + \frac{(1-\gamma)}{2}\sigma_y^i\sigma_y^{i+1}\Big] + \sum_{i=1}^{N}\sigma_z^i, \tag{2.26}$$

with $g, \delta, \gamma \in (-\infty, \infty)$. The phase diagram of this Hamiltonian may be obtained through a procedure similar to the one described in the Section 2.1, and is depicted in Fig. 2.7. The boundary line equations are now :

$$\begin{cases} g^2 = (\gamma\delta)^2 + 1, \\ \delta^2 = (\gamma g)^2 + 1, \end{cases}$$

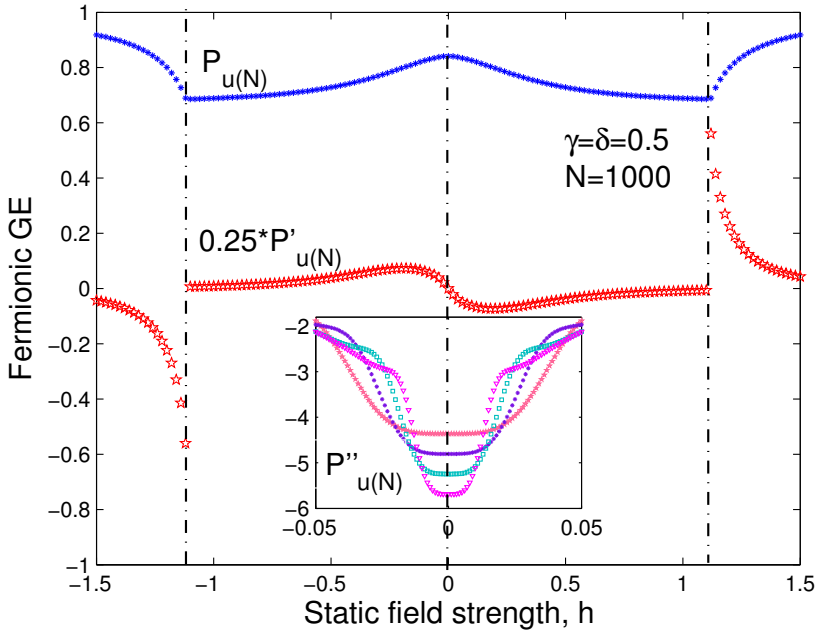

Figure 2.5: $P_{\mathfrak{u}(N)}$ as a static QPT indicator: Using $\mathfrak{u}(N)$ purity and rescaled purity derivative with respect to magnetic field strength to identify QPTs. Inset: second derivative for $N = 1000, 2000, 4000, 8000$ (top to bottom).

where the alternating universality class (4^{th} order QPT) also exists when approaching QCPs at $(g = \pm 1, \delta = 0)$ by changing δ and $(g = 0, \delta = \pm 1)$ by changing g (keeping $\gamma \neq 0$). Interestingly, in the Ising limit $\gamma = 1$, the two alternating models of Eqs. (2.1) and (2.26) may be mapped into each other through a Kramers-Wannier duality transformation as considered in [47]. Let us define the following transformation:

$$\Gamma_z^n = \sigma_x^{n-1}\sigma_x^n, \quad \Gamma_x^n\Gamma_x^{n+1} = \sigma_z^n,$$

which associates a new "dual" chain to our original spatial chain, such that sites of the original chain will be associated with links of the "dual" chain where operators Γ_α^n are placed (and vice-versa). In this way, Γ_z^n "senses" whether spins on the original adjacent sites are aligned or not, and vice-versa. Then the original (Ising-like) Hamiltonian

$$H = -\sum_i \sigma_x^i\sigma_x^{i+1} + \sum_i (h - (-1)^i\delta)\sigma_z^i$$

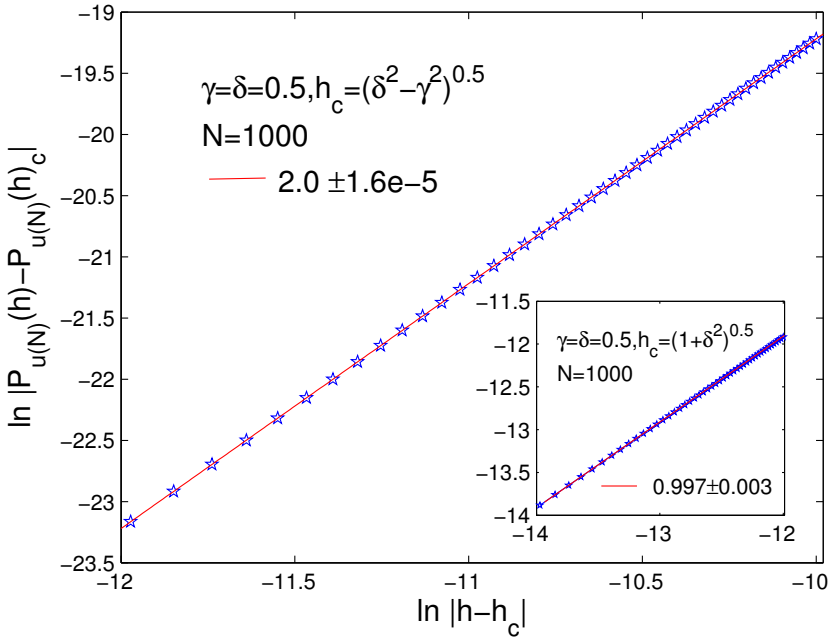

Figure 2.6: $P_{\mathfrak{u}(N)}$ as a static QPT indicator: Determination of ν for both the alternating and Ising (inset) universality class from the Taylor expansion of $\mathfrak{u}(N)$ purity near the QCPs.

is mapped into the new Hamiltonian

$$H' = -\sum_i \Gamma_z^{i+1} + \sum_i (h - (-1)^i \delta) \Gamma_x^i \Gamma_x^{i+1} \,.$$

By invoking PBCs, we obtain

$$H' = -\sum_i \Gamma_z^{i} + \sum_i (h - (-1)^i \delta) \Gamma_x^i \Gamma_x^{i+1},$$

which is exactly the Hamiltonian in Eq. (2.26) at $\gamma = 1$. Since the Hamiltonian in Eq. (2.1) and the Hamiltonian in Eq. (2.26) can be mapped into each other by duality transformation at $\gamma = 1$, all the analysis done for the Hamiltonian Eq. (2.1) is applicable for the Hamiltonian in Eq. (2.26) in the limit $\gamma = 1$.

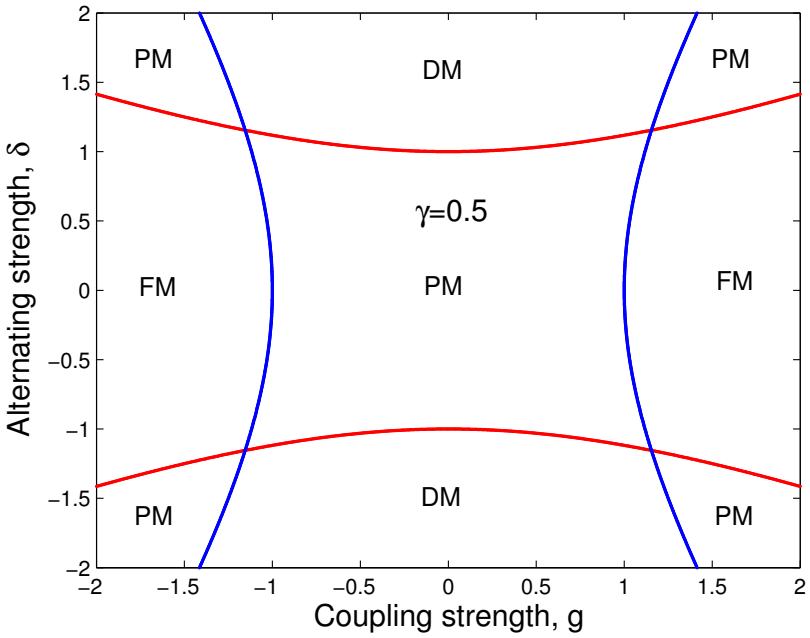

Figure 2.7: Phase diagram of Hamiltonian (2.26) for $\gamma = 0.5$.

Chapter 3

Dynamics in the Alternating XY Chain with Initial Ground State

In this Chapter, we explore the extent to which universal scaling laws persist out of equilibrium and encode information about the equilibrium phase diagram, by focusing on the case where the system is initially in its many-body ground state. In particular, we shall primarily discuss *adiabatic power-law quantum quenches*, where a single control parameter is changed in time according to:

$$\lambda(t) - \lambda_c = |\frac{t - t_c}{\tau}|^{\alpha} \text{sign}(t - t_c), \quad t \in [t_0, t_f], \tag{3.1}$$

so that a QCP is crossed at $t = t_c \equiv 0$. Here, $\alpha > 0$ is the power-law exponent, with $\alpha = 1$ corresponding to a linear quench, and $\alpha = 2$ corresponding to a quadratic quench, respectively.

3.1 Dynamical Response Indicators

Before we go on to explore dynamical scaling, it is important to identify what quantity may be used to capture the adiabaticity loss that happens when the system enters the impulse region, and cannot adiabatically follow the instantaneous ground state, according to the KZ argument. A natural

candidate is:

$$\Delta\mathcal{O}(t) \quad \equiv \quad \langle\Phi(t)|\,\mathcal{O}(t)\,|\Phi(t)\rangle - \langle\tilde{\Phi}(t)|\,\mathcal{O}(t)\,|\tilde{\Phi}(t)\rangle, \tag{3.2}$$

where we consider the "excess expectation value" of an (extensive) observable $\mathcal{O}$, which, in general, can be explicitly time-dependent, with respect to the time-evolved state $\Phi(t)$ relative to the instantaneous ground state $\tilde{\Phi}(t)$. In particular, we will consider the following observables for our system Hamiltonian Eq. (2.1) in this Chapter:

• Quasi-particle excitation density, which is especially attractive from a theory standpoint in view of its simplicity. The final excitation density $n_{\rm ex}(t_f)$ may be computed from the expectation value of the instantaneous quasi-particle number operator over $|\Phi(t)\rangle$:

$$n_{\rm ex}(t_f) = \frac{2}{N}\langle\Phi(t_f)|\sum_{k\in K_+}\left[\gamma^\dagger_{k,3}(t_f)\gamma_{k,3}(t_f) + \gamma^\dagger_{k,4}(t_f)\gamma_{k,4}(t_f)\right]|\Phi(t_f)\rangle. \tag{3.3}$$

• Excitation energy, $\mathcal{O}(t) = H(t)/N$, which has the potential advantage of being more directly accessible in experiments:

$$\Delta H(t_f) = \frac{2}{N}\langle\Phi(t_f)|\sum_{k\in K_+}\left[\epsilon_{k,3}(t_f)\gamma^\dagger_{k,3}(t_f)\gamma_{k,3}(t_f) + \epsilon_{k,4}(t_f)\gamma^\dagger_{k,4}(t_f)\gamma_{k,4}(t_f)\right]|\Phi(t_f)\rangle. \tag{3.4}$$

• Nearest-neighbor spin correlator per site along the x-direction, that is,

$$\mathcal{O} \equiv XX = \frac{1}{N}\sum_{i=1}^{N}\sigma_x^i\sigma_x^{i+1}, \tag{3.5}$$

which corresponds to the density of domain walls where the x-polarization of spins changes its orientation in the center of FM phase in the Ising limit, that is, at $\delta_f = 0, \gamma_f = 1, h_f = 0$.

• Magnetization per site, that is,

$$\mathcal{O} \equiv M_z = \frac{1}{N}\sum_{i=1}^{N}\sigma_z^i, \tag{3.6}$$

which corresponds to the density of flips in the $z-$polarization of spins in certain limit of PM phase,

that is, when $\delta_f = 0, \gamma_f = 1, h_f \mapsto \infty$ [58].

- Generalized $\mathfrak{u}(N)$ purity, that is, $\mathcal{O} \equiv P_{\mathfrak{u}(N)}$[1], with,

$$\Delta P_{\mathfrak{u}(N)}(t_f) \equiv P_{\mathfrak{u}(N)}(|\Phi(t_f)\rangle) - P_{\mathfrak{u}(N)}(|\tilde{\Phi}(t_f)\rangle_{GS}). \tag{3.7}$$

In principle, the sums in Eqs. (3.3)–Eqs. (3.7) after written in momentum space should include all the modes in K_+, as indicated. However, to the purpose of analytically investigating dynamical scaling behavior, it is useful to note that not all the allowed modes will necessarily change their state along the adiabatic quench path, effectively making no contribution to the relative expectation $\Delta\mathcal{O}(t)$. In what follows, we shall refer to the subset of modes $K_R \subseteq K_+$ whose state changes in an adiabatic quench as the *relevant modes*. We may relate the number of relevant modes, $N_R \equiv |K_R|$, to the system size and the quench rate via $N_R(N, \tau) \propto N|k_{\max}(\tau) - k_c|$, where $k_{\max}$ is the largest momentum in the relevant mode set. In a power-law adiabatic quench process, since adiabaticity breaks at a time scale $\hat{t} \sim \tau^{\alpha\nu z/(\alpha\nu z+1)}$, and the typical gap, $\hat{\Delta} \sim \hat{t}^{-1}$, an accessible excited state contributes to the excitation if and only if its minimum gap along the path, $\tilde{\Delta}_k$, matches with this typical gap, $\tilde{\Delta}_k \sim \hat{\Delta}$. In general [112], $\tilde{\Delta}_k$ scales as $\tilde{\Delta}_k \sim (k - k_c)^{z_2}$, where z_2 is a genuinely non-static exponent, whose meaning will become more clear in later discussion. Accordingly, the scaling of $k_{\max}$ can be determined by $\hat{\Delta} \sim (k_{\max} - k_c)^{z_2}$, leading to

$$k_{\max} - k_c \sim \tau^{-\alpha\nu z/[z_2(\alpha\nu z+1)]}. \tag{3.8}$$

3.2 Dynamics in the Anisotropic Limit: Standard Critical Point

Let us start with the simplest situation: Adiabatic linear quenches across an isolated standard (non-multicritical) QCP. As we discussed in Section 2.1.1.1, there are two universality classes in the plane with positive γ (similarly for negative γ): $d = 2$ Ising universality class with critical exponents

[1]Strictly speaking, $P_{\mathfrak{u}(N)}$ is not a *single* observable. However, for some special states (as discussed in Section 2.2), it can be expressed in terms of the fluctuation of the fermion number operator.

$\nu = 1, z = 1$, and alternating universality class with critical exponents $\nu = 2, z = 1$.

3.2.1 Exact Numerical Scaling Results: Kibble-Zurek Scaling

In our model, the time-evolved many-body state at time t, $|\Phi(t)\rangle = \prod_{k\in K^+} |\Phi_k(t)\rangle$, may still be expressed in the form of Eq. (2.8) for time-dependent coefficients $u_k^{(a)}(t)$, $a = 1, \ldots, 6$, computed from the solution of the Schrödinger equation. Alternatively, we can also obtain the solution of $u_k^{(a)}(t)$, $a = 1, \ldots, 6$, from the time-evolved expression of quasi-particle annihilation operators $\tilde{\gamma}_{k,3}$ and $\tilde{\gamma}_{k,4}$, where (recall Eq. (2.9))

$$\begin{cases} \tilde{\gamma}_{k,3}(t) = \tilde{v}_{k,1}(t)a_k + \tilde{v}_{k,2}(t)a_{-k}^\dagger + \tilde{v}_{k,3}(t)b_k + \tilde{v}_{k,4}(t)b_{-k}^\dagger, \\ \tilde{\gamma}_{k,4}(t) = \tilde{w}_{k,1}(t)a_k + \tilde{w}_{k,2}(t)a_{-k}^\dagger + \tilde{w}_{k,3}(t)b_k + \tilde{w}_{k,4}(t)b_{-k}^\dagger. \end{cases}$$

The coefficients $\tilde{v}_{k,n}(t)(\tilde{w}_{k,n}(t))$, $n = 1, \ldots, 4$, can be obtained from solving the Schrödinger equation:

$$i\frac{d}{dt}\begin{pmatrix} \tilde{v}_{k,1}(t) \\ \tilde{v}_{k,2}(t) \\ \tilde{v}_{k,3}(t) \\ \tilde{v}_{k,4}(t) \end{pmatrix} = \begin{pmatrix} 2(h(t)+\delta(t)) & 0 & J_k & \Gamma_k(t) \\ 0 & -2(h(t)+\delta(t)) & -\Gamma_k(t) & J_k \\ J_k^* & -\Gamma_k^*(t) & 2(h(t)-\delta(t)) & 0 \\ \Gamma_k^*(t) & J_k^* & 0 & -2(h(t)-\delta(t)) \end{pmatrix} \begin{pmatrix} \tilde{v}_{k,1}(t) \\ \tilde{v}_{k,2}(t) \\ \tilde{v}_{k,3}(t) \\ \tilde{v}_{k,4}(t) \end{pmatrix},$$

where $J_k = -2\cos(k)$, $\Gamma_k(t) = -2i\gamma(t)\sin(k)$. The coefficients $\tilde{w}_{k,n}(t)$ satisfy the same Schrödinger equation as $\tilde{v}_{k,n}(t)$, but with different initial conditions:

$$\tilde{v}_{k,n}(t_0) = v_{k,n}, \qquad \tilde{w}_{k,n}(t_0) = w_{k,n},$$

where $v_{k,n}$ and $w_{k,n}$ are coefficients in Eq. (2.9) obtained from diagonalizing the initial Hamiltonian $\hat{H}_k(t_0)$. We use 4th-order Runge-Kutta method to obtain $\tilde{v}_{k,n}(t)$ and $\tilde{w}_{k,n}(t)$, subject to the initial condition that the system lies in its ground state at $t = t_0$. Similar to the relation of the ground state coefficients in the static case, that is, $\gamma_{k,3}|\Psi_k\rangle = 0, \gamma_{k,4}|\Psi_k\rangle = 0$, we now have $\tilde{\gamma}_{k,3}(t)|\Psi_k(t)\rangle =$

$0, \tilde{\gamma}_{k,4}(t)|\Psi_k(t)\rangle = 0$, which leads to:

$$\begin{cases} u_k^{(1)}(t) = \tilde{v}_{k,3}(t)\tilde{w}_{k,1}(t) - \tilde{v}_{k,1}(t)\tilde{w}_{k,3}(t), & u_k^{(2)}(t) = \tilde{v}_{k,2}(t)\tilde{w}_{k,3}(t) - \tilde{v}_{k,3}(t)\tilde{w}_{k,2}(t), \\ u_k^{(3)}(t) = \tilde{v}_{k,1}(t)\tilde{w}_{k,4}(t) - \tilde{v}_{k,4}(t)\tilde{w}_{k,1}(t), & u_k^{(4)}(t) = \tilde{v}_{k,4}(t)\tilde{w}_{k,3}(t) - \tilde{v}_{k,3}(t)\tilde{w}_{k,4}(t), \\ u_k^{(5)}(t) = \tilde{v}_{k,2}(t)\tilde{w}_{k,1}(t) - \tilde{v}_{k,1}(t)\tilde{w}_{k,2}(t), & u_k^{(6)}(t) = \tilde{v}_{k,4}(t)\tilde{w}_{k,2}(t) - \tilde{v}_{k,2}(t)\tilde{w}_{k,4}(t). \end{cases}$$

Recall that a main assumption in the KZ argument is the existence of adiabatic and impulse region. Thus, in order to observe KZS, it is essential to guarantee that the system will go through both adiabatic and impulse regions, which in turn depends on the range of τ we choose. Suppose that $\tau \in [\tau_{\min}, \tau_{\max}]$ is the appropriate range of τ to exhibit KZS. Then $\tau_{\min}$ is associated with the existence of an adiabatic region away from criticality, while $\tau_{\max}$ is associated with the existence of impulse region close to QCP for a *finite* system. Thus, from standard adiabaticity requirements away from criticality [64], $\tau_{\min} \sim 1/[\min_{t\in[t_0,t_f]}\mathrm{Gap}(H(t))]^2$. On the other hand, if τ is arbitrarily large, a finite system never enters the impulsive regime, if the size-dependent contribution to the gap dominates over the control-dependent one. From the scaling assumption in Eq. (1.3), we infer that the gap closes polynomially as N^{-z}. Thus, $N^{-z} \sim (\hat{t}/\tau)^{\nu z}$, which leads to the following upper bound of τ: $\tau_{\max} \sim N^{(\nu z+1)/\nu}$. Two remarks are in order: First, in the thermodynamic limit, the adiabaticity condition is broken close to QCP *irrespective* of the quench rate. Consequently, there is no upper limit of τ range in the thermodynamic limit. Second, in a generic power-law quench, the upper limit $\tau_{\max}$ would change accordingly with the change of $\hat{t}_\alpha$, that is, $\tau_{\max} \sim N^{(\alpha\nu z+1)/\nu}$.

Provided that $\tau \in [\tau_{\min}, \tau_{\max}]$ in a finite system, KZS is found to hold irrespective of the details of the QCP and the initial (final) quantum phase, in particular for both 2nd and higher-order QPTs, and independent of the path direction:

$$n_{\mathrm{ex}}^{\mathrm{Ising}}(t_f) \sim \tau^{-1/2}, \qquad n_{\mathrm{ex}}^{\mathrm{Alternating}}(t_f) \sim \tau^{-2/3},$$

as illustrated in Fig. 3.1.

While the excitation density exhibits KZS, one might wonder: Is this the only quantity that shows KZS? How would KZS be generalized to other physical observables? Remarkably, our numerical results indicate that scaling behavior holds *throughout the quench process* (not only at $t = t_f$) for a

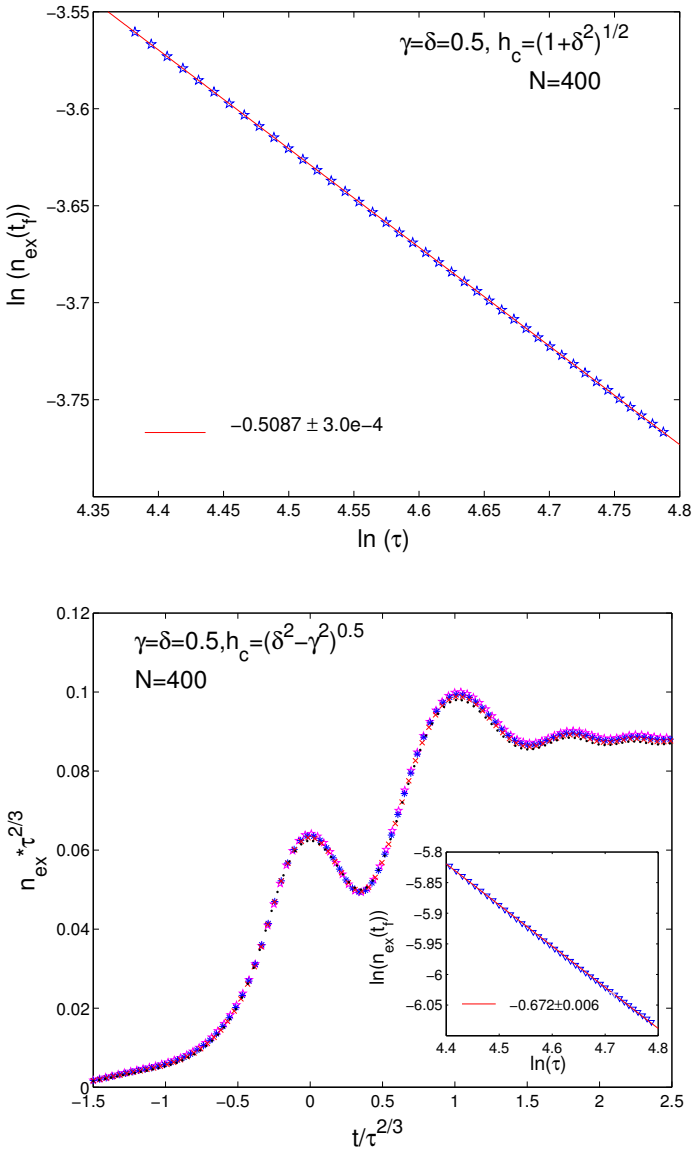

Figure 3.1: Dynamical scaling of the excitation density of quenching the magnetic field strength h by fixing $\delta = \gamma = 0.5$. Top panel: log-log plot for Ising universality class. Bottom panel: alternating universality class, with log-log scaling plot in the inset.

large class of physical observables in the form of Eq. (3.2) [56]. That is,

$$\Delta\mathcal{O}(t) \quad = \quad \tau^{-(\nu+\beta)/(\nu z+1)} F_{\mathcal{O}}\Big(\frac{t-t_c}{\hat{t}}\Big)\,, \tag{3.9}$$

where β is a scaling exponent determined by the physical dimension of $\mathcal{O}$ and F is an observable-dependent scaling function. For instance, under a quench of the magnetic field strength, h, M_z defined in Eq. (3.6) obeys a dynamical scaling law of the form $\Delta M_z(t) = \tau^{(-\nu-\nu z+1)/(\nu z+1)} G((t-t_c)/\hat{t})$, whereas XX defined in Eq. (3.5) obeys a dynamical scaling law $\Delta XX(t) = \tau^{-\nu/(\nu z+1)} W((t-t_c)/\hat{t})$, for appropriate scaling functions G and W, respectively. The exact numerical scaling results of $\Delta XX(t)$ is shown in the main figure of Fig. 3.2.

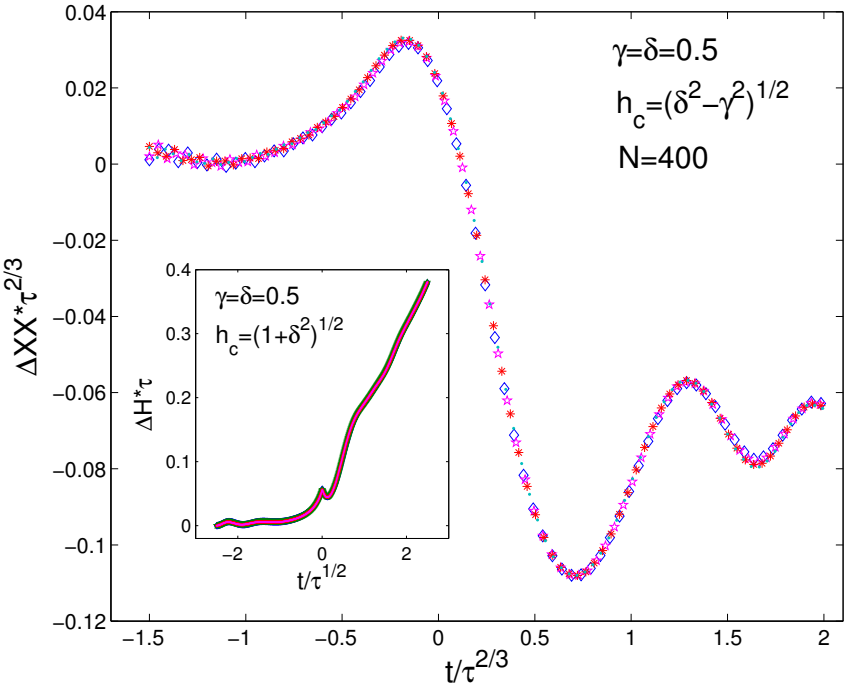

Figure 3.2: Dynamical scaling under a magnetic field quench. Main panel: excess nearest-neighbor spin correlation per particle, ΔXX, vs rescaled time for the alternating universality class from numerical integration of the Schrödinger equation. Inset: excess energy per particle, ΔH, vs rescaled time for the Ising universality class from first-order AR.

3.2.2 Scaling Prediction from First-Order Adiabatic Renormalization

The fact that the system becomes gapless at a *single* instant t_c suggests to seek an explanation of the above scaling results based on the fact that $\dot{\lambda}(t) = 1/\tau$ is a small parameter, motivating us to look for a perturbative approach. While a similar strategy has been implemented in [62], we aim to

provide a firm theoretical foundation and further highlighting important assumptions. By a suitable parametrization ($t_c = 0$), our time-dependent Hamiltonian may be written as:

$$H(t) = H_c + [\lambda(t) - \lambda_c]H_1 = H_c + t/\tau H_1,$$

with H_c quantum-critical in the thermodynamic limit. Let $\{E_m(t)\}$ and $\{|\psi_m(t)\rangle\}$ denote the snapshot eigenvalues and (orthonormal) eigenvectors of $H(t)$, where $|\psi_0(t)\rangle \equiv |\psi_{GS}(t)\rangle$ and let us assume that: (i) no level crossing occurs during the evolution; (ii) the derivatives of all the spectral projectors $\{|\psi_m(t)\rangle\langle\psi_m(t)|\}$ are sufficiently smooth. The (normalized) time-evolved state reads

$$|\psi(t)\rangle = c_0(t)|\psi_0(t)\rangle + \sum_{m\neq 0} c_m(t)|\psi_m(t)\rangle,$$

for coefficients to be determined. Since for a truly adiabatic evolution no excitation is induced in spite of the fact that the eigenstates of $H(t)$ evolve in time, appropriately subtracting (following Berry, "renormalizing") the adiabatic contribution, which is termed "adiabatic renormalization" (AR), is essential for quantifying the leading non-adiabatic correction. This is achieved in two steps [64]: (i) Effect a canonical transformation to a "comoving frame", where in the zeroth-order adiabatic limit $\tau \to \infty$ the comoving state vector $|\tilde{\psi}(t)\rangle = \tilde{U}(t;t_0)|\psi(t_0)\rangle$ is frozen up to a phase factor, that is, $|\tilde{\psi}(t)\rangle = e^{-i\Gamma_0(t)}|\psi_0(t_0)\rangle$, where $\Gamma_0(t)$ includes in general both the Berry phase and the dynamical phase; (ii) Evaluate the first-order correction to the comoving-frame propagator via Dyson series expansion. Transforming back to the physical frame, $c_m(t) = \langle\psi_m(t_0)|\tilde{U}(t;t_0)|\psi_0(t_0)\rangle$, to the first-order in $\dot{\lambda}$ we finally obtain (in units $\hbar = 1$), $c_0^{(1)}(t) = e^{-i\Gamma_0(t)} + O(\dot{\lambda}^2)$, and

$$\begin{cases} c_m^{(1)}(t) = e^{-i\Gamma_m(t)} \int_{t_0}^{t} dt' \dot{\lambda}(t') \frac{\langle\psi_m(t')|H_1|\psi_0(t')\rangle}{E_m(t')-E_0(t')} e^{i\int_{t_0}^{t'} ds \Delta_m(s)}, \\ \Delta_m(t) = E_m(t) - E_0(t). \end{cases} \tag{3.10}$$

Knowledge of the time-dependent state enables arbitrary physical quantities of interest to be computed, in particular the total time-dependent excitation probability $\mathbb{P}_{\rm ex}(t) = \sum_{m\neq 0} |c_m(t)|^2$. Given Eq. (3.10), the latter formally recovers the expression written in [62], which captures the contribution to the density of excitations from states directly connected to $|\psi_0(t)\rangle$ via H_1. Notice

that, generally speaking, the total time-dependent excitation (computed below as $N_{\rm ex}(t)$) and the total excitation probability $\mathbb{P}_{\rm ex}(t)$ are not the same: Suppose that the time-evolved state is expressed in the snapshot eigenstate basis as $\Phi(t) = \sum_m c_m(t)|\psi_m(t)\rangle$, then,

$$\begin{aligned} N_{\rm ex}(t) &= \langle\Phi(t)|\sum_{k\in K}\left(\gamma^\dagger_{k,3}\gamma_{k,3}+\gamma^\dagger_{k,4}\gamma_{k,4}\right)|\Phi(t)\rangle \\ &= \sum_m |c_n(t)|^2\langle\psi_m(t)|\sum_{k\in K}\left(\gamma^\dagger_{k,3}\gamma_{k,3}+\gamma^\dagger_{k,4}\gamma_{k,4}\right)|\psi_m(t)\rangle \\ &= \sum_{m\neq 0} |c_m(t)|^2\langle\psi_m(t)|\sum_{k\in K}\left(\gamma^\dagger_{k,3}\gamma_{k,3}+\gamma^\dagger_{k,4}\gamma_{k,4}\right)|\psi_m(t)\rangle, \end{aligned} \tag{3.11}$$

where the relation that $|\psi_m(t)\rangle$ is also the eigenstate of the quasi-particle operator was used in the second line of Eq. (3.11), and the fact that ground state has no quasi-particle excitation was used in the third line. Thus, $\mathbb{P}_{\rm ex}(t) = N_{\rm ex}(t)$ if and only if $\langle\psi_m(t)|\sum_{k\in K}\left(\gamma^\dagger_{k,3}\gamma_{k,3}+\gamma^\dagger_{k,4}\gamma_{k,4}\right)|\psi_m(t)\rangle = 1$, which is not true in general. However, in first-order AR, since one-body perturbations H_1 are considered in the present analysis, the first-order excitation probability, $\mathbb{P}^{(1)}_{\rm ex}(t) = \sum_{m\neq 0}|c^{(1)}_m(t)|^2$, coincides with the single-mode quasiparticle contribution to the total time-dependent excitation (the case where both $\gamma^\dagger_{k,3}\gamma_{k,3}$ and $\gamma^\dagger_{k,4}\gamma_{k,4}$ are occupied can be ignored in our adiabatic quench process).

Dynamical scaling emerges once the above result is supplemented by scaling assumptions on three fundamental dynamical variables: the time-dependent excitation energy above the ground state; the time-dependent matrix elements of the perturbation; and the density of excited states, $\rho(E)$, at the energy scale $\hat{t}^{-1}$ that characterizes adiabaticity-breaking, which allows to change discrete sums over excited states to integrals. That is, close to the QCP we assume that:

$$\begin{cases} E_m(t) - E_0(t) = \delta\lambda(t)^{\nu z} f_m(\Delta_m(t_c)/\delta\lambda(t)^{\nu z}), \\ \langle\psi_m(t)|H_1|\psi_0(t)\rangle = \delta\lambda(t)^{\nu z-1} g_m(\Delta_m(t_c)/\delta\lambda(t)^{\nu z}), \\ \rho(E) \sim E^{d/z-1}, \end{cases} \tag{3.12}$$

where the scaling functions f_m, g_m satisfy the following condiitons: i) f_m (g_m) is constant when $x \to 0$; ii) f_m (g_m) $\propto x$ when $x \to \infty$. Having the scaling assumptions at hand, integration over excited states is performed by moving to dimensionless variables $\zeta = (t-t_c)/\hat{t} = (t-t_c)\tau^{-\nu z/(\nu z+1)}$ and $\eta = \Delta_m(t_c)\hat{t} = \Delta_m(t_c)\tau^{\nu z/(\nu z+1)}$. Since at the QCP the integrand in Eq. (3.10) develops a simple pole,

while the phase $e^{i\int_{t_0}^{t'} ds\Delta_m(s)}$ becomes stationary, contributions away from the QCP may be neglected, allowing the desired scaling factor to be isolated, up to a regular function depending only on ζ. Thus, the scaling of the diagonal observables with respect to the eigenstate basis such as excitation density and the residual energy are directly determined as $n_{\rm ex}(\zeta) = \tau^{-d\nu/(\nu z+1)}\Xi(\zeta)$, $\Delta H(\zeta) = \tau^{-(d+z)\nu/(\nu z+1)}\Upsilon(\zeta)$, see the inset of Fig. 3.2 for numerical results. For a *generic observable*, if the additional scaling condition

$$\langle\psi_0(t)|\,\mathcal{O}\,|\psi_m(t)\rangle = \delta\lambda(t)^{\beta} q_m(\Delta_m(t_c)/\delta\lambda(t)^{\nu z}), \tag{3.13}$$

holds for all the excitations m involved in the process for an appropriate scaling function q_m, then $\Delta\mathcal{O} \sim \tau^{-(\nu d+\beta)/(\nu z+1)}$ – consistent with Eq. (3.9).

Two remarks are in order: First, notice that the derivation naturally extends to a generic non-linear *power-law* quench. Provided that the typical time scale for adiabaticity breaking is redefined as $\hat{t}_\alpha \sim \tau^{\alpha\nu z/(1+\alpha\nu z)}$, the same scaling assumptions in Eqs. (3.12)-(3.13) lead to dynamical scaling behavior of the form $n_{\rm ex} \sim \tau^{-\alpha d\nu/(\alpha\nu z+1)}$, and $\Delta\mathcal{O} \sim \tau^{-\alpha(d\nu+\beta)/(\alpha\nu z+1)}$, throughout the whole time evolution. Second, the perturbative derivation as presented strictly applies to quenches across an isolated QCP which is *not* multi-critical. The application of the perturbative approach to a MCP will be discussed in Section 3.4.3.

3.2.3 Dynamics of Generalized Entanglement

As we discussed in Section 2.2.3, Fermionic GE has been proved useful in detecting QPTs and identifying the critical exponents for static cases in both the $d = 2$ Ising universality class and the alternating universality class. It is interesting to ask whether fermionic GE shows any scaling behavior for quenches across QCPs which belongs to these two universality classes. Notice that from the definition in Eq. (2.22), $P_{\mathfrak{u}(N)}$ is essentially a sum of square expectation values of the fermion number operators, thus an extensive quantity which satisfies the necessary condition for an observable to obey dynamical scaling. Therefore, besides the observables discussed in Section 3.2.1, we investigated the scaling behavior of the $\mathfrak{u}(N)$ purity relative to the instantaneous ground state

defined in Eq. (3.7). We find that:

$$\Delta P_{\mathrm{u}(N)}(t) = \tau_Q^{-\nu/(\nu z+1)} G\Big(\frac{t-t_c}{\hat{t}}\Big)\,,$$

for an appropriate scaling function G. Interestingly, $\Delta P_{\mathrm{u}(N)}(t)$ has the *same dynamical scaling exponent as* n_{ex} in both universality classes we investigated. Physically, this is related to the fact that $P_{\mathrm{u}(N)}(t)$ is the fluctuation of the fermion number operator, thus its dimension $\beta = 0$ in Eq. (3.9). Exact numerical results are shown in Fig. 3.3, where $\Delta P_{\mathrm{u}(N)}(t)$ shows KZS throughout the whole time evolution for QPT belonging to the Ising universality class, while $\Delta P_{\mathrm{u}(N)}(t)$ obeys KZS close to the QPT belonging to the alternating universality class. This difference is related to the fact that along the path we choose to approach the QCP of the alternating universality class, other QCPs belonging to the Ising universality class are nearby, thus cross-over to a different scaling behavior of $\Delta P_{\mathrm{u}(N)}(t)$ is expected. Therefore, dynamical scaling of $\Delta P_{\mathrm{u}(N)}(t)$ only persists sufficiently close to the QCP of alternating universality class. Instead, along the path we approach the QCP of Ising universality class, no QCPs from other universality class is encountered, allowing for a more robust behavior.

3.3 Dynamics in the Isotropic Limit

So far, we showed how KZS successfully predicts the dynamical scaling for quenches across an *isolated* (non-multicritical) QCP separating two gapped phases in our model Hamiltonian (see also the discussion in other different models and/or quench schemes in Ref. [58, 62, 63, 65, 68, 66, 67, 69, 70]). However, non-KZS has been reported in certain low-dimensional clean systems, whereby non-zero excitation persists (unlike KZS) for $\tau \to \infty$ in the thermodynamic limit [63], and in the case of *disordered* quantum systems, where marked deviations from power-law behavior may be witnessed [71, 72]. Likewise, critical dynamics in the presence of *non-isolated* QCPs reveals a rich landscape. In particular, the need to modify the KZS by replacing the spatial dimension d with the "co-dimension" m of the relevant critical (gapless) surface has emerged through a study of the 2D Kitaev model [75]. Different non-KZS involving gapless phase has also been reported for quenches

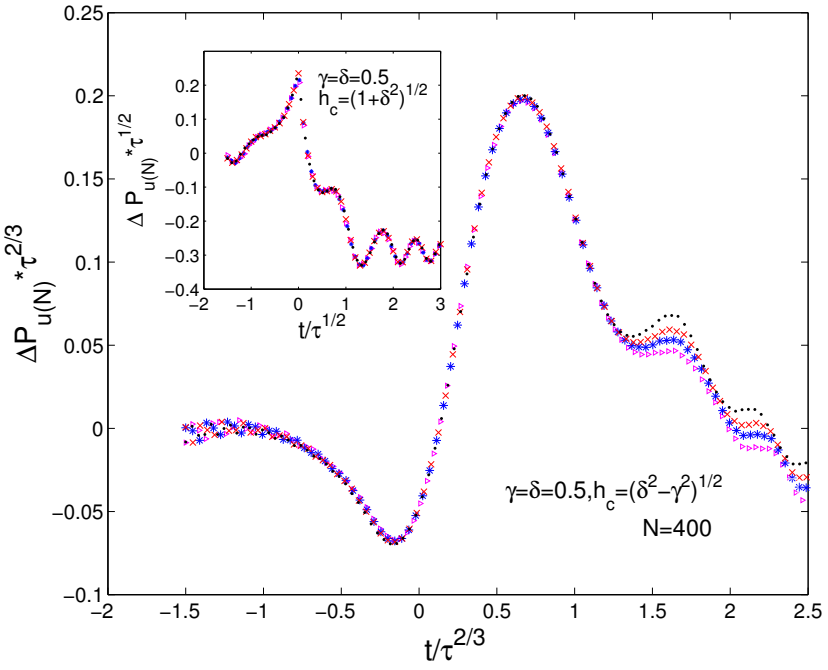

Figure 3.3: Dynamical scaling of $P_{\mathrm{u}(N)}$ for the alternating (main panel) and the Ising (inset panel) universality class.

which originate within an extended quantum critical region [74], and for quenches along a gapless critical line [76].

As we discussed in Chapter 2, in the isotropic limit (the $\gamma = 0$ plane), our phase diagram contains a gapless superfluid phase, for which the standard KZS argument need not be applicable according to the discussion in Refs. [75, 74, 76]. Thus, a main purpose of this Section is to develop an understanding of dynamical scaling for generic (power-law) quenches involving critical regions. To achieve this goal two new notions will be introduced, which are both *path-dependent*: one is the concept of a *dominant critical point* to establish scaling along a critical path, and the other a *mechanism of cancellation* of excitations. Our analysis indicates that details on how different modes of excitation are accessed during the quench process are crucial. We shall mainly consider two different scenarios below. For added clarity, we reproduce the phase diagram for $\gamma = 0$ again with marked points in Fig. 3.4.

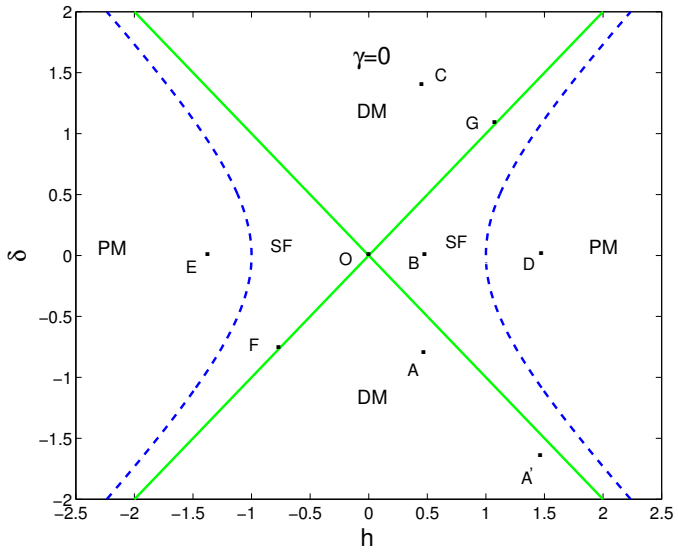

Figure 3.4: Phase diagram in the isotropic limit $\gamma = 0$ with marked points for the discussion on different quench paths.

3.3.1 Quenching along Paths with a Finite Number of Critical Modes

A first situation which is beyond the standard KZS discussed thus far arises in quenches that force the system along a critical line, yet, as we shall explain, are "dominated" by a finite number of participating excitations. *Formally*, this makes it possible to obtain the non-equilibrium exponent for $n_{\rm ex}$ through application of the KZS, provided that care is taken in defining the static exponents through a limiting path-dependent process where, along the quench of interest, a *simultaneous* expansion with respect to both the control parameter *and* the relevant critical mode(s) is taken. Consider a quenching scheme where both h and δ are changed according to t/τ while $\gamma = 0$ (path $F \to O \to G$ in Fig. 3.4). While Eq. (2.6) shows that the critical mode $k_c = \pi/2$ throughout the process ($\Delta_{\pi/2}(t) = 0$, for all $t \in [t_0, t_f]$ as $N \to \infty$), numerical data indicate that excitation sets in *only* when the point O is passed, see Fig. 3.5. For point O, a simultaneous expansion of $\Delta_{\pi/2}(0, h, h)$ around both the control parameter $h(\equiv \delta)$ and $k = \pi/2$ shows that:

$$\Delta_k(0, h, h) = 4(k - \pi/2) + O[k - \pi/2]^3 - 4h + O[h]^2,$$

implying that the static critical exponents at O are $z = 1, \nu = 1$. Similarly, a simultaneous expansion of $\Delta_{\pi/2}(0, h, h)$ around all other critical points along this line, *e.g.* around $(h, \delta) = (1, 1)$, shows:

$$\Delta_k(0, h, h) = 2(k - \pi/2)^2 + O[k - \pi/2]^3 - 2((k - \pi/2)^2 + O[k - \pi/2]^3)(h - 1) + O[h - 1]^2,$$

which yields $z = 2, \nu = 1/2$, different from what obtained at point O. Indeed, the non-equilibrium exponent is solely determined by the static exponents of QCP O along the chosen path, $n_{\rm ex} \sim \tau^{-\nu/(\nu z+1)} = \tau^{-1/2}$. We term a QCP which belongs to a different universality class than all other critical points along a critical line and sets the non-equilibrium scaling a *dominant critical point for that line* [1].

Physically, although the gap $\Delta_{\pi/2}$ closes along the critical line in the thermodynamic limit, a level crossing which brings all bands together only occurs at O – still allowing the time-evolved state to adiabatically follow the snapshot ground state until then. The following independent confirmations may be invoked in support of the above argument. First, consider the anisotropic quench process analyzed in [76], whereby $\gamma(t)$ is changed linearly along the critical line $h^2 = \delta^2 + 1$. By Taylor-expanding Δ_k in Eq. (2.6) around $k = 0, \gamma = 0$ reveals that $\nu = 1, z = 2$ at the dominant QCP $(\gamma = 0, h, \delta)$, whereas $\nu = 1, z = 1$ for $\gamma \neq 0$ along the line. Accordingly, $n_{\rm ex} \sim \tau^{-1/3}$. Plots of the rescaled excitation density $(n_{\rm ex}\tau^{1/3})$ vs the rescaled time $(t/\tau^{2/3})$ collapses onto one another for different τ within the appropriate range, in complete analogy with Fig. 3.5. While our scaling results coincides with the result obtained in [76], the underlying physical explanation is different: In Ref. [76], the $\tau^{-1/3}$ scaling is obtained from the critical exponent z of the non-dominant one, that is $z = 1$ in Eq. (17) of Ref. [76]. However, our simulation clearly shows that the excitation sets in *only when the dominant QCP is passed*, which implies that the critical exponents of the dominant QCP should determine the scaling results. Second, loss of adiabaticity at a single point can also explain the scaling behavior observed for a AFM-to-FM quench (or a gapless phase-to-FM quench) in the XXZ model [74], whereby the control path involves the gapless critical region $-1 \leq \Delta \leq 1$ and the dominant critical point $\Delta = 1$ belongs to a different universality class. Lastly, the concept of a dominant QCP remains useful for a power-law quench, which leads to the scaling behavior

[1] Note that the point O is multi-critical. However, quenches across a MCP need *not* satisfy KZS, see further discussion in Section 3.4 and Ref. [81].

$n_{ex} \sim \tau^{-\alpha d\nu/(\alpha\nu z+1)}$, with ν and z being the critical exponents of the above dominant QCP.

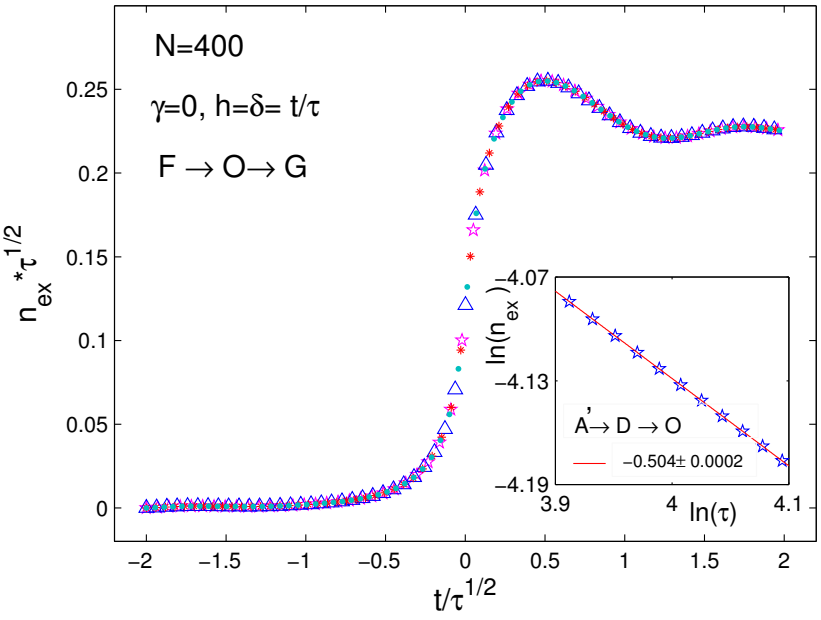

Figure 3.5: Main panel: dynamical scaling of the excitation density for a simultaneous linear quench of h and δ along the gapless critical line $F \to O \to G$. Inset: log-log plot of the final excitation density vs τ along the path $A' \to D \to O$.

3.3.2 Quenching along Paths with an Infinite Number of Critical Modes

More complex scenarios emerge when uncountably many modes of excitations can be important and compete during the quench. We contrast two representative situations where the Lifshitz QPT is involved: (I) Magnetic quenches along the horizontal path $D \to O \to E$ (PM $\to$ SF $\to$ PM); (II) Alternating quenches along the vertical path $A \to B \to C$ (DM $\to$ SF $\to$ DM), as marked in Fig. 3.4. In the isotropic limit, since, as we discussed, the Hamiltonian of Eq. (2.1) has a continuous $U(1)$-symmetry, the total z-magnetization is conserved, $[M_z, H] = 0$. Thus, in both cases, the allowed excitation must comply with a non-trivial dynamical constraint. Along the path $D \to O \to E$, suppose we rewrite the Hamiltonian $H(t)$ as $H(t) = H_0 + h(t)M_z$, where $[H_0, M_z] = 0$ is satisfied. Then, the initial ground state $\Phi(t_0)$ is an eigenstate of both H_0 and M_z, which is always true during the entire time-evolution since both H_0 and M_z are time-independent. Thus, $\Phi(t_0)$ is always

an eigenstate of $H(t)$ along the path $D \to O \to E$, which forces the final state to be the same as the initial ground state up to a global phase factor, leading to $n_{\rm ex}(t_f) \sim \tau^0$. Although for a magnetic quench this may be viewed as a consequence of the fact that the dynamics simply acts as a "relabeling" of the snapshot eigenstates, the same scaling holds for *any* quench which begins or ends in the gapless phase – for instance, a δ-quench along the path $A \to B$. Because these quenches take the system through a critical line in momentum space, $d - m = 1$ (as opposed to $d - m = 0$ for an isolated QCP), and the observed scaling is consistent with the recent prediction $n_{\rm ex}(t_f) \sim \tau^{-m\nu/(\nu z+1)}$ [75].

One may naively expect the same scaling to hold for path (II), which also connects two gapped (DM) phases, albeit different than in (I). Unlike in the standard KZS, however, details about the initial and final phases as well as the time-dependent excitation pattern become important. Specifically, along path (II), we find $n_{\rm ex}(t_f) \sim \tau^{-1/2}$. An explanation may be obtained by exploiting the fact that due to the $U(1)$-symmetry, the fermion number is conserved. This allows the reduced 4×4 matrix $\hat{H}_k$ in Eq. (2.4) to be decoupled into two 2×2 matrices by interchanging the order of the basis vectors a_{-k} and $b_k^\dagger$. Thus, $H'_{\pm k} = W_{\pm k}^\dagger \hat{H}'_{\pm k} W_{\pm k}$, where $W_k^\dagger = (a_k^\dagger, b_k^\dagger)$, $W_{-k}^\dagger = (a_{-k}, b_{-k})$, and

$$\hat{H}'_{\pm k} = \pm 2h \mathbb{I}_2 + \begin{pmatrix} \pm 2\delta & \mp 2\cos k \\ \mp 2\cos k & \mp 2\delta \end{pmatrix}. \tag{3.14}$$

For such a two-level system, the asymptotic excitation probability may be computed from the exact Landau-Zener (LZ) transition formula [82], $P = e^{-2\pi\omega^2/|d\Delta(t)/dt}$, with ω and $\Delta(t)$ being the off-diagonal and diagonal element of the driven two-level system respectively, yielding $p_k = e^{-2\pi\tau\cos^2 k}$. Upon integrating over all modes, we find

$$n_{\rm ex}(t_f) = \frac{1}{\pi}\int_{-\pi/2}^{\pi/2} dk\, p_k \sim \tau^{-1/2}. \tag{3.15}$$

Note that because p_k is independent on h, the result in Eq. (3.15) may be interpreted as implying that traversing the gapless phase produces the *same excitation density* as crossing the single QCP O by translating path (II) at $h = 0$, which determines the non-equilibrium exponent.

Physical insight into what may be responsible for the different behavior observed in the above two

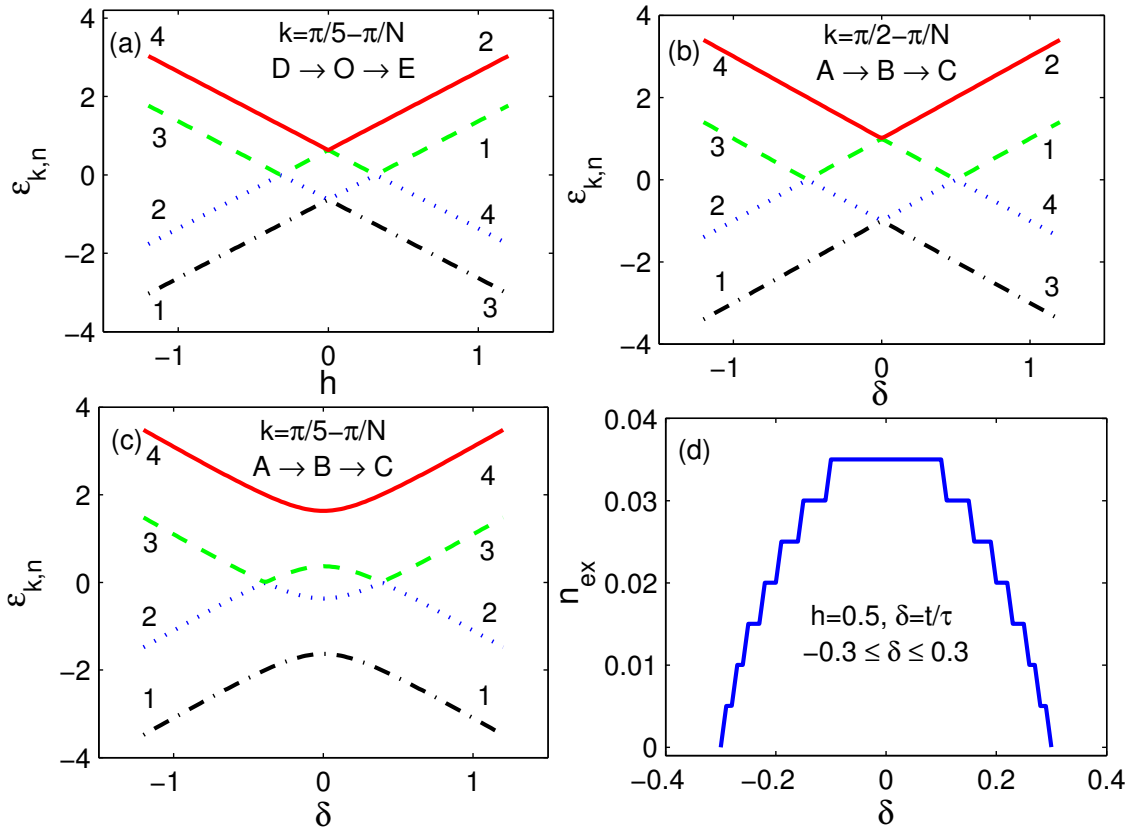

Figure 3.6: Panels (a–c): band structure for different momentum modes k vs quench parameter (*i.e.*, h or δ). Band ordering is determined by band index $n = 1, 2, 3, 4$ at initial time $t = t_{\rm in}$, whereas dash-dotted (black) $\leq$ dotted (blue) $\leq$ dashed (green) $\leq$ solid (red) at a generic time t along the control path. Panel (d): final excitation density, $n_{\rm ex}(t_{\rm fin})$, vs δ for a quench of the alternation strength δ at fixed $h = 0.5$ within the critical region. For all cases, $N = 400$.

quenches can be gained by examining the excitation spectrum along the two paths. Notice that, once the energy eigenvalues are specified at the initial time, ($\epsilon_{k,1}(t_{\rm in}) \leq \epsilon_{k,2}(t_{\rm in}) \leq \epsilon_{k,3}(t_{\rm in}) \leq \epsilon_{k,4}(t_{\rm in})$ in our case), the same relative ordering need not hold at the final time if a level crossing is encountered during the quench – see Fig. 3.6(a),(b). In the critical region, a pair of modes (k, n) and (k, n') undergoes a level crossing if $h^2 - \delta^2 = \cos^2 k$. If the number of such level crossings for fixed n, n' is *even*, the net contribution to the final excitation from momentum k is zero, since the final occupied bands are the same as the initial ones – see Fig. 3.6(c). No cancellation is in place if either an odd

number of level crossings from the same pair or if different pairs (n, n') are involved. The latter situation is realized for all k along path (I) (h-quench, Fig. 3.6(a)) and also for the path $A \to B$ (δ-quench). For a δ-quench along path (II), the net excitation from the gapless phase turns out to be completely canceled (as seen in Fig. 3.6(d), where the quench starts and ends symmetrically within the gapless phase). This only leaves the two boundary critical lines $h = \pm\delta$ as contributing to the excitation, thus *a finite* set of critical modes (a single one in fact, $k_c = \pi/2$, see Fig. 3.6(b)). Interestingly, a similar *cancellation mechanism* was verified for repeated quenches across an isolated QCP [67]. While additional analysis is beyond our scope, we suggest that an even participation from the same (pair of) snapshot excitations may be at the root of this cancellation in both scenarios. Here, we further test this conjecture by examining the path $A' \to D \to O$, for which an effective two-level LZ mapping is no longer possible. Unlike $A \to B \to C$, two intermediate phases are now crossed, and the initial and final phase differ from one another, yet analysis of $\epsilon_{k,n}(t)$ reveals that the two paths are equivalent in terms of participation of critical modes. Numerical results confirm that $n_{\rm ex}(t_f) \sim \tau^{-1/2}$, see inset panel of Fig. 3.5.

3.4 Multi-critical Quantum Quenches

Besides the non-KZS discussed in Section 3.3 for quenches involving critical regions, non-KZS may also occur for the apparently simple situation of a quench across a single quantum *multicritical point* (MCP) in disorder-free spin chains [79, 80, 81]. Here, we show how multicritical quantum quenches dramatically exemplify the dependence of non-equilibrium scaling upon the control path anticipated in Section 3.3, and demonstrate that *anomalous non-ergodic scaling* may emerge in the thermodynamic limit. While a non-KZS $n_{\rm ex}(t_f) \sim \tau^{-1/6}$ was previously reported [79], and an explanation given in terms of an "effective dynamical critical exponent" $z_2 = 3$, the meaning of such exponent relied on the applicability of a LZ-treatment, preventing general insight to be gained. We argue that the failure of KZS is physically rooted in the shift of the center of the impulse region relative to the static picture (see bottom panel in Fig. 1.1), and that z_2 is determined by the scaling of a path-dependent *minimum gap which need not coincide with the critical gap*. Furthermore, we argue that such a dynamical shift may also cause the contribution from *intermediate non-critical*

energy states to dominate the scaling of the excitation density, via an "effective dimensionality exponent" $d_2 \neq 0$. We will show that the latter leads to the emergence of new scaling behavior $n_{\rm ex}(t_f) \sim \tau^{-3/4}$. A unified understanding is obtained by extending the perturbative AR-approach introduced in Section 3.2.2.

3.4.1 Exact Numerical Scaling Results: Anomalous Scaling Behavior

We mainly choose four representative paths to study the dynamical scaling of quenches across MCPs `A` and `B`, which are marked by path $1, 2, 3, 4$ in Fig. 2.4. As showed in the table on page 21, there are two universality classes involved, one is the Lifshitz universality class ($\nu = 1/2, z = 2$) for paths 3 and 4, the other one is a new universality class ($\nu = 1, z = 2$) for paths 1 and 2. So the first question we would like to understand is, will a MCP always introduce anomalous dynamical scaling? In order to quantify the amount of excitation at a generic instant t, again, we monitor both: the excitation density, $n_{\rm ex}$, and the residual energy, ΔH. For a linear quench along either path 1 or 2 (Fig. 3.7 for path 2), we find that $n_{\rm ex}(t) \sim \tau^{-\nu/(\nu z+1)} = \tau^{-1/3}$ and $\Delta H(t) \sim \tau^{-\nu(1+z)/(\nu z+1)} = \tau^{-1}$, which is consistent with KZS [57]. For paths 3 and 4, however (Fig. 3.8 for path 3), we find that $n_{\rm ex}(t) \sim \tau^{-1/6}$ and $\Delta H(t) \sim \tau^{-2/3}$, which is non-KZS (in Ref. [79], the $\tau^{-1/6}$ scaling was pointed out for an equivalent quench scheme across MCP `A`). Similar anomalous exponents are found for non-linear quenches along paths 3 or 4, *e.g.*, $n_{\rm ex}(t) \sim \tau^{-2/9}$ for $\alpha = 2$ (bottom inset panel in Fig. 3.8).

The above results clearly show that, for quenches across a MCP, whether KZS is obeyed depends sensitively on which control path is chosen. A closer inspection reveals the following important differences: (i) Paths $1, 2$ start and end in essentially the same (FM) phase, correspondingly the excitation spectrum is invariant under a transformation $\lambda \mapsto -\lambda$ of the control parameters. Paths $3, 4$ do not exhibit this symmetry; (ii) Along paths $3, 4$, the MCPs `A` and `B` belong to the Lifshitz universality class ($\nu = 1/2$), although all paths share $z = 2$. It is then natural to ask which of these differences may play a role in determining the anomalous dynamical scaling behavior. To answer this question, we introduce another "V-shaped" path across MCP `A` (path 5), which starts and ends in the PM phase but, in each of the two segments, crosses the MCP `A` with Lifshitz exponents (shown in the inset panel of Fig. 3.9). Surprisingly, the observed scaling is $n_{\rm ex}(t) \sim \tau^{-3/4}$ (main panel of

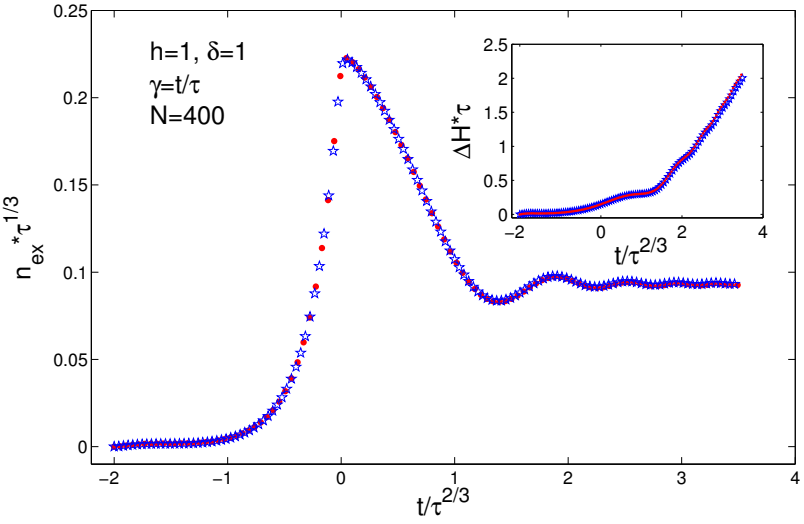

Figure 3.7: Exact scaling of the excitation density (main panel) and excitation energy (inset panel) throughout a linear quench along path 2.

Fig. 3.9), which is neither KZS nor $-1/6$. An identical $-3/4$ scaling holds for a V-shaped path across MCP B, that starts and ends in the DM phase. As finite-size analysis reveals, all the observed anomalous scalings are practically independent upon the system size over a wide range of quench rates (see Fig. 3.10), establishing them as truly thermodynamic in nature [1].

3.4.2 Landau Zener Analysis for Anomalous Scaling Behavior

In order to gain physical understanding of the above anomalous scaling results, we study the limiting cases where an exact solution for $n_{\rm ex}(t_f)$ may be obtained based on the LZ picture. This is possible provided that the quench is linear and the Hamiltonian can be decoupled into effective two-level systems. Among the above-mentioned paths, only paths 4 and 5 (for which $\delta = 0$) can be exactly mapped to a LZ problem, thanks to the possibility of rewriting the Hamiltonian in Eq. (2.1) as

[1]Notice that since $\nu z < z$ along path 5, to leading order the scaling of Δ_k is dominated by the control parameter rather than by the system size.

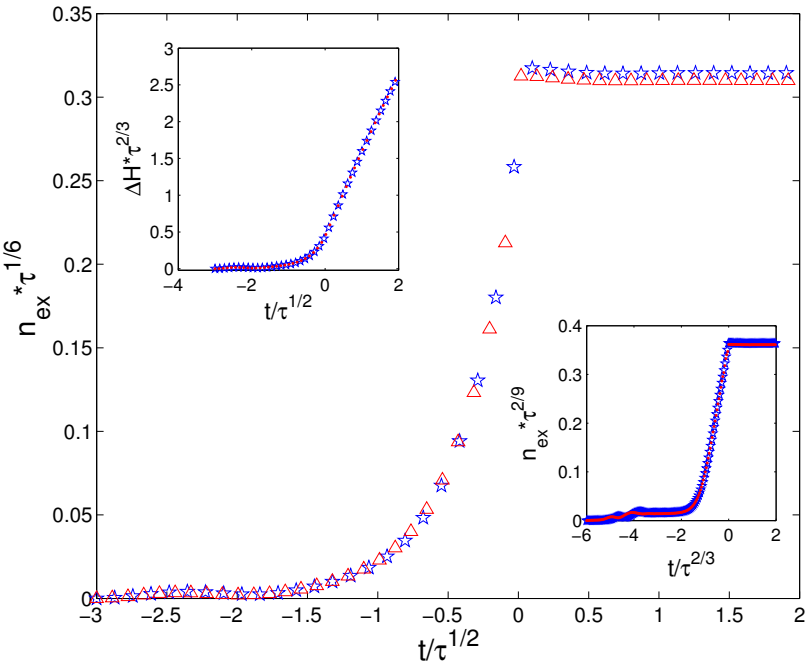

Figure 3.8: Main panel: Exact scaling of the excitation density throughout a linear quench along path 3. Left top inset: Exact scaling of the excitation energy throughout a linear quench along path 3. Right bottom inset: Exact scaling of the excitation density throughout a quadratic quench along path 3. $N = 400$.

$H = \sum_k B_k^\dagger \tilde{H}_k B_k$, where $B_k^\dagger = (c_{-k}, c_k^\dagger)$ and

$$\tilde{H}_k = \begin{pmatrix} \tilde{H}_{k,11} & \tilde{H}_{k,12} \\ \tilde{H}_{k,12}^* & -\tilde{H}_{k,11} \end{pmatrix} = 2 \begin{pmatrix} -h + \cos k & \gamma \sin k \\ \gamma \sin k & h - \cos k \end{pmatrix}. \tag{3.16}$$

A rotation $R_k(q_k)$, $q_k \in [-\pi/2, \pi/2)$, renders the off-diagonal terms in Eq. (3.16) independent upon γ (hence time), allowing a direct use of the LZ formula. Consider path 4 first. By choosing $\tan 2q_k = -\sin k$, the transformed Hamiltonian matrix elements become:

$$\tilde{H}'_{k,11} = -2(1 - \cos k)\cos 2q_k - 2t/\tau(\cos 2q_k - \sin k \sin 2q_k), \quad \tilde{H}'_{k,12} = 2(1 - \cos k)\sin 2q_k.$$

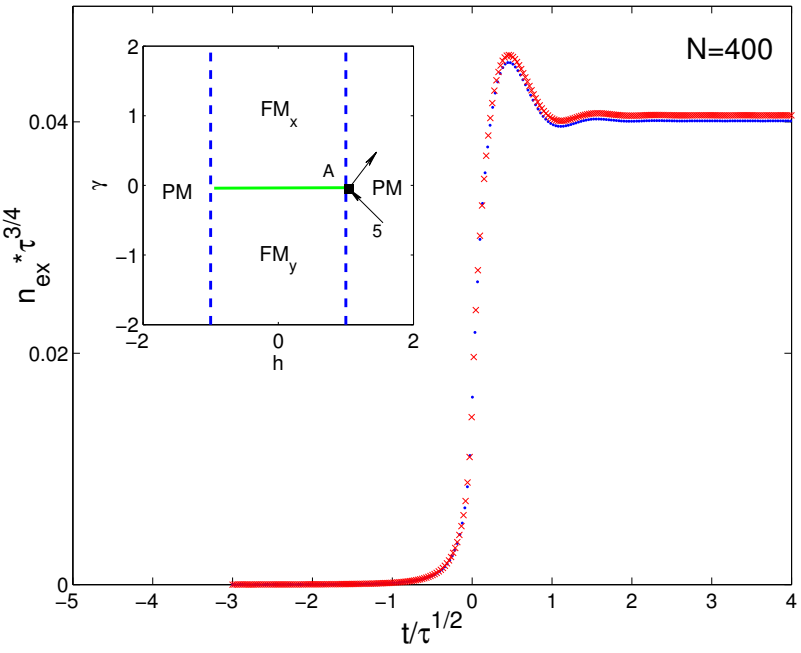

Figure 3.9: Inset panel: The V-shaped path 5 across MCP A, which can be implemented as $h(t) = 1 + |\gamma(t)| = 1 + |t/\tau|$ in a linear quench process. Main panel: Exact scaling of the excitation density throughout a linear quench along path 5.

Notice that the critical mode $k_c = 0$ for the MCP A. We may then let $\tan 2q_k \approx \sin 2q_k$, and the appropriate $q_k \approx -k/2$. From the LZ formula, the asymptotic ($t_f \to \infty$) excitation probability reads:

$$p_k = e^{-2\pi\tau(1-\cos k)^2 \sin^2 2q_k/(\cos 2q_k - \sin k \sin 2q_k)} \approx e^{-\pi\tau k^6/2},$$

where the approximation follows from a Taylor expansion around k_c. Integrating over all modes yields $n_{\rm ex}(t_f) \sim \tau^{-1/6}$, which is consistent with our exact numerical result. Therefore, mathematically, the $\tau^{-1/6}$ scaling follows from the fact that the exponent in p_k scales as $k^6 = k^{2z_2}$, with $z_2 = 3$. In turn, this originates from the scaling of the off-diagonal terms $H'_{k,12} \sim k^{z_2}$. Physically, as we shall later see by invoking AR, $H'_{k,12}$ may in fact be interpreted as the minimum gap for mode k along path 4.

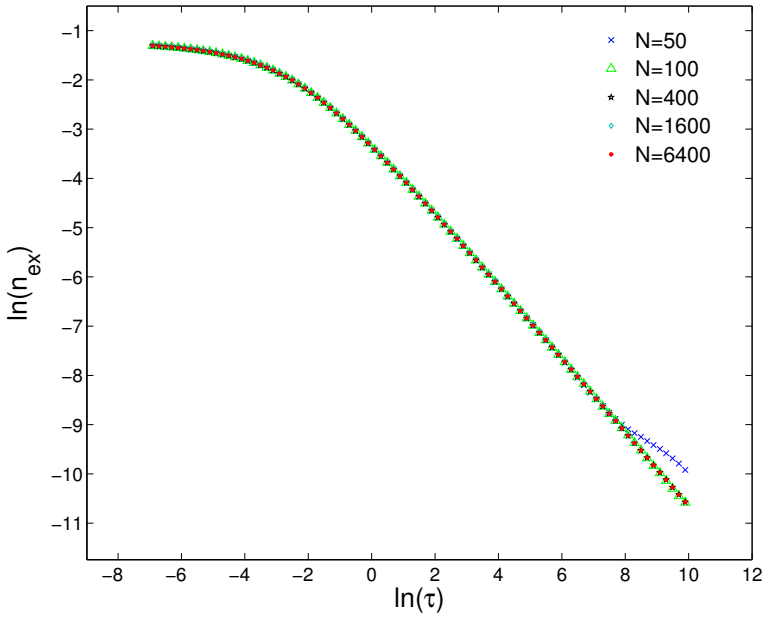

Figure 3.10: Scaling of the final excitation density in path 5 for different system size: $n_{\rm ex}(t_f)$ is the same to a numerical accuracy of 10^{-6}, up to $\tau < 2\times 10^5$. A linear fit yields -0.747 ± 0.001 over the range $200 < \tau < 2000$.

To unveil the $\tau^{-3/4}$ scaling, it is necessary to invoke the *exact finite-time* LZ solution. For simplicity, we restrict to half of path 5, by quenching the system from the PM phase up to the MCP `A`. This has the benefit of avoiding the non-analytic time-dependence of the control parameters that path 5 exhibits at `A`, while leaving the $\tau^{-3/4}$ scaling unchanged thanks to the symmetry of the excitation spectrum. Starting from Vitanov's expression (Eq. (7) in Ref. [83]), the excitation probability $p_k(t_f)$ can be computed via the parabolic cylinder function $D_v(z)$,

$$p_k(t_f) \quad = e^{-\pi\omega^2/4}\left| D_{i\omega^2/2}(T_f\sqrt{2}e^{i3\pi/4})\cos\theta(T_f) - \tfrac{\omega}{\sqrt{2}}e^{-i\pi/4}D_{i\omega^2/2-1}(T_f\sqrt{2}e^{i3\pi/4})\sin\theta(T_f))\right|^2,$$

where $\omega = (1-\cos k)\sin 2q_k\sqrt{\tau}/\sqrt{\cos 2q_k + \sin 2q_k \sin k} \sim k^3\sqrt{\tau}$ is the rescaled coupling strength, $T_f = -\omega/\sin k \sim -k^2\sqrt{\tau}$ is the rescaled time, $\tan 2q_k = \sin k$, and $\theta(T_f) = 1/2\arctan(\omega/T_f) + \pi/2$. Since for our quench process $|T_f| \ll 1$ around k_c, we may estimate $p_k(t_f)$ by Taylor-expanding $D_v(z)$ around $T_f = 0$ up to the second order:

$$
\begin{aligned}
p_k(t_f) &= (1-e^{-\pi\omega^2/2})/2 + \cos^2\theta(T_f)e^{-\pi\omega^2/2} - \sin 2\theta(T_f)/2 \sin\chi_k\sqrt{1-e^{-\pi\omega^2}} \\
&- \cos 2\theta(T_f)\cos\chi_k\sqrt{1-e^{-\pi\omega^2}}T_f\omega + O[T_f]^2, \qquad (3.17)
\end{aligned}
$$

where $\chi_k \approx \pi/4$ around k_c. Note that this approximation breaks when $T_f \sim 1$, setting the scaling of the largest momentum-mode in the relevant modes set as $k_{\max} \sim \tau^{-1/4}$. Since $\omega/T_f \ll 1$ for modes around k_c, $\arctan(\omega/T_f) \sim \omega/T_f$, which leads to $\cos\theta(T_f) \sim \omega/T_f$, and $\sin\theta(T_f) \sim \omega/T_f$. Thus, we can analyze the contribution to $p_k(t_f)$ by the scaling behavior of each term in Eq. (3.17) for modes within $k_{\max}$:

$$
\begin{aligned}
(1-e^{-\pi\omega^2/2})/2 \sim \omega^2, \quad \cos^2\theta(T_f)e^{-\pi\omega^2/2} \sim \cos^2\theta(T_f) \sim (\omega/T_f)^2, \\
\sin 2\theta(T_f)/2 \sin\chi_k\sqrt{1-e^{-\pi\omega^2}} \sim \omega^2/T_f, \quad \cos 2\theta(T_f)\cos\chi_k\sqrt{1-e^{-\pi\omega^2}}T_f\omega \sim \omega^2 T_f.
\end{aligned}
$$

Because $\omega/T_f \ll 1$ and $\omega \ll 1$, the dominant term is $\cos^2\theta(T_f)e^{-\pi\omega^2/2}$, which indicates $p_k(t_f) \sim (\omega/T_f)^2 \sim k^2$. Thus finally,

$$
n_{\text{ex}}(t_f) = \int_0^{k_{\max}} p_k(t_f)dk \sim k_{\max}^3 \sim \tau^{-3/4},
$$

in agreement with our numerical results. Remarkably, the fact that $p_k(t_f) \sim (k-k_c)^{d_2}$, $d_2 = 2$, indicates that k_c is *not* excited despite a static QCP being crossed, and also that the *excitation is dominated by intermediate (excited) energy states*. In fact, at the MCP `A`, the modes around k_c are still far from entering the impulse region, since $|T_f| \gg \omega$, which sets the LZ transition time scale [83]. This is in stark contrast with the main assumption underlying KZS, where the center of the impulse region is the static QCP, and excitations are dominated by modes near k_c, as reflected in the typical scaling $p_k \sim (k-k_c)^0 = O(1)$. Therefore, the shift of the actual (dynamical) impulse region relative to the static one is ultimately responsible for the observed anomalous $\tau^{-3/4}$ scaling.

3.4.3 Scaling Prediction from First-Order Adiabatic Renormalization

Since the system becomes gapless at a single MCP along all the paths under study, first-order AR is still a viable approach. Let, as before, $|\psi_m(t)\rangle$ be a basis of snapshot eigenstates of $H(t)$, with snapshot eigenvalues $E_m(t)$, $m = 0$ labelling the ground state. The time-evolved state may be

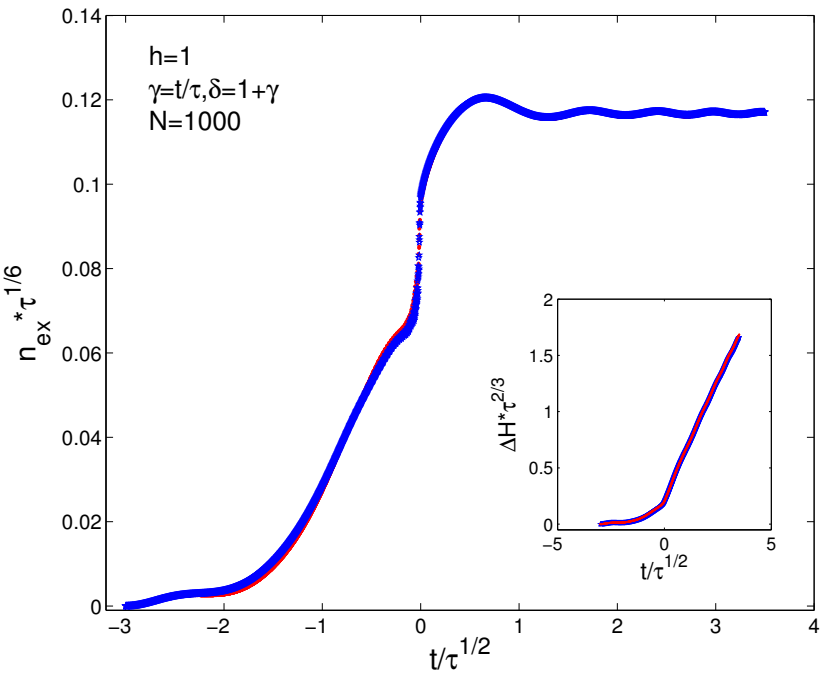

Figure 3.11: Scaling of the excitation density (main) and excitation energy (inset) from first-order AR for a linear quench along path 3.

expanded as $|\psi(t)\rangle = c_0^{(1)}(t)|\psi_0(t)\rangle + \sum_{m\neq 0} c_m^{(1)}(t)|\psi_m(t)\rangle$, where the coefficients $c_m^{(1)}(t)$ are given by Eq. (3.10). First-order AR calculations of $n_{\rm ex}(t)$ demonstrate that for linear quenches along paths 1 and 2, $n_{\rm ex} \sim \tau^{-1/3}$ and $\Delta H \sim \tau^{-1}$, whereas $n_{\rm ex} \sim \tau^{-1/6}$, $\Delta H \sim \tau^{-2/3}$ along paths 3 and 4 (Fig. 3.11). Since the non-analyticity at A in path 5 might cause problems in AR, again we choose to study half of path 5 (see main panel of Fig. 3.12), where we start at MCP A, and then quench towards the PM phase. All the AR results agree with the exact simulation results, confirming that AR is able to reproduce the correct dynamical scaling across a *generic* isolated QCP.

Predicting the scaling exponent based on AR requires scaling assumptions for the contributions entering $c_m^{(1)}(t)$ [*i.e.*, $\Delta_m(t) = E_m(t) - E_0(t)$ and $\langle\psi_m(t)|H_1|\psi_0(t)\rangle$] and the ability to change discrete sums of all the contributing excited states into integrals, for which the density of excited states $\rho(E)$ is required. Since typically the AR prediction is consistent with KZS, anomalous behavior must stem from anomalous scaling assumptions of (one or more of) these ingredients. We first examine the excitation spectrum along different paths. Notice that since H_1 is a one-body perturbation,

only single-mode excitations are relevant, thus the index m labeling many-body excitations may be identified with a momentum mode. Along paths 1 and 2, it turns out that the minimum gap among all modes is *always* located at k_c, whereas along paths 3 and 4, the minimum gap is located at k_c *only* at the MCP. This suggests that knowing the critical exponents of the MCP alone *need not* suffice to determine the dynamical scaling due to the existence of "quasi-critical" modes along paths 3 and 4. In fact, along path 4 (for instance), there is a value of $\tilde{\gamma}$ for each k such that the gap for this mode k reach its minimum value. This location can be obtained by requiring:

$$\frac{\partial \Delta_k(\gamma, 1+\gamma, 0)}{\partial \gamma} = (1+\gamma-\cos k+\gamma \sin^2 k)/\sqrt{(1+\gamma-\cos k)^2+(\gamma \sin k)^2)} = 0,$$

thus $\tilde{\gamma} = (\cos k - 1)/(1+\sin k^2) \approx (\cos k - 1)(1-\sin k^2)$ around $k_c = 0$, which is largely shifted into the FM phase (see inset in Fig. 3.12). By inserting this relation back into Δ_k, the composite function $\Delta_k(\tilde{\gamma})$ has the following scaling behavior

$$\Delta_k(\tilde{\gamma}) \equiv \tilde{\Delta}_k \approx \sqrt{(1+(\cos k-1)(1-\sin k^2)-\cos k)^2+((\cos k-1)(1-\sin k^2)\sin k)^2} \sim k^{z_2},$$

where $z_2 = 3$. Following the same procedure also yields $\tilde{\Delta}_k \sim (k-k_c)^3$ along path 3, while $\tilde{\Delta}_k$ has the same scaling as Δ_k at the MCP along paths 1 and 2. This motivates modifying the AR scaling in Eq. (3.12) as follows:

$$E_m(t) - E_0(t) = \delta\lambda(t)^{\nu z} f_m\Big(\frac{\Delta_m(t_{\min})}{\delta\lambda(t)^{\nu z}}\Big),$$

where $\Delta_m(t_{\min})$ is the minimum gap of mode m attained at $t_{\min}$ along the path, and f_m is a scaling function. Confirmation of this scaling assumption is shown in panel (a), (b) of Fig. 3.13 for path 3.

The above modification requires the scaling of $\rho(E)$ to be modified by letting $\rho(E) \sim E^{d/z_2-1}$, where z_2 comes from the dispersion relation of $\Delta_m(t_{\min})$. If the minimum gap of any mode is below a certain energy along the path, that mode should be counted into the contributing excited states. Accordingly, we have $z_2 = z = 2$ along paths 1, 2, half-5, and $z_2 = 3$ along paths 3, 4. Back to the LZ analysis, note that the off-diagonal term $H'_{12}(k)$ *is* the minimum gap of mode k along the path if there exists a time at which the diagonal term $H'_{11}(k) = 0$, as it happens for path 4. For path 5, however, the off-diagonal term never becomes the minimum gap since the system never leaves

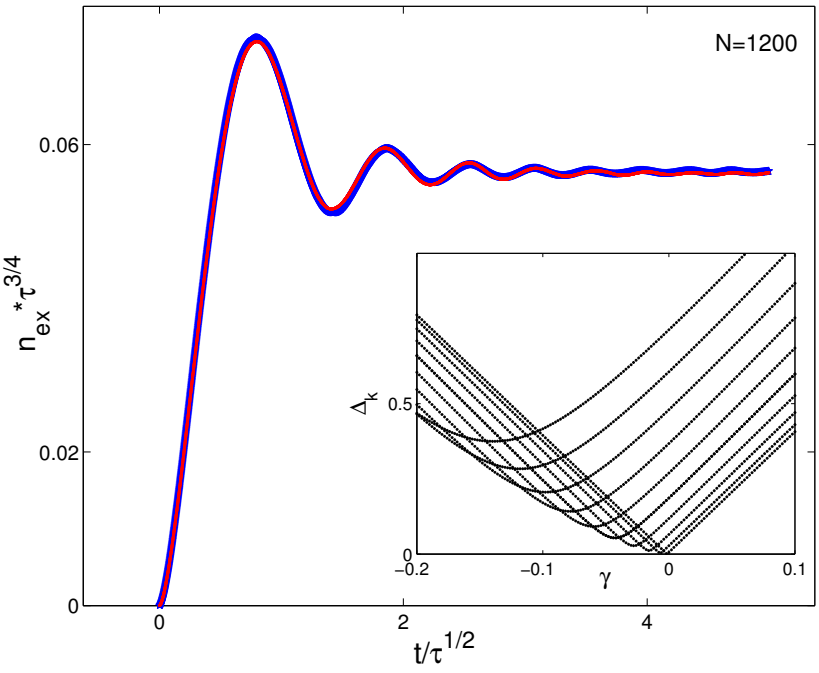

Figure 3.12: Scaling of the excitation density from first-order AR for a linear quench along path half-5 starting at MCP `A` (main). Inset: Low-lying single-mode excitation spectrum along path 4 for $N = 100$.

the PM phase. Therefore, the off-diagonal term in the LZ picture need not suffice to determine the dynamical scaling, and the shift of the location of the minimum gap for each mode from the static QCP is at the root of the anomalous behavior we observe. Lastly, we consider the matrix elements of H_1. Numerical simulations suggest that $\langle\psi_m(t)|H_1|\psi_0(t)\rangle = \delta\lambda(t)^{\nu z-1} g_m(\Delta_m(t_{\min})/\delta\lambda(t)^{\nu z})$, where g_m is a scaling function, and $\Delta_m(t_{\min})$ is the minimum gap of mode m along a path that *extends* the actual path to $t_f \to \infty$ when the quench is stopped at the MCP, and coincides with the actual path otherwise. Then along paths 1 and 2, $\Delta_m(t_{\min}) \sim k^2$, whereas along paths 3, 4, and half-5, $\Delta_m(t_{\min}) \sim k^3$. The confirmation of the scaling assumption for $\langle\psi_m(t)|H_1|\psi_0(t)\rangle$ is shown in panels (c) and (d) of Fig. 3.13 for path 3. Together with the other scaling assumptions, and taking the linear case $\alpha = 1$ as an example, AR yields $|c_m^{(1)}| \sim k^0$, $n_{\rm ex} \sim \tau^{-(z/z_2)(\nu/(\nu z+1))}$ along paths 1 to 4, and $|c_m^{(1)}| \sim k^1$, $n_{\rm ex} \sim \tau^{-3\nu/(\nu z+1)}$ along half-5 path, which completely agrees with the numerical results.

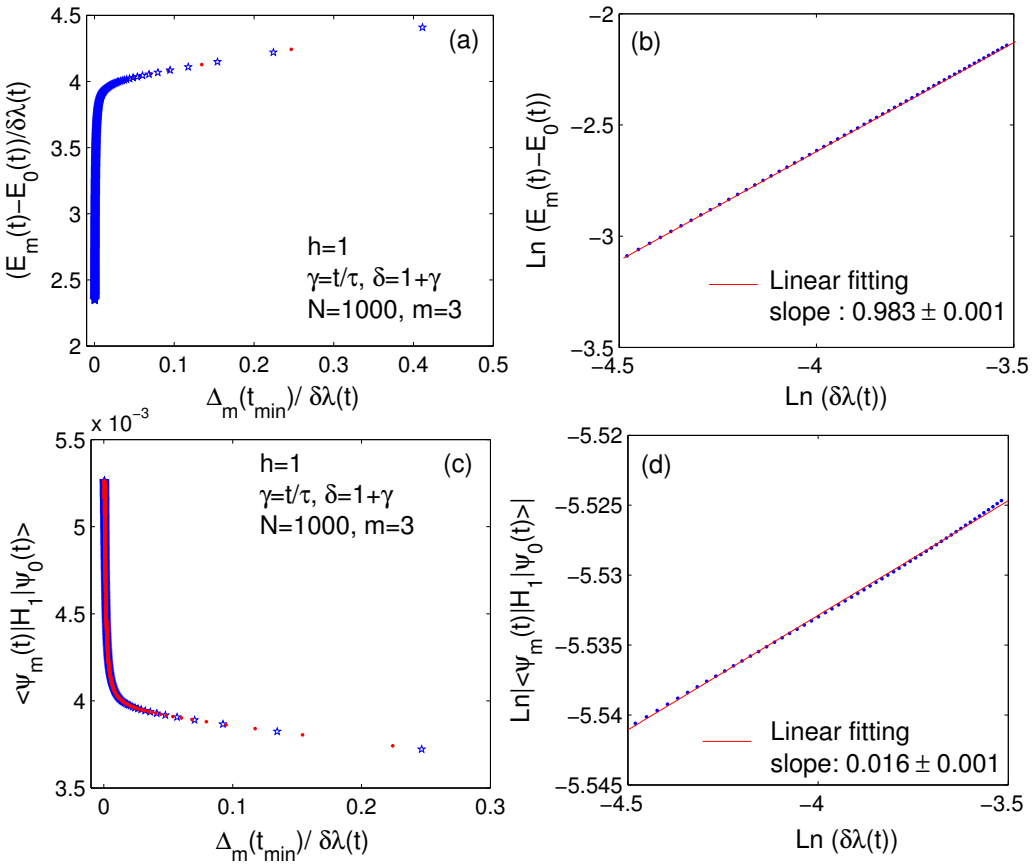

Figure 3.13: Scaling behavior of $E_m(t) - E_0(t)$ [panel (a),(b)] and $\langle\psi_m(t)|H_1|\psi_0(t)\rangle$ [panel (c),(d)] along path 3.

Building on the above analysis, we argue on physical grounds that the scaling of the excitation density for quenches across an *arbitrary (standard or multicritical) isolated QCP* is determined by the following three conditions:

(i) From the condition of adiabaticity breaking, the typical gap, $\hat{\Delta}$, must scale as

$$\hat{\Delta} \sim \tau^{-\alpha\nu z/(\alpha\nu z+1)};$$

(ii) An accessible excited state contributes to the excitation if and only if its minimum gap along

the path matches with this typical gap, $\tilde{\Delta}_k \sim \hat{\Delta}$, with

$$\tilde{\Delta}_k \sim (k - k_c)^{z_2};$$

(iii) The excitation probability, p_k, scales as $p_k \sim (k - k_c)^{d_2}$, where d_2 can differ from 0 if the center of the impulse region is greatly shifted relative to the static limit. Then, upon integrating up to energy $\hat{\Delta}$, and using $p_E \sim p_{k(E)} \sim E^{d_2/z_2}$, we obtain

$$n_{\rm ex} = \int_0^{\hat{\Delta}} p_E dE \sim \hat{\Delta}^{(d+d_2)/z_2} \sim \tau^{-(d+d_2)\alpha\nu z/[z_2(\alpha\nu z+1)]}, \tag{3.18}$$

which is consistent with all the results found thus far.

While KZS corresponds to $z_2 = z$, $d_2 = 0$, situations where $z_2 \neq z$ and/or $d_2 \neq 0$ are *genuinely dynamical*: knowledge about the path-dependent excitation process becomes crucial and non-equilibrium exponents can no longer be fully predicted from equilibrium ones. Interestingly, in the model under examination the Lifshitz universality class appears to be the only universality class for which anomalous scaling occurs, among all possible paths involving MCPs. Whether Lifshitz behavior may constitute a *sufficient* condition for anomalous behavior requires further investigation in other many-body systems.

Chapter 4

Dynamics in the XY Chain with Initial Finite-Energy States

With a few exceptions where quenches at finite temperature and the associated thermal corrections have also been examined [101, 102, 88, 100, 85], the large majority of the existing investigations have focused on quench dynamics originating from the ground state of the initial Hamiltonian $H(t_0)$. Our goal in this Chapter is to present a dedicated analysis of *finite-energy quantum quenches*, with a twofold motivation in mind. First, elucidating to what extent and how universal scaling properties depend upon the details of the system's initialization is needed to gain a more complete picture of non-equilibrium QPTs. While one might, for instance, naively expect that a sizable overlap with the initial ground state would be essential in determining the applicability of ground-state scaling results, one of our main results is that the support of the initial state on those excitations relevant to the path-dependent excitation process is key in a dynamical scenario, in a sense to be made precise later. Second, from a practical standpoint, perfect initialization of a many-body Hamiltonian in its exact ground state is both NP-hard in general [103, 104, 105], and experimentally unfeasible due to limited control. In this sense, our investigation extends previous studies on finite-temperature signatures of static QPTs [123], and may be directly relevant to experiments using ultracold atoms [7, 10, 9, 106] as well as nuclear magnetic resonance (NMR) quantum simulators [107, 108, 109].

Here, we address non-equilibrium dynamics originating from a large class of (bulk) initial states of a quantum XY spin chain for a variety of different quench schemes involving either a regular QCP or a MCP. Both pure and mixed initial states carrying a finite excitation energy above the ground state are examined, under the main assumption that, subsequent to initialization, the system can be treated as (nearly) isolated, hence still evolving unitarily under a time-dependent Hamiltonian. In particular, dynamical scaling in adiabatic and sudden quenches [84, 85, 86, 87, 88] starting from an *excited energy eigenstate* are analyzed in Sec. 4.2.1 and Sec. 4.2.2 respectively, with emphasis on making contact with previously introduced AR approaches [62, 77] and on clarifying connections between scaling behavior in sudden and adiabatic dynamics. The case of a *generic excited pure state* prepared by a sudden parameter quench is also considered in Sec. 4.2.3, and criteria are identified for KZS to be obeyed. Sec. 4.3 is devoted to quench dynamics resulting from an *initial thermal mixture*, with the main goals of characterizing the robustness of dynamical scaling behavior in realistic finite-temperature conditions, and of further exploring the conditions leading to *effective thermalization* of certain physical observables following a sudden quench toward criticality. In the process, we extend the analysis undertaken in Sec. 4.3.1, by presenting finite-temperature generalizations of the scaling predictions obtained for adiabatic (both linear and non-linear) *multicritical quantum quenches*, as well as evidence of how the peculiar nature of a MCP may also result in *anomalous thermalization*.

4.1 Model Hamiltonian

4.1.1 Energy Spectrum

To simplify our discussion, let us consider the homogeneous limit ($\delta = 0$) of the alternating XY spin chain we discussed in the Chapters 2 and 3, that is:

$$H = -\sum_{j=1}^{N} \Big(\frac{1+\gamma}{2} \sigma_x^j \sigma_x^{j+1} + \frac{1-\gamma}{2} \sigma_y^j \sigma_y^{j+1} - h\sigma_z^j \Big), \tag{4.1}$$

where, as before, periodic boundary conditions are assumed, that is, $\sigma_\alpha^j \equiv \sigma_\alpha^{j+N}$, and N is taken to be even. The diagonalization of the Hamiltonian (4.1) is well-known [37, 12, 50], and proceeds along steps similar to those we followed in Chapter 2, but without introducing two sets of fermionic

operators. Here, we recall the basic steps and provide a more detailed discussion on the eigenstate properties, as needed to discuss the quench dynamics from initial excited states. Upon introducing canonical fermionic operators $\{c_j, c_j^\dagger\}$ via the Jordan-Wigner mapping $c_j^\dagger \equiv \prod_{\ell=1}^{j}(-\sigma_z^\ell)\sigma_+^j$, H rewrites as a quadratic form

$$\begin{aligned} H &= -\sum_{j=1}^{N-1}\left(c_j^\dagger c_{j+1} + \gamma c_j^\dagger c_{j+1}^\dagger + \text{h.c.}\right) + 2h\sum_{j=1}^{N} c_j^\dagger c_j - hN + \mathcal{P}\left(c_N^\dagger c_1 + \gamma c_N^\dagger c_1^\dagger + \text{h.c.}\right) \\ &\equiv H^{(+)} + H^{(-)}, \end{aligned} \tag{4.2}$$

where $\mathcal{P}$, the parity of the total fermionic number, was defined in Eq. (2.3), but without the need of differentiating two sets of fermionic operators, and $H^{(+)}$ ($H^{(-)}$) corresponds to $+1$ (-1) eigenvalue of $\mathcal{P}$, respectively.

As discussed in Chapter 2, in finite systems the ground state and excited energy eigenstates with an even number of fermions belong to the $\mathcal{P} = +1$ sector. By using a Fourier transformation to momentum space, $c_k^\dagger = \frac{1}{\sqrt{N}}\sum_{j=1}^{N} e^{-ikj} c_j^\dagger$, followed by a Bogoliubov rotation to fermionic quasiparticles $\{\gamma_k, \gamma_k^\dagger\}$, with $\gamma_k = u_k c_k - i v_k c_{-k}^\dagger$, $u_k = u_{-k}$, $v_k = -v_{-k}$, and $u_k^2 + v_k^2 = 1$, the Hamiltonian in Eq. (4.2) rewrites as a sum of non-interacting terms:

$$H^{(+)} \equiv \sum_{k\in K_+} H_k = \sum_{k\in K_+} \epsilon_k(h,\gamma)(\gamma_k^\dagger\gamma_k + \gamma_{-k}^\dagger\gamma_{-k} - 1). \tag{4.3}$$

Here, the set $K \equiv K_+ + K_-$ of allowed momentum modes is determined by the anti-periodic boundary conditions on the fermions in the even sector, $c_{j+N} \equiv -c_j$, which yields $K_\pm = \Big\{ \pm \frac{\pi}{N}, \pm\frac{3\pi}{N}, \ldots, \pm\Big(\pi - \frac{\pi}{N}\Big)\Big\}$, and

$$\epsilon_k(h,\gamma) = 2\sqrt{(h-\cos k)^2 + \gamma^2 \sin k^2} \tag{4.4}$$

is the quasi-particle energy of mode k. For each k, let $\mathcal{H}_k \equiv \text{span}\{|0_k\rangle, |1_k\rangle\}$, where $\{|0_k\rangle, |1_k\rangle = \gamma_k^\dagger|0_k\rangle\}$ are orthonormal states corresponding, respectively, to zero and one Bogoliubov quasiparticle with momentum k, that is, $\langle 0_k|\gamma_k^\dagger\gamma_k|0_k\rangle = 0$, $\langle 1_k|\gamma_k^\dagger\gamma_k|1_k\rangle = 1$, and similarly for $-k$. Thus, the four

eigenstates of H_k provide a basis for $\mathcal{H}_k \otimes \mathcal{H}_{-k}$,

$$\mathcal{B}_k=\{|0_k,0_{-k}\rangle,|1_k,1_{-k}\rangle,|0_k,1_{-k}\rangle,|1_k,0_{-k}\rangle\} \equiv \mathcal{B}_k^{(+)} \oplus \mathcal{B}_k^{(-)}, \tag{4.5}$$

where the corresponding eigenenergies are given by $-\epsilon_k$, ϵ_k, 0, 0, and a further separation into even (odd) sector for each k is possible due to the fact that $[\mathcal{P}_k, H_k] = 0$, with

$$\mathcal{P}_k \equiv e^{i\pi(\gamma_k^\dagger\gamma_k+\gamma_{-k}^\dagger\gamma_{-k})} = e^{i\pi(c_k^\dagger c_k+c_{-k}^\dagger c_{-k})}.$$

The ground state of $H^{(+)}$ corresponds to the BCS state with no Bogoliubov quasiparticles, that is,

$$|\Psi_0^{(+)}\rangle = \bigotimes_{k\in K_+} |0_k 0_{-k}\rangle = \bigotimes_{k\in K_+} (u_k + iv_k c_k^\dagger c_{-k}^\dagger)|\mathtt{vac}\rangle. \tag{4.6}$$

Many-body excited states in the even sector can be obtained by applying pairs of Bogoliubov quasiparticle operators to $|\Psi_0^{(+)}\rangle$. In particular, excited eigenstates with support only on the even sector $\mathcal{B}_k^{(+)}$ for each mode are obtained by exciting only pairs of quasiparticles with opposite momentum and have the form

$$|\Psi_E^{(+)}\rangle = \Big(\bigotimes_{k\in K_+^e} |1_k 1_{-k}\rangle\Big)\Big(\bigotimes_{k\in K_+-K_+^e} |0_k 0_{-k}\rangle\Big), \tag{4.7}$$

where K_+^e labels the subset of excited modes.

For finite N, the ground state and excited energy eigenstates with an odd number of fermions belong to the sector $\mathcal{P} = -1$, which implies periodic boundary conditions on the fermions, $c_{j+N} \equiv c_j$, and a different set $\bar{K}$ of allowed momentum modes, $\bar{K} \equiv \bar{K}_+ + \bar{K}_- + \{0, -\pi\}$, where $\bar{K}_\pm = \Big\{\pm\frac{2\pi}{N}, \pm\frac{4\pi}{N}, \ldots, \pm\Big(\pi - \frac{2\pi}{N}\Big)\Big\}$. Since one may show that $\epsilon_{k=0} = h - 2$ and $\epsilon_{k=-\pi} = h + 2$, occupying mode 0 has always lower energy than occupying mode $-\pi$, thus the ground state of $H^{(-)}$ is now

$$|\Psi_0^{(-)}\rangle = |1_0 0_{-\pi}\rangle \bigotimes_{k\in\bar{K}_+} |0_k 0_{-k}\rangle,$$

and excitations may be generated by applying Bogoliubov quasiparticle operators in such a way that

the constraint on the total fermionic number parity is obeyed. Similar to modes in the even sector, $k \in K_+$, the subspace of each mode $k \in \bar{K}_+$ yields four eigenstates of H_k and, in principle, a basis formally identical to the one in Eq. (4.5) for the odd Hilbert-space sector. Although for finite N $\mathcal{P}$ is always a good quantum number under dynamics induced by H, the error in the computation of observables arising from identifying the two sets of modes K and $\bar{K}$ is vanishingly small as N increases, as discussed in Section 2.1.1. Thus, for sufficiently large N, a simplified description in terms of a unique set of momentum modes is possible by using the basis

$$\mathcal{B} \equiv \bigotimes_{k \in K_+} \mathcal{B}_k, \tag{4.8}$$

to characterize arbitrary states in the full Hilbert space $\mathcal{H} = \bigotimes_{k \in K_+} (\mathcal{H}_k \otimes \mathcal{H}_{-k})$. This becomes accurate in the thermodynamic limit $N \to \infty$, where the many-body ground state becomes twofold degenerate and the $\mathbb{Z}_2$-symmetry spontaneously breaks, causing different $\mathcal{P}$-sectors to mix.

The equilibrium phase diagram of the Hamiltonian in Eq. (4.1) is shown in the bottom panel of Fig. 2.4. Throughout this Chapter, we will mainly investigate scaling behavior in quenches involving either the regular QCP C ($h_c = 1, \gamma_c = 1$), which has equilibrium critical exponents $\nu = z = 1$ and belongs to the $d = 2$ Ising universality class, or the MCP A ($h_c = 1, \gamma_c = 0$), which has $\nu = 1/2, z = 2$ and belongs instead to the Lifshitz universality class, as marked in Fig. 2.4. For both the QCPs A and C of interest, we have critical mode $k_c = 0$ in the large-N limit.

4.1.2 Dynamical Response Indicators

In Chapter 3, the excess expectation value relative to the instantaneous ground state, defined in Eq. (3.2), was shown to successfully characterize dynamical scaling behavior for a large class of observables in adiabatic quenches originating from the ground state. For a generic quench process, where in principle *both* the time-dependence in $H(t)$ and the initial state $\rho(t_0)$ can be arbitrary, it is desirable to characterize the response of the system in such a way that no excitation is generated by purely adiabatic dynamics and zero-energy quenches are included as a special case. This motivates

extending the definition given in Eq. (3.2) to

$$\Delta\mathcal{O}(t) \quad \equiv \quad \mathrm{Tr}[\mathcal{O}(t)\rho(t)] - \mathrm{Tr}[\mathcal{O}(t)\tilde{\rho}(t)]\,, \tag{4.9}$$

where now $\rho(t)$ and $\tilde{\rho}(t)$ are the actual time-evolved density operator and the density operator resulting from adiabatic evolution of $\rho(t_0)$ respectively. Let $H(t)|\Psi_i(t)\rangle = E_i(t)|\Psi_i(t)\rangle$ define snapshot eigenstates and eigenvalues of $H(t)$ along a given control path. Then the adiabatically steered state is $\tilde{\rho}(t) = \sum_{i,j}\rho_{i,j}(t_0)|\Psi_i(t)\rangle\langle\Psi_j(t)|$, with $\rho_{i,j}(t_0)$ being the matrix elements of the initial state $\rho(t_0)$ in the eigenstate basis $|\Psi_i(t_0)\rangle\langle\Psi_j(t_0)|$ of the initial Hamiltonian $H(t_0)$.

With respect to the basis given in Eq. (4.8), a generic (uncorrelated) state in momentum space may be expressed in the form $\rho(t) = \bigotimes_{k\in K_+}\rho_k(t)$, where $\rho_k(t)$ is the four-dimensional density operator for mode k. Relative to a snapshot eigenbasis

$$\mathcal{B}_k(t) \equiv \{|\psi_k^j(t)\rangle\}, \quad j = 0,\ldots,3,$$

similar to the one given in Eq. (4.5), but constructed from time-dependent quasiparticle operators such that $\gamma_k(t)|0_k(t)\rangle = 0$, $\gamma_k^\dagger(t)|0_k(t)\rangle = |1_k(t)\rangle$, $\rho_k(t)$ may be expressed as:

$$\rho_k(t) = \sum_{i,j=0,3}\rho_{ij,k}(t)|\psi_k^i(t)\rangle\langle\psi_k^j(t)|.$$

Suppose that the time-evolution operator for mode k is $U_k(t)$, that is, $\rho_k(t) = U_k(t)\rho_k(t_0)U_k^\dagger(t)$. Direct calculation shows that $|0_k(t),1_{-k}(t)\rangle = c_{-k}^\dagger|\mathtt{vac}\rangle$, and $|1_k(t),0_{-k}(t)\rangle = c_k^\dagger|\mathtt{vac}\rangle$ for all t, which indicates that the snapshot eigenstates belonging to the $\mathcal{P}_k = -1$ eigenvalues are frozen in time, $|0_k(t),1_{-k}(t)\rangle = |0_k(t_0),1_{-k}(t_0)\rangle$, $\quad |1_k(t),0_{-k}(t)\rangle = |1_k(t_0),0_{-k}(t_0)\rangle$. As long as $\mathcal{P}_k$ is conserved under $H_k(t)$, the even and odd sectors for each k are thus decoupled. As a consequence, upon letting

$$U_k^\dagger(t)|1_k(t),1_{-k}(t)\rangle \equiv a_{0,k}(t)|0_k(t_0),0_{-k}(t_0)\rangle + a_{1,k}(t)|1_k(t_0),1_{-k}(t_0)\rangle,$$

we can evaluate the time-dependent excitation probability for mode k as follows:

$$\begin{aligned} P_k(t) &\equiv \mathrm{Tr}[\rho_k(t)\gamma_k^\dagger(t)\gamma_k(t)] \\ &= \mathrm{Tr}[\rho_k(t)(|1_k(t),1_{-k}(t)\rangle\langle 1_k(t),1_{-k}(t)|]+\mathrm{Tr}[\rho_k(t)|1_k(t),0_{-k}(t)\rangle\langle 1_k(t),0_{-k}(t)|] \\ &= (\rho_{00,k}(t_0)-\rho_{11,k}(t_0))|a_{0,k}(t)|^2+\rho_{11,k}(t_0)+2\mathrm{Re}[\rho_{01,k}(t_0)a_{0,k}^*(t)a_{1,k}(t)]+\rho_{33,k}(t_0), \end{aligned} \tag{4.10}$$

where the relationships $|a_{0,k}(t)|^2 + |a_{1,k}(t)|^2 = 1$ and $\rho_{10,k} = \rho_{01,k}^*$ have been exploited. Notice that from the above definition of $a_{0,k}(t)$, it follows that $|a_{0,k}(t)|^2$ determines the time-dependent probability that mode k is excited when it is in its ground state at $t = t_0$. Similarly, we may express the adiabatically evolved density operator $\tilde{\rho}(t) = \bigotimes_{k\in K_+}\tilde{\rho}_k(t)$, with $\tilde{\rho}_k(t) = \sum_{i,j=0,3}\rho_{ij,k}(t_0)|\psi_k^i(t)\rangle\langle\psi_k^j(t)|$. Thus, the time-dependent excitation probability of mode k relative to the adiabatic path is simply

$$\tilde{P}_k(t) = \mathrm{Tr}[\tilde{\rho}_k(t)\gamma_k^\dagger(t)\gamma_k(t)] = \rho_{11,k}(t_0) + \rho_{33,k}(t_0) \equiv P_k(t_0). \tag{4.11}$$

Upon combining Eqs. (4.11)-(4.11), the *relative excitation probability* of mode k is given by

$$\Delta P_k(t)\equiv P_k(t) - P_k(t_0)=(\rho_{00,k}(t_0) - \rho_{11,k}(t_0))|a_{0,k}(t)|^2+2\mathrm{Re}[\rho_{01,k}(t_0)a_{0,k}^*(t)a_{1,k}(t)]. \tag{4.12}$$

Physically, a non-zero contribution $P_k(t_0)$ may account for initial excitations due to either a coherent preparation into an excited state or to a finite temperature T. Two relevant limiting cases of Eq. (4.12) will play a special role in what follows. First, if mode k is initially in a generic pure state of the form

$$|\psi_k(t_0)\rangle \equiv \sum_{j=0,3} c_{j,k}|\psi_k^j(t_0)\rangle,$$

then $\rho_{00,k}(t_0) = |c_{0,k}|^2$, $\rho_{01,k}(t_0) = c_{0,k}c_{1,k}^*$, $\rho_{11,k}(t_0) = |c_{1,k}|^2$, hence

$$\Delta P_k(t) = (|c_{0,k}|^2 - |c_{1,k}|^2)|a_{0,k}(t)|^2 + 2\mathrm{Re}[c_{0,k}c_{1,k}^*a_{0,k}^*(t)a_{1,k}(t)]. \tag{4.13}$$

Second, if the initial state $\rho(t_0)$ is a statistical mixture, then $\rho_{10,k}(t_0) = \rho_{01,k}(t_0) = 0$, and we have

$$\Delta P_k(t) = (\rho_{00,k}(t_0) - \rho_{11,k}(t_0))|a_{0,k}(t)|^2. \tag{4.14}$$

The time-dependent excess expectation value $\Delta\mathcal{O}(t)$ in Eq. (4.9) may be expressed *directly in terms of the relative excitation probability* provided that the observables obeys $[\mathcal{O}(t), H(t)] = 0$ at all times. In this Chapter, we shall focus on the following three choices:

- $\mathcal{O}(t) = \frac{1}{N}\sum_{k\in K^+}[\gamma_k^\dagger(t)\gamma_k(t) + \gamma_{-k}^\dagger(t)\gamma_{-k}(t)]$, leading to the relative total density of excitations:

$$\Delta n_{\rm ex}(t) = \frac{2}{N}\sum_{k\in K_+}\mathrm{Tr}[(\rho_k(t) - \tilde{\rho}_k(t))\gamma_k^\dagger(t)\gamma_k(t)] = \frac{2}{N}\sum_{k\in K_+}\Delta P_k(t). \tag{4.15}$$

- $\mathcal{O}(t) = H(t)/N$, leading to the relative excitation energy density:

$$\Delta H(t) = \frac{2}{N}\sum_{k\in K_+}\mathrm{Tr}[(\rho_k(t) - \tilde{\rho}_k(t))H_k(t)] = \frac{2}{N}\sum_{k\in K_+}\epsilon_k(h(t),\gamma(t))\Delta P_k(t). \tag{4.16}$$

As a representative example of an observable *not* commuting with the system's Hamiltonian, we shall additionally include results on the scaling behavior of:

- $\mathcal{O} \equiv XX = \frac{1}{N}\sum_{i=1}^{N}\sigma_x^i\sigma_x^{i+1}$, corresponding to the nearest-neighbor spin correlator per site along the x-direction [77]. We have:

$$\Delta XX(t) = \frac{2}{N}\sum_{k\in K_+}\Delta\big[-2\cos k\, c_k^\dagger c_k + i\gamma(t)\sin k\,(c_k^\dagger c_{-k}^\dagger - \text{h.c.})\big] \tag{4.17}$$

Notice that Eqs. (4.15), (4.16) and (4.17) coincide with Eqs. (3.3), (3.4) and (3.5), respectively, in the uniform magnetic field limit when the initial state is the ground state, as expected.

4.2 Quantum Quenches from a Pure Excited State

4.2.1 Adiabatic Quench Dynamics from an Excited Energy Eigenstate

As we discussed in Chapter 3, adiabatic quenches from the ground state of the initial Hamiltonian $H(t_0)$ have been extensively studied and are well understood in this model. In order to explore

the role of initialization, a first natural step is to investigate dynamical scaling behavior when the initial state is an excited *eigenstate* of $H(t_0)$. In this subsection, we will show that both exact and perturbative methods would give consistent results with respect to the condition to exhibit KZS with an initial excited energy eigenstate.

4.2.1.1 Exact Numerical Scaling Results

Since, as remarked, the time-evolution of excited components along $|0_k, 1_{-k}\rangle$ and $|1_k, 0_{-k}\rangle$ is trivial, we focus on excited energy eigenstates with support only on the even sector of each mode k, that is, on states of the form given in Eq. (4.7). Noting that there are only two possibilities for each mode, either $c_{0,k} = 1$ or $c_{0,k} = 0$, Eq. (4.13) yields

$$\Delta P_k(t) = (|c_{0,k}|^2 - |c_{1,k}|^2)|a_{0,k}(t)|^2 = \pm|a_{0,k}(t)|^2, \tag{4.18}$$

and, correspondingly,

$$\Delta n_{\rm ex}(t_f) = \frac{2}{N}\sum_{k\in K_R}\Big[\pm|a_{0,k}(t_f)|^2\Big]. \tag{4.19}$$

Thus, the relative excitation density is the same, up to a sign, in two limiting cases: (i) the many-body ground state, corresponding to $c_{0,k} = 1$ for all k and to an overall positive sign in Eq. (4.19); and (ii) the state where all allowed pairs of quasiparticles are excited, corresponding to $c_{0,k} = 0$ for all k and to an overall negative sign in Eq. (4.19). Since KZS is known to hold for a linear quench process with initial condition (i), and a global sign difference would not change the scaling behavior, KZS is expected to persist for the maximally excited initial eigenstate (ii) as well. This is to some extent surprising both in view of the fact that such an initial state has *zero overlap* with the BCS state $|\Psi_0^{(+)}\rangle$, and because one would not *a priori* expect highly energetic eigenstates to be sensitive to the ground-state QPT.

Interestingly, critical properties of excited eigenstates in the XY chain have recently attracted attention in the context of *static* QPTs [110]. Suppose that each excited eigenstate is associated with an ordered binary strings of length $|K| = N$, where 0 (1) represents a mode in its ground

(excited) state, respectively. Then a compact description of the eigenstate may be given in terms of the "discontinuities" of the characteristic function of the corresponding occupied mode set: thus, no discontinuity is present when all modes are 0 or 1, and a discontinuity is counted every time the occupation of a given mode changes along the string. Alba *et al.* [110] have analytically proved, in particular, that the block entanglement entropy, S_L, of an excited eigenstate of the critical XY chain may still obey conformal scaling as in the ground state provided that the number of discontinuities remains *finite* in the thermodynamic limit, that is, $S_L \sim \log L$, where $L \gg 1$ is the block size. Conversely, S_L exhibits non-critical scaling, $S_L \sim L$, when the number of discontinuities becomes itself an extensive quantity as $N \to \infty$. Thus, certain highly excited states (including the fully excited state considered above) can still display critical behavior, the number of discontinuities in the *full* set of momentum modes being the essential factor in determining the *static* scaling behavior. While, intuitively, non-analyticities in the characteristic mode occupation function need not play a direct role for simple observables such as the excitation density, these results prompt the following question: to what extent does a distinction between "critical" (leading to KZS) and "non-critical" excited eigenstates exist for *dynamical* QPTs?

A key difference with respect to the static situation is that only the *relevant* modes matter in a dynamical QPT, $k \in K_R \equiv [k_c, k_{\max}]$, with $k_{\max}$ given in Eq. (3.8). In Fig. 4.1, we present exact numerical results, obtained by direct numerical integration of the time-dependent Schrödinger equation, for the relative excitation density in a linear adiabatic quench of the magnetic field h around the QCP $\mathtt{C}$ of the critical Ising chain ($\gamma = 1$). Different initial eigenstates are compared over a common range of τ, which is chosen to be well within the appropriate τ-range (recall Section 3.2) for ground-state quenches (see also next paragraph and Fig. 4.2 for further discussion of this point). In panel (a), the system is initialized in the first excited state, where only the critical mode is initially excited (thus only one discontinuity is present), whereas in panel (b), the five lowest-energy modes are initially excited (leading to one discontinuity as well). In case (a), while no scaling is visible for a system with size $N = 400$, progressively better scaling behavior emerges as N is increased, with the value at $N = 3200$ approaching the asymptotic KZS value (and better agreement being achievable by optimizing the τ-range, see below). In constrast, for the data in panel (b), a system size as large as $N = 12800$ is required for a scaling of comparable quality to be established. Since the only

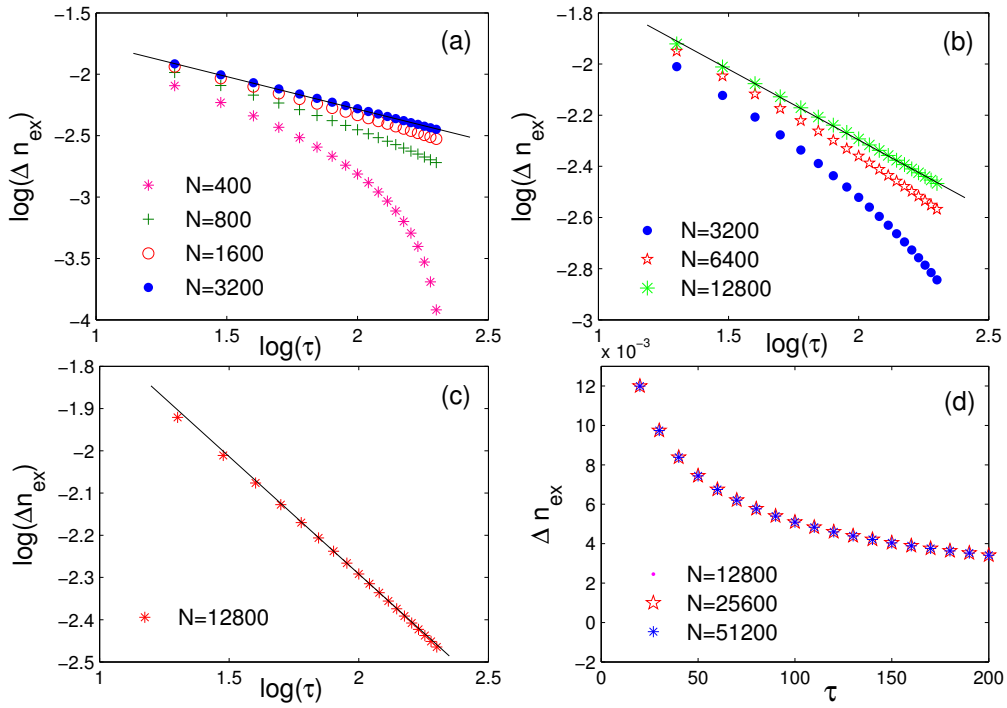

Figure 4.1: Scaling behavior of the final relative excitation density in a linear quench of the magnetic field h around the QCP —tt C in the Ising chain, starting with different excited eigenstates of $H(h_c)$. Panel (a): only $k_c = \pi/N$ is excited initially. The linear fit for $N = 3200$ yields -0.535 ± 0.002. Panel (b): the five lowest-energy modes are initially excited. A linear fitting slope of -0.549 ± 0.003 is now reached at $N = 12800$. Panel (c): five modes ($k = k_c$, $5\pi/N$, $9\pi/N$, $13\pi/N$, and $17\pi/N$) are initially excited. The linear fit for $N = 12800$ yields -0.546 ± 0.002. Panel (d): the five lowest-energy modes are initially excited for $N = 12800$ as in (b), but as the system size is increased linearly, the number of excited modes is increased accordingly. In all cases, the relevant τ-range $\tau_{\rm min} < 20 \leq \tau \leq 250 < \tau_{\rm max}$ (see text and Fig. 4.2).

difference between cases (a) and (b) is a different (fixed) number of initially excited modes in N_R, the fact that upon increasing N (thereby increasing N_R accordingly) a better KZS is comparatively obtained in (a) suggests that the *ratio between the number of initially excited (or non-excited) modes and* N_R is crucial for dynamical scaling behavior – not (as intuitively expected) the discontinuity properties which characterize the initial mode occupation *per se*. More explicitly, let N_E denote the number of modes in K_R that are excited at time t_0, with $N_R - N_E$ correspondingly denoting the

number of non-excited modes in K_R, and let

$$M_R \equiv \min\{N_E, N_R - N_E\}.$$

Motivated by the above observations and also recalling the symmetric role played by initially non-excited vs. excited modes in determining the time-dependent relative probability of excitation [Eq. (4.18)], we conjecture that KZS emerges in the thermodynamic limit provided that the initial excited eigenstate satisfies

$$\frac{M_R}{N_R} = \varepsilon \ll 1. \tag{4.20}$$

Clearly, the case of ground-state initialization corresponds to $N_E = M_R = 0$, and the fully excited state coincides with $N_E = N_R, M_R = 0$. For a generic initial excited eigenstate, Eq. (4.20) allows in principle M_R to be an extensive quantity in the thermodynamic limit. Two additional results are included in Fig. 4.1 to illustrate the above possibility. In panel (c), we still have five excited modes in N_R as in (b), but five discontinuities as opposed to just one. For the same system size (thus also the same ε), the scaling is not worse than in panel (b), further supporting the conclusion that the number of discontinuities does not play a role towards the emergence of dynamical scaling. In panel (d), a fixed value of ε, equal to the one in (b) at $N = 12800$, is explored for different values of N, by also proportionally increasing N_E. As the data show, the resulting $\Delta n_{\rm ex}$ is the same, indicating that M_R may indeed be allowed to be an extensive quantity as long as Eq. (4.20) is obeyed.

It is important to address how the choice of a range of τ-values affects the above scaling conclusions. Let $\tau_{\rm min} \leq \tau \leq \tau_{\rm max}$ and $\tilde{\tau}_{\rm min} \leq \tau \leq \tilde{\tau}_{\rm max}$ denote the valid range for ground-state, and for excited-state initialization, respectively. As discussed in Section 3.2, since $\tau_{\rm min}$ is determined from the requirement that an adiabatic regime exists away from criticality, whereas $\tau_{\rm max}$ follows from ensuring that adiabaticity can be broken in a finite-size system, both $\tau_{\rm min}$ and $\tau_{\rm max}$ are related to the scaling of the *many-body gap* between the ground state and first (available) excited state. Thus, $\tilde{\tau}_{\rm min}$ ($\tilde{\tau}_{\rm max}$) could in *a priori* be substantially different from $\tau_{\rm min}$ ($\tau_{\rm max}$), respectively. In our case, however, the Hamiltonian in Eq. (4.1) can be exactly decoupled into two-level systems for each mode k. Therefore, the relevant gap is always $\Delta_{k_c} \equiv \varepsilon_{k_c}(h, \gamma)$, *irrespective of the initial condition.* For this

reason, the relation $\tau_{\min} \leq \tilde{\tau}_{\min}$ and $\tilde{\tau}_{\max} \leq \tau_{\max}$ must hold, as any finite-energy initial state might imply more restrictive constraints as compared to the zero-energy case. In particular, according to Eq. (4.20), not all the excited eigenstates can lead to KZS, and the better Eq. (4.20) is satisfied, the closer KZS will be approached. This explains why, for instance, the fitting slope -0.549 from panel (b) of Fig. 4.1 is not as close to the KZ value as the one obtained for a ground-state quench with the same range of τ. In the setting of Fig. 4.1(b), the majority of the relevant modes stay in their ground state. In order to reduce the contribution to $\Delta n_{\rm ex}$ from the five lowest-energy modes, we can decrease τ such that N_R will be increased in Eq. (4.20). Numerical support for this strategy is shown in Fig. 4.2, where an optimal range of τ is identified for the same initial states as in Fig. 4.1(d), and very good agreement with KZS is recovered. Thus, we conjecture that if the majority of modes that enter M_R are low-energy modes, we can reduce their contribution to $\Delta n_{\rm ex}$ by decreasing the upper bound to τ. That is, we choose $\tau_{\min} \leq \tau \leq \tilde{\tau}_{\max}$, where $\tilde{\tau}_{\max} < \tau_{\max}$. Conversely, if the majority of modes that enter M_R are high-energy modes, then we reduce the contribution from these modes by increasing the lower bound to τ. That is, we let $\tilde{\tau}_{\min} \leq \tau \leq \tau_{\max}$, with $\tilde{\tau}_{\min} > \tau_{\min}$.

4.2.1.2 Results from First-Order Adiabatic Renormalization

Additional theoretical understanding of the criterion given in Eq. (4.20) may be sought by invoking the perturbative AR [64], which, as discussed in Section 3.2.2, was successfully applied to explain the scaling results for adiabatic quenches starting from the ground state. Can first-order AR still capture dynamical scaling for initial excited eigenstates? Let us focus on linear quenches ($\alpha = 1$), and let the time-dependent Hamiltonian be parametrized as $H(t) = H_c + [\lambda(t) - \lambda_c]H_1 = H_c + (t/\tau)H_1$, with H_c quantum-critical in the thermodynamic limit, so that the relevant QCP is crossed at $t_c \equiv 0$. If the system is prepared in the ℓ-th eigestate of $H(t_0)$, with $t_0 \to t_c$ as in the examples previously considered, the time-evolved state from first-order AR may be expressed in the form

$$|\Psi^{(1)}(t)\rangle = e^{-i\Gamma_\ell(t)}|\Psi_\ell(t)\rangle - \sum_{m\neq\ell} c_m^{(1)}(t)|\Psi_m(t)\rangle,$$

where $\Gamma_\ell(t)$ includes both the Berry phase and the dynamical phase, and $c_m^{(1)}(t)$ gives the time-dependent amplitude along the m-th snapshot eigenstate. Following a derivation similar to the one

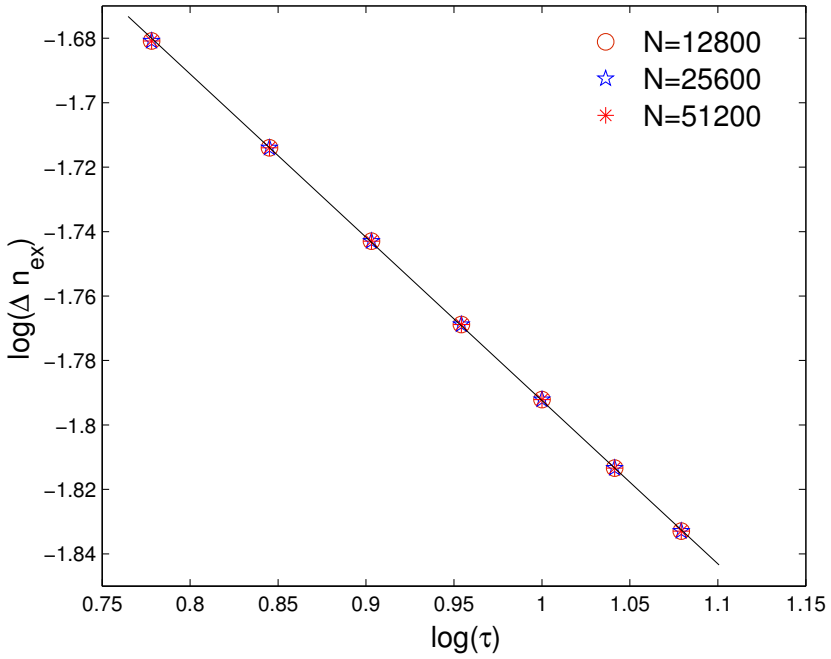

Figure 4.2: Scaling behavior of the final relative excitation density in a linear magnetic-field quench around the QCP C in the Ising chain, starting with an eigenstate of $H(t_c)$ where the five, ten, and twenty lowest-energy modes are initially excited for $N = 12800, N = 25600, N = 51200$, respectively [same as in Fig. 4.1(d)]. The relevant τ-range is now $\tilde{\tau}_{\rm min} \sim \tau_{\rm min} = 5 \leq \tau \leq \tilde{\tau}_{\rm max} = 20 \ll \tau_{\rm max}$. A linear fitting slope of -0.5019 ± 0.002 is now reached for all these cases, in agreement with the KZS prediction.

described in Section 3.2.2, and letting $\Delta_m(t) \equiv E_m(t) - E_\ell(t)$, we find:

$$c_m^{(1)}(t) \;=\; \frac{e^{-i\Gamma_m(t)}}{\tau}\int_{t_0}^{t} dt' \frac{\langle \Psi_m(t')|H_1|\Psi_\ell(t')\rangle}{E_m(t') - E_\ell(t')}\, e^{i\int_{t_0}^{t'} ds \Delta_m(s)}.$$

Thus, to the first order in the quench rate $1/\tau$ the adiabaticity loss can be quantified by $\Delta\mathcal{O}(t) = \langle\Psi^{(1)}(t)|\mathcal{O}(t)|\Psi^{(1)}(t)\rangle - \langle\Psi_\ell(t)|\mathcal{O}(t)|\Psi_\ell(t)\rangle$. In particular, this yields

$$\Delta n_{\rm ex}(t) = \frac{2}{N}\sum_{m\neq\ell} |c_m^{(1)}(t)|^2 \Big(\langle\Psi_m(t)| \sum_{k\in K_+} \gamma_k^\dagger(t)\gamma_k(t)|\Psi_m(t)\rangle - \langle\Psi_\ell(t)| \sum_{k\in K_+} \gamma_k^\dagger(t)\gamma_k(t)|\Psi_\ell(t)\rangle \Big).$$

Since H_1 is a one-body operator in our case, the only non-vanishing matrix elements $\langle\Psi_m(t)|H_1|\Psi_\ell(t)\rangle$ include many-body eigenstates $|\Psi_m(t)\rangle$ which differ from $|\Psi_\ell(t)\rangle$ in the *occupation of precisely one*

mode. Thus,

$$\langle\Psi_m(t)|\sum_k \gamma_k^\dagger(t)\gamma_k(t)|\Psi_m(t)\rangle - \langle\Psi_\ell(t)|\sum_k \gamma_k^\dagger(t)\gamma_k(t)|\Psi_\ell(t)\rangle = \pm 1,$$

which implies

$$\Delta n_{\rm ex}(t_f) = \frac{1}{N}\sum_{m\neq\ell}\Big[\pm|c_m^{(1)}(t_f)|^2\Big]. \tag{4.21}$$

Except for a possible sign difference for each m, the above expression is formally identical to the one holding for ground-state initialization ($\ell = 0$), in analogy with the exact Eq. (4.19). Numerical calculations of the relative excitation density according to Eq. (4.21) [for instance with the same initial condition as in Fig. 4.1(a)] confirm that the condition for initial excited eigenstates to support KZS is the same in first-order AR as the one conjectured based on exact numerical results.

4.2.2 Sudden Quench Dynamics from an Excited Energy Eigenstate

Scaling results for sudden quenches of the control parameter λ around its critical value λ_c have been recently obtained by De Grandi *et al.* [88] under the assumptions that the system is in the ground state of the initial Hamiltonian and the quench has a *small amplitude*, leading to a final excitation density

$$n_{\rm ex}(t_f) \sim |\lambda - \lambda_c|^{d\nu} \equiv \delta\lambda^{d\nu}, \tag{4.22}$$

with $\delta\lambda \ll 1$ in suitable units. Before addressing, in analogy to the case of adiabatic dynamics, the extent to which the expected scaling behavior may be robust against initialization in a finite-energy eigenstate, it is useful to explore more quantitatively the connection between ground-state adiabatic vs. sudden quenches implied by Eq. (4.22).

Suppose, specifically, that the amplitude of a sudden magnetic-field quench near the QCP C of the Ising chain is directly related to the rate τ of a corresponding linear adiabatic sweep across the same QCP via $h_f = h_c \pm \hat{h}$, where $\hat{h} \propto \hat{t}/\tau$ and $\hat{t}$ is the KZ freeze-out time scale, that is, $\hat{t} \sim \tau^{\nu z/(\nu z+1)}$. Eq. (4.22) then yields

$$n_{\rm ex}(t_f) \sim |h_f - h_c|^{d\nu} \sim \tau^{-d\nu/(\nu z+1)}. \tag{4.23}$$

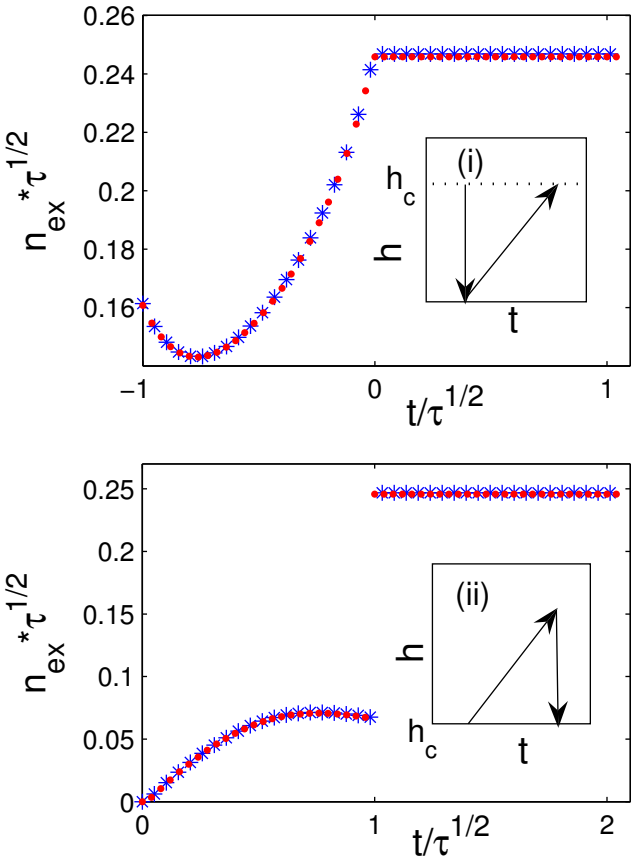

Figure 4.3: Scaling behavior of the final excitation density in combined magnetic-field ground-state quenches across QCP C in the Ising chain. Top: Sudden quench $h_c \mapsto h_f$ (see text) followed by a linear quench back to h_c, with the system finally kept at h_c. Bottom: Linear quench from h_c followed by a sudden quench $h_f \mapsto h_c$, with the system finally kept at h_c. In both cases, $N = 400$.

In other words, the scaling behavior resulting from Eq. (4.22) is essentially equivalent to KZS. While this could be quantitatively demonstrated by direct calculation of $n_{\rm ex}(t)$ in a sudden quench, it can also be nicely illustrated by examining *combined* sudden-adiabatic quenches, which have not been explicitly addressed to our knowledge [1], and will also be relevant in Sec. 4.2.3. Two possible "control loops" starting from $h(t_0) = h_c$ are depicted in Fig. 4.3: we can either (i) suddenly change

[1] In a recent work [121], the behavior of the *decoherence factor* has been advocated as a dynamical indicator of the QPT in an Ising environment. Formally, the required procedure of first turning on the system-environment coupling at the initial time, followed by adiabatic evolution of the Ising chain across the QCP A, can be interpreted in terms of a combined sudden-adiabatic quench scheme on the joint system-plus-environment Hamiltonian. Interestingly, KZS is found to occur in the exponent of the decoherence factor as well. See Chapter 5 for additional discussion.

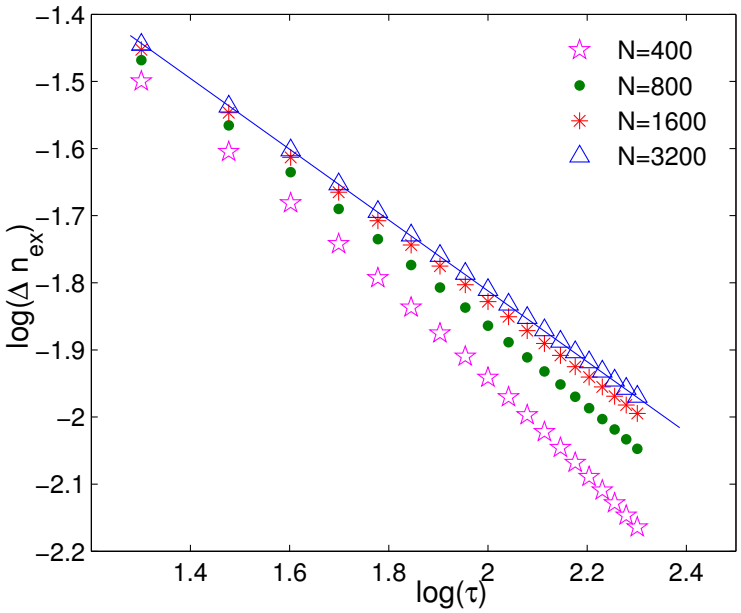

Figure 4.4: Scaling behavior of the final relative excitation density in a sudden magnetic-field quench across QCP C in the Ising chain, starting with the first excited state of $H(h_c)$. The linear fitting slope for $N = 3200$ is -0.5244 ± 0.0004 for $20 \leq \tau \leq 250$. Closer agreement with the KZS may be reached by optimizing over τ as in Fig. 4.2.

the magnetic field amplitude $h_c \mapsto h_f$, and then adiabatically change it back to h_c (top panel); or we can (ii) slowly ramp up h_c to h_f, and then suddenly quench $h_f \mapsto h_c$ (bottom panel). As it is clear from the numerical data, the total excitation density created from the combined sudden-adiabatic quench shows KZS throughout the entire process in both cases, provided that τ is within the appropriate scaling range $\tau_{\min} \leq \tau \leq \tau_{\max}$. Notice that the quench process depicted in Fig. 4.3 is similar to the repeated linear quench across QCP C studied in Ref. [67], in the sense that the initial and final value of the control parameter coincide. While KZS was found to hold in such a repeated linear quench, the difference is now that *half of the linear adiabatic sweep* is replaced by a sudden quench. Since, however, the interval $[h_c - \hat{h}, h_c + \hat{h}]$ corresponds to the impulse region in the KZ scenario for a pure linear quench, the scaling results of the combined quenches under consideration may be understood as a consequence of the fact that the sudden quench component can only further *enforce* the impulse mechanism by which excitation is generated in the KZS argument. Interestingly,

as long as the scaling exists, we can also observe that (i) and (ii) lead to almost the same final excitation density, even if the intermediate values of the excitation density after the sole sudden [in (i)] or linear [in (ii)] quench are different. In summary, the existence of KZS in ground-state sudden and combined sudden-adiabatic quenches with *small amplitude* is essentially a reflection of the fact that the system goes through an impulse region around the QCP no matter how slow or fast the quench is effected.

While sudden quenches of *arbitrary amplitude* will be further considered in the next Subsection, we now return to the question of whether dynamical scaling also holds in small-amplitude sudden quenches when the system is initially prepared in an excited eigenstate of $H(t_0) = H_c$. Exact numerical results are presented in Fig. 4.4, where in order to ease the comparison with a linear quench, we have again explicitly related the sudden-quench amplitude to τ as $h_f - h_c \propto \tau^{-1/2}$. The data for $N = 3200$ indicate that the scaling exponent is slightly closer to the KZS prediction than the one obtained in a pure linear quench with the same initial condition and τ-range [cf. Fig. 3(a)]. Since a sudden quench effectively *strengthens* the impulse mechanism in the KZS argument, the number of relevant modes N_R is larger than the one involved in an adiabatic linear quench. Thus, for the same initial condition (the same M_R), the ratio ε in Eq. (4.20) is smaller in a sudden quench than in a linear quench, comparatively leading to a scaling exponent closer to KZS. Therefore, our conclusions for excited-state sudden quenches are consistent with the ones reached for excited-state adiabatic quenches, and reaffirm how *small-amplitude sudden quench dynamics and adiabatic dynamics near a QCP are essentially equivalent over a wide range of initializations.*

4.2.3 Adiabatic Dynamics Following a Sudden Quench from the Ground State

In addition to eigenstates of the initial Hamiltonian, another physically relevant class of initial preparations is provided by pure states that are reachable from the many-body ground state via a sudden parameter quench of *arbitrary amplitude*. For concreteness, let us focus on adiabatic dynamics following a sudden quench of the magnetic field h to its critical value h_c in the Ising chain. Thus, the initial state for the adiabatic quench is a superposition of different eigenstates of the Hamiltonian $H(h_c)$ after the (instantaneous) sudden quench. Since for each mode k the parity

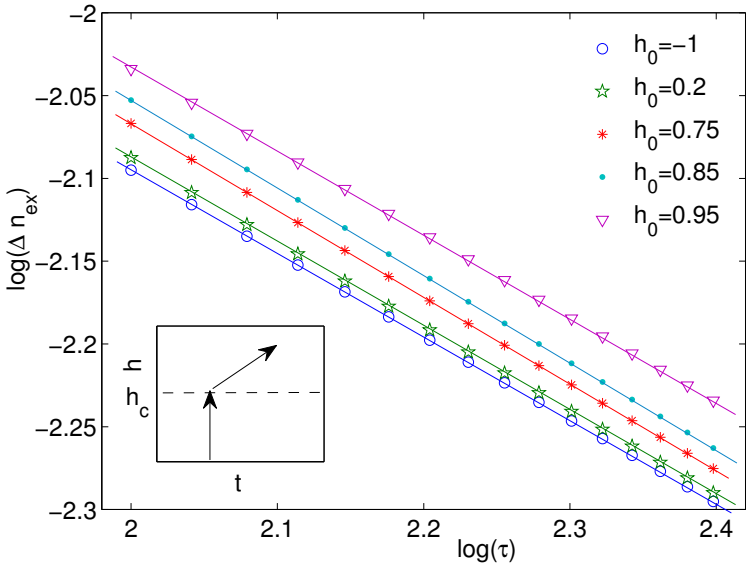

Figure 4.5: Scaling of the final relative excitation density in an adiabatic magnetic-field quench across QCP C in the Ising chain, starting from an excited state prepared by suddenly quenching $h_0 \mapsto h_c$ for different initial values of h_0. The combined control path is illustrated in the inset. The linear fitting slope for $h_0 = -1, 0.2, 0.75, 0.85, 0.95$ is $-0.50283 \pm 5.0 \times 10^{-5}$, $-0.50697 \pm 6.0 \times 10^{-5}$, $-0.5237 \pm 1.0 \times 10^{-4}$, $-0.52800 \pm 5.0 \times 10^{-5}$, and $-0.5037 \pm 8.0 \times 10^{-4}$ respectively. In all cases, the system size $N = 400$.

quantum number $\mathcal{P}_k$ is conserved, and the ground state of H_k lies in the even sector $\mathcal{P}_k = 1$, the expansion coefficients $c_{2,k} = c_{3,k} = 0$, whereas $c_{0,k}$ and $c_{1,k}$ are obtained from expanding the ground state before the sudden quench in the eigenstate basis $\{|\psi_k^j(t_0^+)\rangle\}$ of the quenched Hamiltonian $H(h_c)$.

We can picture the resulting dynamics in terms of a combined sudden-adiabatic quench process (see Fig. 4.5, inset), except that unlike in Sec. 4.2.2 we only focus on the scaling behavior of the relative excitation density $\Delta n_{\rm ex}(t)$ created after the sudden quench. Exact numerical results are plotted in the main panel of Fig. 4.5, showing that for a large range of sudden-quench initializations, the final excitation density still obeys the same KZS,

$$\Delta n_{\rm ex}(t_f) \sim \tau^{-d\nu/(\nu z+1)} \sim \tau^{-1/2},$$

as in adiabatic dynamics starting from the ground state. The above scaling result can be derived

analytically in two limiting cases, starting from Eq. (4.13). Upon integrating over all the relevant modes, we find

$$\Delta n_{\rm ex}(t)=\frac{1}{\pi}\int_0^{k_{\rm max}}\Delta P_k(t)dk=\int_0^{k_{\rm max}}\left[(2|c_{0,k}|^2-1)|a_{0,k}(t)|^2+2{\rm Re}[c_{0,k}c_{1,k}^*a_{0,k}^*(t)a_{1,k}(t)]\right]\frac{dk}{\pi}. \qquad (4.24)$$

There are two contributions in $\Delta P_k(t)$. If the initial state of mode k is close to either a non-excited or to a fully excited state ($|c_{0,k}|^2\approx 1$ or $|c_{0,k}|^2\approx 0$ for all $k\in K_R$, respectively), the first term is the dominant one. In this case, KZS clearly holds. In the opposite limit where each mode $k\in K_R$ is initially half-excited ($|c_{0,k}|^2\approx 1/2$), the second term is the dominant one. Since, for a sudden quench to h_c, the latter is the center of the impulse region (recall Fig. 1, top) and at most half of the impulse region can be crossed, all the relevant modes can at most be close to half-excitation, making this second limiting case directly relevant to the sudden-quench state preparation for suitable h_0. Assuming that $|c_{0,k}|^2\approx 1/2$ and ignoring relative phases thus yields

$$\Delta P_k(t)\sim|a_{0,k}(t)a_{1,k}(t)|\sim|a_{0,k}(t)|\sqrt{1-|a_{0,k}(t)|^2}.$$

By invoking the LZ formula [79], the asymptotic ($t_f\to\infty$) excitation probability for modes near k_c scales like $e^{-2\pi k^2\tau}$ when $t_0\to-\infty$. Starting from QCP C (the center of the impulse region) will not, however, affect the exponential behavior [114]. Therefore, $|a_{0,k}(t)|^2\sim e^{-2\pi k^2\tau}$ as long as t_f is deep in the adiabatic region, and $1-|a_{0,k}(t)|^2\sim k^2\tau$. Integrating over the relevant modes then gives the anticipated KZS result:

$$\int_0^{k_{\rm max}}dk\,|a_{0,k}(t)|\sqrt{(1-|a_{0,k}(t)|^2)}\sim\int_0^{\tau^{-1/2}}dk\,k\,\tau^{1/2}\sim\tau^{-1/2},$$

where we used the fact that $k_{\rm max}\sim\tau^{-1/2}$ [Eq. (3.8)] in the upper integration limit.

While the above argument suffices to explain the emergence of KZS starting from *special* sudden-quench initializations, for generic quenches the dominant term in Eq. (4.24) need not be the same for different modes. In order to gain further insight, it is necessary to inspect the distribution of the excitation probability for each relevant mode after a sudden quench from a generic value $h_0\mapsto h_c$. Numerical results for the low-lying modes are presented in Fig. 4.6 for a wide range of

initial magnetic-field strength h_0. For each mode k, we can identify two boundary values, $h_{0,k}^{\min}$ and $h_{0,k}^{\max}$, such that when $h_{0,k}^{\min} \leq h_0 \leq h_{0,k}^{\max}$, mode k is close to its ground state after the sudden quench ($|c_{0,k}|^2 \approx 1$), whereas if $h_0 \ll h_{0,k}^{\min}$ or $h_0 \gg h_{0,k}^{\max}$, mode k is close to half-excitation ($|c_{0,k}|^2 \approx 1/2$). Since $h_{0,k}^{\min}$ and $h_{0,k}^{\max}$ are approximately symmetric with respect to the critical value $h_c = 1$, let us for simplicity take $h_{0,k}^{\mathrm{m}} \equiv h_{0,k}^{\max}$, with $h_{0,k}^{\min} \approx 2h_c - h_{0,k}^{\mathrm{m}}$. Qualitatively, $h_{0,k}^{\mathrm{m}}$ can be determined by the condition $\Delta(h_0, k) \approx \Delta(h_c, k)$, which yields approximately $|c_{0,k}|^2 \approx 1$. If, conversely, $\Delta(h_0, k) \gg \Delta(h_c, k)$ ($|h_0 - h_c| \gg |h_{0,k}^{\mathrm{m}} - h_c|$), we can consider $|c_{0,k}|^2 \approx 1/2$. Altogether, the results in Figs. 4.5-4.6 indicate that the limiting analytical condition of requiring the same dominant term in Eq. (4.24) for *all* the relevant modes is too strong for $\Delta n_{\mathrm{ex}}(t)$ to show KZS. For instance, when $h_0 = 0.95$, not all the relevant modes are staying in their ground state (k_c is not), yet KZS holds. In general, however, the variation of $|c_{0,k}|^2$ with k does affect the scaling result. For instance, when h_0 is around 0.75, agreement with the KZS prediction for the same system size is relatively poor, motivating one to roughly identify the range $0.6 \lesssim h_0 \lesssim 0.9$ with a cross-over region. Based on these observations, we conjecture that a necessary (and sufficient) condition for the relative excitation density $\Delta n_{\mathrm{ex}}(t)$ to approach KZS in the thermodynamic limit is that *the dominant term in Eq. (4.24) is the same for the majority of the relevant modes.*

An alternative physical interpretation of the above conjecture may be obtained by observing that for a generic value of h_0, there exist modes $k_e, k_g \in K_+$ such that if $k_c \leq k \leq k_e$, $\Delta(h_0, k) \gg \Delta(h_c, k)$, whilst if $k_g \leq k \leq \pi$, $\Delta(h_0, k) \approx \Delta(h_c, k)$, and we also assume $k_e < k_g$ for concreteness. Since, in an adiabatic sweep with speed τ, the set of relevant modes $K_R = [k_c, k_{\max}]$ is determined according to Eq. (3.8), we can distinguish three different regimes depending on how $k_{\max}$ is positioned relative to the interval $[k_e, k_g]$:

(i) $k_{\max} \leq k_e$: in this case, all the relevant modes are half-excited, recovering one of the limiting situations (analytically) leading to KZS, as already discussed (*e.g.*, $h_0 = -1$ in Fig. 4.5);

(ii) $k_e < k_{\max} < k_g$: in this case, by a reasoning similar to the one leading to Eq. (4.20), KZS is predicted to emerge provided that $(k_{\max} - k_e) = \varepsilon k_{\max}$, $\varepsilon \ll 1$, in such a way that the majority of the relevant modes are half-excited (*e.g.*, $h_0 = 0.2$ in Fig. 4.5);

(iii) $k_g \leq k_{\max}$: in this case, KZS is predicted provided that $k_g = \varepsilon k_{\max}$, $\varepsilon \ll 1$, in such a way that the majority of the relevant modes stay in their ground state (*e.g.*, $h_0 = 0.95$ in Fig. 4.5).

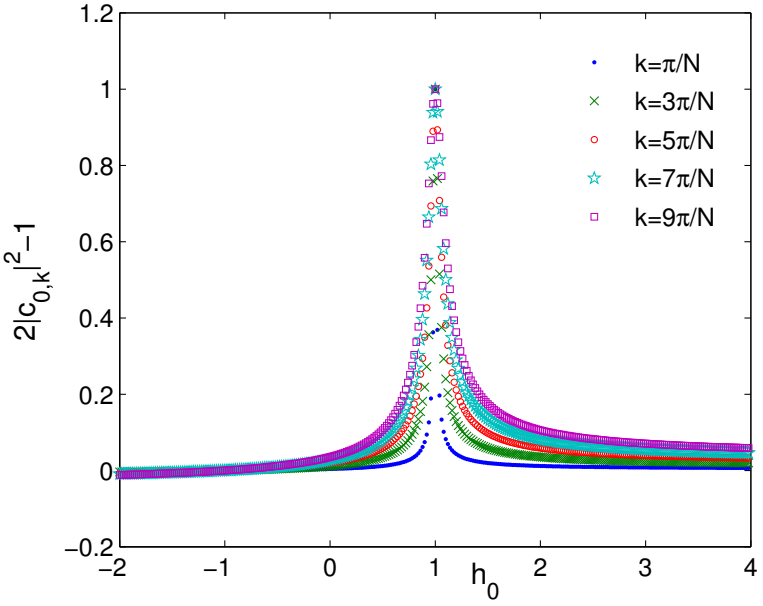

Figure 4.6: Dependence of the excitation coefficient $2|c_{0,k}|^2 - 1$ upon the initial magnetic-field strength h_0 in a state prepared by a sudden quench $h_0 \mapsto h_c$ in the Ising chain ($\gamma = 1$). The values $c_{0,k}$ are obtained by expanding the ground state of $H(h_0)$ in terms of the eigenbasis of $H(h_c = 1)$ at QCP C. The five lowest-energy modes are considered, for system size $N = 400$.

Thus, for both $h_0 = 0.75$ and $h_0 = 0.85$, the initial state prepared by the sudden quench may be interpreted to lie in the cross-over region between cases (ii) and (iii), explaining why the resulting scaling deviates appreciably from the KZ prediction.

Similarly to the excited-eigenstate initialization, sudden-quench initialization will also add more constraints on the appropriate τ range for KZS to hold. If the initial state is prepared via a sudden quench that guarantees one of the above conditions (i)–(iii) to be fulfilled for any $\tau \in [\tau_{\min}, \tau_{\max}]$, then the latter range is also appropriate for KZS to emerge under excited-eigenstate initialization. If not, the situation is more involved, and the range of τ may need to be adjusted such that either (ii) or (iii) is enforced. If condition (ii) is more likely to be obeyed (*e.g.*, if $h_0 \approx 0.6$), we can choose $\tilde{\tau}_{\min} > \tau_{\min}$ in such a way that the number of modes between k_e and k_g is decreased, and the majority of relevant modes is thus half-excited. If instead condition (iii) is more likely to be obeyed (*e.g.*, if $h_0 \approx 0.9$), we can choose $\tilde{\tau}_{\max} < \tau_{\max}$ in such a way that the number of relevant modes staying

in their ground state is increased. While the strategy for adjusting the τ-range in a sudden-quench initialization is similar to the one advocated in excited-eigenstate initialization, conditions (i)–(iii) are in fact easier to fulfill than Eq. (4.20). For instance, for $N = 400$, the worst scaling in Fig. 4.5 is still relatively close to KZS, whereas the latter is completely lost when initially only k_c is excited in Fig. 4.1(a). This difference is due to the fact that the initial occupation of modes in the relevant set changes less abruptly in a sudden-quench initialization than in excited-eigenstate initialization.

We conclude our discussion of quench processes originating from a (pure) excited state by commenting on the fact that the analysis developed for $\Delta n_{\rm ex}(t)$ can be extended to different observables without requiring major conceptual modifications. While an explicit example involving the spin correlator defined in Eq. (4.17) will be included in the next Section, the basic idea is to proceed in analogy with ground-state quenches, by taking into consideration the appropriate scaling exponent as determined by the physical dimension of the observable $\mathcal{O}$. Consider, for instance, the relative excitation energy $\Delta H(t)$ defined in Eq. (4.16) which, as remarked, can be experimentally more accessible than the relative excitation density. In all the situations where KZS holds for the latter, $\Delta n_{\rm ex}(t_f) \sim \tau^{-d\nu/(\nu z+1)} \sim \tau^{-1/2}$ (in particular, in the case of excited-state initialization via a sudden quench just discussed), we also find for our model that

$$\Delta H(t_f) \sim \tau^{-(d+z)\nu/(\nu z+1)} \sim \tau^{-1},$$

consistent with the corresponding ground-state scaling behavior.

4.3 Quantum Quenches from a Thermal State

4.3.1 Adiabatic Quench Dynamics

While we have only focused thus far on initialization mechanisms resulting in a *pure* excited state, another large class of initial states with a finite excitation energy may be obtained through dissipative means, in particular because the system may find itself (or be placed) in contact with a thermal bath. After a time sufficient for equilibration to occur, the system would then relax to a canonical ensemble at temperature T. In equilibrium, it is well known that the influence of a ground-state

QCP can cross over to a finite range of temperatures, the so-called "quantum critical regime," which is often broader than naively expected [116, 117, 1, 118]. In a dynamical scenario, how robust is dynamical scaling (in particular, KZS) to initialization at a finite-temperature? If scaling persists, how do the relevant non-equibrium exponents depend upon the initial temperature? Motivated by these questions, scaling behavior in a system initially prepared in a thermal equilibrium state *at criticality* and then adiabatically quenched away from the QCP has been analyzed in Ref. [88]. In particular, it is shown that for fermionic quasi-particles, the excess excitation due to a quench across a standard QCP obeys

$$\Delta n_{\rm ex}(t_f) \sim \frac{1}{T}\,\tau^{-(d+z)\nu/(\nu z+1)}, \tag{4.25}$$

provided that the initial temperature is high enough ($T \gg \epsilon_k(t_0)$, for all $k \in K_R$). Our goal here is to both present quantitative evidence for the above scaling law and, most importantly, to extend the analysis to multicritical QCPs.

Let T denote the initial thermal equilibrium temperature, so that the initial density operator has the form $\rho(t_0) = \bigotimes_{k\in K_+} \rho_k(t_0)$, with $\rho_k(t_0)$ given by:

$$\rho_{00,k}(t_0) = \frac{1}{\mathcal{Z}} e^{+\epsilon_k(h,\gamma)/T},\ \ \rho_{11,k}(t_0) = \frac{1}{\mathcal{Z}} e^{-\epsilon_k(h,\gamma)/T},\ \ \rho_{22,k}(t_0) = \rho_{33,k}(t_0) = \frac{1}{\mathcal{Z}}, \tag{4.26}$$

in units where $\hbar = k_B = 1$ and with

$$\mathcal{Z} \equiv 2 + e^{+\epsilon_k(h,\gamma)/T} + e^{-\epsilon_k(h,\gamma)/T}.$$

For clarity, we focus on linear adiabatic dynamics first. We shall study both the standard Ising QCP `C` under a magnetic-field quench of the form $h(t) = 1 - t/\tau$ [$h = h_c = 1, \gamma = 1$ in Eq. (4.26)], and the MCP `A` under a simultaneous quench of the magnetic field and the anisotropic parameter, $h(t) = 1 - \gamma(t) = 1 - t/\tau$ [$h = h_c = 1, \gamma = \gamma_c = 1$ in Eq. (4.26)]. At $T = 0$, the scaling of the excitation density can be in both cases described by $n_{\rm ex}(t_f) \sim \tau^{-d\nu z/[z_2(\nu z+1)]}$, where z_2 is determined from the scaling of the minimal gap along the path with respect to k [cf. Eq. 3.18, with $\alpha = 1$ and $d_2 = 0$]. Thus, $z_2 = z$ in the quench across QCP `C`, leading to KZS, whereas $z_2 = 3 \neq z$ in

the quench across MCP A, leading to anomalous scaling $n_{\rm ex}(t_f) \sim \tau^{-1/6}$. Given the above thermal initial condition, starting from Eq. (4.14) for the relative excitation probability, we find:

$$\Delta P_k(t) = \tanh\Big(\frac{\epsilon_k(h_c,\gamma_c)}{2T}\Big)|a_{0,k}(t)|^2, \tag{4.27}$$

where for both paths we simply write $\epsilon_k(h_c,\gamma_c)$ to mean that critical parameter values are assumed at $t = t_0$. When $T \leq \epsilon_k(h_c,\gamma_c)$, $\tanh\big(\frac{\epsilon_k(h_c,\gamma_c)}{2T}\big) \approx 1$ and $\Delta P_k(t)$ is the same as starting from the ground state of mode k. Thus, in order for the same ground-state scaling (either KZS or $\tau^{-1/6}$) to emerge in the low-temperature limit, the condition $T \leq \epsilon_k(h_c,\gamma_c)$ needs to be satisfied for all the relevant modes. Since $\epsilon_{k_c}(h_c,\gamma_c) = 0$, this means that in the thermodynamic limit, the only allowed initial temperature is $T = 0$ if a thermal state of $H(h_c,\gamma_c)$ is considered. In the opposite limit of high temperature, where $T \gg \epsilon_k(h_c,\gamma_c)$, $\tanh\big(\frac{\epsilon_k(h_c,\gamma_c)}{2T}\big) \approx \epsilon_k(h_c,\gamma_c)/(2T) \sim (k-k_c)^z/T$ for modes k near k_c. Upon integrating over the relevant modes and recalling Eq. (3.8), the relative excitation density is then:

$$\Delta n_{\rm ex}(t_f) = \frac{1}{\pi}\int_0^{k_{\rm max}} \Delta P_k(t_f) d^d k \sim \frac{1}{T}\int_0^{\tau^{-\nu z/[z_2(\nu z+1)]}} k^z d^d k = \frac{1}{T}\,\tau^{-(d+z)\nu z/[z_2(\nu z+1)]}. \tag{4.28}$$

For the standard QCP C, this yields $\Delta n_{\rm ex}(t_f) \sim \tau^{-1}/T$, recovering the result of Eq. (4.25), whilst $\Delta n_{\rm ex}(t_f) \sim \tau^{-1/2}/T$ in the multicritical quench across QCP A. As argued in Section 3.4 that the time-dependent excitation process in ground-state quenches need not be dominated by the critical mode k_c for certain paths across MCPs and $P_k = \Delta P_k \sim k^{d_2}$, with d_2 playing the role of an "effective dimensionality exponent". For a thermal quench, it is interesting to note that, formally, one may interpret $d_2 = z \neq 0$ in the above equation, also implying that the dominant contribution does *not* originate from modes around k_c. In the high temperature limit, $\rho_k(t_0)$ is, indeed, almost fully mixed for modes near k_c, causing the contribution of $\rho_{00,k}$ and $\rho_{11,k}$ to Eq. (4.14) to be nearly cancelled, and consistently leading to $\Delta P_k(t) \approx 0$ for those modes.

The scaling prediction in Eq. (4.28) can be further generalized to a *non-linear thermal quench*, whereby for instance $h(t) = 1-\gamma(t) = 1-(t/\tau)^\alpha$ in the case of a quench away from the MCP A. When $T = 0$, Eq. 3.18 yields $n_{\rm ex}(t_f) \sim \tau^{-d\alpha\nu z/[z_2(\alpha\nu z+1)]}$ [1]. Correspondingly, in the high-temperature

[1] We note that our prediction differs from the one recently established in [111], where a linearization procedure around the QCP is invoked in order to use the LZ formula.

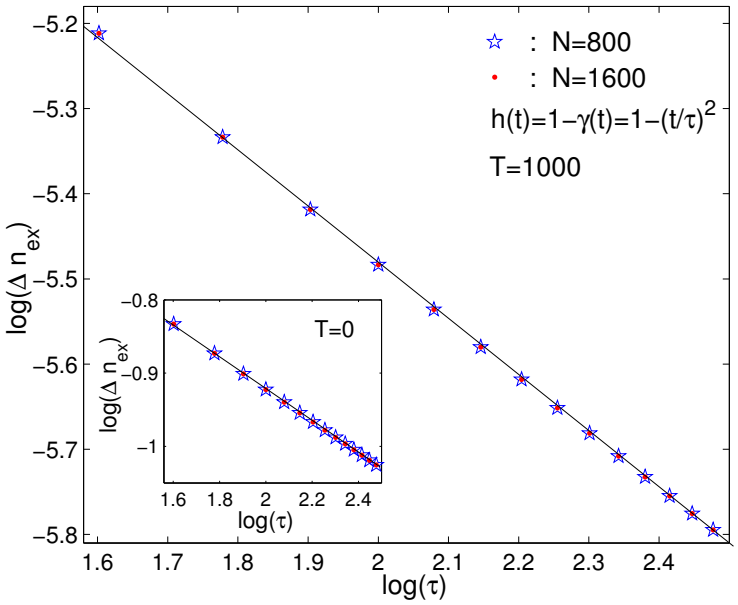

Figure 4.7: Exact scaling behavior of $\Delta n_{\rm ex}(t_f)$ in a quadratic adiabatic quench $h(t) = 1 - \gamma(t) = 1 - (t/\tau)^2$, starting from a thermal state at MCP B ($t_0 = t_c = 0$) toward the FM phase. The initial temperature $T = 1000$, yielding a linear fitting slope -0.663 ± 0.002, in good agreement with the value $2/3$ predicted by Eq. (4.29). For comparison, the case of a ground-state quench is reproduced in the inset, with a linear fitting slope of -0.2190 ± 0.0006, which is also in good agreement with the predicted $2/9$ exponent [112]. The data for different sizes ($N = 800$ and $N = 1600$) coincide up to 10^{-13}.

limit,

$$\Delta n_{\rm ex}(t_f) \sim \frac{1}{T}\,\tau^{-(d+z)\alpha\nu z/[z_2(\alpha\nu z+1)]}. \tag{4.29}$$

Exact numerical results for a quadratic quench ($\alpha = 2$) are reported in Fig. 4.7, the inset corresponding to the ground-state $T = 0$ case. Within numerical accuracy, the observed behavior is in excellent agreement with the predicted scaling, $\tau^{-2/9}$ for $T = 0$ and $\tau^{-2/3}$ for high-T, respectively.

We further examine how dynamical scaling is detected by other observables and how it is influenced by temperature away from the limiting regimes discussed above by considering the behavior of the spin correlator, $\Delta XX(t)$, defined in Eq. (4.17). Since XX does not commute with the Hamiltonian in Eq. (4.1), no analytical treatment is possible. Exact numerical results are presented in Fig. 4.8 for both the regular and the multicritical QCPs C and A (inset vs. main panel, respectively),

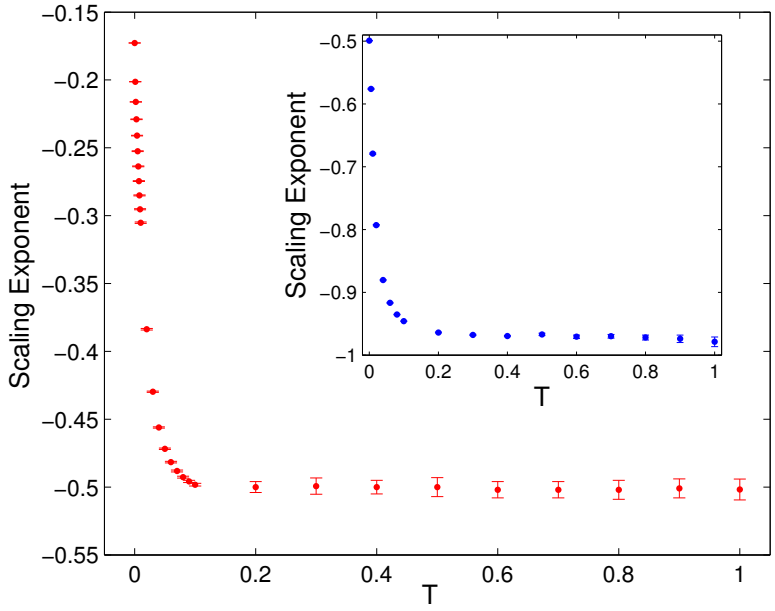

Figure 4.8: Main panel: Scaling exponent $\Delta XX(t_f)$ as a function of temperature T in a linear quench $h(t) = 1 - \gamma(t) = 1 - t/\tau$ away from the MCP `A`, starting with a thermal equilibrium state of $H(h_c, \gamma_c)$. Inset: Scaling exponent of $\Delta XX(t_f)$ as a function of temperature in a linear quench $h(t) = 1 + t/\tau$ away from the regular QCP `C`, starting with a thermal equilibrium state of $H(h_c = 1)$. In both cases, $N = 800$.

starting from the same thermal initial condition at criticality as considered above. As the data show, similar features emerge in both cases: the scaling exponent of $\Delta XX(t)$, which is expected to be the same as for $\Delta n_{\rm ex}$, deviates from its zero-temperature value ($-1/2$ or $-1/6$, respectively) as soon as the temperature is nonzero, and as the latter is gradually increased, it continuously changes until for sufficiently high temperature ($T \gg \epsilon_k(h_c, \gamma_c)$, for all $k \in K_R$), it stabilizes at the value predicted by Eq. (4.29) (-1 or $-1/2$, respectively). All these observations are consistent with the predictions in the previous paragraph.

In summary, we see that ground-state dynamical scaling (and KZS in particular) is fragile with respect to temperature fluctuations if the initial state is a thermal equilibrium state *at criticality*. In this case, the two situations where scaling exists are the zero-temperature and the high-temperature limit, with Eq. (4.29) holding in the latter regime. This requires *all* the relevant modes to either stay in their ground state or be highly mixed at the initial time, which is a stronger condition in

comparison to the ones identified in the previous sections for coherently-prepared (pure) excited states. From a practical standpoint, the high-temperature regime could potentially be relevant to liquid-state NMR simulators [108, 109]. In order for tests of dynamical scaling/KZS in the low-temperature regime to be experimentally viable, however, the initial thermal state needs to be (or be prepared) sufficiently *far away from criticality* (*e.g.*, $|h_0 - h_c| \gg 1$ for QCP C), in such a way that the condition $T \leq \Delta(k, h_0)$ for all $k \in K_R$ can still be fulfilled with a non-zero temperature.

4.3.2 Effective Thermalization

Before discussing the concept of effective thermalization, let us recall the standard meaning of thermalization, that is, the relaxation towards thermal equilibrium of a system in contact with reservoir (or bath). More precisely, let $\rho_{\rm B}$ be the thermal state of the bath, and $\rho_{\rm th}$ the state of the system at thermal equilibrium. A thermalization process may be defined by the following two requirements: (I) The state $\rho_{\rm th} \otimes \rho_{\rm B}$ is stationary; (II) If the system is prepared in a state ($\rho_{\rm ini}$) different from $\rho_{\rm th}$, at the end of the relaxation process we have a total state $\rho_{\rm SB}$ such that $\mathrm{Tr}_{\rm B}(\rho_{\rm SB}) = \rho_{\rm th}$ and $\mathrm{Tr}_{\rm S}(\rho_{\rm SB}) = \rho_{\rm B}$, where $\mathrm{Tr}_{\rm B(S)}$ is the partial trace over the bath (system) [119].

While the above approach focuses on a system in contact with a bath that has already reach thermal equilibrium, a related question is whether it is possible for an isolated system to reach a stationary state with thermal characteristics in the long-time limit. In this context, sudden quenches have recently attracted considerable interest as a setting for probing the long-time dynamics of isolated quantum many-body systems and the approach to equilibrium [85, 94, 95, 96, 97, 98]. Since the quadratic Hamiltonian in Eq. (4.1) describes a simple (non-interacting) integrable model, it is well known that no thermalization can occur in a proper sense, that is, the behavior of *generic* observables is not governed by a conventional statistical equilibrium ensemble [102, 90, 91, 92, 93]. The above investigations have nevertheless shown that information about the asymptotic behavior of an appropriate subset of observables may still be encoded in a finite *effective temperature* $T_{\rm eff}$, independent on the fine details of the initial state and the dynamics but only determined by the total energy of the process. Let $\rho(t_0) \equiv \rho_0$ and H_f denote, respectively, the density operator describing the initial state of the system, and the final Hamiltonian after the (instantaneous) quench. Following Rossini *et al.* [94], the effective temperature is defined by the requirement that the average energy

of the initial state relative to the quenched Hamiltonian equals the one corresponding to a *fictitious* thermal state at temperature $T_{\rm eff}$ in the canonical ensemble, that is,

$$\mathrm{Tr}[\rho_0 H_f] = \mathrm{Tr}[\rho_{T_{\rm eff}} H_f]. \tag{4.30}$$

Under the assumption that $T = 0$ initially [that is, ground-state initialization in Eq. (4.30)], the emergence of effective thermal behavior has been related to the *locality* properties of different physical observables relative to the quasi-particle language that diagonalizes the model [95, 96]. For a generic quench in a Ising chain, only non-local observables (such as the two-point correlation functions of the order parameter) have been found to thermalize, with both their asymptotic average value and the finite-time transient being determined by *equilibrium* statistical mechanics at $T_{\rm eff}$. Remarkably, however, thermal behavior has also been established for certain *local* observables (the transverse magnetization per site, $1/N \sum_j \sigma_z^j$, and the kink density, $\mathcal{N}$) *in quenches towards criticality*, the long-time value being still univocally determined by $T_{\rm eff}$.

Physically, it is clear that the concept of an effective temperature has a restricted validity and, for the model under investigation, it does *not* imply that an actual thermal ensemble emerges as a result of a sudden quench followed by free evolution under the quenched Hamiltonian. With that in mind, we further explore next the emergence of effective thermal behavior in *critical* quenches, by focusing on a different local observable and by extending the analysis in two directions: first, initialization in a thermal state at finite $T > 0$ and, second, sudden quenches to a multicritical QCP.

4.3.2.1 Sudden Quenches to a Standard Critical Point

Let us first consider a sudden quench of the magnetic field $h_0 \mapsto h_f$ in the Ising chain ($\gamma = 1$), starting from an initial state of the form given in Eq. (4.26), and focus on the long-time behavior of the number of quasiparticle excitations with momentum k. Since the corresponding observable commutes with the time-dependent Hamiltonian, the long-time expectation value $\langle \gamma_k^\dagger \gamma_k \rangle$ coincides with the one right after the quench. In order for the latter to be consistent with the equilibrium

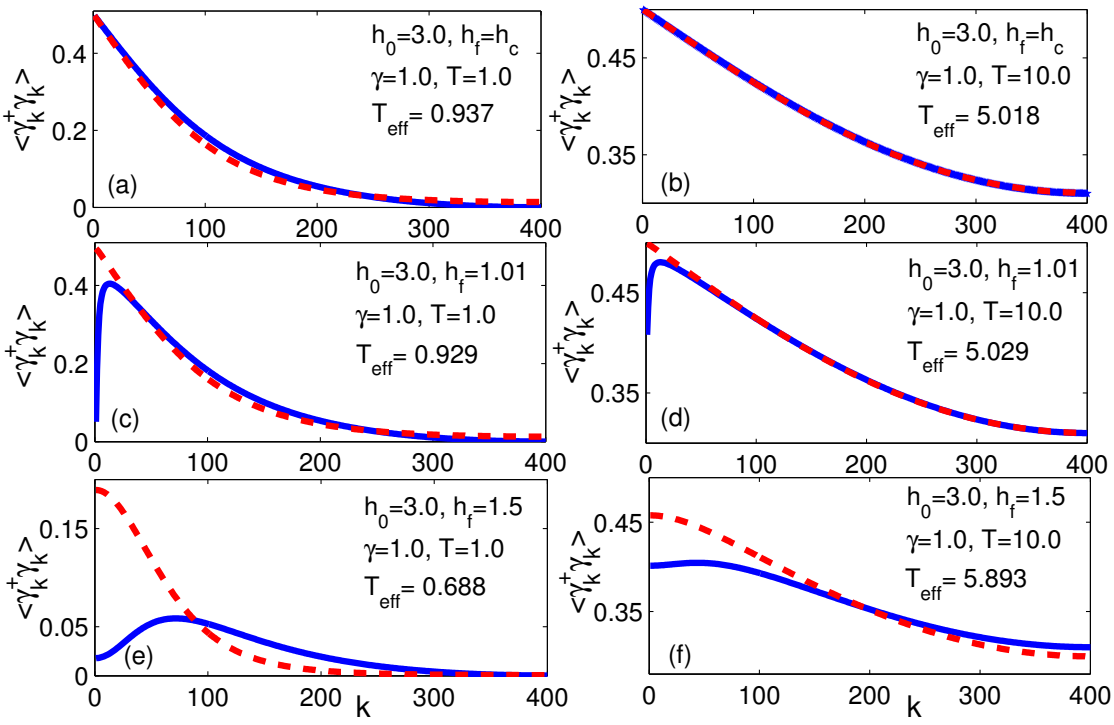

Figure 4.9: Comparison between the long-time average quasiparticle excitation following a sudden quench $h_0 \mapsto h_f$ starting from a thermal initial state at temperature T (dashed red) and the equilibrium value predicted by a fictitious thermal canonical ensemble at $T_{\rm eff}$ (solid blue). Panels (a), (c), (e): sudden quenches to $h_f = h_c = 1$, $h_f = 1.01$, $h_f = 1.5$, respectively, with initial temperature $T = 1.0$. The behavior for a ground-state quench ($T = 0$, data not shown) is qualitatively similar, with deviations from the thermal prediction being further pronounced. Panels (b), (d), (f): sudden quenches to $h_f = h_c = 1$, $h_f = 1.01$, $h_f = 1.5$, respectively, with initial temperature $T = 10.0$. In all cases, $N = 800$, and the value of $T_{\rm eff}$ obtained from is Eq. (4.30) is also given.

value at $T_{\rm eff}$, the following identity must hold:

$$(\rho_{00,k}(t_0) - \rho_{11,k}(t_0))|a_{0,k}|^2 + \rho_{11,k}(t_0) + \rho_{33,k}(t_0) = (1 + e^{+\epsilon_k(h_f,\gamma=1)/T_{\rm eff}})^{-1}, \tag{4.31}$$

where $|a_{0,k}|^2$ is the excitation probability of mode k due to the quench and Eq. (4.11) has been used in the left hand-side. The right hand-side is the fermionic thermal equilibrium prediction $\mathrm{Tr}[\rho^k_{T_{\rm eff}} \gamma^\dagger_k \gamma_k]$. Exact numerical results are presented in Fig. 4.9. Altogether, these data indicate that similar to the behavior of other local observables in a ground-state quench [95, 96], no effective thermalization is observed outside criticality [panels (c)–(f)], as expected. Even for a quench toward QCP C, however,

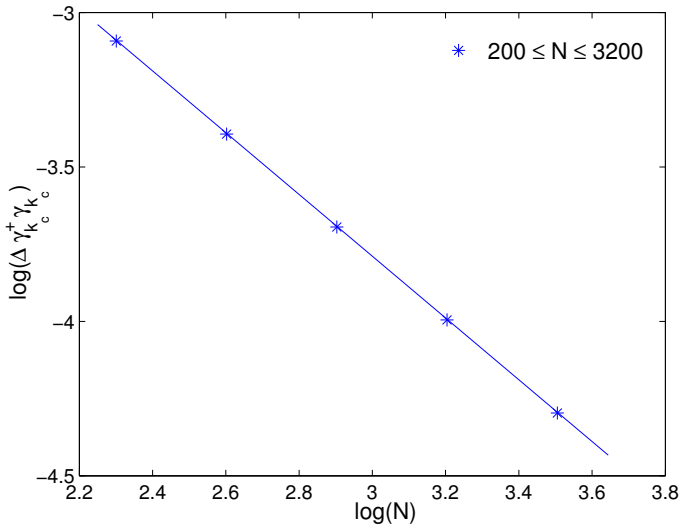

Figure 4.10: Difference between the long-time quasiparticle excitation of the critical mode k_c from its thermal equilibrium prediction as a function of system size for a sudden magnetic-field quench to h_c in the Ising chain. An initial thermal state with temperature $T = 1.0$ is considered. The linear fitting slope is $-0.99992 \pm 3 \times 10^{-5}$.

the initial temperature T *must be sufficiently high* in order for our chosen observable to thermalize [panel (a) vs. (b)].

In order to gain physical insight into what distinguishes a critical vs. non-critical quench in our case, and understand why effective thermal behavior fails to emerge outside criticality even for high initial temperature, it is useful to take a closer look at Fig. 4.9(d): clearly, the main difference between the equilibrium and the actual quasiparticle distribution arises from momentum modes close to k_c. On the one hand, since $\Delta(k_c, h_f)$ is the smallest gap at h_f, the maximum quasiparticle excitation is expected to occur at k_c from the equilibrium prediction [right hand side of Eq. (4.31)]. On the other hand, the peak of the observed distribution is located at modes close to k_c, but not exactly at k_c. Because the system is far from h_c, note that the difference of $\rho_{00,k}$, $\rho_{11,k}$, and $\rho_{33,k}$ for modes close to k_c is negligible. Thus, the main difference is due to $|a_{0,k}|^2$, which, as remarked, is the excitation probability of mode k at $T = 0$ after a sudden quench to h_c. Upon re-interpreting $|a_{0,k}|^2 \leftrightarrow 1 - |c_{0,k}|^2$, it is possible to make contact with the results shown in Fig. 4.6: clearly, the excitation probability of mode k_c changes dramatically for h_0 close to h_c, which suggests that k_c does

not contribute appreciably *unless* $h_f = h_c$. Instead, other modes close to k_c can be excited for values $h_f \approx h_c$ at which k_c is not yet excited. Since the excitation contribution from such "quasi-critical modes" would then be larger than the one from k_c, Eq. (4.31) would not hold. Accordingly, the only way to enforce the validity of Eq. (4.31) is through a sudden quench towards h_c, as observed.

Having clarified why criticality is essential, we need to assess whether the requirement of a sufficiently high initial T may be related to the finite system size or will persist in the thermodynamic limit. We focus on a sudden quench $h_0 = 3.0 \mapsto h_c$ at $T = 1.0$, and analyze how the long-time average of the total quasiparticle density $1/N \sum_k \gamma_k^\dagger \gamma_k$ deviates from the thermal equilibrium prediction at T_{eff} as N is increased. While we found that the observed deviations are practically constant over the range of N explored (data not included), the difference between $\langle \gamma_{k_c}^\dagger \gamma_{k_c} \rangle$ and its corresponding thermal prediction at T_{eff} *does decrease* with increasing N: as seen in Fig. 4.10, such a difference $\Delta \gamma_{k_c}^\dagger \gamma_{k_c} \sim N^{-0.99992}$ at $T = 1.0$, implying a vanishing difference and effective thermal behavior also at low temperature *for the critical mode* as $N \to \infty$. This property, however, stems from the fact that the gap of k_c closes in the thermodynamic limit, which is not true for the gap of other modes. For either the number of quasiparticles in a generic mode or for the total quasiparticle density, we thus conjecture that even in the thermodynamic limit, thermal behavior will be observed following sudden quenches to the QCP `A` *only if* $T \gg \Delta_k(h_c, \gamma = 1)$ *for all the relevant modes.*

4.3.2.2 Sudden Quenches to a Multi-critical Point

In view of the peculiar features that distinguish a multicritical QCP, as reflected in particular in anomalous scaling behavior, it is not obvious whether the above condition would still suffice for the same observables to thermalize in a sudden quench towards MCP `A`. Exact results for two sudden multicritical quenches of the form $(h_0 = 1 + \gamma_0 \mapsto h_f = 1 + \gamma_f, \gamma_0 \mapsto \gamma_f)$ are given in Fig. 4.11, starting from a thermal state at high temperature: specifically, MCP `A` is both reached via a sudden quench from the PM phase (left panel) and via a sudden quench from the FM phase (right panel). Contrary to the high-temperature scenario for the regular QCP `C` [Fig. 4.9(b)], *no* thermal behavior emerges, the observed expectation value $\langle \gamma_k^\dagger \gamma_k \rangle$ for modes close to k_c being significantly smaller or larger than the thermal equilibrium prediction, respectively.

This anomalous long-time behavior can be traced back to the asymmetry of the impulse region

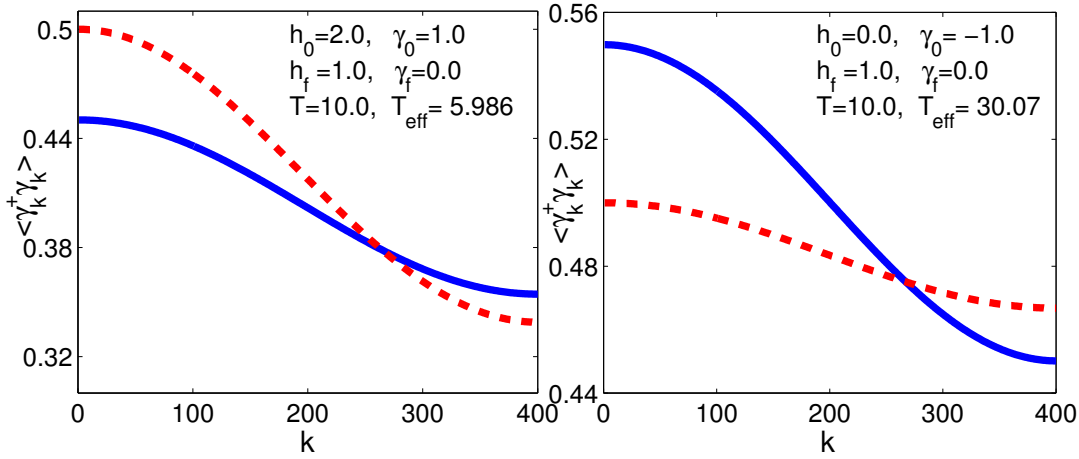

Figure 4.11: Comparison between the long-time quasiparticle excitation following a sudden quench $h_0 \mapsto h_f = h_c = 1, \gamma_0 \mapsto \gamma_f = \gamma_c = 0$ towards the MCP `B` (blue) and the equilibrium value predicted by a fictitious thermal ensemble at T_{eff} (red). The system is initially in a thermal state with temperature $T = 10$. Left: Initial state is the thermal state at $h_0 = 2.0, \gamma_0 = 1.0$ (inside the PM phase). Right: Initial state is the thermal state at $h_0 = 0.0, \gamma_0 = -1.0$ (inside the FM phase). Notice that due to the fact that the excitation probability of low-energy modes exceeds $1/2$, T_{eff} is much higher than in any other situation with the same initial T, cf. Fig. 4.9(b, d, f) and Fig. 4.11(a).

along the control path, as sketched in Fig. 1.1(bottom). Recalling the discussion in Section 3.4, the location of the minimum gap for each mode k along the path $h = 1 + \gamma$ is determined by requiring $\partial \Delta_k(\gamma, 1+\gamma)/\partial\gamma = 0$, that is,

$$\tilde{\gamma}(k) = (\cos k - 1)/(1 + \sin k^2) < 0,$$

which indicates that the center of the impulse region is largely shifted into the FM phase for each k. As a result, after a sudden quench to the MCP `A` from the FM phase, the excitation probability of low-energy modes tends to be greater than $1/2$, whereas for a sudden quench to MCP `A` from the PM phase, the excitation probability of low-energy modes tends to be smaller than $1/2$. Since the thermal equilibrium value is close to $1/2$ in the high-temperature limit for low-energy modes, thermal behavior is not realized in either quench process.

Based on the above results, we conjecture that *quenching toward the center of the impulse region* is a necessary requirement for $\gamma_k^\dagger \gamma_k$ or $1/N \sum_k \gamma_k^\dagger \gamma_k$ to thermalize following a sudden quench. While

typically this is the case in a quench to a regular QCP (for instance, a sudden quench of h to QCP C at fixed $\gamma = 1$), for a sudden quench to MCP A along the path $h = 1+\gamma$, the location of the minimum gap (hence the center of the impulse region) is different for each mode k, preventing thermalization to be possible along this path irrespective of the final values h_f, γ_f. More generally, we expect the above requirement to be *necessary* for local observables other than those examined here. In this context, it would be interesting to explore, for instance, whether the transverse magnetization or the density of kinks would still effectively thermalize in a multicritical quench to QCP A from the ground state.

We also remark that in a recent work [97], general conclusions have been reached for the equilibrium distribution after a sudden quench, predicting, in particular, effective thermal behavior for generic observables when the quench is performed around a non-critical point, and poor equilibration otherwise. While at first these results seem to contradict both our present conclusions for critical quenches towards QCP C in the appropriate temperature regime as well as earlier results for zero temperature [95, 96], a crucial assumption in Ref. [97] is a small quench amplitude, causing only a small number of excited states to effectively contribute around a QCP. The opposite condition is implied throughout our discussion, the sudden quench amplitude being in fact large enough for the number of excited states involved in a critical quench to outweigh those involved in a non-critical one (cf. Fig. 4.6). In the light of that, we also conjecture that having a *sufficiently large number of states* involved in the excitation process is a general necessary condition for effective thermalization after a sudden quench.

Chapter 5

Quantum-Critical Decoherence Dynamics in the XY Chain

The superposition principle in quantum mechanics allows arbitrary linear combinations of any states as a possible quantum state. However, in reality, no system is completely isolated from its surounding environment. Thus, the environment can destroy coherence between the states of a quantum system, and irreversibly degrade pure states into statistical mixtures. This is *decoherence* [126]. From the point of view of QIS, decoherence tends to destroy the entanglement of a quantum state, and it is thus crucial that decoherence can be controlled. On the other hand, from the point of view of condensed-matter physics, just similar to using entanglement as a bridge between QIS and condensed-matter physics, a natural question is, Can we borrow concepts from the theory of open quantum systems, in particular exploit decoherence properties, to detect and further study QPTs?

It has been shown in Ref. [122] that, when a spin qubit is transversely coupled to a Ising chain with transverse magnetic field, that is, the coupling Hamiltonian is proportional to $\sigma_S^z \sum_{i=1}^N \sigma_i^z$, the decay of the qubit coherence (quantified by a factor $D(t)$) is enhanced when the Ising-chain environment undergoes a QPT. Thus, the decoherence of the qubit can be used as a probe of the static quantum-criticality of the environment. In a dynamical secnario, would the decoherence factor still be a useful indicator of the dynamical QPT of the environment, in the sense of exhibiting (generalized) KZS?

In a recent work [121], it is found that the exponent of the decoherence factor of the test qubit exhibits KZS when the Ising environment is driven through the QPT with a constant quench speed. How universal the scaling of the decoherence factor would be, given that it is an dynamical indicator based on a *reduced* (as opposed to full) dynamics? Would the way in which various critical properties reflect into decoherence behavior be different than for other criticality indicators studied in previous Chapters? Since the excitation density shows anomalous scaling behavior for certain quench paths across a MCP, how would the scaling behavior of $D(t)$ change when a MCP is involved, in particular, will $D(t)$ still exhibit KZS or will the scaling change accordingly, just like the excitation density?

In Chapter 4, the robustness of KZS was studied with respect to different finite-energy initial states. In particular, when a thermal equilibrium initial state is considered, the relative excitation density has been found to exhibit a different scaling behavior in the high-temperature limit, compared with the low-temperature limit. Since the decoherence factor is, in principle, measurable in experiments [124, 125], and since in realistic experiments zero-temperature is unaccessible, a relevant question would also be, To what extent can scaling behavior be usefully detected and extracted for initial thermal states? Would a similar crossover scaling behavior from low-temperature to high-temperature exist for the decoherence factor as well? Or would it exhibits a behavior similar to the static case, where the signature of critical behavior of the environment would only exist in a finite (small) temperature window [123]?

With these questions in mind, in this last Chapter we present preliminary results on the decoherence of a central qubit,

$$|\psi\rangle = c_+|\uparrow\rangle + c_-|\downarrow\rangle,$$

coupled to a quantum spin XY chain transversely. The Hamiltonian for the whole system-environment reads:

$$H = H_E + H_{SE} = -\sum_{i=1}^{N}\left(\frac{1+\gamma}{2}\sigma_i^x\sigma_{i+1}^x + \frac{1-\gamma}{2}\sigma_i^y\sigma_{i+1}^y - h\sigma_i^z\right) - \delta\sigma_S^z\sum_{i=1}^{N}\sigma_i^z, \tag{5.1}$$

where the first term is the Hamiltonian of the environment, the second term describes the coupling between the environment and the central qubit [1], and δ is the coupling strength between the two. In

[1] In principle, the total Hamiltonian H should also include the system Hamiltonian H_S. Here, to simplify our calculation, H_S is taken to be zero.

Section 5.1, we will consider the scaling behavior of the decoherence factor $D(t)$ when the environment undergoes a standard QCP by a linear quench of the magnetic field strength, $h \mapsto h(t) = 1 - t/\tau$ (without loss of generality, $\gamma = 1$ is fixed), *e.g.* QCP `C` in the phase diagram Fig. 2.4, for both zero-temperature and finite-temperature cases. In Section 5.2, we will instead discuss the scaling behavior of $D(t)$ when the environment crosses a MCP along the paths where the excitation density shows anomalous KZS, *e.g.* from FM (PM) to MCP `A` in the phase diagram of Fig. 2.4.

5.1 Scaling of the Decoherence Factor in Adiabatic Quenches: Standard Critical Point

5.1.1 Zero-Temperature Results

Let us first revisit the results obtained in Ref. [121]. Initially, the state of the whole system is:

$$|\psi(t_0) = |\varphi_{GS}(t_0)\rangle \otimes (c_+|\uparrow\rangle + c_-|\downarrow\rangle), \tag{5.2}$$

where $|\varphi_{GS}(t_0)\rangle$ is the ground state of the environment with Hamiltonian $H_E(h(t_0))$. Thus, we can express $|\varphi_{GS}(t_0)\rangle = \prod_{k\in K_+} |0_k 0_{-k}(t_0)\rangle$, defined in Eq. (4.6). From Eq. (5.1), we can tell that when the central spin is in the $|\uparrow\rangle$ state, the environment will evolve with the Hamiltonian $H_E(h(t) + \delta)$, whereas when the central spin is in the $|\downarrow\rangle$ state, the environment will evolve with the Hamiltonian $H_E(h(t) - \delta)$. Thus, let $U_\uparrow(t)$ be the time propagator of the environment with an effective Hamiltonian $H_E(h(t) + \delta)$, that is:

$$U_\uparrow(t) = \hat{T} e^{-i\int_{t_0}^{t} dt H_E(h(t)+\delta)},$$

where $\hat{T}$ is the time-ordering operator. Similarly,

$$U_\downarrow(t) = \hat{T} e^{-i\int_{t_0}^{t} dt H_E(h(t)-\delta)}$$

is the time propagator of the environment with an effective Hamiltonian $H_E(h(t)-\delta)$. Thus, the total propagator for the whole system becomes:

$$U(t) = U_{\uparrow}(t) \otimes |\uparrow\rangle_S\langle\uparrow| + U_{\downarrow}(t) \otimes |\downarrow\rangle_S\langle\downarrow|. \tag{5.3}$$

Therefore, the time-evolved state of the whole system at time t is:

$$\begin{aligned} |\psi(t)\rangle &= U(t)|\varphi_{GS}(t_0)\rangle \otimes (c_+|\uparrow\rangle + c_-|\downarrow\rangle) \\ &= c_+|\uparrow\rangle \otimes U_{\uparrow}(t)|\varphi_{GS}(t_0)\rangle + c_-|\downarrow\rangle \otimes U_{\downarrow}(t)|\varphi_{GS}(t_0)\rangle \\ &= c_+|\uparrow\rangle \otimes |\varphi_+(t)\rangle + c_-|\uparrow\rangle \otimes |\varphi_-(t)\rangle. \end{aligned} \tag{5.4}$$

Then the time-dependent reduced density matrix of the central qubit in the σ_z basis is:

$$\rho_S(t) = \begin{pmatrix} |c_+|^2 & c_+^* c_- \langle\varphi_+(t)|\varphi_-(t)\rangle \\ c_-^* c_+ \langle\varphi_-(t)|\varphi_+(t)\rangle & |c_-|^2 \end{pmatrix},$$

The decoherence factor is defined as $D(t) \equiv |\langle\varphi_+(t)|\varphi_-(t)\rangle|^2$ in Ref. [121], which means that in the limit $D(t) = 0$, any coherent relation between $|\uparrow\rangle$ and $|\downarrow\rangle$ is completely lost, while in the limit $D(t) = 1$, the coherent relation is maintained. Effectively speaking, turning on the system-environment coupling at the initial time is like a sudden quench of the environment Hamiltonian from $H_E(h(t_0))$ to $H_E(h(t_0) \pm \delta)$ for the $|\varphi_\pm(t)\rangle$ branch, respectively. Then the environment Hamiltonian is followed by an adiabatic linear quench. Thus, the procedure for obtaining $|\varphi_+(t)\rangle$ ($|\varphi_-(t)\rangle$) is similar to our calculation for combined (sudden-plus-adiabatic) quenches described in Section 4.2.3. Because of the non-interacting picture of different momentum modes, each momentum mode evolves independently, thus: $U_{\uparrow}(t) = \prod_{k\in K_+} U_{k,\uparrow}(t)$, and $U_{\downarrow}(t) = \prod_{k\in K_+} U_{k,\downarrow}(t)$, leading to $|\varphi_+(t)\rangle = \prod_{k\in K_+} |\varphi_{k,+}(t)\rangle$, $|\varphi_-(t)\rangle = \prod_{k\in K_+} |\varphi_{k,-}(t)\rangle$.

In Ref. [121], it was assumed that $|\varphi_{k,\pm}(t)\rangle = \tilde{u}_k^{\pm}(t)|\mathtt{vac}\rangle - \tilde{v}_k^{\pm} c_k^\dagger c_{-k}^\dagger |\mathtt{vac}\rangle$, then the evolution of

$\tilde{u}_k^{\pm}$ and $\tilde{v}_k^{\pm}$ satisfies the following Schrödinger equation:

$$i\frac{d}{dt}\begin{pmatrix} \tilde{u}_k^{\pm}(t)_k(t) \\ \tilde{v}_k^{\pm}(t)_k(t) \end{pmatrix} = \begin{pmatrix} 2(h(t)\pm\delta - cosk) & 2\sin k \\ 2\sin k & -2(h(t)\pm\delta - cosk) \end{pmatrix}\begin{pmatrix} \tilde{u}_k^{\pm}(t)_k(t) \\ \tilde{v}_k^{\pm}(t)_k(t) \end{pmatrix}. \tag{5.5}$$

From the Landau-Zener analysis of the time-evolution of each mode k, we have

$$\begin{aligned}
\tilde{u}_k^{\pm}(t)_k(t) &= e^{-\pi\tau'/16}e^{i\pi/4}\big[(1+n)D_{-n-2}(iz_{\pm} + iz_{\pm}D_{-n-1}(iz_{\pm})\big] \\
\tilde{v}_k^{\pm}(t)_k(t) &= \frac{\sqrt{\tau'}}{2}e^{-\pi\tau'/16}D_{-n-1}(iz_{\pm}),
\end{aligned}$$

where $D_\nu(z)$ is the Weber function, τ' is the rescaled quench rate (see Eqs. (11) and (12) in Ref. [121]). If we express

$$D(t) = \prod_{k\in K_+} |\langle\varphi_{k,+}(t)|\varphi_{k,-}(t)\rangle|^2 \equiv \prod_{k\in K_+} F_k,$$

in the large N limit, one may approximate

$$D(t) \approx e^{-\frac{N}{2\pi}\int_0^{\pi}\ln F_k^{-1}}. \tag{5.6}$$

Then, it is predicted that for quenches across QCP C the following scaling behavior holds:

$$D(t) \sim e^{-\tau^{-N\nu/(\nu z+1)}}, \tag{5.7}$$

in which an expansion of the Weber functions was used to obtain the approximate behavior of $u_k'(t)$ and $v_k'(t)$. The physical understanding of the scaling result in Eq. (5.7) is that the time-evolution of the whole mode set can be separated into two parts: relevant modes vs. non-relevant modes. The number of relevant modes scales with $\tau^{-1/2}$, which enters into the integral of F_k, while the integral for the non-relevant modes does not depend on τ.

Since there is an oscillating behavior of $D(t)$ when the final magnetic field $h(t_f)$ is not at QCP C, as it was shown in Ref. [121], it would not be easy to observe dynamical scaling behavior. Thus, in our numerical simulation, we choose to quench from large negative $h(t_0)$ (say $h(t_0) = -10$) to

$h(t_f) = h_c = 1$, and we find that, instead of Eq. (5.7), the following scaling holds:

$$D(h_c = 1, \gamma_c = 1) \sim e^{-\tau^{1/2}}, \tag{5.8}$$

which is presented in Fig. 5.1. It was clearly stated in Ref. [121] that the Weber function expansion that was used is only valid when the final $h(t_f)$ is *not* at the QCP. However, it would be interesting to know what physical difference corresponds to this change of scaling behavior of the decoherence factor for quenches to a critical vs. non-critical point. This is different from the scaling results of other dynamical indicators we studied before, for which the same scaling behavior exist throughout the entire time-evolution [1].

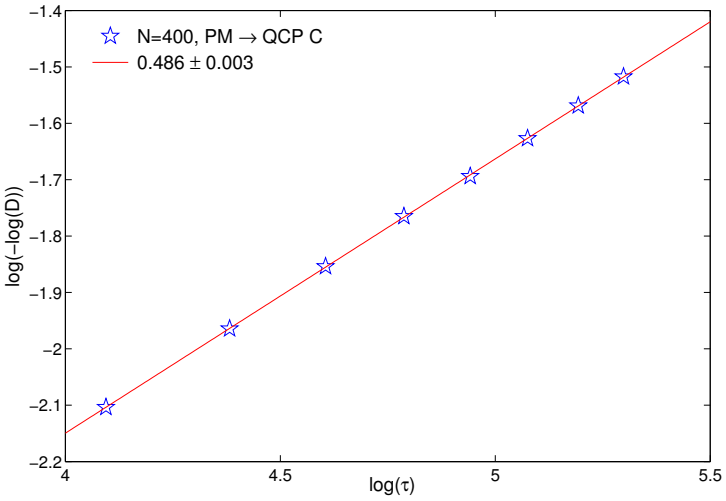

Figure 5.1: Scaling behavior of the decoherence factor in a linear quench of the magnetic field strength $h(t)$ towards the QCP C, with initial ground state of the Ising environment Hamiltonian.

[1] Notice that this is, in some sense, in analogy to our observation in Section 4.3.2, where a sudden quench to standard QCP vs. non-QCP shows different effective thermalization behavior.

5.1.2 Finite-Temperature Results

Next, let us assume that the environment is initially in a thermal equilibrium state at temperature T. The initial density matrix for the whole system would then be:

$$\rho_{SE}(t_0) = \rho_E(t_0) \otimes \rho_S(t_0) = \Big(\bigotimes_{k \in K_+} \rho_k(t_0)\Big) \otimes \rho_S(t_0), \tag{5.9}$$

where the expression of $\rho_k(t_0)$ is given in Eq. (4.26), that is:

$$\begin{aligned} \rho_k(t_0) &= \frac{1}{\mathcal{Z}} e^{+\epsilon_k(h(t_0),1)/T} |0_k, 0_{-k}\rangle\langle 0_k, 0_{-k}| + \frac{1}{\mathcal{Z}} e^{+\epsilon_k(h(t_0),1)/T} |1_k, 1_{-k}\rangle\langle 1_k, 1_{-k}| \\ &+ \frac{1}{\mathcal{Z}} |0_k, 1_{-k}\rangle\langle 0_k, 1_{-k}| + \frac{1}{\mathcal{Z}} |1_k, 0_{-k}\rangle\langle 1_k, 0_{-k}|. \end{aligned} \tag{5.10}$$

Accordingly, the time-evolved density matrix for the whole system is $\rho_{SE}(t) = U(t)\rho_{SE}(t_0)U^\dagger(t)$, whereby

$$\rho_S(t) = \mathrm{Tr_E}\rho_{\mathrm{SE}}(t) = \begin{pmatrix} |c_+|^2 & c_+^* c_- d(t) \\ c_-^* c_+ d(t)^* & |c_-|^2 \end{pmatrix}, \tag{5.11}$$

with

$$\begin{aligned} d(t) &= \mathrm{Tr_E}\left[U_\uparrow(t)\rho_{\mathrm{E}}(t=0)U_\downarrow^\dagger(t)\right] \\ &= \prod_{k \in K_+} \Big(\frac{1}{\mathcal{Z}} e^{+\epsilon_k(h(t_0),1)/T} \langle 0_k, 0_{-k}(t_0)|U_{k,\uparrow}(t)U_{k,\downarrow}^\dagger(t)|0_k, 0_{-k}(t_0)\rangle \\ &+ \frac{1}{\mathcal{Z}} e^{-\epsilon_k(h(t_0),1)/T} \langle 1_k, 1_{-k}(t_0)|U_{k,\uparrow}(t)U_{k,\downarrow}^\dagger(t)|1_k, 1_{-k}(t_0)\rangle + \frac{2}{\mathcal{Z}}\Big). \end{aligned}$$

In order to investigate the role of the temperature on the scaling behavior of the decoherence factor $D(t) = |d(t)|^2$, we choose the same quench path as in Section 5.1, but now with a different initial temperature. Exact numerical results are shown in Fig. 5.2, where KZS still exists for $T = 1.5$, however, for $T = 1.9$, $D(h_c)$ exhibits oscillation behavior. Interestingly, the latter is also seen for a quench towards a non-critical point at zero temperature. Thus, the oscillating behavior for finite temperature might be an indication of the fact that the thermal fluctuations wash out the critical

behavior of the environment, which is also true for the static behavior of the decoherence factor [123]. Since one of the motivation to study the scaling behavior of decoherence factor is to detect QPT in a realistic setting, one might wonder whether $T = 1.5$ is realizable in an accessible experiment. Notice that in Eq. (5.10), we set $\hbar = k_B = 1$. Thus, temperature is roughly of the same order of energy units, that is, the coupling strength J between nearest spins in the xy plane. Suppose that the spin coupling strength is a few meV [1], then $T = 1$ corresponds to about $10K$. The initial magnetic field strength $h(t_0) = 10$ implies that $\frac{eB\hbar}{mc}$ is on the order of 10meV, thus the magnetic field strength $B \sim 100T$, which is too high to access. However, the initial magnetic field does not need to be so high since as along as the starting point is deep in the PM or FM phase, that is, when $B \sim 10T$, the scaling behavior should still be observed. Thus, it might be possible to test the scaling of $D(t)$ in an experiment.

5.2 Scaling of the Decoherence Factor in Adiabatic Quenches: Multi-Critical Point

In order to understand whether the scaling of the exponent of the decoherence factor is related to KZS, we further explore the behavior of $D(t)$ for quenches equivalent to path 4 and path 5 across the MCP `A` studied in Section 3.4, where anomalous scaling behavior of the excitation density was found. To simplify our discussion, initial zero temperature of the environment is considered. Thus, the only difference between the discussion in this Section and Section 5.1 is the quench paths. Because of the oscillating behavior of $D(t)$ for quenches towards a non-critical point, we choose two paths parameterized as follows: (I) $h(t) = 1 + \gamma(t) = 1 + t/\tau$, say from $h(t_0) = 0(\gamma(t_0) = -1)$ to MCP `A`; (II) $h(t) = 1 + \gamma(t) = 1 - t/\tau$, say from $h(t_0) = 10(\gamma(t_0) = 9)$ to MCP `A`, in which the excitation density scales as $\tau^{-1/6}$, $\tau^{-3/4}$ respectively. Surprisingly, our numerical results (shown in Fig. 5.3) indicate that for path (I):

$$D^{(I)}(h_c = 1, \gamma_c = 0) \sim e^{-\tau^{0.835}} \approx e^{-\tau^{5/6}}, \tag{5.12}$$

[1] In a recent experiment [127], the magnetic $Co2^+$ ions in $CoNb_2O_6$ are arranged into near-isolated ferromagnetic Ising chain, where the sufficiently low exchange energy J of a few meV can be matched by experimentally attainable magnetic fields ($10T \sim 1meV$) to access the QCP.

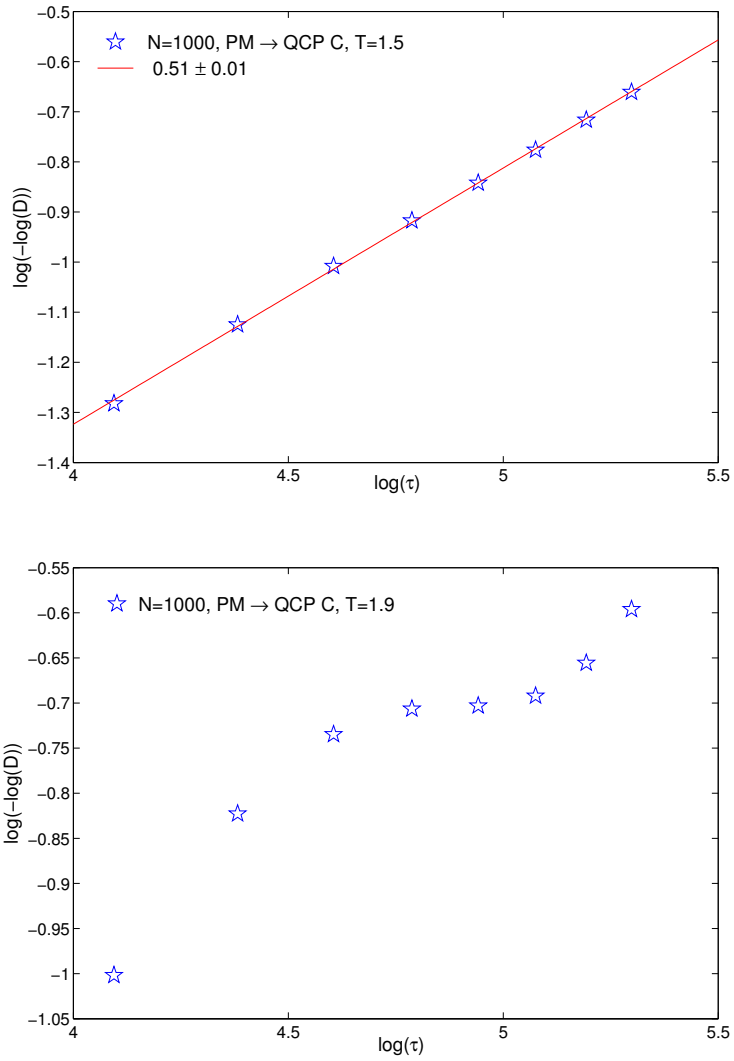

Figure 5.2: Scaling behavior of the decoherence factor in a linear quench of the magnetic field strength $h(t)$ towards the QCP C for different initial temperature of the environment. $T = 1.5$ ($T = 1.9$) for the top (bottom) panel.

while for path (II):

$$D^{(II)}(h_c = 1, \gamma_c = 0) \sim e^{-\tau^{0.277}} \approx e^{-\tau^{1/4}}. \tag{5.13}$$

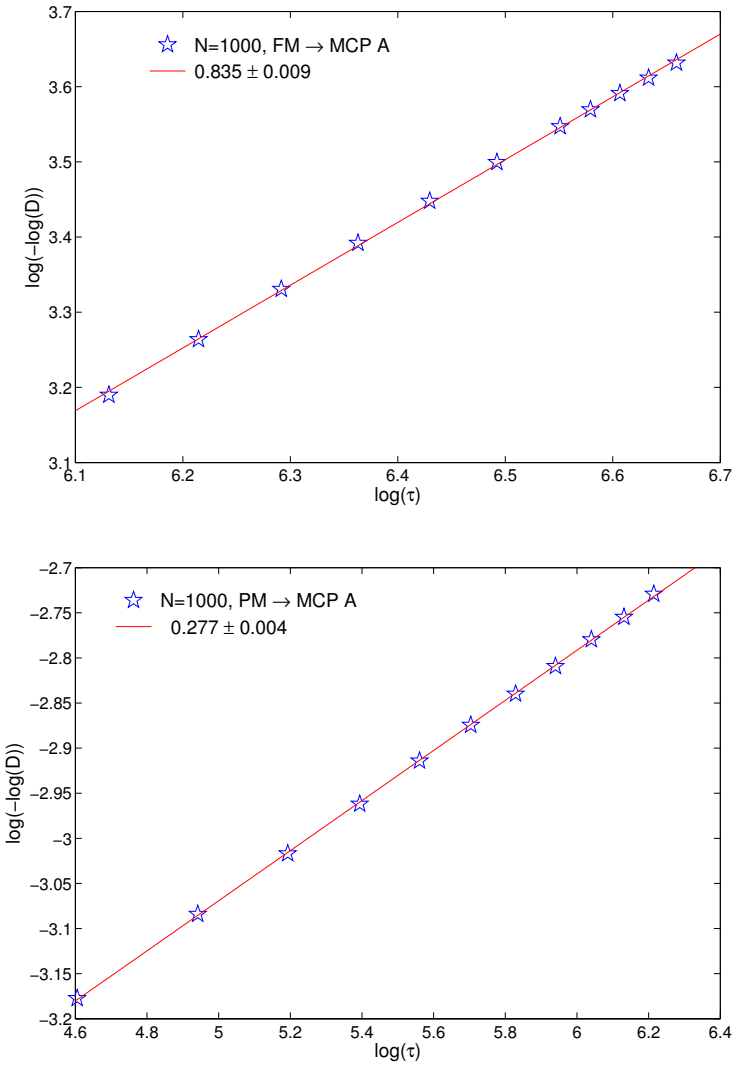

Figure 5.3: Scaling behavior of the decoherence factor for the quench path (I) (top panel) and (II) (bottom panel) at zero temperature.

Interestingly, the results obtained in this Section, together with the results in Section 5.1 imply that the scaling behavior of $D(t)$ at a QCP may be described as follows:

$$D \sim e^{-\tau^{1+\eta}}, \tag{5.14}$$

where η is the scaling behavior of the excitation density along the same path. $\eta = -1/2, -1/6, -3/4$, respectively, for quenches towards QCP C, and MCP A along paths 4, 5. However, what is the physical understanding of the above $(1 + \eta)$ scaling needs further investigation. I think that a possible explanation might be the role of the quench time. In fact, in decoherence dynamics, one important difference between the decoherence factor and other dynamical indicators we studied is that decoherence is closely related to the total time of evolution: The longer the time evolution of the central qubit is, the larger the amount of decoherence becomes. In all our discussion, when we choose the initial and final point on the phase diagram, the evolution time scales with τ^1. Perhaps this is the origin of τ^1 in Eq. (5.14).

Chapter 6

Conclusion and Outlook

In summary, in my Thesis research, I have addressed the non-equilibrium dynamics of a class of one-dimensional exactly solvable XY models perturbed by both adiabatic and sudden quenches. The main findings emerging from this study may be itemized as follows:

- **Kibble-Zurek Scaling.**

(i) Initial ground state: In an appropriate range of quench rate, KZS is found to exist for a large variety of extensive observables throughout the whole time evolution for adiabatic quench across an isolated (non-multicritical) QCP provided that the excess amount relative to the adiabatic process is considered. In order to have KZS, it is essential that the system evolves through both adiabatic and impulse regions, and that the impulse region only exists symmetrically around one (finite-number of) QCP(s), as illustrated in the top panel of Fig. 1.1. Thus, in some sense, KZS reflects the scaling behavior of the *static properties of the phase diagram*, since only the equilibrium critical exponents are encoded in KZS.

(ii) Initial pure excited states: Besides the conditions stated in (i) above, adiabatic quench dynamics can still encode the ground-state equilibrium critical exponents for a large class of initial energy eigenstates as well as for pure excited states prepared by a sudden parameter quench. A crucial role is played by how the initial excitation is distributed over the set of *relevant* quasi-particle modes that effectively evolve in an adiabatic quench. In particular, a unifying criterion that ensures the emergence of KZS in both the above scenarios in the thermodynamic limit is obtained

by requiring that the *majority of the relevant modes share a common initial excitation pattern*, as expressed by Eq. (4.20).

(iii) Initial mixed states: In general, more restrictive conditions on the distribution of the initial excitation over relevant modes must be obeyed for universal dynamical scaling to emerge in adiabatic quench dynamics that originates from a statistical (incoherent) mixture as compared to a (coherently prepared) pure state. In particular, *all* the relevant modes, as opposed to *majority* of the relevant modes, must share a common excitation pattern (not thermally excited) for the initial thermal state. This implies that KZS is fragile against thermal fluctuations if the initial thermal state is prepared *at criticality*, that is, the scaling exponent deviating from the KZ prediction as soon as $T \neq 0$. However, from a practical standpoint, it is important to note that a *finite range of temperatures* can still support KZS if the system is initially at thermal equilibrium *sufficiently far from criticality*.

•Anomalous Dynamical Scaling.

(i) Initial ground state: There are two situations in our model that the dynamical scaling exponent can not be solely determined by equilibrium critical exponents. First, when a critical region is involved in the adiabatic quench process, non-equilibrium scaling exponents remain expressible by combinations of equilibrium (path-dependent) ones, however a detailed characterization of both the static phase diagram and the accessible low-lying excitations is necessary for quantitative predictions. Second, for certain paths across MCP, the center of the impulse region may not be located at the MCP (see bottom panel of Fig. 1.1), leading to a genuinely non-static exponent in the non-equilibrium scaling. It is interesting to notice that in the latter scenario, although there is only one isolated MCP involved in the quench process, there is potentially a *quasi-critical region* around the MCP, which, in some sense, is similar to the first scenario.

(ii) Initial mixed states: When the system is driven away from an isolated (non-multicritical) QCP with a fully mixed thermal state at criticality initially (high-temperature limit), the KZS no longer holds. The scaling property of the initial excitation probability plays a role in the dynamical scaling exponent.

• First-Order Adiabatic Renormalization.

First-order AR is found to be useful in predicting the non-equilibrium scaling exponent when an isolated (standard or multi-critical) QCP is involved in the quench process originating from the

many-body ground state. We also generalized AR to adiabatic quench processes from an excited eigenstate, and found that the perturbative scaling result is consistent with exact numerical results as well.

• **Effective thermalization.**

Effective thermal behavior may emerge in the relaxation dynamics of the quasiparticle density following a sudden quench from a thermal state under appropriate conditions. Specifically, the long-time expectation value of this observable is determined by a *fictitious* thermal equilibrium ensemble at temperature T_{eff} provided that i) the system is quenched toward the *center of the impulse region*, and ii) the initial temperature is *sufficiently high* with respect to all the relevant gaps. For a standard QCP, the first requirement is met by a sudden quench *toward criticality*, which has been found sufficient for local observables such as the transverse magnetization per site and the kink density to thermalize starting from the ground state [94, 96, 95]. Our results indicate that, in general, condition i) alone need *not* suffice for arbitrary local observables. It remains an interesting open question to precisely characterize what subclass of local observables may exhibit effective thermal behavior under the sole condition i). Our results additionally show that for the quasiparticle density, effective thermalization may fail to occur altogether (or possibly require yet more stringent requirements) for sudden quenches to a *multicritical* QCP. Physically, we have traced this behavior back to the existence of a quasi-critical region and the corresponding shift of the impulse region.

• **Generalized Entanglement.**

Fermionic GE, in particular the $\mathfrak{u}(N)$-purity, was found to be able to identify the QCPs and the associated critical exponents of *all* the equilibrium QPTs in the anisotropic limit of the alternating XY spin chain. The $\mathfrak{u}(N)$-purity can also exhibit non-equilibrium dynamical scaling (KZS) throughout the whole time-evolution for quenches across an isolated standard QCP, provided that the excess amount relative to the ground state is considered.

While the above analysis provides a more complete picture of non-equilibrium dynamics in a paradigmatic class of spin chains than available thus far, there are still many open questions that require further investigation. Some important questions are as follows:

• **Robustness of KZS under decoherence.** Since our analysis is restricted to the dynamics

of an isolated quantum system, a natural question that arises is, How robust is the KZS when the quantum system is coupled to an environment? This problem is studied in Ref. [101, 102] with Ising model coupled to an Ohmic bath with temperature T, and found that there is a cross-over between KZS to a scaling mainly caused by thermal incoherent excitation. The universality of this result with respect to the properties of the bath and the system needs to be further elucidated.

• **The role of initialization for non-integrable models.** It is interesting to ask how crucially our results related to initial excited states rely on the XY chain being an exactly solvable non-interacting model. In particular, it would be worthwhile to explore whether dynamical critical scaling may still exist for finite-energy initial states in non-integrable models, or even in more complex but still integrable systems such as a Bethe-Ansatz solvable one-dimensional Heisenberg XXZ chain [110] or an infinitely coordinated Lipkin-Meshkov-Glick model [73].

• **Thermalization for initial surface states.** The effective thermalization we discussed thus far is restricted to initial *bulk thermal* states. How would the thermalization behavior change for an initial edge state (that is, an eigenstate of XY spin chain with open boundary condition within FM phase [37]). These edge states might exhibit different thermalization behavior in the sense that they are gapless in an otherwise gapped phase, thus there is a finite gap separating these edge states with the bulk states. It may be interesting to compare the relaxation time scale of initial edge vs. bulk states.

• **Generalized entanglement around MCPs.** While the $\mathfrak{u}(N)$ purity is faithful in detecting the QPTs of our system Hamiltonian in the anisotropic limit, the behavior of the $\mathfrak{u}(N)$ purity around MCPs was not discussed. Would the $\mathfrak{u}(N)$ purity still be able to identify the critical exponent of MCPs? How will the $\mathfrak{u}(N)$ purity scale for those paths where anomalous dynamical scalings were observed with respect to the quasi-particle excitation density?

• **Physical understanding of the critical decoherence scaling.** In Chapter 5, we showed our numerical results for the scaling behavior of decoherence factor for a central spin when the environment Hamiltonian is linearly quenched towards a QCP. This suggests that the scaling behavior of the decoherence factor for quenches towards QCP and non-QCP is completely different (see Ref. [121] for analytical analysis for quenches towards non-QCP). The physical understanding of the observed anomalous scaling behavior requires further study.

Appendix A

Ground-state $\mathfrak{u}(N)$-purity in the presence of alternation

The equality we would like to prove is the following:

$$P_{\mathfrak{u}(N)} \quad = \quad 1 - \frac{2}{N}\Big[\langle\Psi_{GS}|\hat{N}^2|\Psi_{GS}\rangle - \langle\Psi_{GS}|\hat{N}|\Psi_{GS}\rangle^2\Big], \tag{A.1}$$

where $\hat{N} = \sum_{k\in K_+}\left(a_k^\dagger a_k + b_k^\dagger b_k + a_{-k}^\dagger a_{-k} + b_{-k}^\dagger b_{-k}\right)$. Recall the ground state wavefunction expression from Eq. (2.8):

$$|\Psi_{GS}\rangle = \prod_{k\in K^+}|\Psi_k\rangle = \Big(u_k^{(1)} + u_k^{(2)} a_k^\dagger a_{-k}^\dagger + u_k^{(3)} b_k^\dagger b_{-k}^\dagger + u_k^{(4)} a_k^\dagger b_{-k}^\dagger + u_k^{(5)} a_{-k}^\dagger b_k^\dagger + u_k^{(6)} a_k^\dagger a_{-k}^\dagger b_k^\dagger b_{-k}^\dagger\Big)|\mathtt{vac}\rangle.$$

Thus, we need to evaluate the following quantity (by leaving $\Psi_{GS}\rangle$ understood):

$$\begin{aligned}
\langle\hat{N}^2\rangle - \langle\hat{N}\rangle^2 &= \sum_{k,k'\in K_+}\langle(a_k^\dagger a_k + b_k^\dagger b_k + a_{-k}^\dagger a_{-k} + b_{-k}^\dagger b_{-k})(a_{k'}^\dagger a_{k'} + b_{k'}^\dagger b_{k'} + a_{-k'}^\dagger a_{-k'} + b_{-k'}^\dagger b_{-k'})\rangle \\
&\quad - \sum_{k,k'\in K_+}\langle a_k^\dagger a_k + b_k^\dagger b_k + a_{-k}^\dagger a_{-k} + b_{-k}^\dagger b_{-k}\rangle\langle a_{k'}^\dagger a_{k'} + b_{k'}^\dagger b_{k'} + a_{-k'}^\dagger a_{-k'} + b_{-k'}^\dagger b_{-k'}\rangle \\
&= \sum_k \langle(a_k^\dagger a_k + b_k^\dagger b_k + a_{-k}^\dagger a_{-k} + b_{-k}^\dagger b_{-k})^2\rangle - \langle a_k^\dagger a_k + b_k^\dagger b_k + a_{-k}^\dagger a_{-k} + b_{-k}^\dagger b_{-k}\rangle^2, \quad \text{(A.2)}
\end{aligned}$$

where the fact that $k \neq k'$ terms do not survive in $\langle \hat{N}^2 \rangle - \langle \hat{N} \rangle^2$ is exploited in the derivation of the last line in Eq. (A.2) because of the factorized expression of $|\Psi_{GS}\rangle$ for different modes. Since

$$\langle a_k^\dagger a_k \rangle = |u_k^{(2)}|^2 + |u_k^{(4)}|^2 + |u_k^{(6)}|^2, \qquad \langle a_{-k}^\dagger a_{-k} \rangle = |u_k^{(2)}|^2 + |u_k^{(5)}|^2 + |u_k^{(6)}|^2,$$
$$\langle b_k^\dagger b_k \rangle = |u_k^{(3)}|^2 + |u_k^{(5)}|^2 + |u_k^{(6)}|^2, \qquad \langle b_{-k}^\dagger b_{-k} \rangle = |u_k^{(3)}|^2 + |u_k^{(4)}|^2 + |u_k^{(6)}|^2,$$
$$\langle a_k^\dagger a_k a_{-k}^\dagger a_{-k} \rangle = |u_k^{(2)}|^2 + |u_k^{(6)}|^2, \quad \langle a_k^\dagger a_k b_k^\dagger b_k \rangle = |u_k^{(6)}|^2, \quad \langle a_k^\dagger a_k b_{-k}^\dagger b_{-k} \rangle = |u_k^{(4)}|^2 + |u_k^{(6)}|^2,$$
$$\langle a_{-k}^\dagger a_{-k} b_k^\dagger b_k \rangle = |u_k^{(5)}|^2 + |u_k^{(6)}|^2, \quad \langle a_{-k}^\dagger a_{-k} b_{-k}^\dagger b_{-k} \rangle = |u_k^{(6)}|^2, \quad \langle b_k^\dagger b_k b_{-k}^\dagger b_{-k} \rangle = |u_k^{(3)}|^2 + |u_k^{(6)}|^2,$$

we also have:

$$\begin{aligned}
&\langle (a_k^\dagger a_k + b_k^\dagger b_k + a_{-k}^\dagger a_{-k} + b_{-k}^\dagger b_{-k})^2 \rangle = \langle a_k^\dagger a_k + b_k^\dagger b_k + a_{-k}^\dagger a_{-k} + b_{-k}^\dagger b_{-k} \rangle \\
&+ 2\langle a_k^\dagger a_k a_{-k}^\dagger a_{-k} + a_k^\dagger a_k b_k^\dagger b_k + a_k^\dagger a_k b_{-k}^\dagger b_{-k} + a_{-k}^\dagger a_{-k} b_k^\dagger b_k + a_{-k}^\dagger a_{-k} b_{-k}^\dagger b_{-k} + b_k^\dagger b_k b_{-k}^\dagger b_{-k} \rangle \\
&= 4(|u_k^{(2)}|^2 + |u_k^{(3)}|^2 + |u_k^{(4)}|^2 + |u_k^{(5)}|^2) + 16|u_k^{(6)}|^2,
\end{aligned}$$

$$\langle a_k^\dagger a_k + b_k^\dagger b_k + a_{-k}^\dagger a_{-k} + b_{-k}^\dagger b_{-k} \rangle^2 = 4(|u_k^{(2)}|^2 + |u_k^{(3)}|^2 + |u_k^{(4)}|^2 + |u_k^{(5)}|^2 + 2|u_k^{(6)}|^2).$$

On the other hand, from the expression of $P_{\mathfrak{u}(N)}$ in Eq. (2.22), we obtain:

$$\begin{aligned}
P_{\mathfrak{u}(N)} = 1 - \frac{4}{N} \sum_{k \in K_+} &(2|u_k^{(2)}|^2 + 2|u_k^{(4)}|^2 + 2|u_k^{(3)}|^2 + 2|u_k^{(4)}|^2 + 4|u_k^{(6)}|^2) - (|u_k^{(2)}|^2 + |u_k^{(4)}|^2 + |u_k^{(6)}|^2)^2 \\
&- (|u_k^{(2)}|^2 + |u_k^{(5)}|^2 + |u_k^{(6)}|^2)^2 - (|u_k^{(3)}|^2 + |u_k^{(5)}|^2 + |u_k^{(6)}|^2)^2 - (|u_k^{(3)}|^2 + |u_k^{(4)}|^2 + |u_k^{(6)}|)^2 \\
&- 2(|u_k^{(3)} u_k^{(4)^*} - u_k^{(5)} u_k^{(2)^*}|^2 + |u_k^{(4)} u_k^{(2)^*} - u_k^{(3)} u_k^{(5)^*}|^2),
\end{aligned}$$

where the following relationships were used in the derivation

$$\langle a_k^\dagger b_k \rangle = u_k^{(3)} u_k^{(4)^*} - u_k^{(5)} u_k^{(2)^*}, \qquad \langle a_{-k}^\dagger b_{-k} \rangle = u_k^{(4)} u_k^{(2)^*} - u_k^{(3)} u_k^{(5)^*}.$$

Thus, in order to prove Eq. (A.1), we need to show that:

$$\sum_{k \in K_+} \left[|u_k^{(2)}|^2 |u_k^{(3)}|^2 + |u_k^{(4)}|^2 |u_k^{(5)}|^2 + 2\mathrm{Re}(u_k^{(2)} u_k^{(4)^*} u_k^{(3)} u_k^{(5)^*}) - |u_k^{(1)}|^2 |u_k^{(6)}|^2 \right] = 0. \tag{A.3}$$

First, $|\Psi_k\rangle = |\Psi_{-k}\rangle$ (thanks to the symmetry between k and $-k$); second, from the matrix expression of H_k in Eq. (2.7), when k is changed to $-k$, H_k is changed to H_k^*, thus, we have $u_k^{(n)^*} = u_{-k}^{(n)}$. Then, considering these two relations together, we obtain:

$$\begin{aligned} u_k^{(1)} &= u_{-k}^{(1)} = u_k^{(1)^*}, \quad u_k^{(2)} = -u_{-k}^{(2)} = -u_k^{(2)^*}, \quad u_k^{(3)} = -u_{-k}^{(3)} = -u_k^{(3)^*}, \\ u_k^{(4)} &= u_{-k}^{(5)} = u_k^{(5)^*}, \quad u_k^{(5)} = -u_{-k}^{(4)} = u_k^{(4)^*}, \qquad u_k^{(6)} = -u_{-k}^{(6)} = -u_k^{(6)^*}, \end{aligned}$$

which implies that $u_k^{(1)}$ and $u_k^{(6)}$ are real numbers, $u_k^{(2)}$ and $u_k^{(3)}$ are pure imaginary numbers, and $u_k^{(4)} = u_k^{(5)^*}$. Consider, in addition, that the 4-th column in H_k is equal to minus the 5-th column in H_k, implying that the real part of $u_k^{(4)}, u_k^{(5)}$ is irrelevant in diagonalizing H_k. Thus, we also know that $u_k^{(4)}$ and $u_k^{(5)}$ can be taken to be pure imaginary numbers. With all these information at hand, we can rewrite $Re(u_k^{(2)} u_k^{(4)^*} u_k^{(3)} u_k^{(5)^*}) = \pm |u_k^{(2)} u_k^{(3)}||u_k^{(4)} u_k^{(5)}|$, where the + sign corresponds to $u_k^{(2)} u_k^{(3)} = |u_k^{(2)} u_k^{(3)}|$, while the − sign corresponds to $u_k^{(2)} u_k^{(3)} = -|u_k^{(2)} u_k^{(3)}|$. Now, for the first situation that $u_k^{(2)} u_k^{(3)} = |u_k^{(2)} u_k^{(3)}|$, to prove Eq. (A.3) is equivalent to prove:

$$\sum_{k \in K_+} (|u_k^{(2)} u_k^{(3)}| + |u_k^{(4)} u_k^{(5)}| + |u_k^{(1)} u_k^{(6)}|)(|u_k^{(2)} u_k^{(3)}| + |u_k^{(4)} u_k^{(5)}| - |u_k^{(1)} u_k^{(6)}|) = 0, \tag{A.4}$$

while for the second situation where $u_k^{(2)} u_k^{(3)} = -|u_k^{(2)} u_k^{(3)}|$, to prove Eq. (A.3) is equivalent to prove:

$$\sum_{k \in K_+} (|u_k^{(2)} u_k^{(3)}| - |u_k^{(4)} u_k^{(5)}| + |u_k^{(1)} u_k^{(6)}|)(|u_k^{(2)} u_k^{(3)}| - |u_k^{(4)} u_k^{(5)}| - |u_k^{(1)} u_k^{(6)}|) = 0. \tag{A.5}$$

Since the Hamiltonian Eq. (2.1) exhibits particle-hole symmetry, applying a particle-hole transformation $\hat{U}_{\text{ph}}$ to $|\Psi_k\rangle$, which interchanges particle and hole, yields another eigenstate of H_k. Specifically, for each mode k, we can have the equations:

$$\begin{aligned} \hat{U}_{\text{ph}}|\texttt{vac}\rangle = a_k^\dagger a_{-k}^\dagger b_k^\dagger b_{-k}^\dagger |\texttt{vac}\rangle, \quad \hat{U}_{\text{ph}}|(a_k^\dagger a_{-k}^\dagger b_k^\dagger b_{-k}^\dagger |\texttt{vac}\rangle) = |\texttt{vac}\rangle, \\ \hat{U}_{\text{ph}}|(a_k^\dagger a_{-k}^\dagger |\texttt{vac}\rangle) = b_k^\dagger b_{-k}^\dagger |\texttt{vac}\rangle, \quad \hat{U}_{\text{ph}}|(b_k^\dagger b_{-k}^\dagger |\texttt{vac}\rangle) = a_k^\dagger a_{-k}^\dagger |\texttt{vac}\rangle, \\ \hat{U}_{\text{ph}}|(a_k^\dagger b_{-k}^\dagger |\texttt{vac}\rangle) = a_{-k}^\dagger b_k^\dagger |\texttt{vac}\rangle, \quad \hat{U}_{\text{ph}}|(a_{-k}^\dagger b_k^\dagger |\texttt{vac}\rangle) = a_k^\dagger b_{-k}^\dagger |\texttt{vac}\rangle, \end{aligned}$$

Thus,

$$\langle\Psi_k|\hat{U}_{\rm ph}|\Psi_k\rangle=\langle\Psi_k|u_k^{(6)}+u_k^{(3)}a_k^\dagger a_{-k}^\dagger+u_k^{(2)}b_k^\dagger b_{-k}^\dagger+u_k^{(5)}a_k^\dagger b_{-k}^\dagger+u_k^{(4)}a_{-k}^\dagger b_k^\dagger+u_k^{(1)}a_k^\dagger a_{-k}^\dagger b_k^\dagger b_{-k}^\dagger|\mathtt{vac}\rangle=0,$$

leading to the following equation:

$$u_k^{(1)}u_k^{(6)^*}+u_k^{(6)}u_k^{(1)^*}+u_k^{(2)}u_k^{(3)^*}+u_k^{(3)}u_k^{(2)^*}+u_k^{(4)}u_k^{(5)^*}+u_k^{(5)}u_k^{(4)^*}=2(u_k^{(1)}u_k^{(6)}-u_k^{(2)}u_k^{(3)}-|u_k^{(4)}u_k^{(5)}|)=0,$$

which guarantees Eq. (A.4) (Eq. (A.5)) to be true provided that either $u_k^{(2)}u_k^{(3)} = |u_k^{(2)}u_k^{(3)}|$ or $u_k^{(2)}u_k^{(3)} = -|u_k^{(2)}u_k^{(3)}|$.

Appendix B

Generalized entanglement in static and dynamic quantum phase transitions

This Appendix includes the following paper:

S. Deng, L. Viola and G. Ortiz, "Generalized entanglement in static and dynamic quantum phase transitions", *Recent Progress in Many-Body Theories*, Vol. **11** (World Scientific, Singapore, 2008), p. 387, arXiv:0802.3941.

GENERALIZED ENTANGLEMENT IN STATIC AND DYNAMIC QUANTUM PHASE TRANSITIONS

Shusa Deng and Lorenza Viola*

Department of Physics and Astronomy, Dartmouth College, Hanover, NH 03755, USA
**E-mail: Lorenza.Viola@Dartmouth.edu*

Gerardo Ortiz

Department of Physics, Indiana University, Bloomington, IN 47405, USA
E-mail: ortizg@indiana.edu

We investigate a class of one-dimensional, exactly solvable anisotropic XY spin-1/2 models in an alternating transverse magnetic field from an entanglement perspective. We find that a physically motivated Lie-algebraic *generalized entanglement* measure faithfully portraits the static phase diagram – including second- and fourth-order quantum phase transitions belonging to distinct universality classes. In the simplest time-dependent scenario of a slow quench across a quantum critical point, we identify parameter regimes where entanglement exhibits *universal dynamical scaling* relative to the static limit.

Keywords: Entanglement; Quantum Phase Transitions; Quantum Information Science

1. Introduction

Developing methodologies for probing, understanding, and controlling quantum phases of matter under a broad range of equilibrium and non-equilibrium conditions is a central goal of condensed-matter physics and quantum statistical mechanics. Since novel forms of matter tend to emerge in the deep quantum regime where thermal effects are frozen out, a key prerequisite is to obtain an accurate theoretical understanding of zero-temperature *quantum phase transitions* (QPTs).[1] Aside from its broad conceptual significance, such a need is heightened by the growing body of experimental work which is being performed at the interface between material science, quantum device technology, and experimental implementations of quantum information processing (QIP). Following the experimental realization of the Bose-Hubbard model in a confined ^{87}Rb Bose-Einstein condensate and the spectacular observation of the superfluid-to-Mott-insulator QPT,[2] ultracold atoms are enabling investigations into strongly interacting many-body systems with an unprecedented degree of control and flexibility – culminating in the observation of topological defects in a rapidly quenched spinor Bose-Einstein condensate.[3] Remarkably, the

occurrence of a QPT influences physical properties well into the finite-temperature regime where real-world systems live, as vividly demonstrated by the measured low-temperature resistivity behavior in heavy-fermion compounds.[4]

From a theoretical standpoint, achieving as a complete and rigorous quantum-mechanical formulation as desired is hindered by the complexity of quantum correlations in many-body states and dynamical evolutions. Motivated by the fact that QIP science provides, first and foremost, an organizing framework for addressing and quantifying different aspects of "complexity" in quantum systems, it is natural to ask: Can QIP concepts and tools contribute to advance our understanding of many-body quantum systems? In recent years, *entanglement theory* has emerged as a powerful bridging testbed for tackling this broad question from an information-physics perspective. On one hand, entanglement is intimately tied to the inherent complexity of QIP, by constituting, in particular, a *necessary* resource for computational speed-up in pure-state quantum algorithms.[5] On the other hand, critically reassessing traditional many-body settings in the light of entanglement theory has already resulted in a number of conceptual, computational, and information-theoretic developments. Notable advances include efficient representations of quantum states based on so-called *projected entangled pair states*,[6] improved renormalization-group methods for both static 2D and time-dependent 1D lattice systems,[7] as well as rigorous results on the computational complexity of such methods and the solvability properties of a class of generalized mean-field Hamiltonians.[8]

In this work, we focus on the problem of characterizing quantum critical models from a *Generalized Entanglement* (GE) perspective,[9,10] by continuing our earlier exploration with a twofold objective in mind: first, to further test the usefulness of GE-based criticality indicators in characterizing static quantum phase diagrams with a higher degree of complexity than considered so far (in particular, multiple competing phases); second, to start analyzing time-dependent, non-equilibrium QPTs, for which a number of outstanding physics questions remain. In this context, special emphasis will be devoted to establish the emergence and validity of *universal scaling laws for non-equilibrium observables*.

2. Generalized Entanglement in a Nutshell

2.1. *The need for GE*

Because a QPT is driven by a purely quantum change in the many-body ground-state correlations, the notion of entanglement appears naturally suited to probe quantum criticality from an information-theoretic standpoint: What is the structure and role of entanglement near and across criticality? Can appropriate entanglement measures detect and classify quantum critical points (QCPs) according to their universality properties? Extensive investigations have resulted in a number of suggestive results, see e.g. Ref. 11 for a recent review. In particular, pairwise entanglement, quantified by so-called *concurrence*, has been found to develop distinctive singular behavior at criticality in the thermodynamic limit, universal scaling laws

being obeyed in both 1D and 2D systems. Additionally, it has been established that the crossing of a QCP point is typically signaled by a logarithmic divergence of the *entanglement entropy* of a block of nearby particles, in agreement with predictions from conformal field theory. While this growing body of results well illustrates the usefulness of an entanglement-based view of quantum criticality, a general theoretical understanding is far from being reached. With a few exceptions, the existing entanglement studies have focused on analyzing how (i) *bipartite* quantum correlations (among two particles or two contiguous blocks) behave near and across a QCP under the assumption that the underlying microscopic degrees of freedom correspond to (ii) *distinguishable* subsystems (iii) *at equilibrium*.

GE provides an entanglement framework which is uniquely positioned to overcome the above limitations, while still ensuring consistency with the standard "subsystem-based" entanglement theory in well-characterized limits.[9,10,12] Physically, GE rests on the idea that entanglement is an *observer-dependent* concept, whose properties are determined by the expectations values of a *distinguished subspace of observables* Ω, without reference to a preferred decomposition of the overall system into subsystems. The starting point is to generalize the observation that standard entangled pure states of a composite quantum system look mixed relative to an "observer" whose knowledge is restricted to *local* expectation values. Consider, in the simplest case, two distinguishable spin-1/2 subsystems in a singlet (Bell) state,

$$|\text{Bell}\rangle = \frac{|\uparrow\rangle_A \otimes |\downarrow\rangle_B - |\downarrow\rangle_A \otimes |\uparrow\rangle_B}{\sqrt{2}}, \tag{1}$$

defined on a tensor-product state space $\mathcal{H} = \mathcal{H}_A \otimes \mathcal{H}_B$. First, the statement that $|\text{Bell}\rangle$ is entangled – $|\text{Bell}\rangle$ cannot be expressed as $|\psi\rangle_A \otimes |\varphi\rangle_B$ for arbitrary $|\psi\rangle_A \in \mathcal{H}_A$, $|\varphi\rangle_B \in \mathcal{H}_B$ – is unambiguously defined only after a preferred tensor-product decomposition of $\mathcal{H}$ is fixed: Should the latter change, so would entanglement in general.[12] Second, the statement that $|\text{Bell}\rangle$ is entangled is equivalent to the property that (either) *reduced subsystem state* – as given by the partial trace operation, $\rho_A = \text{Tr}_B\{|\text{Bell}\rangle\langle\text{Bell}|\}$ – is *mixed*, $\text{Tr}\{\rho_A^2\} = 1/2(1 + \sum_{\alpha=x,y,z}\langle\sigma_\alpha^A\rangle^2) < 1$, in terms of expectations of the Pauli spin-1/2 matrices σ_α^A acting on A.

To the purposes of defining GE, the key step is to realize that a meaningful notion of a *reduced state* may be constructed for any pure state $|\psi\rangle \in \mathcal{H}$ without invoking a partial trace, by specifying such a reduced "Ω-state" as a list of expectations of operators in the preferred set Ω. The fact that the space of all Ω-states is *convex* then motivates the following:[9]

Definition (Pure-state GE). A pure state $|\psi\rangle \in \mathcal{H}$ is *generalized unentangled relative to* Ω *if its reduced* Ω*-state is pure, generalized entangled otherwise.*

For applications to quantum many-body theories, two major advantages emerge with respect to the standard entanglement definition: first, GE is directly applicable to both distinguishable and indistinguishable degrees of freedom, allowing to naturally incorporate quantum-statistical constraints; second, the property of a many-body state $|\psi\rangle$ to be entangled or not is independent on both the choice

of "modes" (e.g. position, momentum, etc) and the operator language used to describe the system (spins, fermions, bosons, etc) – depending only on the observables Ω which play a distinguished physical and/or operational role.

2.2. *GE by example*

For a large class of physical systems, the set of distinguished observables Ω may be identified with a *Lie algebra* consisting of Hermitian operators, $\Omega \simeq \mathfrak{h}$, which generate a corresponding distinguished unitary Lie group via exponentiation, $\mathfrak{h} \mapsto \mathcal{G} = e^{i\mathfrak{h}}$. While the assumption of a Lie-algebraic structure is not necessary for the GE framework to be applicable,[9,12] it has the advantage of both suggesting simple GE measures and allowing a complete characterization of generalized unentangled states. In particular, a geometric measure of GE is given by the square length (according to the trace norm) of the projection of $|\psi\rangle\langle\psi|$ onto $\mathfrak{h}$:

Definition (Relative purity). Let $\{O_\ell\}$, $\ell = 1, \ldots, M$, be a Hermitian, orthogonal basis for $\mathfrak{h}$, $\dim(\mathfrak{h}) = M$. The *purity of* $|\psi\rangle$ *relative to* $\mathfrak{h}$ is given by

$$P_{\mathfrak{h}}(|\psi\rangle) = \mathsf{K} \sum_{\ell=1}^{M} \langle\psi|O_\ell|\psi\rangle^2 \,, \tag{2}$$

where K is a global normalization factor chosen so that $0 \leq P_{\mathfrak{h}} \leq 1$.

Notice that $P_{\mathfrak{h}}$ is, by construction, invariant under group transformations, that is, $P_{\mathfrak{h}}(|\psi\rangle) = P_{\mathfrak{h}}(G|\psi\rangle)$, for all $G \in \mathcal{G}$, as desirable on physical grounds. If, additionally, $\mathfrak{h}$ is a semi-simple Lie algebra *irreducibly* represented on $\mathcal{H}$, generalized unentangled states coincide[9] with *generalized coherent states* (GCSs) of $\mathcal{G}$, that is, they may be seen as "generalized displacements" of an appropriate reference state, $|\mathsf{GCS}(\{\eta_\ell\})\rangle = \exp(i \sum_\ell \eta_\ell O_\ell)|\mathsf{ref}\rangle$. Physically, GCSs correspond to unique ground states of Hamiltonians in $\mathfrak{h}$: States of matter such as BCS superconductors or normal Fermi liquids are typically described by GCSs. While we refer the reader to previous work[9,10,12] for additional background, we illustrate here the GE notion by example, focusing on two limiting situations of relevance to the present discussion.

2.2.1. *Example 1: Standard entanglement revisited*

The standard entanglement definition builds on the assumption of *distinguishable* quantum degrees of freedom, the prototypical QIP setting corresponding to N local parties separated in real space, and $\mathcal{H} = \mathcal{H}_1 \otimes \ldots \otimes \mathcal{H}_N$. Available means for manipulating and observing the system are then naturally restricted to arbitrary local transformations, which translates into identifying the Lie algebra of arbitrary local (traceless) observables, $\mathfrak{h}_{loc} = \mathfrak{su}(\dim(\mathcal{H}_1)) \oplus \ldots \oplus \mathfrak{su}(\dim(\mathcal{H}_N))$, as the distinguished algebra in the GE approach. If, for example, each of the factors $\mathcal{H}_\ell$ supports a spin-1/2, $\mathfrak{h}_{loc} = \mathrm{span}\{\sigma_\alpha^\ell \,; \alpha = x, y, z, \ell = 1, \ldots, N\}$, and Eq. (2) yields

$$P_{\mathfrak{h}_{loc}}(|\psi\rangle) = \frac{1}{N} \sum_{\ell,\alpha} \langle\psi|\sigma_\alpha^\ell|\psi\rangle^2 = \frac{1}{N}\Big(\sum_\ell \mathrm{Tr}\rho_\ell^2 - \frac{1}{2} \Big) \,, \tag{3}$$

which is nothing but the average (normalized) subsystem purity. Thus, $P_{\mathfrak{h}_{loc}}$ quantifies multipartite subsystem entanglement in terms of the average bipartite entanglement between each spin and the rest. Maximum local purity, $P_{\mathfrak{h}} = 1$, is attained if and only if the underlying state is a pure product state, that is, a GCS of the local unitary group $\mathcal{G}_{loc} = SU(2)_1 \otimes \ldots \otimes SU(2)_N$.

2.2.2. *Example 2: Fermionic GE*

Consider a system of indistinguishable spinless fermions able to occupy N modes, which could for instance correspond to distinct lattice sites or momentum modes, and are described by canonical fermionic operators $c_j, c_j^\dagger$ on the 2^N-dimensional Fock space $\mathcal{H}_{Fock}$. Although the standard definition of entanglement can be adapted to the distinguishable-subsystem structure associated with a given choice of modes (resulting in so-called "mode entanglement"), privileging a specific mode description need not be physically justified, especially in the presence of many-body interactions.[13] These difficulties are avoided in the GE approach by associating "generalized local" resources with *number-preserving* bilinear fermionic operators, which identifies the unitary Lie algebra $\mathfrak{u}(N) = \text{span}\{c_j^\dagger c_j \,; 1 \leq i, j \leq N\}$ as the distinguished observable algebra for fermionic GE. Upon re-expressing $\mathfrak{u}(N)$ in terms of an orthogonal Hermitian basis of generators, Eq. (2) yields

$$P_{\mathfrak{u}(N)}(|\psi\rangle) = \frac{2}{N} \sum_{j<k=1}^{N} \left[\langle c_j^\dagger c_k + c_k^\dagger c_j \rangle^2 - \langle c_j^\dagger c_k - c_k^\dagger c_j \rangle^2 \right] + \frac{4}{N} \sum_{j=1}^{N} \langle c_j^\dagger c_j - 1/2 \rangle^2 \,. \quad (4)$$

One may show[10] that a many-fermion pure state is generalized unentangled relative to $\mathfrak{u}(N)$ if and only if it is a single Slater determinant (with any number of fermions), whereas $P_{\mathfrak{u}(N)} < 1$ for any state containing fermionic GE. Note that a Bell pure state as in Eq. (1) rewrites, via a Jordan-Wigner isomorphic mapping, in the form

$$|\text{Bell}\rangle = \frac{|\uparrow\rangle_A \otimes |\downarrow\rangle_B - |\downarrow\rangle_A \otimes |\uparrow\rangle_B}{\sqrt{2}} = \frac{c_1^\dagger |\text{vac}\rangle - c_2^\dagger |\text{vac}\rangle}{\sqrt{2}} \,, \quad (5)$$

in terms of the fermionic vacuum $|\mathsf{vac}\rangle = |\downarrow\rangle_A \otimes |\downarrow\rangle_B \equiv |\downarrow,\downarrow\rangle$. Thus, while $|\text{Bell}\rangle$ is maximally mode-entangled relative to the local spin algebra $\mathfrak{su}(2) \oplus \mathfrak{su}(2)$, it is $\mathfrak{u}(N)$-*un*entangled – consistent with the fact that it is a one-particle state.

3. Generalized Entanglement and Quantum Critical Phenomena

3.1. *Static QPTs*

Let us focus in what follows on a class of exactly solvable spin-1/2 one-dimensional models described by the following Hamiltonian:

$$H = -\sum_{i=1}^{N} \left[\frac{(1+\gamma)}{2} \sigma_x^i \sigma_x^{i+1} + \frac{(1-\gamma)}{2} \sigma_y^i \sigma_y^{i+1} \right] + \sum_{i=1}^{N} \Big(h - (-1)^i \delta \Big) \sigma_z^i, \quad (6)$$

where periodic boundary conditions are assumed, that is, $\sigma_\alpha^i \equiv \sigma_\alpha^{i+N}$. Here, $\gamma \in [0,1]$, $h \in [-\infty,\infty]$, and $\delta \in [-\infty,\infty]$ are the anisotropy in the XY plane, the uniform magnetic field strength, and the alternating magnetic field strength, respectively. For $\delta = 0$, the above Hamiltonian recovers the anisotropic XY model in a transverse field studied in Ref. 10, whereas $\delta > 0$, $\gamma = 1$ corresponds to the Ising model in a alternating transverse field recently analyzed in Ref. 15.

While full detail will be presented elsewhere,[17] an exact solution for the energy spectrum of the above Hamiltonian may be obtained by generalizing the basic steps used in the standard Ising case,[14] in order to account for the existence of a two-site primitive cell introduced by the alternation. By first separately applying the Jordan-Wigner mapping to even and odd lattice sites,[16] and then using a Fourier transformation to momentum space, Hamiltonian (6) may be rewritten as:

$$H = \sum_{k\in K_+} H_k = \sum_{k\in K_+} \hat{A}_k^\dagger \hat{H}_k \hat{A}_k\,, \quad K_+ = \left\{\frac{\pi}{N}, \frac{3\pi}{N}, \ldots, \left(\frac{\pi}{2} - \frac{\pi}{N}\right)\right\},$$

where $\hat{H}_k$ is a four-dimensional Hermitian matrix, and $\hat{A}_k^\dagger = (a_k^\dagger, a_{-k}, b_k^\dagger, b_{-k})$ is a vector operator, $a_k^\dagger$ ($b_k^\dagger$) denoting canonical fermionic operators that create a spinless fermion with momentum k for even (odd) sites, respectively. Thus, the problem reduces to diagonalizing each of matrices $\hat{H}_k$, for $k \in K_+$. If $\epsilon_{k,1}, \epsilon_{k,2}, \epsilon_{k,3}, \epsilon_{k,4}$, with $\epsilon_{k,1} \le \epsilon_{k,2} \le 0 \le \epsilon_{k,3} \le \epsilon_{k,4}$ denote the energy eigenvalues of $\hat{H}_k$, then

$$H_k = \sum_{n=1,\ldots,4} \epsilon_{k,n} \gamma_{k,n}^\dagger \gamma_{k,n}\,,$$

where $\gamma_{k,n}^\dagger, \gamma_{k,n}$ are quasi-particle excitation operators for mode k in the nth band. At $T = 0$, the $\epsilon_{k,1}$ and $\epsilon_{k,2}$ bands are occupied, whereas $\epsilon_{k,3}$ and $\epsilon_{k,4}$ are empty, thus the ground-state energy $E_{GS} = \sum_{k\in K_+}(\epsilon_{k,1} + \epsilon_{k,2})$, with $\epsilon_{k,1} < 0, \epsilon_{k,2} \le 0$.

By denoting with $|\text{vac}\rangle$ the fermionic vacuum, and by exploiting the symmetry properties of the Hamiltonian, the many-body ground state may be expressed in the form $|\Psi\rangle_{GS} = \prod_{k\in K^+} |\Psi_k\rangle$, with

$$|\Psi_k\rangle = \left(u_k^{(1)} + u_k^{(2)} a_k^\dagger a_{-k}^\dagger + u_k^{(3)} b_k^\dagger b_{-k}^\dagger + u_k^{(4)} a_k^\dagger b_{-k}^\dagger + u_k^{(5)} a_{-k}^\dagger b_k^\dagger + u_k^{(6)} a_k^\dagger a_{-k}^\dagger b_k^\dagger b_{-k}^\dagger\right)|\text{vac}\rangle, \tag{7}$$

for complex coefficients determined by diagonalizing H_k, with $\sum_{a=1}^6 |u_k^{(a)}|^2 = 1$. Since QPTs are caused by non-analytical behavior of E_{GS}, QCPs correspond to zeros of $\epsilon_{k,2}$. The quantum phase boundaries are determined by the following pair of equations: $h^2 = \delta^2 + 1$; $\delta^2 = h^2 + \gamma^2$. The resulting *anisotropic* ($\gamma > 0$) quantum phase diagram is showed in Fig. 1 where, without loss of generality, we set $\gamma = 0.5$. Quantum phases corresponding to disordered (paramagnetic, PM) behavior, dimer order (DM), and ferromagnetic long-range order (FM) emerge as depicted. In the general case, the boundaries between FM and PM phases, as well as between FM and DM phases, are characterized by second-order broken-symmetry QPTs. Interestingly, however, E_{GS} develops weak singularities at

$$(h_c, \delta_c) = (0, \delta = \pm\gamma)\,, \qquad (h_c, \delta_c) = (\pm 1, \delta = 0)\,, \tag{8}$$

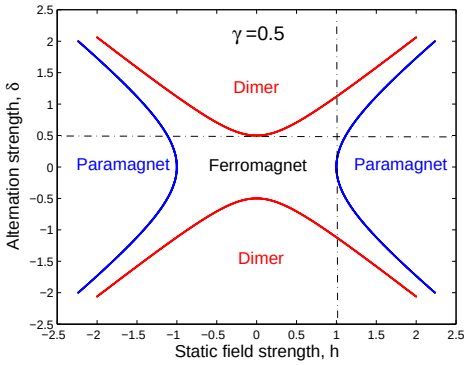

Fig. 1. Phase diagram of the spin-1/2 XY alternating Hamiltonian given in Eq. (6) with $\gamma = 0.5$.

where fourth-order broken-symmetry QPTs occur along the paths approaching the QCPs (Fig. 1, dashed-dotted lines). In the *isotropic* limit ($\gamma = 0$), an insulator-metal Lifshitz QPT occurs from a gapped to a gapless phase, with no broken-symmetry order parameter. For simplicity, we shall primarily focus on *gapped* quantum phases in what follows, thus $\gamma > 0$. Standard finite-size scaling analysis reveals that new quantum critical behavior emerges in connection with the alternating fourth-order QCPs in Eq. (8).[15] Thus, in addition to the usual Ising universality class, characterized by critical exponents $\nu = 1, z = 1$, an alternating universality class occurs, with critical exponents $\nu = 2, z = 1$.

The key step toward applying GE as a QPT indicator is to identify a (Lie) algebra of observables whose expectations reflect the changes in the GS as a function of the control parameters. It is immediate to realize that Hamiltonian Eq. (6), once written in fermionic language, is an element of the Lie algebra $\mathfrak{so}(2N)$, which includes *arbitrary* bilinear fermionic operators. As a result, the GS is always a GCS of $\mathfrak{so}(2N)$, and GE relative to $\mathfrak{so}(2N)$ carries no information about QCPs. However, the GS becomes a GCS of the number-conserving sub-algebra $\mathfrak{u}(N)$ in both the fully PM and DM limit. This motivates the choice of the fermionic $\mathfrak{u}(N)$-algebra discussed in *Example 2* as a natural candidate for this class of systems. Taking advantage of the symmetries of this Hamiltonian, the fermionic purity given in Eq. (4) becomes:

$$P_{\mathfrak{u}(N)} = \frac{8}{N} \sum_{k \in K_+} \Big\{ \Big[|\langle a_k^\dagger b_k \rangle|^2 + |\langle a_{-k}^\dagger b_{-k} \rangle|^2 \Big] \\ + \frac{4}{N} \Big[\langle a_k^\dagger a_k - 1/2 \rangle^2 + \langle a_{-k}^\dagger a_{-k} - 1/2 \rangle^2 + \langle b_k^\dagger b_k - 1/2 \rangle^2 + \langle b_{-k}^\dagger b_{-k} - 1/2 \rangle^2 \Big] \Big\} \tag{9}$$

Analytical results for $P_{\mathfrak{u}(N)}$ are only available for $\delta = 0$, where GE sharply detects the PM-FM QPT in the XY model.[10] Remarkably, ground-state fermionic GE still faithfully portraits the full quantum phase diagram with alternation. First, derivatives of $P_{\mathfrak{u}(N)}$ develop singular behavior only at QCPs, see Fig. 2 (left). Furthermore,

GE exhibits the correct scaling properties near QCPs.[10] By taking a Taylor expansion, $P_{\mathrm{u}(N)}(h) - P_{\mathrm{u}(N)}(h_c) \sim \xi^{-1} \sim (h - h_c)^{\nu}$, where ξ is the correlation length, the static critical exponent ν may be extracted from a log-log plot of $P_{\mathrm{u}(N)}$ for both the Ising and the alternating universality class, as demonstrated in Fig. 2 (right).

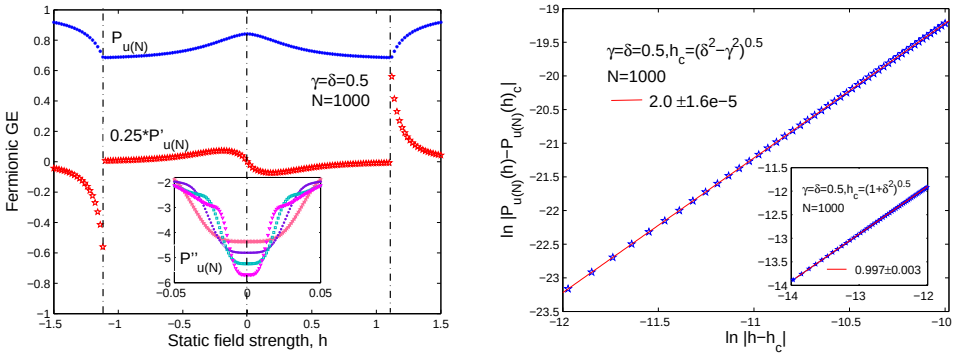

Fig. 2. $P_{\mathrm{u}(N)}$ as a static QPT indicator. Left panel: Purity and rescaled purity derivative vs magnetic field strength. Inset: second derivative for $N = 1000, 2000, 4000, 8000$ (top to bottom). Right panel: Determination of ν for both the alternating and Ising (inset) universality class.

3.2. *Dynamic QPTs*

While the above studies provide a satisfactory understanding of *static* quantum critical properties, *dynamical* aspects of QPTs present a wealth of additional challenges. To what extent can non-equilibrium properties be predicted by using equilibrium critical exponents? The simplest dynamical scenario one may envision arises when a single control parameter is slowly changed in time with constant speed $\tau_q > 0$, that is, $g(t) - g_c = (t - t_c)/\tau_q$, so that a QCP is crossed at $t = t_c$ ($t_c = 0$ without loss of generality). The typical time scale characterizing the response of the system is the *relaxation time* $\tau = \hbar/\Delta \sim |g(t) - g_c|^{-z\nu}$, Δ being the gap between the ground state and first accessible excited state and z the dynamic critical exponent.[1] Since the gap closes at QCPs in the thermodynamic limit, τ diverges even for an arbitrarily slow quench, resulting in a *critical slowing-down*. According to the so-called Kibble-Zurek mechanism (KZM),[18] a crossover between an (approximately) adiabatic regime to an (approximately) impulse regime occurs at a freeze-out time $-\hat{t}$, whereby the system's instantaneous relaxation time matches the transition rate,

$$\tau(\hat{t}) = |(g(\hat{t}) - g_c)/g'(\hat{t})|\,, \qquad \hat{t} \sim \tau_q^{\nu z/(\nu z+1)}\,,$$

resulting in a predicted scaling of the final density of excitations as

$$n(t_F) \sim \tau_q^{-\nu/(\nu z+1)}\,. \tag{10}$$

While agreement with the above prediction has been verified for different quantum systems,[19] several key points remain to be addressed: What are the required physical ingredients for the KZM to hold? What features of the initial (final) quantum phase are relevant? How does dynamical scaling reflect into entanglement and other observable properties?

In our model, the time-evolved many-body state at instant time t, $|\Phi(t)\rangle = \prod_{k\in K^+} |\Phi_k(t)\rangle$, may still be expressed in the form of Eq. (7) for time-dependent coefficients $u_k^{(a)}(t)$, $a = 1,\ldots,6$, computed from the solution of the Schrödinger equation, subject to the initial condition that $|\Phi(t\to-\infty)\rangle = |\Psi_{GS}(-\infty)\rangle$. The final excitation density is then obtained from the expectation value of the appropriate quasi-particle number operator over the final state,

$$n(t_F) = \frac{1}{N}\langle\Phi(t_F)| \sum_{k\in K_+} (\gamma^\dagger_{k,3}\gamma_{k,3} + \gamma^\dagger_{k,4}\gamma_{k,4}) \,|\Phi(t_F)\rangle\,.$$

As shown in Fig. 3 (left), the resulting value agrees with Eq. (10) over an appropriate τ_q-range *irrespective of the details of the QCP and the initial (final) quantum phase*:

$$n(t_F)^{Ising} \sim \tau_q^{-1/2}\,, \qquad n(t_F)^{Alternating} \sim \tau_q^{-2/3}\,.$$

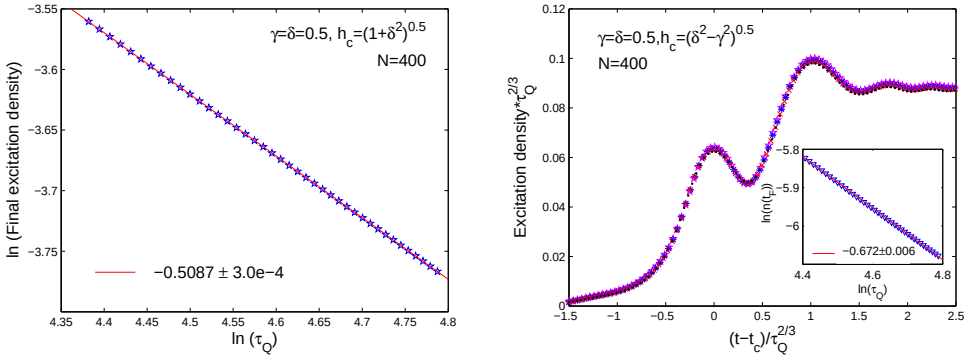

Fig. 3. Dynamical scaling of the excitation density. Left panel: log-log plot for Ising universality class (FM to PM). Right panel: alternating universality class (FM to FM), with log-log scaling plot in the inset.

Remarkably, however, our results indicate that *scaling behavior holds throughout the entire time evolution* (see Fig. 3, right), implying the possibility to express the time-dependent excitation density as:

$$n(t) = \tau_q^{-\nu/(\nu z+1)} F\Big(\frac{t-t_c}{\hat{t}}\Big)\,,$$

where F is a universal scaling function. Numerical results support the conjecture that similar *universal dynamical scaling* holds for arbitrary observables.[17] In particular, fermionic GE obeys scaling behavior across the entire dynamics provided

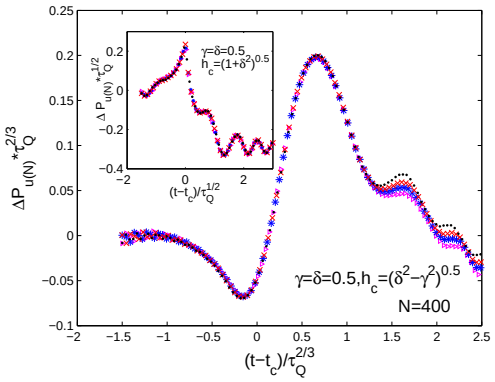

Fig. 4. Dynamical scaling of $P_{\mathrm{u}(N)}$ for the alternating and the Ising (inset) universality class.

that the amount relative to the instantaneous ground state $|\Psi(t)\rangle_{GS}$ is considered:

$$\Delta P_{\mathrm{u}(N)}(t) \equiv P_{\mathrm{u}(N)}(|\Phi(t)\rangle) - P_{\mathrm{u}(N)}(|\Psi(t)\rangle_{GS}) = \tau_q^{-\nu/(\nu z+1)} G\Big(\frac{t-t_c}{\hat{t}}\Big)\,,$$

for an appropriate scaling function G, see Fig. 4.

It is important to stress that the above discussion applies to control paths which originate and end in gapped phases. In the isotropic limit $\gamma = 0$, we observe no scaling of the form Eq. (10) if the system is driven to/from the superfluid gapless phase.

4. Conclusion

In addition to further demonstrating the usefulness of the GE notion toward characterizing static quantum critical phenomena, we have tackled the study of time-dependent QPTs in a simple yet illustrative scenario. Our analysis points to the emergence of suggestive physical behavior and a number of questions which deserve to be further explored. In particular, while for *gapped* systems as considered here, the origin of the observed universal dynamical scaling is likely to be rooted in the existence of a well-defined adiabatic (though non-analytic) limit – as independently investigated in Ref. 20, a rigorous understanding remains to be developed. We expect that a GE-based perspective will continue to prove valuable to gain additional insight in quantum-critical physics.

Acknowledgments

It is a pleasure to thank Rolando Somma and Anatoli Polkovnikov for useful discussions and input. Shusa Deng gratefully ackowledges partial support from Constance and Walter Burke through their *Special Project Fund in Quantum Information Science*.

References

1. S. Sachdev, *Quantum Phase Transitions* (Cambridge UP, Cambridge, 1999).
2. M. Greiner, O. Mandel, T. Esslinger, T. W. Hänsch, and I. Bloch, *Nature* **415**, p. 39 (2002).
3. L. E. Sadler, J. M. Higbie, S. R. Leslie, M. Vengalattore, and D. M. Stamper-Kurn, *Nature* **443**, p. 312 (2006).
4. P. Gegenwart *et al.*, *Phys. Rev. Lett.*, **89**, p. 056402 (2002).
5. R. Jozsa and N. Linded, *Proc. Roy. Soc. London A* **459**, p. 2001 (2003); G. Vidal, *Phys. Rev. Lett.* **91**, p. 147902 (2003).
6. F. Verstraete and J. I. Cirac, arXiv: cond-mat/0407066 (2004); *Phys. Rev. A* **70**, p. 060302(R) (2004).
7. D. Porras, F. Verstraete, and J. I. Cirac, *Phys. Rev. B* **73**, p. 014410 (2006); G. Vidal, *Phys. Rev. Lett.* **93**, p. 040502 (2004).
8. J. Eisert, *Phys. Rev. Lett.* **97**, p. 260501 (2006); R. Somma, H. Barnum, G. Ortiz, and E. Knill, *Phys. Rev. Lett.* **97**, p. 190501 (2006).
9. H. Barnum, E. Knill, G. Ortiz, and L. Viola, *Phys. Rev. A*, **68**, p. 032308 (2003); H. Barnum, E. Knill, G. Ortiz, R. Somma, and L. Viola, *Phys. Rev. Lett.*, **92**, p. 107902 (2004).
10. R. Somma, G. Ortiz, H. Barnum, E. Knill, L. Viola, *Phys. Rev. A* **70**, p. 042311 (2004); R. Somma, H. Barnum, E. Knill, G. Ortiz, and L. Viola, *Int. J. Mod. Phys. B* **20**, 2760 (2006).
11. L. Amico, R. Fazio, A. Osterloh, and V. Vedral, arXiv: quant-ph/0703044 (2007).
12. L. Viola and H. Barnum, arXiv:quant-ph/0701124 (2007), and references therein.
13. M. Kindermann, *Phys. Rev. Lett.* **96**, p. 240403 (2006).
14. P. Pfeuty, *Ann. Phys.* **57**, p. 79 (1970); E. Barouch, B. M. McCoy, and M. Dresden, *Phys. Rev. A* **2**, p. 1075 (1970).
15. O. Derzhko and T. Krokhmalskii, *Czech. J. Phys.* **55**, p. 605 (2005); O. Derzhko, J. Richter, and T. Krokhmalskii, *Phys. Rev. E* **69**, p. 066112 (2004).
16. K. Okamoto and K. Yasumura, *J. Phys. Soc. Japan* **59**, p. 993 (1990).
17. S. Deng, G. Ortiz, and L. Viola, in preparation.
18. W. H. Zurek, U. Dorner, and P. Zoller, *Phys. Rev. Lett.* **95**, p. 105701 (2005).
19. J. Dziarmaga, *Phys. Rev. Lett.* **95**, p. 245701 (2005); F. M. Cucchietti, B. Damski, J. Dziarmaga, and W. H. Zurek, *Phys. Rev. A* **75**, p. 023603 (2007).
20. A. Polkovnikov, *Phys. Rev. B*, **72**, p. 161201 (2005); A. Polkovnikov and V. Gritsev, cond-mat/0706.0212 (2007).

Appendix C

Dynamical non-ergodic scaling in continuous finite-order quantum phase transitions

This Appendix includes the following paper:

S. Deng, G. Ortiz, and L. Viola, "Dynamical non-ergodic scaling in continuous finite-order quantum phase transitions", Europhys. Lett. **84**, 67008 (2008).

A Letters Journal Exploring the Frontiers of Physics

December 2008

EPL, **84** (2008) 67008
doi: 10.1209/0295-5075/84/67008

www.epljournal.org

Dynamical non-ergodic scaling in continuous finite-order quantum phase transitions

S. Deng[1], G. Ortiz[2] and L. Viola[1(a)]

[1] *Department of Physics and Astronomy, Dartmouth College, 6127 Wilder Laboratory - Hanover, NH 03755, USA*
[2] *Department of Physics, Indiana University - Bloomington, IN 47405, USA*

received 23 July 2008; accepted in final form 13 November 2008
published online 12 January 2009

PACS 73.43.Nq – Quantum phase transitions
PACS 05.70.Jk – Critical point phenomena
PACS 75.10.Jm – Quantized spin models

Abstract – We investigate the emergence of universal dynamical scaling in quantum critical spin systems adiabatically driven out of equilibrium, with emphasis on quench dynamics which involves non-isolated critical points (*i.e.*, critical regions) and cannot be *a priori* described through standard scaling arguments nor time-dependent perturbative approaches. Comparing to the case of an isolated quantum critical point, we find that non-equilibrium scaling behavior of a large class of physical observables may still be explained in terms of equilibrium critical exponents. However, the latter are in general non-trivially path-dependent, and detailed knowledge about the time-dependent excitation process becomes essential. In particular, we show how multiple level crossings within a gapless phase may completely suppress excitation depending on the control path. Our results typify non-ergodic scaling in continuous finite-order quantum phase transitions.

The response of a physical system to external probes is an invaluable technique for unveiling the system's properties. If the probe is dynamic, so that the Hamiltonian becomes explicitly time-dependent, the system is forced out of equilibrium – a subject of prime practical importance which can soon prove full of challenges and surprises. In particular, understanding and manipulating the dynamics of zero-temperature quantum phase transitions (QPTs) [1] in matter has a broad significance across fields as diverse as quantum-statistical mechanics, material science, quantum information processing, and cosmology. The extent to which universal quantum scaling laws persist out of equilibrium and encode information about the equilibrium phase diagram is the topic of this work.

As early as 1970, Barouch and coworkers [2] studied the time-dependent $T = 0$ magnetization of the anisotropic XY chain, and showed that equilibrium is not reached at the final evolution time. This *non-ergodic* behavior was later confirmed for other physical observables [3], and the analysis extended to the case where the system is driven across its quantum critical point (QCP) by changing a control parameter $\lambda(t)$ (*e.g.*, the magnetic field along the z-axis) in time with constant quench rate $\tau > 0$. The emergence of non-equilibrium scaling, however, was not discussed. An important step was taken in ref. [4], starting from the observation that irrespective of how slowly the quench occurs, adiabaticity is lost in the thermodynamic limit at a "freeze-out" time $(t_c - \hat{t})$ before the QCP is crossed. This yields a power-law prediction for the final density of excitations, $n_{\rm ex}(t_{\rm fin}) \sim \xi^{-1}(\hat{t}) \sim \tau^{-\ell}$, where the *non-equilibrium critical exponent* $\ell = d\nu/(\nu z + 1)$ is solely determined by the equilibrium correlation length (ξ) the dynamic critical exponents of the QCP (ν and z, respectively), and the spatial dimension, d. While it is suggestive to realize that defect formation is a manifestation of broken ergodicity in Barouch's sense [3], continuous experimental advances in systems ranging from ultracold atomic gases to quantum magnets [5] demand the applicability of the above *Kibble-Zurek scaling* (KZS) to be carefully scrutinized, and the potential for more general *non-ergodic* scaling to be explored. How much information on the equilibrium physics is needed for reliable scaling predictions to be possible?

The KZS for linear quenches across an *isolated* QCP separating two gapped phases has been confirmed by now for a variety of control schemes in one-dimensional (1D) models [6–8], including QCPs of topological nature [9] and noisy driving fields [10] – generalizations to repeated [11]

(a) E-mail: Lorenza.Viola@Dartmouth.EDU

and non-linear quenches [12,13] having also been established. Leaving aside the case of *disordered* quantum systems, where marked deviations from power law behavior may be witnessed [14], the possibility of genuinely *non-adiabatic* scaling in low-dimensional clean systems, whereby non-zero excitation persists (unlike KZS) for $\tau \to \infty$ in the thermodynamic limit, has been pointed out in [8]. Likewise, critical dynamics in the presence of *non-isolated* QCPs reveals a rich landscape. The need to modify the KZS by replacing d with the "co-dimension" m of the relevant critical (gapless) surface has emerged through a study of the 2D Kitaev model [15]. Evidence of non-KZS has also been reported for quenches which originate within an extended quantum critical region [16], cross a multi-critical point [13,17], or steer the system along a gapless critical line [18].

A main purpose of this work is to develop a theory and understanding of non-ergodic scaling for generic (power law) quenches along critical regions. To achieve this goal two new notions are introduced, which are both *path-dependent*: one is the concept of a *dominant critical point* to establish scaling along a critical path, and the other a *mechanism of cancellation* of excitations. Besides elucidating several results recently reported in the literature, our analysis indicates that details on how different modes of excitation are accessed throughout the quench process are crucial. We consider several different scenarios within a unifying illustrative testbed, the 1D anisotropic XY model in a transverse alternating magnetic field [19]. In particular, we push beyond the KZS domain – notably, by investigating quenches that involve a continuous Lifshitz QPT to a gapless phase. We also revisit the standard KZS and clarify how, for arbitrary continuous QPTs, it can be accounted for by the *iterative adiabatic renormalization* approach of Berry [20], as long as two gapped quantum phases are involved. Most importantly, we find that universal dynamical scaling is obeyed by a large class of extensive physical observables *throughout the quench dynamics*, a result with practical implications in the experimental detection of non-ergodic scaling.

Model Hamiltonian. – The spin-1/2 anisotropic XY model in a transverse alternating field is defined by [19]

$$H = -\sum_{i=1}^{N} \Big\{ \frac{1+\gamma}{2}\sigma_x^i \sigma_x^{i+1} + \frac{1-\gamma}{2}\sigma_y^i \sigma_y^{i+1} - [h-(-)^i\delta]\sigma_z^i \Big\}, \tag{1}$$

where periodic boundary conditions are assumed, that is, $\sigma_\alpha^i \equiv \sigma_\alpha^{i+N}$. Here, $\gamma \in [0,1]$, $h, \delta \in [-\infty, \infty]$, are the anisotropy in the XY plane, and the uniform and alternating magnetic field strength, respectively. This model can be exactly solved by following the steps outlined in [19,21]. The Hamiltonian (1) rewrites as $H = \sum_{k\in K_+} \hat{H}_k = \sum_{k\in K_+} A_k^\dagger H_k A_k$, where $K_+ = \{\pi/N, 3\pi/N, \ldots, \pi/2 - \pi/N\}$ specifies allowed momentum values, and $A_k^\dagger = (a_k^\dagger, a_{-k}, b_k^\dagger, b_{-k})$ is a vector operator, with $a_k^\dagger$ ($b_k^\dagger$) denoting canonical fermionic operators that create a spinless fermion with momentum k for even (odd) sites. Diagonalization of the reduced 4×4 Hamiltonian matrix H_k further yields a collection of non-interacting quasi-particles,

$$H = \sum_{k\in K_+}^{n=1,\ldots,4} \epsilon_{k,n} N_{k,n},$$

in terms of an appropriate number operator $N_{k,n}$ for mode (k,n). Assuming that n labels bands in increasing energy order, only $\epsilon_{k,1}, \epsilon_{k,2} \leqslant 0$ bands are occupied at $T=0$, with an excitation gap $\Delta_k = \epsilon_{k,3} - \epsilon_{k,2}$ being given by

$$\Delta_k(\gamma,h,\delta) = 4\Big[h^2 + \delta^2 + \cos^2 k + \gamma^2 \sin^2 k - 2\sqrt{h^2\cos^2 k + \delta^2(h^2 + \gamma^2 \sin^2 k)}\Big]^{1/2}. \tag{2}$$

Quantum phase boundaries are determined by the equations $h^2 = \delta^2 + 1$; $\delta^2 = h^2 + \gamma^2$. The phase diagram with both $\gamma = 0.5$ and $\gamma = 0$ is shown in fig. 1. Quantum phases corresponding to disordered paramagnetic (PM) and dimer (DM) behavior emerge as depicted for arbitrary γ. For $\gamma > 0$, ferromagnetic order (FM phase) develops in the center of the phase diagram, whereas for the isotropic chain a superfluid (SF) phase with a gapless spectrum and non-broken $U(1)$-symmetry emerges. Finite-size analysis reveals that this model supports four distinct universality classes: i) When $\gamma > 0$, generic QCPs belong to the $d=2$ Ising universality class with critical exponents $\nu = 1, z = 1$. Different critical behavior occurs at $(h \to 0, \delta = \pm\gamma)$ and $(h = \pm 1, \delta \to 0)$, where weak singularities in the ground-state energy develop (4th-order QCPs [19]), and $\nu = 2, z = 1$, corresponding to the alternating universality class. ii) When $\gamma = 0$, generic QCPs on the boundary

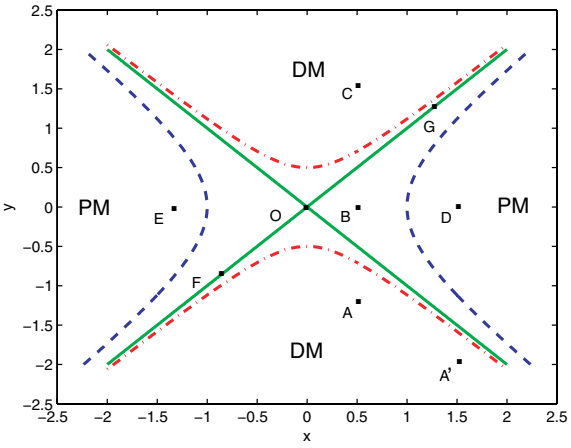

Fig. 1: (Colour on-line) Phase diagram of the alternating spin chain, eq. (1). Dashed (blue) and dashed-dotted (red) lines define the phase boundaries for $\gamma = 0.5$, the enclosed area corresponding to the FM phase. Dashed (blue) and solid (green) lines correspond to $\gamma = 0$, the enclosed area being the SF gapless phase.

lines belong to the Lifshitz universality class, with critical exponents $\nu = 1/2, z = 2$. Different critical behavior still occurs at $(h = \pm 1, \delta \to 0)$, where now $\nu = 1, z = 2$. Furthermore, Ising critical exponents are recovered while approaching the point $(h = 0, \delta = 0) \equiv O$ along every path other than $(\delta = 0, h \to 0)$ (when there is no QCP). In what follows, we focus on quenching schemes where h and δ are individually or simultaneously varied with time. We address separately different representative scenarios.

Quenching across an isolated critical point. – Suppose first that the system is *linearly* quenched across an isolated (non-multicritical) QCP that separates two gapped phases upon changing a single control parameter as $\delta\lambda(t) = \lambda(t) - \lambda_c = (t - t_c)/\tau$, where $t \in [t_{\rm in}, t_{\rm fin}]$. Without loss of generality we may assume that the system becomes critical at $t_c = 0$. For finite N, the exact time-evolved many-body state $|\psi(t)\rangle$ may be determined from numerical integration of the Schrödinger equation with Hamiltonian $H(t)$, subject to $|\psi(t_{\rm in})\rangle = |\psi_{GS}(t_{\rm in})\rangle$, the latter being the ground state of $H(t_{\rm in})$. The final excitation density $n_{\rm ex}(t_{\rm fin})$ may then be computed from the expectation value of the instantaneous quasi-particle number operator over $|\psi(t)\rangle$. Provided that the quench rate τ belongs to the appropriate range[1], KZS is found to hold irrespective of the details of the QCP and the initial (final) quantum phase, in particular for both 2nd- and higher-order QPTs, and independent of the path direction:

$$n_{\rm ex}^{\rm Ising}(t_{\rm fin}) \sim \tau^{-1/2}, \quad n_{\rm ex}^{\rm Alternating}(t_{\rm fin}) \sim \tau^{-2/3}.$$

While the excitation density is an accurate measure of the loss of adiabaticity in exactly solvable models, identifying manifestations of the KZS in quantities that can be more directly accessible in experiments and/or meaningful in more general systems is essential. Remarkably, numerical results indicate that scaling behavior holds throughout the quench process for a large class of physical observables, provided that the excess expectation value relative to the instantaneous ground state is considered [19]. That is

$$\begin{aligned} \Delta\mathcal{O}(t) &\equiv \langle\psi(t)|\,\mathcal{O}\,|\psi(t)\rangle - \langle\psi_{GS}(t)|\,\mathcal{O}\,|\psi_{GS}(t)\rangle \\ &= \tau^{-(\nu+\beta)/(\nu z+1)} F_{\mathcal{O}}\Big(\frac{t - t_c}{\hat{t}}\Big), \end{aligned} \tag{3}$$

where β is a scaling exponent determined by the physical dimension of $\mathcal{O}$ and F is an observable-dependent scaling function. For instance, under a quench of the magnetic field strength, h, the magnetization per site, $M_z = (\sum_{i=1}^N \sigma_z^i)/N$, obeys dynamical scaling of the form $\Delta M_z(t) = \tau^{(-\nu-\nu z+1)/(\nu z+1)} G((t - t_c)/\hat{t})$, whereas the nearest-neighbor spin correlator along the x-direction, $XX = (\sum_{i=1}^N \sigma_x^i \sigma_x^{i+1})/N$, obeys dynamical scaling of the form $\Delta XX(t) = \tau^{-\nu/(\nu z+1)} W((t - t_c)/\hat{t})$, for appropriate scaling functions G and W, respectively – see fig. 2.

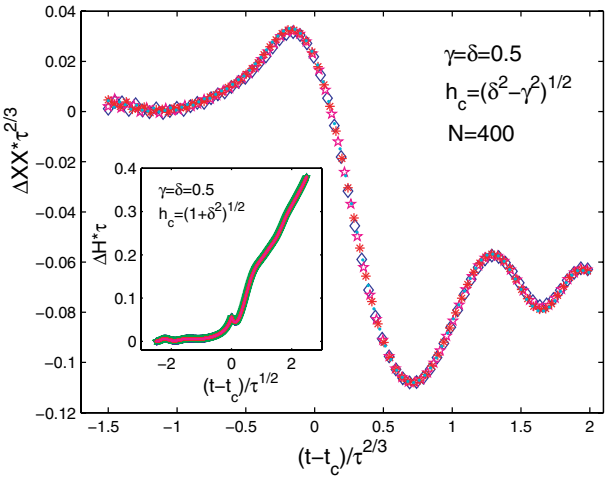

Fig. 2: (Colour on-line) Dynamical scaling under a magnetic field quench. Main panel: excess nearest-neighbor spin correlation per particle, ΔXX, *vs.* rescaled time for the alternating universality class from numerical integration of the Schrödinger equation. Inset: excess energy per particle, ΔH, *vs.* rescaled time for the Ising universality class from first-order adiabatic renormalization.

The fact that the system becomes gapless at a single instant t_c suggests to seek an explanation of the above results based on the fact that $\dot{\lambda}(t) = 1/\tau$ is a small parameter. While a similar strategy has been implemented in [8], our emphasis is on providing a firm theoretical foundation and further highlighting important assumptions. By a suitable parametrization, the relevant time-dependent Hamiltonian may be written as $H(t) = H_c + [\lambda(t) - \lambda_c]H_1 = H_c + (t - t_c)/\tau H_1$, with H_c quantum-critical in the thermodynamic limit. Let $\{E_m(t)\}$ and $\{|\psi_m(t)\rangle\}$ denote the snapshot eigenvalues and (orthonormal) eigenvectors of $H(t)$, where $|\psi_0(t)\rangle \equiv |\psi_{GS}(t)\rangle$ and assume that: i) no level crossing occurs throughout the evolution; ii) the derivatives of all the spectral projectors $\{|\psi_m(t)\rangle\langle\psi_m(t)|\}$ are sufficiently smooth. The (normalized) time-evolved state reads

$$|\psi(t)\rangle = c_0(t)|\psi_0(t)\rangle + \sum_{m\neq 0} c_m(t)|\psi_m(t)\rangle,$$

for coefficients to be determined. Since for a truly adiabatic evolution no excitation is induced in spite of the fact that the eigenstates of $H(t)$ evolve in time, appropriately subtracting (following Berry, "renormalizing") the adiabatic contribution is essential for quantifying the leading non-adiabatic correction. This is achieved in two steps [22]: i) effect a canonical transformation to a "comoving frame," where in the zeroth-order adiabatic limit $\tau \to \infty$ the comoving state vector $|\tilde{\psi}(t)\rangle = \tilde{U}(t; t_{\rm in})|\psi(t_{\rm in})\rangle$ is frozen up

[1] That $\tau \geqslant \tau_{\rm min}$ follows from standard adiabaticity requirements away from criticality, $\tau_{\rm min} \sim 1/[\min_{t\in[t_{\rm in},t_{\rm fin}]} {\rm Gap}(H(t))]^2$. The existence of a finite upper bound $\tau_{\rm max}$ follows from the fact that if τ is arbitrarily large, a *finite* system never enters the impulsive regime, if the size-dependent contribution to the gap dominates over the control-dependent one. From scaling analysis under the assumption that the gap closes polynomially as N^{-z}, we estimate $\tau_{\rm max} \sim N^{(\nu z+1)/\nu}$.

to a phase factor, that is, $|\tilde{\psi}(t)\rangle = e^{-i\Gamma_0(t)}|\psi_0(t_{\rm in})\rangle$, where $\Gamma_0(t)$ includes in general both the Berry phase and the dynamical phase; ii) evaluate the first-order correction to the comoving-frame propagator via Dyson series expansion. Transforming back to the physical frame, $c_m(t) = \langle\psi_m(t_{\rm in})|\tilde{U}(t;t_{\rm in})|\psi_0(t_{\rm in})\rangle$, to first order in $\dot{\lambda}$ we finally obtain (in units $\hbar = 1$), $c_0^{(1)}(t) = e^{-i\Gamma_0(t)} + O(\dot{\lambda}^2)$, and

$$c_m^{(1)}(t) = e^{-i\Gamma_m(t)}\int_{t_{\rm in}}^{t} {\rm d}t'\,\dot{\lambda}(t')\frac{\langle\psi_m(t')|H_1|\psi_0(t')\rangle}{E_m(t') - E_0(t')} e^{i\int_{t_{\rm in}}^{t'} {\rm d}s\Delta_m(s)},$$
$$\Delta_m(t) = E_m(t) - E_0(t)\,. \qquad (4)$$

Knowledge of the time-dependent state enables arbitrary physical quantities of interest to be computed, in particular the total time-dependent excitation probability $\mathbb{P}_{\rm ex}(t) = \sum_{m\neq 0}|c_m(t)|^2$. Given eq. (4), the latter formally recovers the expression given in [8], which captures the contribution to the density of excitations from states directly connected to $|\psi_0(t)\rangle$ via H_1 (see footnote [2]). Dynamical scaling emerges once the above result is supplemented by scaling assumptions on three fundamental dynamical variables: the time-dependent excitation energy above the ground state; the time-dependent matrix elements of the perturbation; and the density of excited states, $\rho(E)$, at the energy scale $\hat{t}^{-1}$ characterizing adiabaticity-breaking, which allows to change discrete sums over excited states to integrals. That is, close to the QCP we assume that

$$\begin{aligned} E_m(t) - E_0(t) &= \delta\lambda(t)^{\nu z} f_m(\Delta_m(t_c)/\delta\lambda(t)^{\nu z}),\\ \langle\psi_m(t)|H_1|\psi_0(t)\rangle &= \delta\lambda(t)^{\nu z-1} g_m(\Delta_m(t_c)/\delta\lambda(t)^{\nu z}),\\ \rho(E) &\sim E^{d/z-1}, \end{aligned} \qquad (5)$$

where the scaling functions f_m, g_m satisfy i) f_m (g_m) is constant when $x\to 0$; ii) f_m (g_m) $\propto x$ when $x\to\infty$ (see footnote [3]). Having the scaling assumptions at hand, integration over excited states is performed by moving to dimensionless variables $\zeta = (t-t_c)/\hat{t} = (t-t_c)\tau^{-\nu z/(\nu z+1)}$ and $\eta = \Delta_m(t_c)\hat{t} = \Delta_m(t_c)\tau^{\nu z/(\nu z+1)}$. Since at the QCP the integrand in eq. (4) develops a simple pole, while the phase $e^{i\int_{t_{\rm in}}^{t'} {\rm d}s\Delta_m(s)}$ becomes stationary, contributions away from the QCP may be neglected, allowing the desired scaling factor to be isolated, up to a regular function depending only on ζ. Thus, the scaling of the excitation density and *diagonal observables* such as the residual energy is directly determined as $n_{\rm ex}(\zeta) = \tau^{-d\nu/(\nu z+1)}\Xi(\zeta)$, $\Delta H(\zeta) = \tau^{-(d+z)\nu/(\nu z+1)}\Upsilon(\zeta)$, see also fig. 2. For a *generic observable*, if the additional scaling condition

$$\langle\psi_0(t)|\,\mathcal{O}\,|\psi_m(t)\rangle = \delta\lambda(t)^{\beta} q_m(\Delta_m(t_c)/\delta\lambda(t)^{\nu z}), \qquad (6)$$

holds for all the excitations m involved in the process for an appropriate scaling function q_m, then $\Delta\mathcal{O}\sim\tau^{-(\nu d+\beta)/(\nu z+1)}$ – consistent with eq. (3).

Two remarks are in order. First, the above argument directly explains the dynamical scaling reported in [19] for generalized entanglement relative to the fermionic algebra $u(N)$ [23], whose ground-state equilibrium behavior directly reflects the fluctuations of the total number operator. Second, the derivation naturally extends to a generic non-linear *power law* quench, that is, $\delta\lambda(t) = \lambda(t) - \lambda_c = |(t-t_c)/\tau|^{\alpha}{\rm sign}(t-t_c)$, $\alpha > 0$. Provided that the typical time scale for adiabaticity breaking is redefined as $\hat{t}_\alpha \sim \tau^{\alpha\nu z/(1+\alpha\nu z)}$, the same scaling assumptions in eqs. (5), (6) lead to dynamical scaling behavior of the form $n_{ex}\sim\tau^{-\alpha d\nu/(\alpha\nu z+1)}$, and $\Delta\mathcal{O}\sim\tau^{-\alpha(d\nu+\beta)/(\alpha\nu z+1)}$, throughout the whole time evolution[4].

Quenching along paths involving a finite number of critical modes. – A first situation which is beyond the standard KZS discussed thus far arises in quenches that force the system along a critical line, yet are dominated by a finite number of participating excitations. *Formally*, this makes it possible to obtain the non-equilibrium exponent for $n_{\rm ex}$ through application of the KZS, provided care is taken in defining the static exponents through a limiting path-dependent process where, along the quench of interest, a *simultaneous* expansion with respect to both the control parameter *and* the relevant critical mode(s) is taken. Consider a quenching scheme where both h and δ are changed according to t/τ while $\gamma = 0$ (path $F\to O\to G$ in fig. 1). While eq. (2) shows that the mode $k = \pi/2$ is critical throughout the process ($\Delta_{\pi/2}(t) = 0$, for all $t\in[t_{\rm in}, t_{\rm fin}]$ as $N\to\infty$), numerical data indicate that excitation sets in only when the point O is passed, see fig. 3. As remarked, the static critical exponents at O are $z = 1, \nu = 1$, which differ from the critical exponents ($z = 2, \nu = 1/2$) of all other critical points along this line. Indeed, the non-equilibrium exponent is solely determined by the static exponents of this QCP along the chosen path, $n_{\rm ex}\sim\tau^{-\nu/(\nu z+1)} = \tau^{-1/2}$. We term a QCP which belongs to a different universality class than all other critical points along a critical line and sets the non-ergodic scaling a *dominant critical point for that line*[5]. Physically, although $\Delta_{\pi/2}$ closes along the critical line in the thermodynamic limit, a level crossing which brings all bands together only occurs at O – still allowing the time-evolved state to adiabatically follow the snapshot ground state until then. The following independent confirmations may be invoked in support of the above argument. First, consider the anisotropic quench process analyzed in [18], whereby $\gamma(t)$ is changed linearly along the critical line $h^2 = \delta^2 + 1$. By Taylor-expanding Δ_k in eq. (2) around $k = 0, \gamma = 0$

[2] In particular, since one-body perturbations H_1 are considered in the present analysis, the first-order excitation probability, $\mathbb{P}_{\rm ex}^{(1)}(t) = \sum_{m\neq 0}|c_m^{(1)}(t)|^2$, coincides with the single-mode quasiparticle contribution, $\langle N_{k,n}\rangle = 1$, to the total time-dependent excitation density.

[3] Note that $\rho\sim\xi^{-d}/E$, with $\xi^d\sim\xi^m\xi^{d-m}\sim E^{-m/z}L^{d-m}$ for a $(d-m)$-dimensional critical surface.

[4] The perturbative derivation as presented strictly applies to quenches across an isolated QCP which is *not* multi-critical. We defer application of the perturbative derivation to a multi-critical point to a forthcoming analysis.

[5] The point O is multi-critical. However, quenches across a multi-critical point need *not* satisfy KZS, see [13].

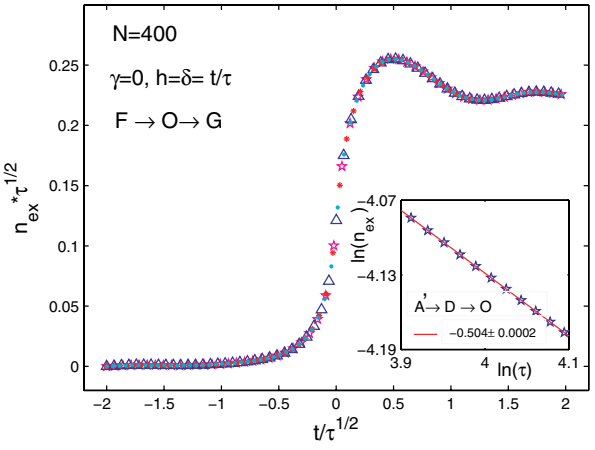

Fig. 3: (Colour on-line) Main panel: dynamical scaling of the excitation density for a simultaneous linear quench of h and δ along the gapless critical line $h=\delta$ $(F\to O\to G)$. Inset: log-log plot of the final excitation density *vs.* τ along the path $A'\to D\to O$.

reveals that $\nu=1, z=2$ at the dominant QCP $(\gamma=0,h,\delta)$, whereas $\nu=1, z=1$ for $\gamma\neq 0$ along the line. Accordingly, $n_{\rm ex}\sim\tau^{-1/3}$. While this coincides with the result obtained in [18], the underlying physical explanation is different. Plots of the rescaled excitation density $(n_{\rm ex}\tau^{1/3})$ *vs.* the rescaled time $(t/\tau^{2/3})$ would collapse onto one another for different τ within the appropriate range, in complete analogy with fig. 3. Second, loss of adiabaticity at a single point can also explain the scaling behavior observed for an AFM-to-FM quench (or a critical-to-FM quench) in the XXZ model [16], whereby the control path involves the gapless critical region $-1\leqslant\Delta\leqslant 1$ and the dominant critical point $\Delta=1$ belongs to a different universality class. Lastly, the concept of a dominant QCP remains useful for a power law quench, which leads to the scaling behavior $n_{ex}\sim\tau^{-\alpha d\nu/(\alpha\nu z+1)}$, with ν and z being the critical exponents of the dominant QCP along the critical line.

Quenching along paths involving an infinite number of critical modes. – More complex scenarios emerge when uncountably many modes of excitations can compete during the quench. Focusing on the isotropic limit $\gamma=0$, we contrast two representative situations where the Lifshitz QPT is involved: I) magnetic quenches along the path $D\to O\to E$ (PM → SF → PM); II) alternating quenches along the path $A\to B\to C$ (DM → SF → DM). Since $[M_z,H]=0$, in both cases the allowed excitation must comply with a non-trivial dynamical constraint. Along the path $D\to O\to E$, this forces the final state to be the same as the initial ground state up to a global phase factor, leading to $n_{\rm ex}(t_{\rm fin})\sim\tau^0$. Although for a magnetic quench this may be viewed as a consequence of the fact that the dynamics simply acts as a relabeling of the snapshot eigenstates, the same scaling holds for any quench which begins or ends in the gapless phase – for instance, a δ-quench along the path $A\to B$. Because these quenches take the system through a critical line in momentum space, $d-m=1$ (as opposed to $d-m=0$ for an isolated QCP), the observed scaling is consistent with the recent prediction $n_{\rm ex}(t_{\rm fin})\sim\tau^{-m\nu/(\nu z+1)}$ [15].

One may naively expect the same scaling to hold for path II), which also connects two gapped phases, albeit different than in I). Unlike in the standard KZS, however, details about the initial and final phases as well as the time-dependent excitation pattern become important. Specifically, along path II) we find $n_{\rm ex}(t_{\rm fin})\sim\tau^{-1/2}$. An explanation may be obtained by exploiting the fact that, due to $U(1)$-symmetry, the fermion number is conserved. This allows the reduced 4×4 matrix H_k to be decoupled into two 2×2 matrices by interchanging the order of the basis vectors a_{-k} and $b_k^\dagger$. Thus, $\hat{H}_{\pm k}=W_{\pm k}^\dagger H'_{\pm k}W_{\pm k}$, where $W_k^\dagger=(a_k^\dagger,b_k^\dagger)$, $W_{-k}^\dagger=(a_{-k},b_{-k})$, and

$$H'_{\pm k}=\pm 2h\mathbb{I}_2+\begin{pmatrix}\pm 2\delta & \mp 2\cos k\\ \mp 2\cos k & \mp 2\delta\end{pmatrix}. \qquad (7)$$

For such a two-level system, the asymptotic excitation probability may be computed from the Landau-Zener transition formula [24], yielding $p_k=e^{-2\pi\cos^2 k\tau}$. Upon integrating over all modes, we find

$$n_{\rm ex}(t_{\rm fin})=\frac{1}{\pi}\int_{-\pi/2}^{\pi/2}{\rm d}k\,p_k\sim\tau^{-1/2}. \qquad (8)$$

Note that because p_k is independent of h, the result in eq. (8) may be interpreted as implying that traversing the gapless phase produces the same excitation density as crossing the single QCP O by translating path II) at $h=0$, which determines the non-equilibrium exponent.

Physical insight into what may be responsible for the different behavior observed in the two quenches is gained by looking at the excitation spectrum along the two paths. Notice that, once the energy eigenvalues are specified at the initial time, $(\epsilon_{k,1}(t_{\rm in})\leqslant\epsilon_{k,2}(t_{\rm in})\leqslant\epsilon_{k,3}(t_{\rm in})\leqslant\epsilon_{k,4}(t_{\rm in})$ in our case), the same relative ordering need not hold at the final time if a level crossing is encountered during the quench – see fig. 4(a), (b). In the critical region, a pair of modes (k,n) and (k,n') undergoes a level crossing if $h^2-\delta^2=\cos^2 k$. If the number of such level crossings for fixed n,n' is *even*, the net contribution to the final excitation from momentum k is zero, since the final occupied bands are the same as the initial ones – see fig. 4(c). No cancellation is in place if either an odd number of level crossings from the same pair or if different pairs (n,n') are involved. The latter situation is realized for all k along path I) (h-quench, fig. 4(a)) and also for the path $A\to B$ (δ-quench). For a δ-quench along path II), the net excitation from the gapless phase turns out to be completely canceled (as seen in fig. 4(d), where the quench starts and ends symmetrically within the gapless phase). This only leaves the two boundary critical lines $h=\pm\delta$ as contributing to the excitation, thus a finite set of critical modes (a single one in fact, $k=\pi/2$, see fig. 4(b)).

Interestingly, a similar *cancellation mechanism* was verified for repeated quenches across an isolated QCP [11].

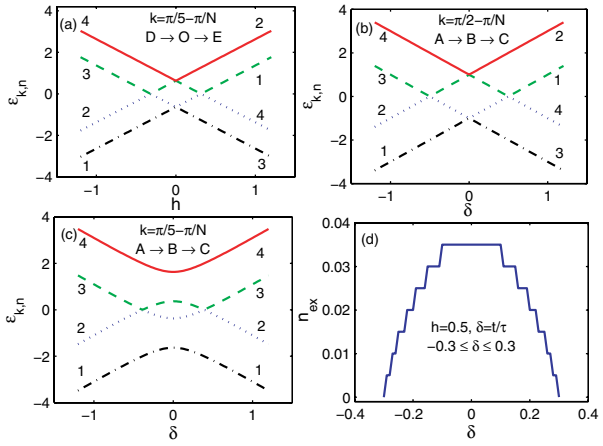

Fig. 4: (Colour on-line) Panels (a)–(c): band structure for different momentum modes k *vs.* quench parameter (*i.e.*, h or δ). Band ordering is determined by band index $n = 1, 2, 3, 4$ at initial time $t = t_{\rm in}$, whereas dash-dotted (black) $\leqslant$ dotted (blue) $\leqslant$ dashed (green) $\leqslant$ solid (red) at a generic time t along the control path. Panel (d): final excitation density, $n_{\rm ex}(t_{\rm fin})$, *vs.* δ for a quench of the alternation strength δ at fixed $h = 0.5$ within the critical region. For all cases, $N = 400$.

While a thorough analysis is beyond our current scope, we suggest that even participation from the same (pair of) snapshot excitations may be at the root of this cancellation in both scenarios. Here, we further test this conjecture by examining the path $A' \to D \to O$, for which an effective two-level LZ mapping is no longer possible. Unlike $A \to B \to C$, two intermediate phases are now crossed, and the initial and final phase differ from one another, yet analysis of $\epsilon_{k,n}(t)$ reveals that the two paths are equivalent in terms of participation of critical modes. Numerical results confirm that $n_{\rm ex}(t_{\rm fin}) \sim \tau^{-1/2}$, fig. 3.

Conclusions. – Non-ergodic dynamical scaling is fully captured by first-order adiabatic renormalization for sufficiently slow quenches involving a simple isolated QCP. Beyond this regime, we find that non-equilibrium exponents remain expressible by combinations of equilibrium (path-dependent) ones in all the scenarios under examination, however a detailed characterization of both the static phase diagram and the accessible low-lying excitations is necessary for quantitative predictions. Ultimately, scaling behavior appears to be the same for control paths which share an equivalent excitation structure. While yet different non-ergodic scaling may arise in more complex systems (*e.g.*, infinite-order Berezinskii-Kosterlitz-Thouless QPTs [16] as well as models with infinite coordination [25]), a deeper analysis of how competing many-body excitations contribute and interfere during a quench may shed further light on non-equilibrium quantum critical physics.

* * *

SD acknowledges partial support from Constance and Walter Burke through their Special Projects Fund in QIS.

REFERENCES

[1] Sachdev S., *Quantum Phase Transitions* (Cambridge University Press, Cambridge) 1999.
[2] Barouch E., McCoy B. M. and Dresden M., *Phys. Rev. A*, **2** (1970) 1075.
[3] Vallespir J. B., arXiv:quant-ph/0603124; Sen(De) A., Sen U. and Lewenstein M., *Phys. Rev. A*, **70** (2004) 060304.
[4] Zurek W. H., Dorner U. and Zoller P., *Phys. Rev. Lett.*, **95** (2005) 105701.
[5] Greiner M. *et al.*, *Nature*, **415** (2002) 39; Micheli A., Brennen G. K. and Zoller P., *Nat. Phys.*, **2** (2006) 341; Sadler L. E. *et al.*, *Nature*, **443** (2006) 312; Xu G. *et al.*, *Science*, **24** (2007) 317; Kummamuru R. K. and Soh Y.-A., *Nature*, **452** (2008) 859.
[6] Dziarmaga J., *Phys. Rev. Lett.*, **95** (2005) 245701; Damski B., *Phys. Rev. Lett.*, **95** (2005) 035701; Damski B. and Zurek W. H., *Phys. Rev. A*, **73** (2006) 063405; Cucchietti F. M. *et al.*, *Phys. Rev. A*, **75** (2007) 023603.
[7] Cherng R. W. and Levitov L. S., *Phys. Rev. A*, **73** (2006) 043614.
[8] Polkovnikov A., *Phys. Rev. B*, **72** (2005) 161201; Polkovnikov A. and Gritsev V., *Nat. Phys.*, **4** (2008) 477.
[9] Mondal S., Sen D. and Sengupta K., *Phys. Rev. B*, **78** (2008) 045101.
[10] Fubini A., Falci G. and Osterloh A., *New J. Phys.*, **9** (2007) 134.
[11] Mukherjee V., Dutta A. and Sen D., *Phys. Rev. B*, **77** (2008) 214427.
[12] Sen D., Sengupta K. and Mondal S., *Phys. Rev. Lett.*, **101** (2008) 016806; Barankov R. and Polkovnikov A., *Phys. Rev. Lett.*, **101** (2008) 076801.
[13] Divakaran U., Mukherjee V., Dutta A. and Sen D., arXiv:0807.3606; Mondal S., Sengupta K. and Sen D., arXiv:0808.1175.
[14] Dziarmaga J., *Phys. Rev. B*, **74** (2006) 064416; Caneva T., Fazio R. and Santoro G. E., *Phys. Rev. B*, **76** (2007) 144427.
[15] Sengupta K., Sen D. and Mondal S., *Phys. Rev. Lett.*, **100** (2008) 077204.
[16] Pellegrini F. *et al.*, *Phys. Rev. B*, **77** (2008) 140404.
[17] Mukherjee V. *et al.*, *Phys. Rev. B*, **76** (2007) 174303.
[18] Divakaran U., Dutta A. and Sen D., *Phys. Rev. B*, **78** (2008) 144301.
[19] Deng S., Viola L. and Ortiz G., in *Recent Progress in Many-Body Theories*, Vol. **11** (World Scientific, Singapore) 2008, p. 387, arXiv:0802.3941.
[20] Berry M. V., *Proc. R. Soc. A*, **14** (1987) 31.
[21] Okamoto K. and Yasumura K., *J. Phys. Soc. Jpn.*, **59** (1990) 993; Derzhko O., Richter J., Krokhmalskii T. and Zaburannyi O., *Phys. Rev. E*, **69** (2004) 066112.
[22] Messiah A., *Quantum Mechanics* (North-Holland, Amsterdam) 1962, Chapt. XVII.
[23] Barnum H. *et al.*, *Phys. Rev. Lett.*, **92** (2004) 107902; Somma R. *et al.*, *Phys. Rev. A*, **70** (2004) 042311.
[24] Zener C., *Proc. R. Soc. London, Ser. A*, **137** (1932) 696.
[25] Caneva T., Fazio R. and Santoro G. E., arXiv:0806.4455.

Appendix D

Anomalous nonergodic scaling in adiabatic multicritical quantum quenches

This Appendix includes the following paper:

S. Deng, G. Ortiz, and L. Viola, "Anomalous nonergodic scaling in adiabatic multicritical quantum quenches", Phys. Rev. B **80**, 241109(R) (2009).

PHYSICAL REVIEW B **80**, 241109(R) (2009)

Anomalous nonergodic scaling in adiabatic multicritical quantum quenches

Shusa Deng,[1] Gerardo Ortiz,[2] and Lorenza Viola[1]
[1]*Department of Physics and Astronomy, Dartmouth College, 6127 Wilder Laboratory, Hanover, New Hampshire 03755, USA*
[2]*Department of Physics, Indiana University, Bloomington, Indiana 47405, USA*
(Received 31 August 2009; published 30 December 2009)

We investigate nonequilibrium dynamical scaling in adiabatic quench processes across quantum multicritical points. Our analysis shows that the resulting power-law scaling *depends sensitively on the control path* and that anomalous critical exponents may emerge depending on the universality class. We argue that the observed anomalous behavior originates in the fact that the dynamical excitation process takes place asymmetrically with respect to the static multicritical point and that noncritical energy modes may play a dominant role. As a consequence, dynamical scaling requires introducing genuinely nonstatic exponents.

DOI: 10.1103/PhysRevB.80.241109 PACS number(s): 73.43.Nq, 75.10.Jm, 64.60.Kw, 05.30.−d

I. INTRODUCTION

Establishing dynamical scaling relations in many-body systems adiabatically driven out-of-equilibrium across a quantum phase transition has important implications for both condensed-matter physics[1] and adiabatic quantum computation.[2] A paradigmatic scenario is the Kibble-Zurek scaling (KZS),[3,4] whereby a homogeneous d-dimensional system is linearly driven with a constant speed $1/\tau$ across an isolated quantum critical point (QCP) described by equilibrium critical exponents ν and z. Assuming that in the thermodynamic limit, the system loses adiabaticity throughout an "impulse region" $[t_c-\hat{t},t_c+\hat{t}]$ centered around the QCP and with a characteristic width $2\hat{t}$, excitations are generated in the final state with a density $n_{\mathrm{ex}}(t_f)\sim\tau^{-d\nu/(\nu z+1)}$. While the KZS and its nonlinear generalizations have been verified in several exactly solvable models,[5] departures from the KZ prediction may occur for more complex quench processes, involving isolated QCPs in disordered[6] and infinitely coordinated systems[7] or nonisolated QCPs (that is, quantum critical regions).[8–10] Evidence of non-KZS, however, has also been reported in the apparently simpler situation of a quench across a single quantum multicritical point (MCP) in clean spin chains.[11,12]

In this work, we show how multicritical quantum quenches dramatically exemplify the dependence of nonequilibrium scaling upon the control path anticipated in Ref. 9 and demonstrate that anomalous "nonergodic" scaling may emerge in the thermodynamic limit. While a non-KZS $n_{\mathrm{ex}}(t_f)\sim\tau^{-1/6}$ was previously reported[11] and an explanation given in terms of an "effective dynamical critical exponent" $z_2=3$, the meaning of such exponent relied on the applicability of a Landau-Zener (LZ) treatment, preventing general insight to be gained. We argue that the failure of KZS is physically rooted in the shift of the center of the impulse region relative to the static picture and that z_2 is determined by the scaling of a path-dependent *minimum gap*, which need not coincide with the critical gap. Furthermore, such a dynamical shift may also cause the contribution from *intermediate noncritical energy states* to dominate the scaling of the excitation density, via an "effective dimensionality exponent" $d_2\neq 0$. We show that the latter leads to the emergence of a new scaling behavior $n_{\mathrm{ex}}(t_f)\sim\tau^{-3/4}$. A unified understanding is obtained by extending the adiabatic renormalization (AR) approach of Ref. 9.

II. MODEL HAMILTONIAN

We focus on the alternating spin-1/2 XY chain described by the Hamiltonian[9,13]

$$H=-\sum_{i=1}^{N}(\gamma_+\sigma_x^i\sigma_x^{i+1}+\gamma_-\sigma_y^i\sigma_y^{i+1}-h_i\sigma_z^i), \tag{1}$$

where $\gamma_\pm=(1\pm\gamma)/2$, $h_i=h-(-)^i\delta$, and periodic boundary conditions are assumed. Here, $h,\delta\in\mathbb{R}$ are the uniform and alternating magnetic field strength, respectively, whereas $\gamma\in\mathbb{R}$ is the anisotropy (lifting the restriction $\gamma\in[0,1]$ is essential for the present analysis). An exact solution for the energy spectrum of H may be obtained through the steps outlined in Ref. 13. The problem maps into a collection of noninteracting quasiparticle labeled by momentum modes $k\in K_+=\{\pi/N,3\pi/N,\ldots,\pi/2-\pi/N\}$, whose excitation gap is given by $\Delta_k(\gamma,h,\delta)=4[h^2+\delta^2+\cos^2 k+\gamma^2\sin^2 k-2\sqrt{h^2\cos^2 k+\delta^2(h^2+\gamma^2\sin^2 k)}]^{1/2}$. The quantum phase boundaries are determined by the equations[9,13] $h^2=\delta^2+1$, $\delta^2=h^2+\gamma^2$. Thus, the critical lines on the $\gamma=0$ plane consist entirely of MCPs.

III. QUENCH DYNAMICS: EXACT RESULTS

We assume that the system is initially in the ground state and that (in the simplest case) a slow quench across a MCP is implemented upon changing a single control parameter according to $\delta\lambda(t)=\lambda(t)-\lambda_c=|(t-t_c)/\tau|^\alpha\mathrm{sign}(t-t_c)$ over a time interval $t\in[t_0,t_f]$, where $\alpha=1$ corresponds to a linear driving, and λ_c is the critical value. Thus, the time-dependent Hamiltonian $H(t)$ may be written as $H(t)=H_c+\delta\lambda(t)H_1$, where H_c is quantum multicritical at time t_c in the thermodynamic limit, and H_1 is the contribution that couples to the external control (a similar parametrization is possible for quenches involving multiple parameters). Without loss of generality, we may let $t_c=0$. In what follows, we shall focus on two representative MCPs, A and B as marked in Fig. 1, each approached through two different paths (path 5 will be

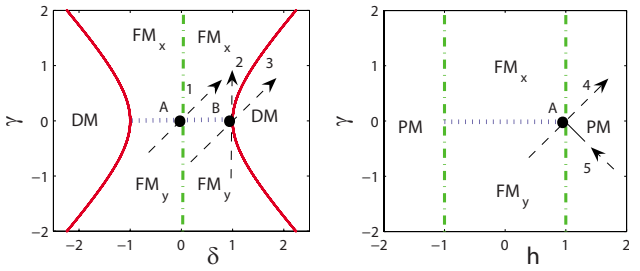

FIG. 1. (Color online) Phase diagram of H in Eq. (1) when $h=1$ (left) and $\delta=0$ (right). The dashed-dotted (green) line separates the ferromagnetic (FM) and paramagnetic (PM) phases, the solid (red) lines separate dimer (DM) and FM, whereas the dotted (blue) line is the superfluid phase (SF). The arrows indicate the relevant control paths for A and B.

introduced later), whose properties are summarized in Table I.

In order to quantify the amount of excitation at a generic instant t, we numerically integrate the time-dependent Schrödinger equation for $H(t)$ and monitor two standard "nonadiabaticity" indicators:[7,9,13] the excitation density $n_{\rm ex}$ and the residual energy ΔH. For a linear quench along either path 1 or 2 (left panel of Fig. 2), we find that $n_{\rm ex}(t) \sim \tau^{-\nu/(\nu z+1)}=\tau^{-1/3}$ and $\Delta H(t)\sim\tau^{-\nu(1+z)/(\nu z+1)}=\tau^{-1}$, which is consistent with KZS[3] and our conclusion in Ref. 9. For paths 3 and 4, however (right panel of Fig. 2), we find that $n_{\rm ex}(t) \sim \tau^{-1/6}$ and $\Delta H(t)\sim\tau^{-2/3}$, which is non-KZS (in Ref. 11, the $\tau^{-1/6}$ scaling was pointed out for an equivalent quench scheme across MCP A). Similar anomalous exponents are found for nonlinear quenches along path 3 or 4, e.g., $n_{\rm ex}(t) \sim \tau^{-2/9}$ for $\alpha=2$.

The above results show that for quenches across a MCP, whether KZS is obeyed depends sensitively on which control path is chosen. A closer inspection reveals the following important differences: (i) paths 1,2 start and end in essentially the same phase, correspondingly, the excitation spectrum is invariant under a transformation $\lambda\mapsto-\lambda$ of the control parameters. Paths 3,4 do not exhibit this symmetry; (ii) along paths 3,4, the MCPs A and B belong to the Lifshitz universality class ($\nu=1/2$), although all paths share $z=2$. It is then natural to ask which of these differences may play a role in determining the anomalous dynamical scaling behavior. To answer this question, we introduce another "V-shaped" path across MCP A (path 5), $h(t)=1+|\gamma(t)|=1+|t/\tau|$, which starts and ends in the PM phase but, in each of the two segments, crosses the MCP A with Lifshitz exponents. Surprisingly, the observed scaling is $n_{\rm ex}(t)\sim\tau^{-3/4}$ (left panel of Fig. 3), which

TABLE I. Critical exponents and parametrization of the relevant control paths for MCPs A and B.

Path	ν	z	Quenching scheme
1	1	2	$\gamma(t)=\delta(t)=\lvert t/\tau\rvert^{\alpha}\mathrm{sign}(t);\ h=1$
2	1	2	$\gamma(t)=\lvert t/\tau\rvert^{\alpha}\mathrm{sign}(t);\ h=1,\delta=1$
3	1/2	2	$\gamma(t)=\delta(t)-1=\lvert t/\tau\rvert^{\alpha}\mathrm{sign}(t);\ h=1$
4	1/2	2	$\gamma(t)=h(t)-1=\lvert t/\tau\rvert^{\alpha}\mathrm{sign}(t);\ \delta=0$

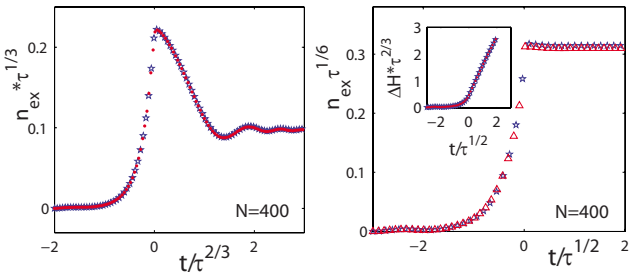

FIG. 2. (Color online) Exact scaling of the excitation density during a linear quench along path 2 (left) and path 3 (right). Right inset: scaling of the residual energy along path 3.

is neither KZS nor $-1/6$. An identical $-3/4$ scaling holds for a similar V-path across MCP B that starts and ends in the DM phase. As finite-size analysis reveals, all the observed anomalous scalings are practically independent upon system size over a wide range of quench rates (see, e.g., right panel of Fig. 3), establishing them as truly thermodynamic in nature.[14]

IV. LANDAU-ZENER ANALYSIS

We begin to seek an understanding from limiting cases, where an exact solution for $n_{\rm ex}(t_f)$ may be obtained based on the LZ picture.[15] This is possible provided that $\alpha=1$ and the Hamiltonian can be decoupled into effective two-level systems. Among the above-mentioned paths, only paths 4 and 5 (for which $\delta=0$) can be exactly mapped to a LZ problem, thanks to the possibility of rewriting H in Eq. (1) as $H=\Sigma_k\hat{H}_k=\Sigma_k B_k^\dagger H_k B_k$, where $B_k^\dagger=(c_{-k},c_k^\dagger)$ and

$$H_k=\begin{pmatrix} H_{k,11} & H_{k,12} \\ H_{k,12}^* & -H_{k,11}\end{pmatrix}=2\begin{pmatrix} -h+\cos k & \gamma\sin k \\ \gamma\sin k & h-\cos k\end{pmatrix}. \quad (2)$$

A rotation $R_k(q_k)$, $q_k\in[-\pi/2,\pi/2)$, renders the off-diagonal terms in Eq. (2) independent upon γ (hence time), allowing use of the LZ formula. Consider path 4 first. By choosing $\tan 2q_k=-\sin k$, the transformed Hamiltonian matrix elements become $H'_{k,11}=-2(1-\cos k)\cos 2q_k-2t/\tau(\cos 2q_k-\sin k\sin 2q_k)$, and $H'_{k,12}=2(1-\cos k)\sin 2q_k$. If the critical mode k_c is defined by requiring $\Delta_{k_c}=0$ in the thermodynamic

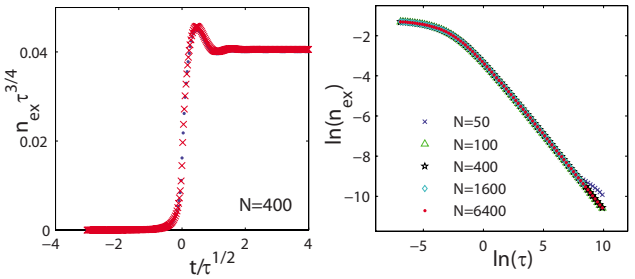

FIG. 3. (Color online) Left: exact scaling of the excitation density during a linear quench along path 5. Right: scaling of the final excitation density in path 5 for different size; $n_{\rm ex}(t_f)$ is the same to a numerical accuracy of 10^{-6}, up to $\tau<2\times10^5$. A linear fit yields -0.747 ± 0.001 over $200<\tau<2000$.

limit, we have $k_c=0$ for the MCP A. We may then let $\tan 2q_k \approx \sin 2q_k$, and the appropriate $q_k \approx -k/2$. From the LZ formula, the asymptotic ($t_f \to \infty$) excitation probability reads as

$$p_k = e^{-2\pi\tau(1-\cos k)^2 \sin^2 2q_k/(\cos 2q_k - \sin k \sin 2q_k)} \approx e^{-\pi\tau k^6/2},$$

where the approximation follows from a Taylor expansion around k_c. Integrating over all modes yields $n_{\rm ex}(t_f) \sim \tau^{-1/6}$, which is consistent with our exact numerical result. Therefore, mathematically, the $\tau^{-1/6}$ scaling follows from the fact that the exponent in p_k scales as $k^6 = k^{2z_2}$, with $z_2=3$. In turn, this originates from the scaling of the off-diagonal terms $H'_{k,12} \sim k^{z_2}$. Physically, as we shall later see by invoking AR, $H'_{k,12}$ may be interpreted as the minimum gap for mode k along path 4.

To unveil the $\tau^{-3/4}$ scaling, it is necessary to use the *exact finite-time* LZ solution. For simplicity, we restrict to half of path 5, by quenching the system from the PM phase up to the MCP A. This has the benefit of avoiding the nonanalytic time dependence of the control parameters that path 5 exhibits at A, while leaving the $\tau^{-3/4}$ scaling unchanged thanks to the symmetry of the excitation spectrum. Starting from Vitanov's expression [Eq. (7) in Ref. 16], the excitation probability $p_k(t_f)$ can be computed via the parabolic cylinder function $D_v(z)$,

$$p_k(t_f) = e^{-\pi\omega^2/4} \left| D_{i\omega^2/2}(T_f\sqrt{2}e^{i3\pi/4}) \cos\,\theta(T_f) - \frac{\omega}{\sqrt{2}} e^{-i\pi/4} D_{i\omega^2/2-1}(T_f\sqrt{2}e^{i3\pi/4}) \sin\,\theta(T_f) \right|^2,$$

where $\omega = (1-\cos k)\sin 2q_k \sqrt{\tau}/\sqrt{\cos 2q_k + \sin 2q_k \sin k} \sim k^3\sqrt{\tau}$ is the rescaled coupling strength, $T_f = -\omega/\sin k \sim -k^2\sqrt{\tau}$ is the rescaled time, $\tan 2q_k = \sin k$, and $\theta(T_f) = 1/2 \arctan(\omega/T_f) + \pi/2$. Since for our quench process $\omega \ll |T_f| \ll 1$ around k_c, we may estimate $p_k(t_f)$ by Taylor expanding $D_v(z)$ around $T_f=0$,

$$p_k(t_f) \approx (1-e^{-\pi\omega^2/2})/2 + \cos^2\,\theta(T_f) e^{-\pi\omega^2/2} - \sin 2\theta(T_f)/2 \sin\chi_k \sqrt{1-e^{-\pi\omega^2}}, \quad (3)$$

where $\chi_k \approx \pi/4$ around k_c. This approximation breaks when $T_f \sim 1$, setting the scaling of the highest-momentum contributing mode $k_{\rm max} \sim \tau^{-1/4}$. In Eq. (3), the dominant term $\cos^2\,\theta(T_f) e^{-\pi\omega^2/2} \sim \cos^2\,\theta(T_f) \sim |\omega/T_f|^2 \sim k^2$ since $e^{-\pi\omega^2/2} \approx 1$ within $k_{\rm max}$, which means $p_k(t_f) \sim k^2$. Thus, $n_{\rm ex}(t_f) = \int_0^{k_{\rm max}} p_k(t_f) \sim k_{\rm max}^3 \sim \tau^{-3/4}$, in agreement with our numerical results. Remarkably, the fact that $p_k(t_f) \sim (k-k_c)^{d_2}$, $d_2=2$, indicates that k_c is *not* excited despite a static QCP being crossed, and also that the *excitation is dominated by intermediate energy states*. In fact, at the MCP A, the modes around k_c are still far from the impulse region, since $|T_f| \gg \omega$, which sets the LZ transition time scale.[16] This is in stark contrast with the main assumption underlying KZS, where the center of the impulse region is the static QCP, and excitations are dominated by modes near k_c, as reflected in the typical scaling $p_k \sim (k-k_c)^0$.

Notice how the *asymmetry* of the dynamical impulse region (due to the asymmetry of the excitation spectrum) underlies the emergence of the observed anomalous scalings, in different ways: along path 4, such an asymmetry shifts the center of the impulse region into the FM phase (see also Fig. 2, right), and whether the LZ solution with $t_f \to \infty$ or $t_f \to 0^-$ is used leads to the same $\tau^{-1/6}$ result. Along half of path 5, instead, stopping the quench at MCP A is a prerequisite for "blocking" low-energy modes, and different scaling $(-1/6)$ would be obtained by extending the quench beyond $t_f=0$ into the FM phase and using the LZ asymptotic result.

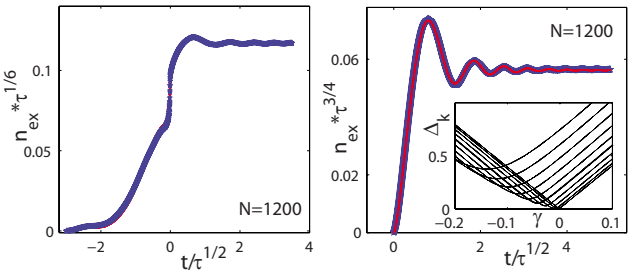

FIG. 4. (Color online) Scaling of the excitation density from first-order AR for a linear quench along path 3 (left) and half-5 starting at MCP A (right). Right inset: low-lying single-mode excitation spectrum along path 4 for $N=100$.

V. PERTURBATIVE SCALING APPROACH

Since the system becomes gapless at a single MCP along all the paths under study, first-order AR is a viable approach.[4,9] Let $|\psi_m(t)\rangle$ be a basis of snapshot eigenstates of $H(t)$, with snapshot eigenvalues $E_m(t)$, $m=0$ labeling the ground state. The time-evolved state may be expanded as $|\psi(t)\rangle = c_0^{(1)}(t)|\psi_0(t)\rangle + \Sigma_{m\neq 0} c_m^{(1)}(t)|\psi_m(t)\rangle$, where the coefficients $c_m^{(1)}(t)$ determine the excitation amplitudes and are given by Eq. (4) in Ref. 9. First-order AR calculations of $n_{\rm ex}(t)$ demonstrate that for linear quenches along paths 1 and 2, $n_{\rm ex} \sim \tau^{-1/3}$, whereas $n_{\rm ex} \sim \tau^{-1/6}$ along paths 3 and 4 (left panel of Fig. 4). Since the nonanalyticity at A in path 5 might cause problems in AR, again we choose to study half of path 5 (right panel of Fig. 4). All the AR results agree with the exact simulation results, confirming that AR reproduces the correct dynamical scaling across a *generic* isolated QCP.

Predicting the scaling exponent based on AR requires scaling assumptions for the contributions entering $c_m^{(1)}(t)$ [i.e., $\Delta_m(t) = E_m(t) - E_0(t)$ and $\langle\psi_m(t)|H_1|\psi_0(t)\rangle$], and the ability to change discrete sums of all the contributing excited states into integrals, for which the density of excited states $\rho(E)$ is required. Since typically the AR prediction is consistent with KZS, anomalous behavior must stem from anomalous scaling assumptions of (one or more of) these ingredients. We first examine the excitation spectrum along different paths. Since H_1 is a one-body perturbation, only single-mode excitations are relevant; thus, the index m labeling many-body excitations may be identified with a momentum mode. Along paths 1 and 2, it turns out that the minimum gap among all modes is *always* located at k_c, whereas along paths 3 and 4, the minimum gap is located at k_c *only* at the MCP. This suggests that knowing the static exponents of the MCP alone

need *not* suffice to determine the dynamical scaling due to the existence of "quasicritical" modes along paths 3 and 4. Mathematically, along path 4, $\partial\Delta_k(\gamma,1+\gamma,0)/\partial\gamma=0$ gives the location of the minimum gap for each mode k at $\tilde{\gamma}=(\cos k-1)/(1+\sin k^2)$, which is largely shifted into the FM phase (see inset in Fig. 4). By inserting this relation back into Δ_k, the function $\Delta_k(\tilde{\gamma})\equiv\tilde{\Delta}_k\sim(k-k_c)^3$. Following the same procedure also yields $\tilde{\Delta}_k\sim(k-k_c)^3$ along path 3, whereas $\tilde{\Delta}_k$ has the same scaling as Δ_k at the MCP along paths 1 and 2. This motivates modifying the AR scaling assumptions of Ref. 9 as follows: $E_m(t)-E_0(t)=\delta\lambda(t)^{\nu z}f_m[\Delta_m(t_{\min})/\delta\lambda(t)^{\nu z}]$, where $\Delta_m(t_{\min})$ is the minimum gap of mode m attained at $t_{\min}$ along the path, and f_m is a scaling function.

The above modification requires the scaling of $\rho(E)$ to be modified by letting $\rho(E)\sim E^{d/z_2-1}$, where z_2 comes from the dispersion relation of $\Delta_m(t_{\min})$. If the minimum gap of any mode is below a certain energy along the path, that mode should be counted into the contributing excited states. Accordingly, we have $z_2=z=2$ along paths 1, 2, half-5, and $z_2=3$ along paths 3, 4. Back to the LZ analysis, note that the off-diagonal term $H'_{12}(k)$ is the minimum gap of mode k along the path if there exists a time at which the diagonal term $H'_{11}(k)=0$, as it happens for path 4. For path 5, however, the off-diagonal term never becomes the minimum gap since the system never leaves the PM phase. Therefore, the off-diagonal term in the LZ picture need not suffice to determine the dynamical scaling, and the shift of the location of the minimum gap for each mode from the static QCP is at the root of the anomalous behavior we observe. Lastly, we consider the matrix elements of H_1. Numerical simulations suggest that $\langle\psi_m(t)|H_1|\psi_0(t)\rangle=\delta\lambda(t)^{\nu z-1}g_m[\Delta_m(t_{\min})/\delta\lambda(t)^{\nu z}]$, where g_m is a scaling function, and $\Delta_m(t_{\min})$ is the minimum gap of mode m along a path that *extends* the actual path to $t_f\to\infty$ when the quench is stopped at the MCP and coincides with the actual path otherwise. Then along paths 1 and 2, $\Delta_m(t_{\min})\sim k^2$, whereas along paths 3, 4, and half-5, $\Delta_m(t_{\min})\sim k^3$. Together with the other scaling assumptions and taking the linear case $\alpha=1$ as an example, AR yields $|c_m^{(1)}|\sim k^0$, $n_{\rm ex}\sim\tau^{-(z/z_2)(\nu/(\nu z+1))}$ along paths 1–4, and $|c_m^{(1)}|\sim k^1$, $n_{\rm ex}\sim\tau^{-3\nu/(\nu z+1)}$ along half-5 path, which completely agrees with the numerical results.

Building on the above analysis, we argue on physical grounds that the scaling of the excitation density for quenches across an *arbitrary* (*standard or multicritical*) *isolated QCP* is determined by three conditions: (i) from the condition of adiabaticity breaking, the typical gap $\hat{\Delta}$ scales as $\hat{\Delta}\sim\tau^{-\alpha\nu z/(\alpha\nu z+1)}$; (ii) an accessible excited state contributes to the excitation if and only if its minimum gap along the path matches with this typical gap $\tilde{\Delta}_k\sim\hat{\Delta}$, with $\tilde{\Delta}_k\sim(k-k_c)^{z_2}$; (iii) the excitation probability p_k scales as $p_k\sim(k-k_c)^{d_2}$, where d_2 can differ from 0 if the center of the impulse region is greatly shifted relative to the static limit. Then upon integrating up to energy $\hat{\Delta}$, and using $p_E\sim p_{k(E)}\sim E^{d_2/z_2}$, yields

$$n_{\rm ex}\sim\hat{\Delta}^{(d+d_2)/z_2}\sim\tau^{-(d+d_2)\alpha\nu z/[z_2(\alpha\nu z+1)]}, \tag{4}$$

which is consistent with all the results found thus far. While KZS corresponds to $z_2=z$, $d_2=0$, situations where $z_2\neq z$ and/or $d_2\neq 0$ are *genuinely dynamical*. The knowledge about the path-dependent excitation process becomes crucial and nonequilibrium exponents cannot be fully predicted from equilibrium ones. Interestingly, in the model under examination the Lifshitz universality class appears to be the only universality class for which anomalous scaling occurs, among all possible paths involving MCPs. Whether Lifshitz behavior may constitute a *sufficient* condition for anomalous behavior requires further investigation in other many-body systems.

ACKNOWLEDGMENTS

We thank T. Caneva for insightful feedback. S.D. acknowledges support from a Hull Graduate Foundation.

[1] S. Sachdev, *Quantum Phase Transitions* (Cambridge University Press, Cambridge, 1999).
[2] E. Farhi, J. Goldstone, S. Gutmann, J. Lapan, A. Lundgren, and D. Preda, Science **292**, 472 (2001); G. E. Santoro and E. Tosatti, J. Phys. A **39**, R393 (2006).
[3] W. H. Zurek, U. Dorner, and P. Zoller, Phys. Rev. Lett. **95**, 105701 (2005); J. Dziarmaga, *ibid.* **95**, 245701 (2005); B. Damski and W. H. Zurek, Phys. Rev. A **73**, 063405 (2006); F. M. Cucchietti, B. Damski, J. Dziarmaga, and W. H. Zurek, *ibid.* **75**, 023603 (2007).
[4] A. Polkovnikov, Phys. Rev. B **72**, 161201(R) (2005); A. Polkovnikov and V. Gritsev, Nat. Phys. **4**, 477 (2008).
[5] R. W. Cherng and L. S. Levitov, Phys. Rev. A **73**, 043614 (2006); A. Fubini, G. Falci, and A. Osterloh, New J. Phys. **9**, 134 (2007); V. Mukherjee, A. Dutta, and D. Sen, Phys. Rev. B **77**, 214427 (2008); S. Mondal, D. Sen, and K. Sengupta, *ibid.* **78**, 045101 (2008); D. Sen, K. Sengupta, and S. Mondal, Phys. Rev. Lett. **101**, 016806 (2008); R. Barankov and A. Polkovnikov, *ibid.* **101**, 076801 (2008).
[6] J. Dziarmaga, Phys. Rev. B **74**, 064416 (2006); T. Caneva, R. Fazio, and G. E. Santoro, *ibid.* **76**, 144427 (2007).
[7] T. Caneva, R. Fazio, and G. E. Santoro, Phys. Rev. B **78**, 104426 (2008).
[8] F. Pellegrini, S. Montangero, G. E. Santoro, and R. Fazio, Phys. Rev. B **77**, 140404(R) (2008).
[9] S. Deng, G. Ortiz, and L. Viola, EPL **84**, 67008 (2008).
[10] D. Chowdhury, U. Divakaran, and A. Dutta, arXiv:0906.1161 (unpublished).
[11] V. Mukherjee, U. Divakaran, A. Dutta, and D. Sen, Phys. Rev. B **76**, 174303 (2007); U. Divakaran, V. Mukherjee, A. Dutta, and D. Sen, J. Stat. Mech.: Theory Exp. 2009, P02007.
[12] S. Mondal, K. Sengupta, and D. Sen, Phys. Rev. B **79**, 045128 (2009).
[13] S. Deng, G. Ortiz, and L. Viola, *14th International Conference on Recent Progress in Many-Body Theories (RPMBT14)* (World Scientific, Singapore, 2008), Vol. 11, p. 387.
[14] Since $\nu z<z$, to leading order the scaling of Δ_k is dominated by the control parameter rather than by the size.
[15] C. Zener, Proc. R. Soc. London, Ser. A **137**, 696 (1932).
[16] N. V. Vitanov, Phys. Rev. A **59**, 988 (1999).

Appendix E

Dynamical critical scaling and effective thermalization in quantum quenches: Role of the initial state

This Appendix includes the following paper:

S. Deng, G. Ortiz, and L. Viola, "Dynamical critical scaling and effective thermalization in quantum quenches: Role of the initial state", Phys. Rev. B **83**, 094304 (2011).

Dynamical critical scaling and effective thermalization in quantum quenches: Role of the initial state

Shusa Deng,[1] Gerardo Ortiz,[2] and Lorenza Viola[1]
[1]*Department of Physics and Astronomy, Dartmouth College, Hanover, New Hampshire 03755, USA*
[2]*Department of Physics, University of Indiana, Bloomington, Indiana 47405, USA*
(Received 2 November 2010; revised manuscript received 28 January 2011; published 25 March 2011)

We explore the robustness of universal dynamical scaling behavior in a quantum system near criticality with respect to initialization in a large class of states with finite energy. By focusing on a homogeneous XY quantum spin chain in a transverse field, we characterize the nonequilibrium response under adiabatic and sudden quench processes originating from a pure as well as a mixed excited initial state, and involving either a regular quantum critical or a multicritical point. We find that the critical exponents of the ground-state quantum phase transition can be encoded in the dynamical scaling exponents despite the finite energy of the initial state. In particular, we identify conditions on the initial distribution of quasiparticle excitation that ensure that Kibble-Zurek scaling persists. The emergence of effective thermal equilibrium behavior following a sudden quench toward criticality is also investigated, with focus on the long-time expectation value of the quasiparticle number operator. Despite the integrability of the XY model, this observable is found to behave thermally in quenches to a regular quantum critical point, provided that the system is initially prepared at sufficiently high temperature. However, a similar thermalization behavior fails to occur in quenches toward a multicritical point. We argue that the observed lack of thermalization originates in this case in the asymmetry of the impulse region that is also responsible for anomalous multicritical dynamical scaling.

DOI: 10.1103/PhysRevB.83.094304 PACS number(s): 73.43.Nq, 75.10.Jm, 05.30.−d, 64.60.Kw

I. INTRODUCTION

Characterizing the nonequilibrium dynamics of quantum many-body systems is of central significance to both condensed-matter physics and quantum statistical mechanics. A quantitative understanding of nonequilibrium quantum phase transitions (QPTs) is, in particular, a fundamental prerequisite for uncovering and controlling quantum phases of matter,[1,2] as well as for assessing the complexity of quantum annealing or adiabatic algorithms.[3,4] Unlike standard phase transitions, which are driven by a change in temperature, QPTs are driven entirely by quantum fluctuations at zero temperature. They nevertheless share with their classical counterpart the generic feature of universality: In equilibrium, the critical properties of a system sufficiently close to a quantum critical point (QCP) depend only on a few relevant characteristics such as its symmetry and dimensionality, thus defining the universality class to which the corresponding (continuous) QPT belongs. The universality class is distinguished by a small set of critical exponents, for instance, ν and z, describing the power-law divergence of the characteristic length scale and the vanishing of the characteristic energy scale, respectively.[1] In a nonequilibrium scenario, the system can be driven across a QCP *dynamically*, that is, through an explicit time dependence of one or more control parameters in the underlying many-body Hamiltonian. This naturally prompts a number of questions: To what extent can universal quantum scaling laws persist out of equilibrium and be solely specified in terms of the equilibrium phase diagram? Conversely, how does quantum criticality influence the ability of a system to relax back to equilibrium?

Historically, the first theoretical studies in these directions date back to the pioneering work by Barouch and co-workers[5–7] which led, in particular, to the discovery of "nonergodic" behavior in the zero-temperature long-time magnetization of a driven XY spin chain.[6] In recent years, the demand for quantitatively addressing the above broad questions has heightened under the impetus of experimental advances in manipulating ultracold atomic gases, which are enabling the unitary dynamics of many-body quantum systems to be explored with an unprecedented level of coherent control and isolation from the environment.[8,9] As a result, nonequilibrium quantum critical physics is being actively investigated both from theoretical and experimental standpoints.

In this framework, an important step forward is provided by the prediction of universal behavior in *adiabatic* dynamics near a QCP based on the *Kibble-Zurek scaling* (KZS) argument[10] (see also Ref. 11 for related independent work and Ref. 12 for a recent review). Originally introduced in the context of classical (finite-temperature) phase transitions in cosmology,[13] the KZ argument rests on the basic intuition that, irrespective of how slowly a system is driven across a continuous phase transition, adiabaticity is necessarily lost in the thermodynamic limit due to the vanishing energy gap at the critical point. Qualitatively, this determines typical time and length scales, $\hat{t}$ and $\hat{\xi}$, respectively, which characterize the adiabatic-to-diabatic crossover and, since "order" cannot be established on distances larger than $\hat{\xi}$, results in the formation of a domain structure and the generation of a *finite* density of "topological defects" in the system. Quantitatively, let the time dependence in the quantum-mechanical Hamiltonian $H(t)$ be introduced through a control parameter $\lambda(t)$, with $\lambda_c \equiv \lambda(t_c)$ corresponding to the crossing of an isolated QCP at time t_c, which can be taken to be $t_c \equiv 0$ without loss of generality. If the system is initially ($t = t_0$) in the ground state, its ability to adiabatically adjust to $H(t)$ is determined by the condition that the typical time scale $\tau(t) \equiv |(\lambda(t) - \lambda_c)/\dot{\lambda}(t)|$ associated with the applied control be sufficiently long relative to the slowest response time $\tau_r \sim \Delta^{-1}$, which is set by the smallest energy gap Δ. Since, as the QCP is approached, the latter vanishes as $\Delta \sim |\lambda(t) - \lambda_c|^{\nu z}$, adiabaticity is broken throughout an

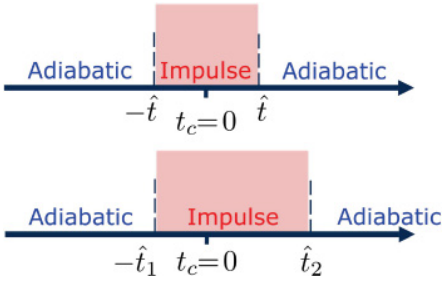

FIG. 1. (Color online) Qualitative sketch of the adiabatic-impulse-adiabatic sequence of regimes relevant to dynamical scaling arguments. Top: Symmetric impulse region, as assumed by the standard KZS scenario. Bottom: Asymmetric impulse region, as resulting from the existence of quasicritical path-dependent energy states; see Ref. 23.

"impulse region" $[t_c - \hat{t}, t_c + \hat{t}]$ symmetrically located around the QCP, where the "freeze-out" time $\hat{t}$ is determined by the condition $\tau(\hat{t}) = \tau_r(\hat{t})$. In the simplest case of a linear sweep across the QCP (Fig. 1, top), $\lambda(t) - \lambda_c \equiv t/\tau$ for a fixed rate $\tau^{-1} > 0$, this yields $\hat{t} \sim \tau^{\nu z/(\nu z+1)}$ and a typical gap $\hat{\Delta} \sim \hat{t}^{-1}$. Correspondingly, the typical correlation length $\hat{\xi} \sim \xi(\hat{t}) \sim \hat{\Delta}^{-z}$ also scales with the quench time τ. Since $\hat{\xi}$ is the universal length scale near criticality, it determines the scaling of the final ($t = t_f$) density of defects and, more generally, the *total* density of excitations, $n_{\rm ex}(t_f)$, created in the system. If d denotes the spatial dimension, the KZS result then follows:

$$n_{\rm ex}(t_f) \sim \tau^{-d\nu/(\nu z+1)}. \tag{1}$$

The validity as well as the limitations of the above KZS have been carefully scrutinized in a number of settings. By now, the original KZS has been confirmed for a variety of models involving a regular isolated QCP,[14–18] and extensions have been introduced for more general adiabatic dynamics, including repeated,[19] nonlinear,[20] and optimal[21] quench processes. In parallel, departures from the KZS predictions have emerged for more complex adiabatic scenarios, involving, for instance, quenches across either an isolated multicritical point (MCP),[20,22–25] or nonisolated QCPs (that is, critical regions),[26–29] as well as QPTs in infinitely coordinated,[30] disordered,[31] and/or spatially inhomogeneous systems.[12,32] A main message that has emerged from the above studies is that, unlike in the standard KZS of Eq. (1) where the nonequilibrium critical exponent is completely specified in terms of static exponents, additional details about the time-dependent excitation may play an essential role in general. As a result, genuinely nonstatic, *path-dependent exponents* may be required for dynamical scaling predictions. This feature is vividly exemplified, for instance, in multicritical quantum quenches, whereby the asymmetry of the KZ impulse region relative to the static QCP (Fig. 1, bottom) causes a path-dependent minimum gap other than the critical gap to be relevant and an effective dynamical exponent $z_2 \neq z$ to emerge.[23]

In addition to characterizing the response to an adiabatic probe, the opposite limit of a *sudden* change of the tuning parameter $\lambda(t)$ near a QCP has also attracted a growing attention recently, in connection with the study of both dynamical quantum-critical properties,[33–35] as well as thermalization dynamics in closed quantum systems and its interplay with quantum integrability.[36–43] In particular, for sudden quenches with a sufficiently *small amplitude*, the existence of universal scaling behavior has been established for various physical observables and qualitatively related to the above KZ argument:[35,44] by associating to a quench with amplitude $\delta\lambda$ the characteristic length scale $\xi \sim |\delta\lambda|^{-\nu}$, and by interpreting ξ as the correlation length in the final state, one immediately infers that $n_{\rm ex}(t_f) \sim \xi^{-d} \sim |\delta\lambda|^{d\nu}$.

With a few exceptions where quenches at finite temperature and the associated thermal corrections have also been examined,[35,36,44,45] the large majority of the existing investigations have focused on quench dynamics originating from the ground state of the initial Hamiltonian $H(t_0)$. Our goal in this work is to present a dedicated analysis of *finite-energy quantum quenches*, with a twofold motivation in mind. Conceptually, elucidating to what extent and how universal scaling properties may depend upon the details of the system's initialization is needed to gain a more complete picture of nonequilibrium quantum-critical physics. While one might, for instance, naively expect that a sizable overlap with the initial ground state would be essential in determining the applicability of ground-state scaling results, a main highlight of our analysis is that the support of the initial state on those excitations relevant to the path-dependent excitation process is key in a dynamical scenario, in a sense to be made precise later. Furthermore, from a practical standpoint, perfect initialization of a many-body Hamiltonian in its exact ground state is both non-deterministic polynomial (NP)-hard in general[46,47] and experimentally unfeasible due to limited control. In this sense, our investigation both extends previous studies on finite-temperature signatures of static QPTs,[48] and may be directly relevant to experiments using ultracold atoms[8] as well as nuclear magnetic resonance (NMR) quantum simulators.[49,50]

While our analysis focuses on the simplest yet paradigmatic case of an exactly solvable XY quantum spin chain (Sec. II), we address nonequilibrium dynamics originating from a large class of (bulk) initial states for a variety of different quench schemes involving either a regular QCP or a MCP. Both pure and mixed initial states carrying finite excitation energy above the ground state are examined, under the main assumption that, subsequent to initialization, the system can be treated as (nearly) isolated, hence evolving under a time-dependent Hamiltonian. In particular, dynamical scaling in adiabatic and sudden quenches starting from an *excited energy eigenstate* are analyzed in Secs. III A and III B, respectively, with emphasis on making contact with previously introduced adiabatic renormalization approaches[15,28] and on clarifying formal connections between scaling behavior in sudden and adiabatic dynamics. The case of a *generic excited pure state* prepared by a sudden parameter quench is also considered in Sec. III C, and criteria are identified for KZS to be obeyed. Section IV is devoted to quench dynamics resulting from an *initial thermal mixture*, with the main goals of characterizing the robustness of dynamical scaling behavior in realistic finite-temperature conditions, and of further exploring the conditions leading to effective thermalization of certain physical observables following a sudden quench toward criticality. In the process, we continue and extend the analysis undertaken in Deng *et al.*[23] by presenting finite-temperature generalizations of the scaling predictions obtained for adiabatic (both linear

and nonlinear) *multicritical quantum quenches*, as well as evidence of how the peculiar nature of a MCP may also result in *anomalous thermalization behavior*. Section V concludes with a discussion of the main findings and their implications, along with further open problems.

II. MODEL HAMILTONIAN

A. Energy spectrum and equilibrium phase diagram

We consider the homogeneous one-dimensional spin-1/2 XY model described by the Hamiltonian

$$H = -\sum_{j=1}^{N}\left(\frac{1+\gamma}{2}\sigma_x^j\sigma_x^{j+1} + \frac{1-\gamma}{2}\sigma_y^j\sigma_y^{j+1} - h\sigma_z^j\right), \quad (2)$$

where periodic boundary conditions are assumed, that is, $\sigma_\alpha^j \equiv \sigma_\alpha^{j+N}$, and N is taken to be even. Here, $\gamma, h \in [-\infty,\infty]$, parametrize the degree of anisotropy in the XY plane, and the uniform magnetic-field strength, respectively, in suitable units. The diagonalization of Hamiltonian (2) is well known,[5,6,51,52] and we only recall the basic steps here. Upon introducing canonical fermionic operators $\{c_j, c_j^\dagger\}$ via the Jordan-Wigner mapping $c_j^\dagger \equiv \prod_{\ell=1}^{j}(-\sigma_z^\ell)\sigma_+^j$, H rewrites as a quadratic form

$$H = -\sum_{j=1}^{N-1}(c_j^\dagger c_{j+1} + \gamma c_j^\dagger c_{j+1}^\dagger + \text{H.c.}) + 2h\sum_{j=1}^{N} c_j^\dagger c_j - hN + \mathcal{P}\,(c_N^\dagger c_1 + \gamma c_N^\dagger c_1^\dagger + \text{H.c.}), \quad (3)$$

where the last term originates from the spin periodic boundary conditions and the parity operator $\mathcal{P} \equiv \prod_{j=1}^{N}(-\sigma_z^j) = e^{i\pi\sum_{j=1}^{N} c_j^\dagger c_j} = +1(-1)$ depending on whether the eigenvalue of the total fermionic number operator is even (odd), respectively. Physically, $\mathcal{P}$ corresponds to a global $\mathbb{Z}_2$ symmetry, which, for finite N, allows the even and odd subspaces to be exactly decoupled, $H \equiv H^{(+)} + H^{(-)}$, and the diagonalization to be carried out separately in each sector.

In finite systems, the ground state as well as excited energy eigenstates with an even number of fermions belong to the $\mathcal{P} = +1$ sector. By using a Fourier transformation to momentum space, $c_k^\dagger = \frac{1}{\sqrt{N}}\sum_{j=1}^{N} e^{-ikj}c_j^\dagger$, followed by a Bogoliubov rotation to fermionic quasiparticles $\{\gamma_k, \gamma_k^\dagger\}$, with $\gamma_k = u_k c_k - i v_k c_{-k}^\dagger$, $u_k = u_{-k}$, $v_k = -v_{-k}$, and $u_k^2 + v_k^2 = 1$, the Hamiltonian in Eq. (3) rewrites as a sum of noninteracting terms:

$$H^{(+)} \equiv \sum_{k\in K_+} H_k = \sum_{k\in K_+} \epsilon_k(h,\gamma)(\gamma_k^\dagger\gamma_k + \gamma_{-k}^\dagger\gamma_{-k} - 1). \quad (4)$$

Here, the set $K \equiv K_+ + K_-$ of allowed momentum modes is determined by the antiperiodic boundary conditions on the fermions in the even sector, $c_{j+N} \equiv -c_j$, which yields $K_\pm = \{\pm\frac{\pi}{N}, \pm\frac{3\pi}{N}, \ldots, \pm(\pi - \frac{\pi}{N})\}$, and

$$\epsilon_k(h,\gamma) = 2\sqrt{(h-\cos k)^2 + \gamma^2\sin k^2} \quad (5)$$

is the quasiparticle energy of mode k. For each k, let $\mathcal{H}_k \equiv \text{span}\{|0_k\rangle, |1_k\rangle\}$, where $\{|0_k\rangle, |1_k\rangle = \gamma_k^\dagger|0_k\rangle\}$ are orthonormal states corresponding, respectively, to zero and one Bogoliubov quasiparticle with momentum k, that is, $\langle 0_k|\gamma_k^\dagger\gamma_k|0_k\rangle = 0$, $\langle 1_k|\gamma_k^\dagger\gamma_k|1_k\rangle = 1$, and similarly for $-k$. Thus the four eigenstates of H_k provide a basis for $\mathcal{H}_k \otimes \mathcal{H}_{-k}$,

$$\mathcal{B}_k = \{|0_k,0_{-k}\rangle, |1_k,1_{-k}\rangle, |0_k,1_{-k}\rangle, |1_k,0_{-k}\rangle\} \equiv \mathcal{B}_k^{(+)} \oplus \mathcal{B}_k^{(-)}, \quad (6)$$

where the corresponding eigenenergies are given by $-\epsilon_k$, ϵ_k, 0, 0, and a further separation into an even (odd) sector for each k is possible due to the fact that $[\mathcal{P}_k, H_k] = 0$, with $\mathcal{P}_k \equiv e^{i\pi(\gamma_k^\dagger\gamma_k + \gamma_{-k}^\dagger\gamma_{-k})} = e^{i\pi(c_k^\dagger c_k + c_{-k}^\dagger c_{-k})}$.

The ground state of $H^{(+)}$ corresponds to the BCS state with no Bogoliubov quasiparticles,

$$|\Psi_0^{(+)}\rangle = \bigotimes_{k\in K_+}|0_k0_{-k}\rangle = \bigotimes_{k\in K_+}(u_k + i v_k c_k^\dagger c_{-k}^\dagger)|\texttt{vac}\rangle,$$

where $|\texttt{vac}\rangle$ is the fermionic vacuum. Many-body excited states in the even sector can be obtained by applying pairs of Bogoliubov quasiparticle operators to $|\Psi_0^{(+)}\rangle$. In particular, excited eigenstates with support only on the even sector $\mathcal{B}_k^{(+)}$ for each mode are obtained by exciting only pairs of quasiparticles with opposite momentum and have the form

$$|\Psi_E^{(+)}\rangle = \left(\bigotimes_{k\in K_+^e}|1_k1_{-k}\rangle\right)\left(\bigotimes_{k\in K_+ - K_+^e}|0_k0_{-k}\rangle\right), \quad (7)$$

where K_+^e labels the subset of excited modes.

For finite N, the ground state and excited energy eigenstates with an odd number of fermions belong to the sector $\mathcal{P} = -1$, which implies periodic boundary conditions on the fermions, $c_{j+N} \equiv c_j$, and a different set $\bar{K}$ of allowed momentum modes, $\bar{K} \equiv \bar{K}_+ + \bar{K}_- + \{0, -\pi\}$, where $\bar{K}_\pm = \{\pm\frac{2\pi}{N}, \pm\frac{4\pi}{N}, \ldots, \pm(\pi - \frac{2\pi}{N})\}$. Since one may show that $\epsilon_{k=0} = h - 2$ and $\epsilon_{k=-\pi} = h + 2$, occupying mode 0 has always lower energy than occupying mode $-\pi$, thus the ground state of $H^{(-)}$ is now

$$|\Psi_0^{(-)}\rangle = |1_0 0_{-\pi}\rangle \bigotimes_{k\in\bar{K}_+}|0_k0_{-k}\rangle,$$

and excitations may be generated by applying Bogoliubov quasiparticle operators in such a way that the constraint on the total fermionic number is obeyed. Similar to modes in the even sector, $k \in K_+$, the subspace of each mode $k \in \bar{K}_+$ yields four eigenstates of H_k and, in principle, a basis formally identical to the one in Eq. (6) for the odd Hilbert-space sector. Although for finite N (thus necessarily in numerical simulations) $\mathcal{P}$ is always a good quantum number under dynamics induced by H, the error in the computation of observables arising from identifying the two sets of modes K and $\bar{K}$ scales like $1/N$. Thus for sufficiently large N, a simplified description in terms of a unique set of momentum modes is possible by using the basis

$$\mathcal{B} \equiv \bigotimes_{k\in K_+}\mathcal{B}_k \quad (8)$$

to characterize arbitrary states in the full Hilbert space $\mathcal{H} = \bigotimes_{k\in K_+}(\mathcal{H}_k \otimes \mathcal{H}_{-k})$. This becomes accurate in the thermodynamic limit $N \to \infty$, where the many-body ground state becomes twofold degenerate and the $\mathbb{Z}_2$ symmetry spontaneously breaks, causing different $\mathcal{P}$ sectors to mix.

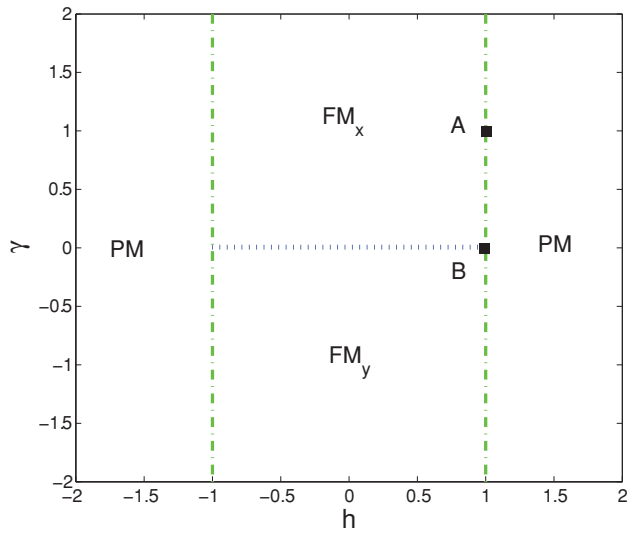

FIG. 2. (Color online) The phase diagram of the XY Hamiltonian in Eq. (2). The regular QCP A ($h_c = 1, \gamma_c = 1$) and the MCP B ($h_c = 1, \gamma_c = 0$) are marked. The dashed-dotted (green) line separates the ferromagnetic (FM) and paramagnetic (PM) phases, whereas the dotted (blue) line represents the superfluid phase (SF).

The equilibrium phase diagram of the model Hamiltonian in Eq. (2) is determined by the behavior of the excitation gap of each mode, $\Delta_k(h,\gamma) \equiv \epsilon_k(h,\gamma)$, with $\epsilon_k(h,\gamma)$ given in Eq. (5), and is depicted in Fig. 2. Throughout this work, we will mainly investigate scaling behavior in quenches involving either the regular QCP A ($h_c = 1, \gamma_c = 1$), which has equilibrium critical exponents $\nu = z = 1$ and belongs to the $d = 2$ Ising universality class, or the MCP B ($h_c = 1, \gamma_c = 0$), which has $\nu = 1/2, z = 2$ and belongs instead to the Lifshitz universality class.[23] In what follows, we shall refer to the *critical mode* k_c as the mode whose gap $\Delta_k(h,\gamma)$ vanishes in the thermodynamic limit. For both the QCPs A and B of interest, we thus have $k_c = 0$ in the large-N limit.

B. Dynamical response indicators

If the system described by Eq. (2) is driven across a QCP by making one (or both) of the control parameter(s) h, γ explicitly time dependent, excitations are induced as a result of the nonequilibrium dynamics. Since the gap vanishes at the QCP in the thermodynamic limit, this happens no matter how slowly the Hamiltonian changes with time. In Refs. 17 and 28, the excess expectation value relative to the instantaneous ground state was shown to successfully characterize dynamical scaling behavior for a large class of physical observables in adiabatic quenches originating from the ground state. That is, for an extensive observable $\mathcal{O}$, the following quantity quantifies the underlying adiabaticity loss:

$$\Delta\mathcal{O}(t) \equiv \langle\Psi(t)|\,\mathcal{O}\,|\Psi(t)\rangle - \langle\tilde{\Psi}(t)|\,\mathcal{O}\,|\tilde{\Psi}(t)\rangle, \qquad (9)$$

where $|\Psi(t)\rangle$ and $|\tilde{\Psi}(t)\rangle$ are the actual time-evolved state and the adiabatically evolved state resulting from $|\Psi(t_0)\rangle$, respectively. For a generic quench process, where in principle both the time dependence in $H(t)$ and the initial state $\rho(t_0)$ can be arbitrary, it is desirable to characterize the response of the system in such a way that no excitation is generated by purely adiabatic dynamics,[15] and zero-energy quenches are included as a special case. This motivates extending the definition of Eq. (9) to

$$\Delta\mathcal{O}(t) \equiv \mathrm{Tr}[\mathcal{O}(t)\rho(t)] - \mathrm{Tr}[\mathcal{O}(t)\tilde{\rho}(t)]\,, \qquad (10)$$

where now $\rho(t)$ and $\tilde{\rho}(t)$ are the actual time-evolved density operator and the density operator resulting from adiabatic evolution of $\rho(t_0)$, respectively, and we also allow, in general, for the observable $\mathcal{O}$ to be explicitly time dependent. Let $H(t)|\Psi_i(t)\rangle = E_i(t)|\Psi_i(t)\rangle$ define snapshot eigenstates and eigenvalues of $H(t)$ along a given control path. Then the adiabatically steered state $\tilde{\rho}(t) = \sum_{i,j}\rho_{i,j}(t_0)|\Psi_i(t)\rangle\langle\Psi_j(t)|$, with $\rho_{i,j}(t_0)$ being the matrix elements of the initial state $\rho(t_0)$ in the eigenstate basis $|\Psi_i(t_0)\rangle\langle\Psi_j(t_0)|$ of the initial Hamiltonian $H(t_0)$.

With respect to the basis given in Eq. (8), a generic uncorrelated state in momentum space may be expressed in the form $\rho(t) = \bigotimes_{k\in K_+}\rho_k(t)$, where $\rho_k(t)$ is the four-dimensional density operator for mode k. Relative to a snapshot eigenbasis

$$\mathcal{B}_k(t) \equiv \left\{\left|\psi_k^j(t)\right\rangle\right\}, \quad j = 0,\ldots,3,$$

similar to the one given in Eq. (6), but constructed from time-dependent quasiparticle operators such that $\gamma_k(t)|0_k(t)\rangle = 0$, $\gamma_k^\dagger(t)|0_k(t)\rangle = |1_k(t)\rangle$, $\rho_k(t)$ may be expressed as

$$\rho_k(t) = \sum_{i,j=0,3}\rho_{ij,k}(t)\left|\psi_k^i(t)\right\rangle\left\langle\psi_k^j(t)\right|.$$

Suppose that the time-evolution operator for mode k is $U_k(t)$, that is, $\rho_k(t) = U_k(t)\rho_k(t_0)U_k^\dagger(t)$. Direct calculation shows that $|0_k(t),1_{-k}(t)\rangle = c_{-k}^\dagger|\mathtt{vac}\rangle$, and $|1_k(t),0_{-k}(t)\rangle = c_k^\dagger|\mathtt{vac}\rangle$ for all t, which indicates that the snapshot eigenstates belonging to the $\mathcal{P}_k = -1$ eigenvalues are frozen in time, $|0_k(t),1_{-k}(t)\rangle = |0_k(t_0),1_{-k}(t_0)\rangle$, $|1_k(t),0_{-k}(t)\rangle = |1_k(t_0),0_{-k}(t_0)\rangle$. As long as $\mathcal{P}_k$ is conserved under $H_k(t)$, the even and odd sectors for each k are decoupled. Thus upon letting

$$\begin{aligned}&U_k^\dagger(t)|1_k(t),1_{-k}(t)\rangle\\ &\quad\equiv a_{0,k}(t)|0_k(t_0),0_{-k}(t_0)\rangle + a_{1,k}(t)|1_k(t_0),1_{-k}(t_0)\rangle,\end{aligned}$$

we can evaluate the time-dependent excitation probability for mode k as follows:

$$\begin{aligned}P_k(t) &\equiv \mathrm{Tr}[\rho_k(t)\gamma_k^\dagger(t)\gamma_k(t)]\\ &= \mathrm{Tr}[\rho_k(t)(|1_k(t),1_{-k}(t)\rangle\langle 1_k(t),1_{-k}(t)|]\\ &\quad + \mathrm{Tr}[\rho_k(t)|1_k(t),0_{-k}(t)\rangle\langle 1_k(t),0_{-k}(t)|]\\ &= [\rho_{00,k}(t_0) - \rho_{11,k}(t_0)]|a_{0,k}(t)|^2 + \rho_{11,k}(t_0)\\ &\quad + 2\mathrm{Re}[\rho_{01,k}(t_0)a_{0,k}^*(t)a_{1,k}(t)] + \rho_{33,k}(t_0), \qquad (11)\end{aligned}$$

where the relationships $|a_{0,k}(t)|^2 + |a_{1,k}(t)|^2 = 1$ and $\rho_{10,k} = \rho_{01,k}^*$ have been exploited. Notice that from the above definition of $a_{0,k}(t)$, it follows that $|a_{0,k}(t)|^2$ is the time-dependent probability that mode k is excited when it is in its ground state at $t = t_0$. Similarly, we may express the adiabatically evolved density operator $\tilde{\rho}(t) = \bigotimes_{k\in K_+}\tilde{\rho}_k(t)$, with $\tilde{\rho}_k(t) = \sum_{i,j=0,3}\rho_{ij,k}(t_0)|\psi_k^i(t)\rangle\langle\psi_k^j(t)|$. Thus the time-dependent excitation probability of mode k relative to the adiabatic path is

simply

$$\tilde{P}_k(t) = \mathrm{Tr}[\tilde{\rho}_k(t)\gamma_k^\dagger(t)\gamma_k(t)] = \rho_{11,k}(t_0) + \rho_{33,k}(t_0) \equiv P_k(t_0). \quad (12)$$

Upon combining Eqs. (11) and (12), the *relative excitation probability* of mode k is given by

$$\Delta P_k(t) \equiv P_k(t) - P_k(t_0) = [\rho_{00,k}(t_0) - \rho_{11,k}(t_0)]|a_{0,k}(t)|^2 + 2\mathrm{Re}[\rho_{01,k}(t_0)a_{0,k}^*(t)a_{1,k}(t)]. \quad (13)$$

Physically, a nonzero contribution $P_k(t_0)$ may account for initial excitations due to either a coherent preparation into an excited state or to a finite temperature T. Clearly, if mode k is initially in its ground state, $P_k(t_0) = 0$, we consistently recover the definitions in Ref. 28 for zero-energy quenches. Two relevant limiting cases of Eq. (13) will play a special role in what follows. First, if mode k is initially in a generic pure state of the form

$$|\psi_k(t_0)\rangle \equiv \sum_{j=0,3} c_{j,k}|\psi_k^j(t_0)\rangle,$$

then $\rho_{00,k}(t_0) = |c_{0,k}|^2$, $\rho_{01,k}(t_0) = c_{0,k}c_{1,k}^*$, $\rho_{11,k}(t_0) = |c_{1,k}|^2$, hence

$$\Delta P_k(t) = (|c_{0,k}|^2 - |c_{1,k}|^2)|a_{0,k}(t)|^2 + 2\mathrm{Re}[c_{0,k}c_{1,k}^*a_{0,k}^*(t)\,a_{1,k}(t)]. \quad (14)$$

Second, if the initial state $\rho(t_0)$ is a statistical mixture, then $\rho_{10,k}(t_0) = \rho_{01,k}(t_0) = 0$, and we have

$$\Delta P_k(t) = [\rho_{00,k}(t_0) - \rho_{11,k}(t_0)]|a_{0,k}(t)|^2. \quad (15)$$

The time-dependent excess expectation value $\Delta\mathcal{O}(t)$ in Eq. (10) may be expressed directly in terms of the relative excitation probability for observables that obey $[\mathcal{O}(t), H(t)] = 0$ at all times. In this work, we shall primarily focus on the following choices:

(1) $\mathcal{O}(t) = \frac{1}{N}\sum_{k\in K^+}[\gamma_k^\dagger(t)\gamma_k(t) + \gamma_{-k}^\dagger(t)\gamma_{-k}(t)]$, leading to the relative total density of excitations:

$$\Delta n_{\mathrm{ex}}(t) = \frac{2}{N}\sum_{k\in K_+}\mathrm{Tr}\{[\rho_k(t) - \tilde{\rho}_k(t)]\gamma_k^\dagger(t)\gamma_k(t)\} = \frac{2}{N}\sum_{k\in K_+}\Delta P_k(t), \quad (16)$$

which coincides with $n_{\mathrm{ex}}(t)$ when the initial state is the ground state.

(2) $\mathcal{O}(t) = H(t)$, leading to the relative excitation energy density:

$$\Delta H(t) = \frac{2}{N}\sum_{k\in K_+}\mathrm{Tr}[(\rho_k(t) - \tilde{\rho}_k(t))H_k(t)] = \frac{2}{N}\sum_{k\in K_+}\epsilon_k(h(t),\gamma(t))\Delta P_k(t). \quad (17)$$

While $\Delta n_{\mathrm{ex}}(t)$ is especially attractive from a theory standpoint in view of its simplicity (possibly enabling analytical calculations), a potential advantage of $\Delta H(t)$ is that it may be more directly accessible in experiments.

As a representative example of an observable *not* commuting with the system's Hamiltonian, we shall additionally include results on the scaling behavior of the following:

(3) $\mathcal{O} \equiv XX = \frac{1}{N}\sum_{i=1}^N \sigma_x^i\sigma_x^{i+1}$, corresponding to the nearest-neighbor spin correlator per site along the x direction.[17] In the Ising limit ($\gamma = 1$), the operator $\mathcal{N} \equiv (1 - XX)/2$ is a natural measure for the "density of kinks" created by the quench, which directly relates to the number of quasiparticles excited at $h = 0$.[12,14,40] We have

$$\Delta XX(t) = \frac{2}{N}\sum_{k\in K_+}\Delta(-2\cos k\, c_k^\dagger c_k) + \Delta[i\gamma(t)\sin k\,(c_k^\dagger c_{-k}^\dagger - \mathrm{H.c.})]. \quad (18)$$

In principle, the sums in Eqs. (16)–(18) should include all the modes in K_+, as indicated. However, for the purpose of analytically investigating dynamical scaling behavior, it is useful to note that not all the allowed modes will necessarily change their state along the adiabatic quench path, effectively making no contribution to the relative expectation $\Delta\mathcal{O}(t)$. In what follows, we shall refer to the subset of modes $K_R \subseteq K_+$ whose state changes in an adiabatic quench as the *relevant modes*. Let a power-law adiabatic quench process be parametrized as $\lambda(t) - \lambda_c = |t/\tau|^\alpha \mathrm{sgn}(t), \alpha = 1$ corresponding to the standard linear case also discussed in the Introduction. We may relate the number of relevant modes, $N_R \equiv |K_R|$, to the system size and the quench rate via $N_R(N,\tau) \propto N|k_{\max}(\tau) - k_c|$, where $k_{\max}$ is the largest momentum in the relevant mode set. Since adiabaticity breaks at a time scale $\hat{t} \sim \tau^{\alpha\nu z/(\alpha\nu z+1)}$, and the typical gap, $\hat{\Delta} \sim \hat{t}^{-1}$, an accessible excited state contributes to the excitation if and only if its minimum gap along the path, $\tilde{\Delta}_k$, matches with this typical gap, $\tilde{\Delta}_k \sim \hat{\Delta}$. In general,[23] $\tilde{\Delta}_k$ scales as $\tilde{\Delta}_k \sim (k - k_c)^{z_2}$, where z_2 is a genuinely nonstatic exponent. Accordingly, the scaling of $k_{\max}$ can be determined by $\hat{\Delta} \sim (k_{\max} - k_c)^{z_2}$, leading to

$$k_{\max} - k_c \sim \tau^{-\alpha\nu z/[z_2(\alpha\nu z+1)]}. \quad (19)$$

III. QUENCHES FROM A PURE EXCITED STATE

A. Adiabatic quench dynamics from an excited energy eigenstate

Adiabatic quenches from the ground state of the initial Hamiltonian $H(t_0)$ have been extensively studied and are well understood in this model.[14–17,23] In order to explore the role of initialization, a first natural step is to investigate dynamical scaling behavior when the initial state is an excited eigenstate of $H(t_0)$. Since, as remarked, the time evolution of excited components along $|0_k,1_{-k}\rangle$ and $|1_k,0_{-k}\rangle$ is trivial, we shall focus on excited energy eigenstates with support only on the even sector of each mode k, that is, on states of the form given in Eq. (7). Noting that there are only two possibilities for each mode, either $c_{0,k} = 1$ or $c_{0,k} = 0$, Eq. (14) yields

$$\Delta P_k(t) = (|c_{0,k}|^2 - |c_{1,k}|^2)|a_{0,k}(t)|^2 = \pm|a_{0,k}(t)|^2, \quad (20)$$

and, correspondingly,

$$\Delta n_{\mathrm{ex}}(t_f) = \frac{2}{N}\sum_{k\in K_R}[\pm|a_{0,k}(t_f)|^2]. \quad (21)$$

Thus the relative excitation density is the same, up to a sign, in two limiting cases: (i) the many-body ground state, corresponding to $c_{0,k} = 1$ for all k and to an overall positive sign in Eq. (21), and (ii) the state where all allowed pairs of quasiparticles are excited, corresponding to $c_{0,k} = 0$ for all k and to an overall negative sign in Eq. (21). Since KZS is known to hold for a linear quench process with initial condition (i), and a global sign difference would not change the scaling behavior, KZS is expected to persist for the maximally excited initial eigenstate (ii) as well. This is to some extent surprising both in view of the fact that such an initial state has zero overlap with the BCS state $|\Psi_0^{(+)}\rangle$, and because one would not *a priori* expect highly energetic eigenstates to be sensitive to the ground-state QPT.

Interestingly, critical properties of excited eigenstates in the XY chain have recently attracted attention in the context of *static* QPTs.[53] Suppose that each excited eigenstate is associated with an ordered binary strings of length $|K| = N$, where 0 (1) represents a mode in its ground (excited) state, respectively. Then a compact description of the eigenstate may be given in terms of the "discontinuities" of a (suitably regularized as $N \to \infty$) characteristic function of the corresponding occupied mode set, where no discontinuity is present when all modes are 0 or 1, and a discontinuity is counted every time the occupation of a given mode changes along the string. Alba *et al.*[53] have analytically proved, in particular, that the block entanglement entropy S_L of an excited eigenstate of the critical XY chain may still obey conformal scaling as in the ground state provided that the number of discontinuities remains *finite* in the thermodynamic limit, that is, $S_L \sim \log L$, where $L \gg 1$ is the block size. Conversely, S_L exhibits noncritical scaling, $S_L \sim L$, when the number of discontinuities becomes itself an extensive quantity as $N \to \infty$. Thus certain highly excited states (including the fully excited state considered above) can still display critical behavior, the number of discontinuities in the *full* set of momentum modes being the essential factor in determining the *static* scaling behavior. While, intuitively, nonanalyticities in the characteristic mode occupation function need not play a direct role for simple observables such as the excitation density, these results still prompt the following question: To what extent does a distinction between "critical" (leading to KZS) and "noncritical" excited eigenstates exist for *dynamical* QPTs?

A key difference with respect to the static situation is that only the *relevant* modes matter in a dynamical QPT, $k \in K_R \equiv [k_c, k_{\max}]$, with $k_{\max}$ given in Eq. (19). In Fig. 3, we present exact numerical results, obtained by direct numerical integration of the time-dependent Schrödinger equation, for

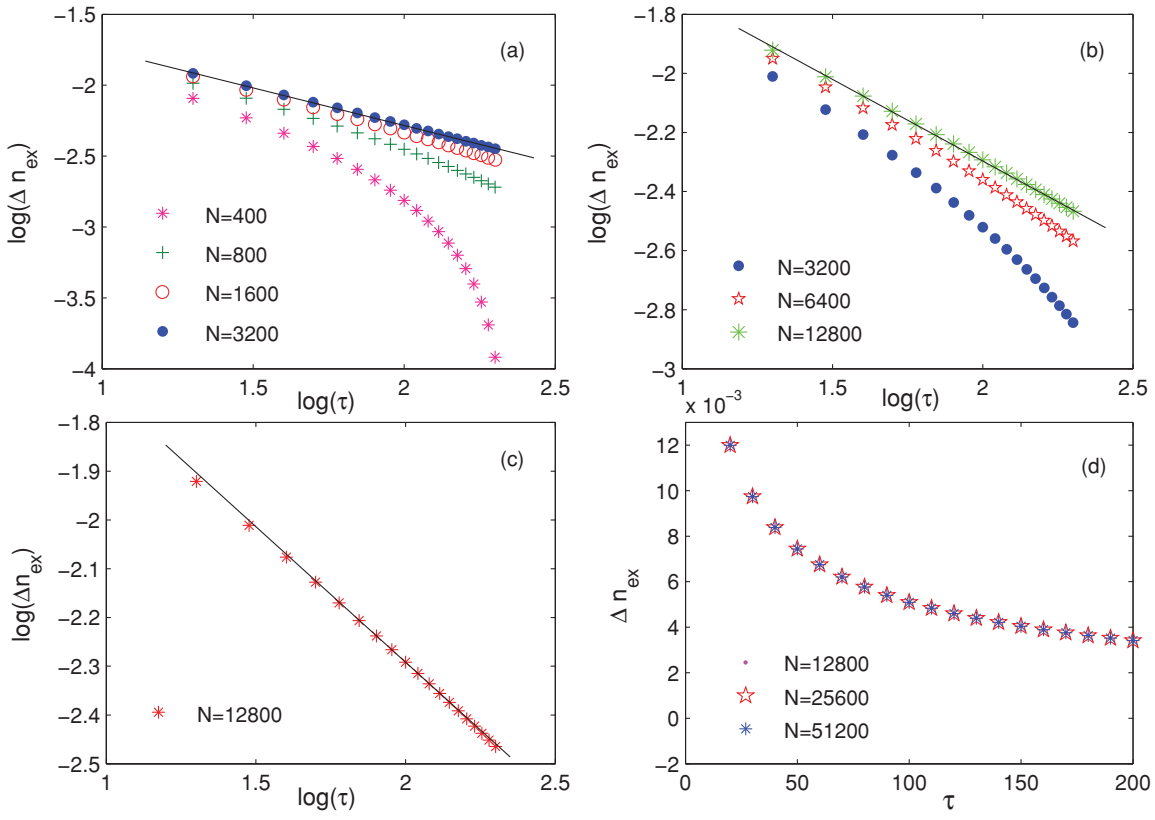

FIG. 3. (Color online) Scaling behavior of the final relative excitation density in a linear quench of the magnetic field h around the QCP A in the Ising chain, starting with different excited eigenstates of $H(h_c)$. (a) Only $k_c = \pi/N$ is excited initially. The linear fit for $N = 3200$ yields -0.535 ± 0.002. (b) The five lowest-energy modes are initially excited. A linear fitting slope of -0.549 ± 0.003 is now reached at $N = 12\,800$. (c) Five modes ($k = k_c$, $5\pi/N$, $9\pi/N$, $13\pi/N$, and $17\pi/N$) are initially excited. The linear fit for $N = 12\,800$ yields -0.546 ± 0.002. (d) The five lowest-energy modes are initially excited for $N = 12\,800$ as in (b), but as the system size is increased linearly, the number of excited modes is increased accordingly. In all cases, the relevant τ range $\tau_{\min} < 20 \leqslant \tau \leqslant 250 < \tau_{\max}$ (see text and Fig. 4).

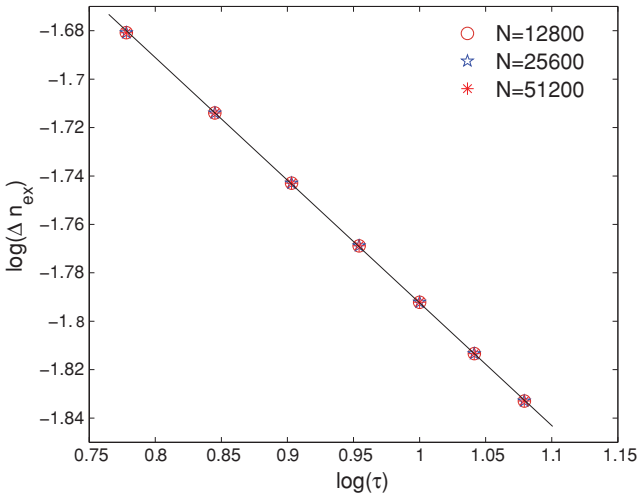

FIG. 4. (Color online) Scaling behavior of the final relative excitation density in a linear magnetic-field quench around the QCP A in the Ising chain, starting with an eigenstate of $H(t_c)$ where the 5, 10, and 20 lowest-energy modes are initially excited for $N = 12\,800, N = 25\,600, N = 51\,200$, respectively [the same as in Fig. 3(d)]. The relevant τ range is now $\tilde{\tau}_{\min} \sim \tau_{\min} = 5 \leqslant \tau \leqslant \tilde{\tau}_{\max} = 20 \ll \tau_{\max}$. A linear fitting slope of -0.5019 ± 0.002 is now reached for all these cases, in agreement with the KZS prediction.

the relative excitation density in a linear adiabatic quench of the magnetic field h around the QCP A of the critical Ising chain ($\gamma = 1$). Different initial eigenstates are compared over a common range of τ, which is chosen to be well within the appropriate τ range[28] for ground-state quenches (see the next paragraph and Fig. 4 for further discussion of this point). In Fig. 3(a), the system is initialized in the first excited state, where only the critical mode is initially excited (thus only one discontinuity is present), whereas in Fig. 3(b), the five lowest-energy modes are initially excited (leading to one discontinuity as well). In case (a), while no scaling is visible for a system with size $N = 400$, progressively better scaling behavior emerges as N is increased, with the value at $N = 3200$ approaching the asymptotic KZS value (and better agreement being achievable by optimizing the τ range, see below). In contrast, for the data in panel (b), a system size as large as $N = 12\,800$ is required for a scaling of comparable quality to be established. Since the only difference between cases (a) and (b) is a different (fixed) number of initially excited modes in N_R, the fact that upon increasing N (thereby increasing N_R accordingly) a better KZS is comparatively obtained in (a) suggests that the *ratio between the number of initially excited (or nonexcited) modes and* N_R is crucial for dynamical scaling behavior—not (as intuitively expected) the discontinuity properties which characterize the initial mode occupation *per se*. More explicitly, let N_E denote the number of modes in K_R that are excited at time t_0, with $N_R - N_E$ correspondingly denoting the number of nonexcited modes in K_R, and let

$$M_R \equiv \min\{N_E, N_R - N_E\}.$$

Motivated by the above observations and also recalling the symmetric role played by initially nonexcited vs excited modes in determining the time-dependent relative probability of excitation [Eq. (20)], we conjecture that KZS emerges in the thermodynamic limit provided that the initial excited eigenstate satisfies

$$\frac{M_R}{N_R} = \varepsilon \ll 1. \tag{22}$$

Clearly, the case of ground-state initialization corresponds to $N_E = M_R = 0$, and the fully excited state coincides with $N_E = N_R, M_R = 0$. For a generic initial excited eigenstate, Eq. (22) allows in principle M_R to be an extensive quantity in the thermodynamic limit. Two additional results are included in Fig. 3 to illustrate the above possibility. In panel (c), we still have five excited modes in N_R as in (b), but five discontinuities as opposed to just one. For the same system size (thus also the same ε), the scaling is not worse than in panel (b), further supporting the conclusion that the number of discontinuities does not play a role toward the emergence of dynamical scaling. In panel (d), a fixed value of ε, equal to the one in (b) at $N = 12\,800$, is explored for different values of N, by also proportionally increasing N_E. As the data show, the resulting $\Delta n_{\rm ex}$ is the same, indicating that M_R may indeed be allowed to be an extensive quantity as long as Eq. (22) is obeyed.

It is important to address how the choice of a range of τ values affects the above scaling conclusions. Let $\tau_{\min} \leqslant \tau \leqslant \tau_{\max}$ and $\tilde{\tau}_{\min} \leqslant \tau \leqslant \tilde{\tau}_{\max}$ denote the valid range for ground-state initialization,[28] and for excited-state initialization, respectively. Since $\tau_{\min}$ is determined from the requirement that an adiabatic regime exists away from criticality, whereas $\tau_{\max}$ follows from ensuring that adiabaticity can be broken in a finite-size system, both $\tau_{\min}$ and $\tau_{\max}$ are related to the scaling of the *many-body* gap between the ground state and first (available) excited state. Thus $\tilde{\tau}_{\min}$ ($\tilde{\tau}_{\max}$) could in general be substantially different from $\tau_{\min}$ ($\tau_{\max}$), respectively. In our case, however, the Hamiltonian in Eq. (2) can be exactly decoupled into two-level systems for each mode k. Therefore the relevant gap is always $\Delta_{k_c} \equiv \varepsilon_{k_c}(h,\gamma)$, *irrespective of the initial condition*. For this reason, the relation $\tau_{\min} \leqslant \tilde{\tau}_{\min}$ and $\tilde{\tau}_{\max} \leqslant \tau_{\max}$ must hold, as any finite-energy initial state might imply more restrictive constraints as compared to the zero-energy case. In particular, according to Eq. (22), not all the excited eigenstates can lead to KZS, and the better Eq. (22) is satisfied, the closer KZS will be approached. This explains why, for instance, the fitting slope -0.549 from Fig. 3(b) is not as close to the KZ value as the one obtained for a ground-state quench with the same range of τ. In the setting of Fig. 3(b), the majority of the relevant modes stay in their ground state. In order to reduce the contribution to $\Delta n_{\rm ex}$ from the five lowest-energy modes, we can decrease τ such that N_R will be increased in Eq. (22). Numerical support for this strategy is shown in Fig. 4, where an optimal range of τ is identified for the same initial states as in Fig. 3(d), and very good agreement with KZS is recovered. Thus we can conjecture that if the majority of modes that enter M_R are low-energy modes, we can reduce their contribution to $\Delta n_{\rm ex}$ by decreasing the upper bound to τ. That is, we choose $\tau_{\min} \leqslant \tau \leqslant \tilde{\tau}_{\max}$, where $\tilde{\tau}_{\max} < \tau_{\max}$. Conversely, if the majority of modes that enter M_R are from high-energy modes, then we reduce the contribution from these modes by increasing the lower bound to τ. That is, we let $\tilde{\tau}_{\min} \leqslant \tau \leqslant \tau_{\max}$, with $\tilde{\tau}_{\min} > \tau_{\min}$.

Additional theoretical understanding of the criterion given in Eq. (22) may be sought by invoking the perturbative

adiabatic renormalization (AR) approach,[54] which was successfully applied to explain the scaling results for adiabatic quenches starting from the ground state.[15,28] Can first-order AR still capture dynamical scaling for initial excited eigenstates? Let us focus on linear quenches ($\alpha = 1$), and let the time-dependent Hamiltonian be parametrized as $H(t) = H_c + [\lambda(t) - \lambda_c]H_1 = H_c + (t/\tau)H_1$, with H_c quantum critical in the thermodynamic limit, so that the relevant QCP is crossed at $t_c \equiv 0$. If the system is prepared in the ℓth eigenstate of $H(t_0)$, with $t_0 \to t_c$ as in the examples previously considered, the time-evolved state from first-order AR may be expressed in the form

$$|\Psi^{(1)}(t)\rangle = e^{-i\Gamma_\ell(t)}|\Psi_\ell(t)\rangle - \sum_{m\neq\ell} c_m^{(1)}(t)|\Psi_m(t)\rangle,$$

where $\Gamma_\ell(t)$ includes in general both the Berry phase and the dynamical phase, and $c_m^{(1)}(t)$ gives the time-dependent amplitude along the mth snapshot eigenstate. Following a derivation similar to the one given in Refs. 54 and 28, and letting $\Delta_m(t) \equiv E_m(t) - E_\ell(t)$, we find

$$c_m^{(1)}(t) = \frac{e^{-i\Gamma_m(t)}}{\tau}\int_{t_0}^{t} dt' \frac{\langle\Psi_m(t')|H_1|\Psi_\ell(t')\rangle}{E_m(t') - E_\ell(t')} e^{i\int_{t_0}^{t'} ds\,\Delta_m(s)}.$$

Thus to first order in the quench rate $1/\tau$ the adiabaticity loss can be quantified by $\Delta\mathcal{O}(t) = \langle\Psi^{(1)}(t)|\mathcal{O}(t)|\Psi^{(1)}(t)\rangle - \langle\Psi_\ell(t)|\mathcal{O}(t)|\Psi_\ell(t)\rangle$. In particular, this yields

$$\Delta n_{\rm ex}(t) = \frac{2}{N}\sum_{m\neq\ell}\left|c_m^{(1)}(t)\right|^2\Bigg(\langle\Psi_m(t)|\sum_{k\in K_+}\gamma_k^\dagger(t)\gamma_k(t)|\Psi_m(t)\rangle - \langle\Psi_\ell(t)|\sum_{k\in K_+}\gamma_k^\dagger(t)\gamma_k(t)|\Psi_\ell(t)\rangle\Bigg).$$

Since H_1 is a one-body operator in our case, the only nonzero matrix elements $\langle\Psi_m(t)|H_1|\Psi_\ell(t)\rangle$ include many-body eigenstates $|\Psi_m(t)\rangle$ which differ from $|\Psi_\ell(t)\rangle$ in the *occupation of precisely one mode*. Thus $\langle\Psi_m(t)|\sum_k \gamma_k^\dagger(t)\gamma_k(t)|\Psi_m(t)\rangle - \langle\Psi_\ell(t)|\sum_k \gamma_k^\dagger(t)\gamma_k(t)|\Psi_\ell(t)\rangle = \pm 1$, which implies

$$\Delta n_{\rm ex}(t_f) = \frac{1}{N}\sum_{m\neq\ell}\left[\pm\left|c_m^{(1)}(t_f)\right|^2\right]. \tag{23}$$

Except for a possible sign difference for each m, the above expression is formally identical to the one holding for ground-state initialization ($\ell = 0$), in analogy with the exact Eq. (21). Numerical calculations of the relative excitation density according to Eq. (23) [for instance, with the same initial condition as in Fig. 3(a), data not shown] confirm that the condition for initial excited eigenstates to support KZS is the same in first-order AR as the one conjectured based on exact numerical results.

B. Sudden quench dynamics from an excited energy eigenstate

As mentioned in the Introduction, scaling results for sudden quenches of the control parameter λ around its critical value λ_c have been recently obtained by De Grandi *et al.*[35] under the assumptions that the system is in the ground state of the initial Hamiltonian and the quench has a *small amplitude*, leading to a final excitation density

$$n_{\rm ex}(t_f) \sim |\lambda - \lambda_c|^{d\nu} \equiv \delta\lambda^{d\nu}, \tag{24}$$

with $\delta\lambda \ll 1$ in suitable units. Before addressing, in analogy to the case of adiabatic dynamics, the extent to which the expected scaling behavior may be robust against initialization in a finite-energy eigenstate, it is useful to explore more quantitatively the connection between ground-state adiabatic vs sudden quenches implied by Eq. (24).

Suppose, specifically, that the amplitude of a sudden magnetic-field quench near the QCP A of the Ising chain is directly related to the rate τ of a corresponding linear adiabatic sweep across the same QCP via $h_f = h_c \pm \hat{h}$, where $\hat{h} \propto \hat{t}/\tau$ and $\hat{t}$ is the KZ freeze-out time scale, i.e., $\hat{t} \sim \tau^{\nu z/(\nu z+1)}$. Equation (24) then yields

$$n_{\rm ex}(t_f) \sim |h_f - h_c|^{d\nu} \sim \tau^{-d\nu/(\nu z+1)}. \tag{25}$$

In other words, the scaling behavior resulting from Eq. (24) is essentially equivalent to KZS. While this could be quantitatively demonstrated by direct calculation of $n_{\rm ex}(t)$ in a sudden quench, it can also be nicely illustrated by examining *combined* sudden-adiabatic quenches, which have not been explicitly addressed, to our knowledge,[55] and will also be relevant in Sec. III C. Two possible "control loops" starting from $h(t_0) = h_c$ are depicted in Fig. 5: we can either (i) suddenly change the magnetic-field amplitude $h_c \mapsto h_f$, and then adiabatically change it back to h_c (top panel); or we can (ii) slowly ramp up h_c to h_f, and then suddenly quench $h_f \mapsto h_c$ (bottom panel). As is clear from the numerical data, the total excitation density created from the combined sudden-adiabatic quench shows KZS throughout the entire process in both cases, provided that τ is within the appropriate scaling range $\tau_{\rm min} \leqslant \tau \leqslant \tau_{\rm max}$. Notice that the quench process depicted in Fig. 5 is similar to the repeated linear quench across QCP A studied in Ref. 19, in the sense that the initial and final value of the control parameter coincide. While KZS was found to hold in such a repeated linear quench, the difference is now that half of the linear adiabatic sweep is replaced by a sudden quench. Since, however, the interval $[h_c - \hat{h}, h_c + \hat{h}]$ corresponds to the impulse region in the KZ scenario for a pure linear quench, the scaling results of the combined quenches under consideration may be understood as a consequence of the fact that the sudden quench component can only further *enforce* the impulse mechanism by which excitation is generated in the KZS argument. Interestingly, as long as the scaling exists, we can also observe that (i) and (ii) lead to almost the same final excitation density, even if the intermediate values of the excitation density after the sole sudden [in (i)] or linear [in (ii)] quench are different. In summary, the existence of KZS in ground-state sudden and combined sudden-adiabatic quenches with *small amplitude* is essentially a reflection of the fact that the system goes through an impulse region around the QCP no matter how slow or fast the quench is effected.

While sudden quenches of *arbitrary amplitude* will be further considered in the next section, we now return to the question of whether dynamical scaling also holds in small-amplitude sudden quenches when the system is initially prepared in an excited eigenstate of $H(t_0) = H_c$. Exact numerical results are presented in Fig. 6, where in order to ease the

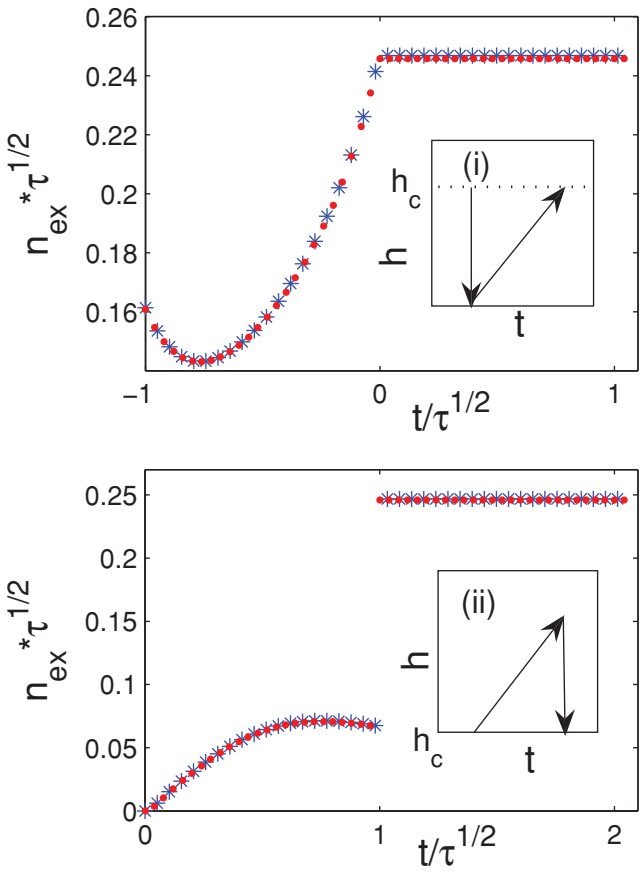

FIG. 5. (Color online): Scaling behavior of the final excitation density in combined magnetic-field ground-state quenches across QCP A in the Ising chain. Top: Sudden quench $h_c \mapsto h_f$ (see text) followed by a linear quench back to h_c, with the system finally kept at h_c. Bottom: Linear quench from h_c followed by a sudden quench $h_f \mapsto h_c$, with the system finally kept at h_c. In both cases, $N = 400$.

comparison with a linear quench, we have again explicitly related the sudden-quench amplitude to τ as $h_f - h_c \propto \tau^{-1/2}$. The data for $N = 3200$ indicate that the scaling exponent is slightly closer to the KZS prediction than the one obtained in a pure linear quench with the same initial condition and τ range [cf. Fig. 3(a)]. Since a sudden quench effectively strengthens the impulse mechanism in the KZS argument, the number of relevant modes N_R is larger than the one involved in an adiabatic linear quench. Thus for the same initial condition (the same M_R), the ratio ε in Eq. (22) is smaller in a sudden quench than in a linear quench, comparatively leading to a scaling exponent closer to KZS. Therefore our conclusions for excited-state sudden quenches are consistent with the ones reached for excited-state adiabatic quenches, and reaffirm how small-amplitude sudden quench dynamics and adiabatic dynamics near a QCP are essentially equivalent over a wide range of initializations.

C. Adiabatic dynamics following a sudden quench from the ground state

In addition to eigenstates of the initial Hamiltonian, another physically relevant class of initial preparations is provided by

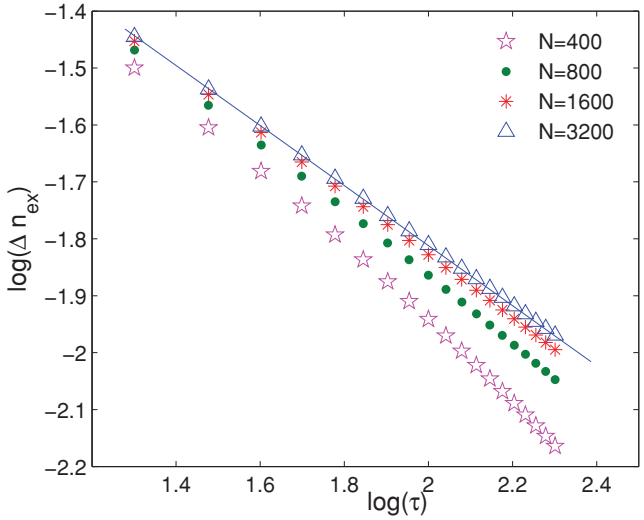

FIG. 6. (Color online) Scaling behavior of the final relative excitation density in a sudden magnetic-field quench across QCP A in the Ising chain, starting with the first excited state of $H(h_c)$. The linear fitting slope for $N = 3200$ is -0.5244 ± 0.0004 for $20 \leqslant \tau \leqslant 250$. Closer agreement with the KZS may be reached by optimizing over τ as in Fig. 4.

pure states that are reachable from the many-body ground state via a sudden parameter quench of *arbitrary amplitude*. For concreteness, let us focus on adiabatic dynamics following a sudden quench of the magnetic field h to its critical value h_c in the Ising chain. Thus the initial state for the adiabatic quench is a superposition of different eigenstates of the Hamiltonian $H(h_c)$ after the (instantaneous) sudden quench. Since for each mode k the parity quantum number $\mathcal{P}_k$ is conserved, and the ground state of H_k lies in the even sector $\mathcal{P}_k = 1$, the expansion coefficients $c_{2,k} = c_{3,k} = 0$, whereas $c_{0,k}$ and $c_{1,k}$ are obtained from expanding the ground state before the sudden quench in the eigenstate basis $\{|\psi_k^j(t_0^+)\rangle\}$ of the quenched Hamiltonian $H(h_c)$.

We can picture the resulting dynamics in terms of a combined sudden-adiabatic quench process (see Fig. 7, inset), except that unlike in Sec. III B we only focus on the scaling behavior of the relative excitation density $\Delta n_{\rm ex}(t)$ created after the sudden quench. Exact numerical results are plotted in the main panel of Fig. 7, showing that for a large range of sudden-quench initializations, the final excitation density still obeys the same KZS,

$$\Delta n_{\rm ex}(t_f) \sim \tau^{-d\nu/(\nu z+1)} \sim \tau^{-1/2},$$

as in adiabatic dynamics starting from the ground state. The above scaling result can be derived analytically in two limiting cases, starting from Eq. (14). Upon integrating over all the relevant modes, we find

$$\Delta n_{\rm ex}(t) = \frac{1}{\pi}\int_0^{k_{\max}} \Delta P_k(t)dk = \int_0^{k_{\max}} \{(2|c_{0,k}|^2 - 1)|a_{0,k}(t)|^2 + 2{\rm Re}[c_{0,k}c_{1,k}^* a_{0,k}^*(t)\, a_{1,k}(t)]\}\frac{dk}{\pi}. \quad (26)$$

There are two contributions in $\Delta P_k(t)$. If the initial state of mode k is close to either a nonexcited or to a fully excited state

($|c_{0,k}|^2 \approx 1$ or $|c_{0,k}|^2 \approx 0$ for all $k \in K_R$, respectively), the first term is the dominant one. In this case, KZS clearly holds. In the opposite limit where each mode $k \in K_R$ is initially half excited ($|c_{0,k}|^2 \approx 1/2$), the second term is the dominant one. Since, for a sudden quench to h_c, the latter is the center of the impulse region (recall Fig. 1, top) and at most half of the impulse region can be crossed, all the relevant modes can at most be close to half excitation, making this second limiting case directly relevant to the sudden-quench state preparation for suitable h_0. Assuming that $|c_{0,k}|^2 \approx 1/2$ and ignoring relative phases thus yields

$$\Delta P_k(t) \sim |a_{0,k}(t)a_{1,k}(t)| \sim |a_{0,k}(t)|\sqrt{1-|a_{0,k}(t)|^2}.$$

By invoking the Landau-Zener formula,[16] the asymptotic ($t_f \to \infty$) excitation probability for modes near k_c scales like $e^{-2\pi k^2 \tau}$ when $t_0 \to -\infty$. Starting from QCP A (the center of the impulse region) will not, however, affect the exponential behavior.[56] Therefore $|a_{0,k}(t)|^2 \sim e^{-2\pi k^2\tau}$ as long as t_f is deep in the adiabatic region, and $1-|a_{0,k}(t)|^2 \sim k^2\tau$. Integrating over the relevant modes then gives the anticipated KZS result:

$$\int_0^{k_{\max}} dk|a_{0,k}(t)|\sqrt{[1-|a_{0,k}(t)|^2]} \sim \int_0^{\tau^{-1/2}} dk\, k\, \tau^{1/2} \sim \tau^{-1/2},$$

where we used the fact that $k_{\max} \sim \tau^{-1/2}$ [Eq. (19)] in the upper integration limit.

While the above argument suffices to explain the emergence of KZS starting from *special* sudden-quench initializations, for generic quenches the dominant term in Eq. (26) need not be the same for different modes. In order to gain further insight, it is necessary to inspect the distribution of the excitation probability for each relevant mode after a sudden quench from a generic value $h_0 \mapsto h_c$. Numerical results for the low-lying modes are presented in Fig. 8 for a wide range of initial magnetic-field strength h_0. For each mode k, we can identify two boundary values, $h_{0,k}^{\min}$ and $h_{0,k}^{\max}$, such that when $h_{0,k}^{\min} \leqslant h_0 \leqslant h_{0,k}^{\max}$, mode k is close to its ground state after the sudden quench ($|c_{0,k}|^2 \approx 1$), whereas if $h_0 \ll h_{0,k}^{\min}$ or $h_0 \gg h_{0,k}^{\max}$, mode k is close to half excitation ($|c_{0,k}|^2 \approx 1/2$). Since $h_{0,k}^{\min}$ and $h_{0,k}^{\max}$ are approximately symmetric with respect to the critical value $h_c = 1$, let us for simplicity take $h_{0,k}^{\mathrm{m}} \equiv h_{0,k}^{\max}$, with $h_{0,k}^{\min} \approx 2h_c - h_{0,k}^{\mathrm{m}}$. Qualitatively, $h_{0,k}^{\mathrm{m}}$ can be determined by the condition $\Delta(h_0,k) \approx \Delta(h_c,k)$, which yields approximately $|c_{0,k}|^2 \approx 1$. If, conversely, $\Delta(h_0,k) \gg \Delta(h_c,k)$ ($|h_0 - h_c| \gg |h_{0,k}^{\mathrm{m}} - h_c|$), we can consider $|c_{0,k}|^2 \approx 1/2$. Altogether, the results in Figs. 7 and 8 indicate that the limiting analytical condition of requiring the same dominant term in Eq. (26) for *all* the relevant modes is too strong for $\Delta n_{\mathrm{ex}}(t)$ to show KZS. For instance, when $h_0 = 0.95$, not all the relevant modes are staying in their ground state (k_c is not), yet KZS holds. In general, however, the variation of $|c_{0,k}|^2$ with k does affect the scaling result. For instance, when h_0 is around 0.75, agreement with the KZS prediction for the same system size is relatively poor, motivating one to roughly identify the range $0.6 \lesssim h_0 \lesssim 0.9$ with a crossover region. Based on these observations, we conjecture that a necessary (and sufficient) condition for the relative excitation density $\Delta n_{\mathrm{ex}}(t)$ to approach KZS in the thermodynamic limit is that

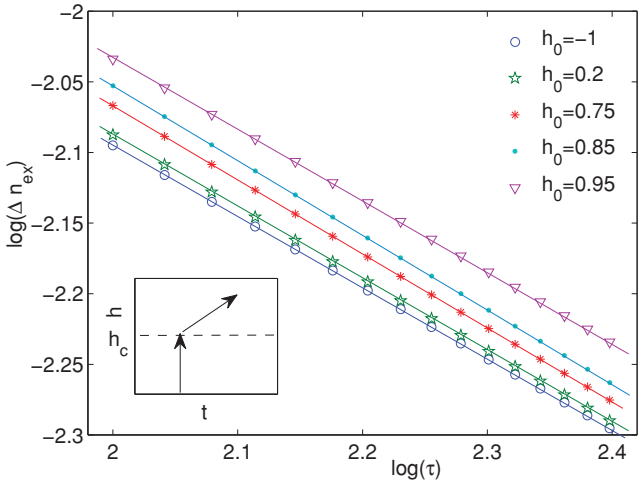

FIG. 7. (Color online) Scaling of the final relative excitation density in an adiabatic magnetic-field quench across QCP A in the Ising chain, starting from an excited state prepared by suddenly quenching $h_0 \mapsto h_c$ for different initial values of h_0. The combined control path is illustrated in the inset. The linear fitting slope for $h_0 = -1,0.2,0.75,0.85,0.95$ is $-0.50283 \pm 5.0 \times 10^{-5}$, $-0.506\,97 \pm 6.0 \times 10^{-5}$, $-0.5237 \pm 1.0 \times 10^{-4}$, $-0.528\,00 \pm 5.0 \times 10^{-5}$, and $-0.5037 \pm 8.0 \times 10^{-4}$, respectively. In all cases, the system size $N = 400$.

the dominant term in Eq. (26) is the same for the majority of the relevant modes.

An alternative physical interpretation of the above conjecture may be obtained by observing that for a generic value of h_0, there exist modes $k_e, k_g \in K_+$ such that if $k_c \leqslant k \leqslant k_e$, $\Delta(h_0,k) \gg \Delta(h_c,k)$, while if $k_g \leqslant k \leqslant \pi$, $\Delta(h_0,k) \approx \Delta(h_c,k)$, and we also assume $k_e < k_g$ for

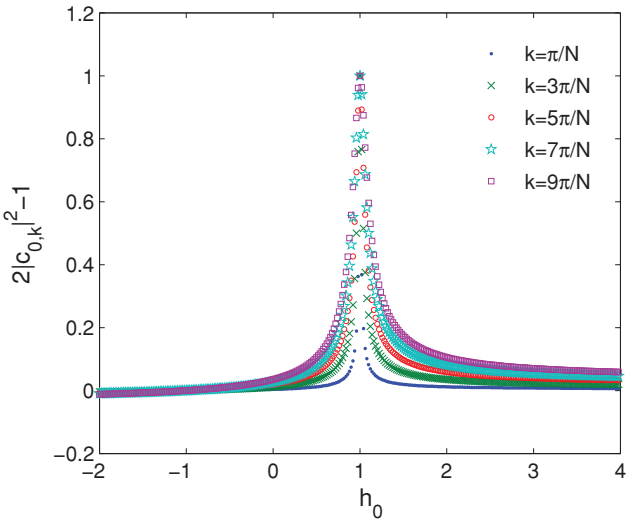

FIG. 8. (Color online) Dependence of the excitation coefficient $2|c_{0,k}|^2 - 1$ upon the initial magnetic-field strength h_0 in a state prepared by a sudden quench $h_0 \mapsto h_c$ in the Ising chain ($\gamma = 1$). The values $c_{0,k}$ are obtained by expanding the ground state of $H(h_0)$ in terms of the eigenbasis of $H(h_c = 1)$ at QCP A. The five lowest-energy modes are considered, for system size $N = 400$.

concreteness. Since, in an adiabatic sweep with speed τ, the set of relevant modes $K_R = [k_c, k_{\max}]$ is determined according to Eq. (19), we can distinguish three different regimes depending on how $k_{\max}$ is positioned relative to the interval $[k_e, k_g]$:

(i) $k_{\max} \leqslant k_e$. In this case, all the relevant modes are half excited, recovering one of the limiting situations (analytically) leading to KZS, as already discussed (e.g., $h_0 = -1$ in Fig. 7);

(ii) $k_e < k_{\max} < k_g$. In this case, by a reasoning similar to the one leading to Eq. (22), KZS is predicted to emerge provided that $(k_{\max} - k_e) = \varepsilon k_{\max}$, $\varepsilon \ll 1$, in such a way that the majority of the relevant modes are half excited (e.g., $h_0 = 0.2$ in Fig. 7);

(iii) $k_g \leqslant k_{\max}$. In this case, KZS is predicted to emerge provided that $k_g = \varepsilon k_{\max}$, $\varepsilon \ll 1$, in such a way that the majority of the relevant modes stay in their ground state (e.g., $h_0 = 0.95$ in Fig. 7).

Thus for both $h_0 = 0.75$ and $h_0 = 0.85$, the initial state prepared by the sudden quench may be interpreted to lie in the crossover region between cases (ii) and (iii), explaining why the resulting scaling deviates appreciably from the KZ prediction.

Similarly to the excited-eigenstate initialization, sudden-quench initialization will also add more constraints on the appropriate τ range for KZS to hold. If the initial state is prepared via a sudden quench that guarantees one of the above conditions (i)–(iii) to be fulfilled for any $\tau \in [\tau_{\min}, \tau_{\max}]$, then the latter range is also appropriate for KZS to emerge under excited-eigenstate initialization. If not, the situation is more involved, and the range of τ may need to be adjusted such that either (ii) or (iii) is enforced. If condition (ii) is more likely to be obeyed (e.g., if $h_0 \approx 0.6$), we can choose $\tilde{\tau}_{\min} > \tau_{\min}$ in such a way that the number of modes between k_e and k_g is decreased, and the majority of relevant modes is thus half excited. If instead condition (iii) is more likely to be obeyed (e.g., if $h_0 \approx 0.9$), we can choose $\tilde{\tau}_{\max} < \tau_{\max}$ in such a way that the number of relevant modes staying in their ground state is increased. While the strategy for adjusting the τ range in a sudden-quench initialization is similar to the one advocated in excited-eigenstate initialization, conditions (i)–(iii) are in fact easier to fulfill than Eq. (22). For instance, for $N = 400$, the worst scaling in Fig. 7 is still relatively close to KZS, whereas the latter is completely lost when initially only k_c is excited in Fig. 3(a). This difference is due to the fact that the initial occupation of modes in the relevant set changes less abruptly in a sudden-quench initialization than in excited-eigenstate initialization.

We conclude our discussion of quench processes originating from a (pure) excited state by commenting on the fact that the analysis developed for $\Delta n_{\rm ex}(t)$ can be extended to different observables without requiring major conceptual modifications. While an explicit example involving the spin correlator defined in Eq. (18) will be included in the next section, the basic idea is to proceed in analogy with ground-state quenches,[28] by taking into consideration the appropriate scaling exponent as determined by the physical dimension of the observable $\mathcal{O}$. Consider, for instance, the relative excitation energy $\Delta H(t)$ defined in Eq. (17), which, as remarked, can be experimentally more accessible than the relative excitation density. In all the situations where KZS holds for the latter, $\Delta n_{\rm ex}(t_f) \sim \tau^{-d\nu/(\nu z+1)} \sim \tau^{-1/2}$ (in particular, in the case of excited-state initialization via a sudden quench just discussed), we also find for our model that

$$\Delta H(t_f) \sim \tau^{-(d+z)\nu/(\nu z+1)} \sim \tau^{-1},$$

consistent with the corresponding ground-state scaling behavior explored in Refs. 28 and 23.

IV. QUENCHES FROM A THERMAL STATE

A. Adiabatic quench dynamics

While we have only focused thus far on initialization mechanisms resulting in a *pure* excited state, another large class of initial states with a finite excitation energy may be obtained through dissipative means, in particular because the system may find itself (or be placed) in contact with a thermal bath. After a time sufficient for equilibration to occur, the system would then relax to a canonical ensemble at temperature T. In equilibrium, it is well known that the influence of a ground-state QCP can cross over to a finite range of temperatures, the so-called "quantum critical regime," which is often broader than naively expected.[1,57,58] In a dynamical scenario, how robust is dynamical scaling (in particular, KZS) to initialization at a finite temperature? If scaling persists, how do the relevant nonequilibrium exponents depend upon the initial temperature? Motivated by these questions, scaling behavior in a system initially prepared in a thermal equilibrium state *at criticality* and then adiabatically quenched away from the QCP has been analyzed in Ref. 35. In particular, it is shown that for fermionic quasiparticles, the excess excitation due to a quench across a standard QCP obeys

$$\Delta n_{\rm ex}(t_f) \sim \frac{1}{T}\,\tau^{-(d+z)\nu/(\nu z+1)}, \tag{27}$$

provided that the initial temperature is high enough [$T \gg \epsilon_k(t_0)$, for all $k \in K_R$]. Our goal here is to both present quantitative evidence for the above scaling law and, most importantly, to extend the analysis to multicritical QCPs.

Let T denote the initial thermal equilibrium temperature, so that the initial density operator has the form $\rho(t_0) = \bigotimes_{k\in K_+} \rho_k(t_0)$, with $\rho_k(t_0)$ given by

$$\rho_{00,k}(t_0) = \frac{1}{\mathcal{Z}} e^{+\epsilon_k(h,\gamma)/T}, \quad \rho_{11,k}(t_0) = \frac{1}{\mathcal{Z}} e^{-\epsilon_k(h,\gamma)/T}, \qquad \rho_{22,k}(t_0) = \rho_{33,k}(t_0) = \frac{1}{\mathcal{Z}}, \tag{28}$$

in units where $\hbar = k_B = 1$ and with

$$\mathcal{Z} \equiv 2 + e^{+\epsilon_k(h,\gamma)/T} + e^{-\epsilon_k(h,\gamma)/T}.$$

For clarity, we focus on linear adiabatic dynamics first. We shall study both the standard Ising QCP A under a magnetic-field quench of the form $h(t) = 1 - t/\tau$ [$h = h_c = 1, \gamma = 1$ in Eq. (28)], and the MCP B under a simultaneous quench of the magnetic field and the anisotropic parameter, $h(t) = 1 - \gamma(t) = 1 - t/\tau$ [$h = h_c = 1, \gamma = \gamma_c = 1$ in Eq. (28)]. At $T = 0$, the scaling of the excitation density can be in both cases described by $n_{\rm ex}(t_f) \sim \tau^{-d\nu z/[z_2(\nu z+1)]}$, where z_2 is determined from the scaling of the minimal gap along the path with respect to k [cf. Eq. (4) in Ref. 23, with $\alpha = 1$ and $d_2 = 0$]. Thus $z_2 = z$ in the quench across QCP A, leading to KZS, whereas $z_2 = 3 \neq z$ in the quench across MCP B,

leading to anomalous scaling $n_{\rm ex}(t_f) \sim \tau^{-1/6}$. Given the above thermal initial condition, starting from Eq. (15) for the relative excitation probability, one finds

$$\Delta P_k(t) = \tanh\left(\frac{\epsilon_k(h_c,\gamma_c)}{2T}\right)|a_{0,k}(t)|^2, \tag{29}$$

where for both paths we simply write $\epsilon_k(h_c,\gamma_c)$ to mean that critical parameter values are assumed at $t = t_0$. When $T \leqslant \epsilon_k(h_c,\gamma_c)$, $\tanh(\frac{\epsilon_k(h_c,\gamma_c)}{2T}) \approx 1$ and $\Delta P_k(t)$ is the same as starting from the ground state of mode k. Thus in order for the same ground-state scaling (either KZS or $\tau^{-1/6}$) to emerge in the low-temperature limit, the condition $T \leqslant \epsilon_k(h_c,\gamma_c)$ needs to be satisfied for all the relevant modes. Since $\epsilon_{k_c}(h_c,\gamma_c) = 0$, this means that in the thermodynamic limit, the only allowed initial temperature is $T = 0$ if a thermal state of $H(h_c,\gamma_c)$ is considered. In the opposite limit of high temperature, where $T \gg \epsilon_k(h_c,\gamma_c)$, $\tanh(\frac{\epsilon_k(h_c,\gamma_c)}{2T}) \approx \epsilon_k(h_c,\gamma_c)/(2T) \sim (k-k_c)^z/T$ for modes k near k_c. Upon integrating over the relevant modes and recalling Eq. (19), the relative excitation density is then

$$\Delta n_{\rm ex}(t_f) = \frac{1}{\pi}\int_0^{k_{\rm max}} \Delta P_k(t_f) d^d k \sim \frac{1}{T}\int_0^{\tau^{-\nu z/[z_2(\nu z+1)]}} k^z d^d k$$
$$= \frac{1}{T}\,\tau^{-(d+z)\nu z/[z_2(\nu z+1)]}. \tag{30}$$

For the standard QCP A, this yields $\Delta n_{\rm ex}(t_f) \sim \tau^{-1}/T$, recovering the result of Eq. (27), while $\Delta n_{\rm ex}(t_f) \sim \tau^{-1/2}/T$ in the multicritical quench across QCP B. In Ref. 23, we argued that the time-dependent excitation process in ground-state quenches need not be dominated by the critical mode k_c for certain paths across MCPs and $P_k = \Delta P_k \sim k^{d_2}$, with d_2 playing the role of an "effective dimensionality exponent." For a thermal quench, it is interesting to note that, formally, one may interpret $d_2 = z \neq 0$ in the above equation, also implying that the dominant contribution does *not* originate from modes around k_c. In the high-temperature limit, $\rho_k(t_0)$ is, indeed, almost fully mixed for modes near k_c, causing the contribution of $\rho_{00,k}$ and $\rho_{11,k}$ to Eq. (15) to be nearly canceled, and consistently leading to $\Delta P_k(t) \approx 0$ for those modes.

The scaling prediction in Eq. (30) can be further generalized to a *nonlinear thermal quench*, whereby, for instance, $h(t) = 1-\gamma(t) = 1-(t/\tau)^\alpha$ in the case of a quench away from the MCP B. When $T = 0$, Eq. (4) in Ref. 23 yields[59] $n_{\rm ex}(t_f) \sim \tau^{-d\alpha\nu z/[z_2(\alpha\nu z+1)]}$. Correspondingly, in the high-temperature limit,

$$\Delta n_{\rm ex}(t_f) \sim \frac{1}{T}\,\tau^{-(d+z)\alpha\nu z/[z_2(\alpha\nu z+1)]}. \tag{31}$$

Exact numerical results for a quadratic quench ($\alpha = 2$) are reported in Fig. 9, the inset corresponding to the ground-state $T = 0$ case. Within numerical accuracy, the observed behavior is in excellent agreement with the predicted scaling, $\tau^{-2/9}$ for $T = 0$ and $\tau^{-2/3}$ for high-T, respectively.

We further examine how dynamical scaling is detected by other observables and how it is influenced by temperature away from the limiting regimes discussed above by considering the behavior of the spin correlator, $\Delta XX(t)$, defined in Eq. (18). Since XX does not commute with the Hamiltonian in Eq. (2), no analytical treatment is possible. Exact numerical

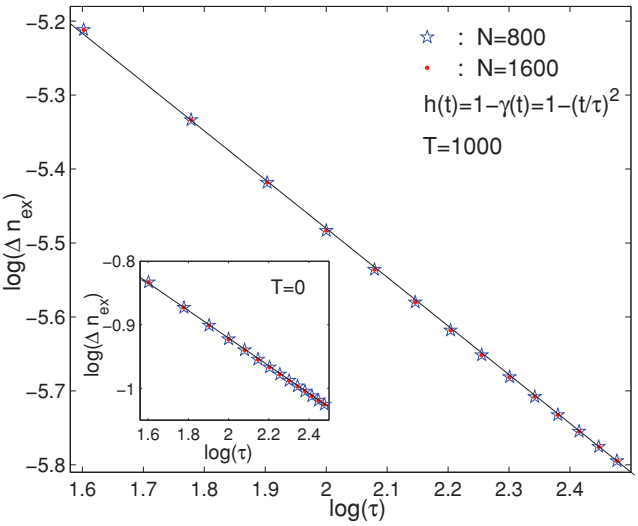

FIG. 9. (Color online) Exact scaling behavior of $\Delta n_{\rm ex}(t_f)$ in a quadratic adiabatic quench $h(t) = 1-\gamma(t) = 1-(t/\tau)^2$, starting from a thermal state at MCP B ($t_0 = t_c = 0$) toward the FM phase. The initial temperature $T = 1000$, yielding a linear fitting slope -0.663 ± 0.002, in good agreement with the value $2/3$ predicted by Eq. (31). For comparison, the case of a ground-state quench is reproduced in the inset, with a linear fitting slope of -0.2190 ± 0.0006, which is also in good agreement with the predicted $2/9$ exponent (Ref. 23). The data for different sizes ($N = 800$ and $N = 1600$) coincide up to 10^{-13}.

results are presented in Fig. 10 for both the regular and the multicritical QCPs A and B (inset vs main panel, respectively), starting from the same thermal initial condition at criticality as considered above. As the data show, similar features emerge in both cases: The scaling exponent of $\Delta XX(t)$, which is expected to be the same as for $\Delta n_{\rm ex}$, deviates from its zero-temperature value ($-1/2$ or $-1/6$, respectively) as soon as the temperature is nonzero, and as the latter is gradually increased, it continuously changes until for sufficiently high temperature ($T \gg \epsilon_k(h_c,\gamma_c)$, for all $k \in K_R$), it stabilizes at the value predicted by Eq. (31) (-1 or $-1/2$, respectively). All these observations are consistent with the predictions in the previous paragraph.

In summary, ground-state dynamical scaling (and KZS in particular) is fragile with respect to temperature fluctuations if the initial state is a thermal equilibrium state *at criticality*. In this case, the two situations where scaling exists are the zero-temperature and the high-temperature limit, with Eq. (31) holding in the latter regime. This requires *all* the relevant modes to either stay in their ground state or be highly mixed at the initial time, which is a stronger condition in comparison to the ones identified in the previous sections for coherently prepared (pure) excited states. From a practical standpoint, the high-temperature regime could potentially be relevant to liquid-state NMR simulators.[50] In order for tests of dynamical scaling or KZS in the low-temperature regime to be experimentally viable, however, the initial thermal state needs to be (or be prepared) sufficiently *far away from criticality* (e.g., $|h_0 - h_c| \gg 1$ for QCP A), in such a way that the condition $T \leqslant \Delta(k,h_0)$ for all $k \in K_R$ can still be fulfilled with a nonzero temperature.

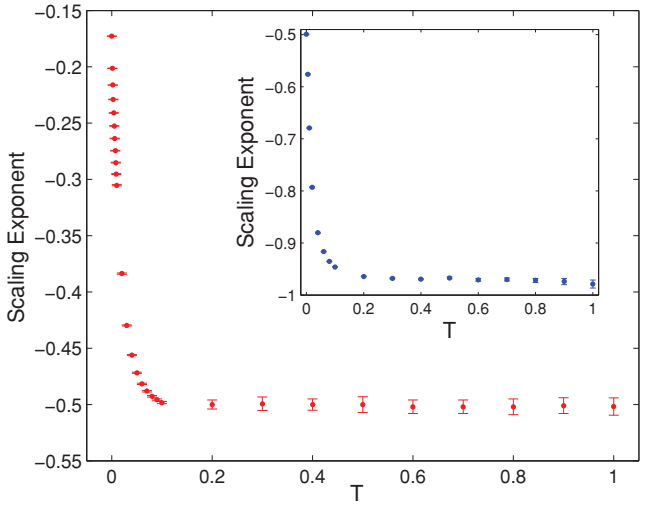

FIG. 10. (Color online) Main panel: Scaling exponent $\Delta XX(t_f)$ as a function of temperature T in a linear quench $h(t) = 1 - \gamma(t) = 1 - t/\tau$ away from the MCP B, starting with a thermal equilibrium state of $H(h_c, \gamma_c)$. Inset: Scaling exponent of $\Delta XX(t_f)$ as a function of temperature in a linear quench $h(t) = 1 + t/\tau$ away from the regular QCP A, starting with a thermal equilibrium state of $H(h_c = 1)$. In both cases, the system size $N = 800$.

B. Sudden quench dynamics and thermalization

Sudden quenches have recently attracted considerable interest as a setting for probing the long-time dynamics of isolated many-body systems and the approach to equilibrium.[36,38–42] Since the quadratic Hamiltonian in Eq. (2) describes a simple (noninteracting) integrable model, it is well known that no thermalization can occur in a proper sense, that is, the behavior of *generic* observables is not governed by a conventional statistical equilibrium ensemble.[37,43] The above investigations have nevertheless shown that information about the asymptotic behavior of an appropriate subset of observables may still be encoded in a finite *effective temperature* $T_{\rm eff}$, independent on the fine details of the initial state and the dynamics but only determined by the total energy of the process. Let $\rho(t_0) \equiv \rho_0$ and H_f denote, respectively, the density operator describing the initial state of the system, and the final Hamiltonian after the (instantaneous) quench. Following Rossini *et al.*,[38] the effective temperature is defined by the requirement that the average energy of the initial state relative to the quenched Hamiltonian equals the one corresponding to a *fictitious* thermal state at temperature $T_{\rm eff}$ in the canonical ensemble, that is,

$$\mathrm{Tr}[\rho_0 H_f] = \mathrm{Tr}[\rho_{T_{\rm eff}} H_f]. \tag{32}$$

Under the assumption that $T = 0$ initially [that is, ground-state initialization in Eq. (32)], the emergence of effective thermal behavior has been related to the *locality* properties of different physical observables relative to the quasiparticle language that diagonalizes the model.[39,40] For a generic quench in an Ising chain, only nonlocal observables (such as the two-point correlation functions of the order parameter) have been found to thermalize, with both their asymptotic average value and the finite-time transient being determined by *equilibrium* statistical mechanics at $T_{\rm eff}$. Remarkably, however, thermal behavior has also been established for certain *local* observables (the transverse magnetization per site, $1/N \sum_j \sigma_z^j$, and the kink density, $\mathcal{N}$) *in quenches toward criticality*, the long-time value being still univocally determined by $T_{\rm eff}$.

Physically, it is clear that the concept of an effective temperature has a restricted validity and, for the model under investigation, it does not imply that an actual thermal ensemble emerges as a result of a sudden quench followed by free evolution under the quenched Hamiltonian. With that in mind, we further explore in what follows the emergence of effective thermal behavior in *critical* quenches, by focusing on a different local observable and by extending the analysis in two directions: first, initialization in a thermal state at finite $T > 0$ and, second, sudden quenches to a multicritical QCP.

Let us first consider a sudden quench of the magnetic field $h_0 \mapsto h_f$ in the Ising chain ($\gamma = 1$), starting from an initial state of the form given in Eq. (28), and focus on the long-time behavior of the number of quasiparticle excitations with momentum k. Since the corresponding observable commutes with the time-dependent Hamiltonian, the long-time expectation value $\langle \gamma_k^\dagger \gamma_k \rangle$ coincides with the one right after the quench. In order for the latter to be consistent with the equilibrium value at $T_{\rm eff}$, the following identity must hold:

$$\begin{aligned}(\rho_{00,k}(t_0) - \rho_{11,k}(t_0))|a_{0,k}|^2 + \rho_{11,k}(t_0) + \rho_{33,k}(t_0) \\ = (1 + e^{+\epsilon_k(h_f,\gamma=1)/T_{\rm eff}})^{-1},\end{aligned} \tag{33}$$

where $|a_{0,k}|^2$ is the excitation probability of mode k due to the quench and Eq. (11) has been used in the left hand-side. The right-hand side is the fermionic thermal equilibrium prediction $\mathrm{Tr}[\rho^k_{T_{\rm eff}} \gamma_k^\dagger \gamma_k]$. Exact numerical results are presented in Fig. 11. Altogether, these data indicate that similar to the behavior of other local observables in a ground-state quench,[39,40] no effective thermalization is observed outside criticality [Figs. 11(c)–11(f)], as expected. Even for a quench toward QCP A, however, the initial temperature T *must be sufficiently high* in order for our chosen observable to thermalize [Figs. 11(a) vs 11(b)].

In order to gain physical insight into what distinguishes a critical vs noncritical quench in our case, and understand why effective thermal behavior fails to emerge outside criticality even for high initial temperature, it is useful to take a closer look at Fig. 11(d): Clearly, the main difference between the equilibrium and the actual quasiparticle distribution arises from momentum modes close to k_c. On the one hand, since $\Delta(k_c, h_f)$ is the smallest gap at h_f, the maximum quasiparticle excitation is expected to occur at k_c from the equilibrium prediction [right-hand side of Eq. (33)]. On the other hand, the peak of the observed distribution is located at modes close to k_c, but not exactly at k_c. Because the system is far from h_c, note that the difference of $\rho_{00,k}$, $\rho_{11,k}$, and $\rho_{33,k}$ for modes close to k_c is negligible. Thus the main difference is due to $|a_{0,k}|^2$, which, as remarked, is the excitation probability of mode k at $T = 0$ after a sudden quench to h_c. Upon re-interpreting $|a_{0,k}|^2 \leftrightarrow 1 - |c_{0,k}|^2$, it is possible to make contact with the results shown in Fig. 8: clearly, the excitation probability of mode k_c changes dramatically for h_0 close to h_c, which suggests that k_c does not contribute appreciably *unless* $h_f = h_c$. Instead, other modes close to k_c can be excited for values $h_f \approx h_c$ at which k_c is not yet excited. Since the

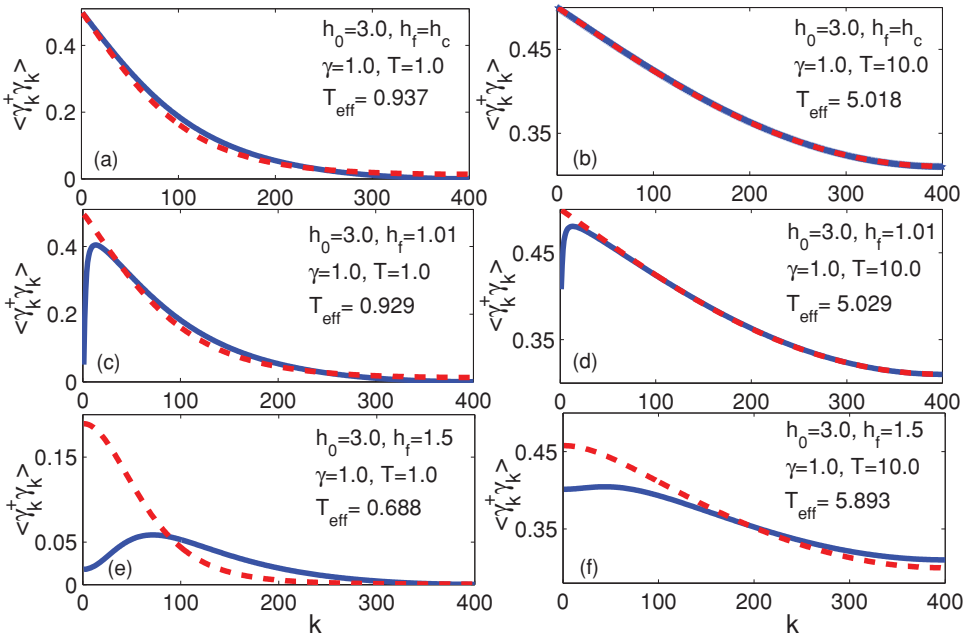

FIG. 11. (Color online) Comparison between the long-time average quasiparticle excitation following a sudden quench $h_0 \mapsto h_f$ starting from a thermal initial state at temperature T (dashed red) and the equilibrium value predicted by a fictitious thermal canonical ensemble at $T_{\rm eff}$ (solid blue). Panels (a), (c), (e): Sudden quenches to $h_f = h_c = 1$, $h_f = 1.01$, $h_f = 1.5$, respectively, with initial temperature $T = 1.0$. The behavior for a ground-state quench ($T = 0$, data not shown) is qualitatively similar, with deviations from the thermal prediction being further pronounced. Panels (b), (d), (f): Sudden quenches to $h_f = h_c = 1$, $h_f = 1.01$, $h_f = 1.5$, respectively, with initial temperature $T = 10.0$. In all cases, $N = 800$, and the value of $T_{\rm eff}$ obtained from is Eq. (32) is also given.

excitation contribution from such "quasicritical modes" would then be larger than the one from k_c, Eq. (33) would not hold. Accordingly, the only way to enforce the validity of Eq. (33) is through a sudden quench toward h_c, as observed.

Having clarified why criticality is essential, we turn to assess whether the requirement of a sufficiently high initial T may be related to the finite system size or will persist in the thermodynamic limit. We focus on a sudden quench $h_0 = 3.0 \mapsto h_c$ at $T = 1.0$, and analyze how the long-time average of the total quasiparticle density $1/N \sum_k \gamma_k^\dagger \gamma_k$ deviates from the thermal equilibrium prediction at $T_{\rm eff}$ as N is increased. While we find that the observed deviations are practically constant over the range of N explored (data not shown), the difference between $\langle \gamma_{k_c}^\dagger \gamma_{k_c} \rangle$ and its corresponding thermal prediction at $T_{\rm eff}$ does decrease with increasing N: As seen in Fig. 12, such a difference $\Delta \gamma_{k_c}^\dagger \gamma_{k_c} \sim N^{-0.999\,92}$ at $T = 1.0$, implying a vanishing difference and effective thermal behavior also at low temperature *for the critical mode* as $N \to \infty$. This property, however, stems from the fact that the gap of k_c closes in the thermodynamic limit, which is not true for the gap of other modes. For either the number of quasiparticles in a generic mode or for the total quasiparticle density, we thus conjecture that even in the thermodynamic limit, thermal behavior will be observed following sudden quenches to the QCP A *only if* $T \gg \Delta_k(h_c, \gamma = 1)$ *for all the relevant modes*.

In view of the peculiar features that distinguish a multicritical QCP, as reflected in particular in anomalous scaling behavior,[23] it is not obvious whether the above condition would still suffice for the same observables to thermalize in a sudden quench toward MCP B. Exact results for two sudden multicritical quenches of the form ($h_0 = 1 + \gamma_0 \mapsto h_f = 1 + \gamma_f, \gamma_0 \mapsto \gamma_f$) are given in Fig. 13, starting from a thermal state at high temperature: Specifically, MCP B is both reached via a sudden quench from the PM phase (left panel) and via a sudden quench from the FM phase (right panel). Contrary to the high-temperature scenario for the

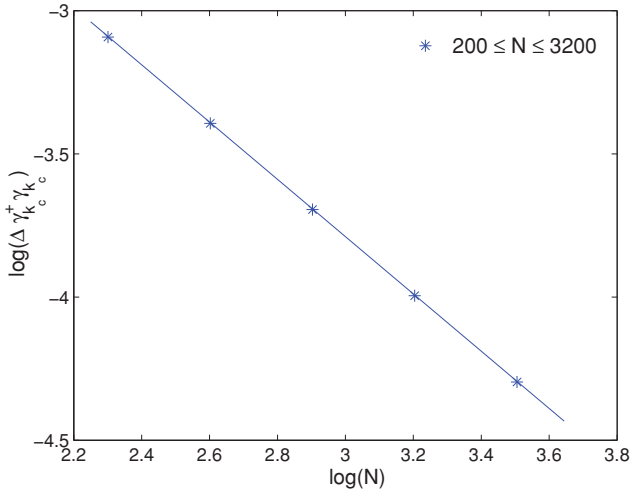

FIG. 12. (Color online) Difference between the long-time quasiparticle excitation of the critical mode k_c from its thermal equilibrium prediction as a function of system size for a sudden magnetic-field quench to h_c in the Ising chain. An initial thermal state with temperature $T = 1.0$ is considered. The linear fitting slope is $-0.999\,92 \pm 3 \times 10^{-5}$.

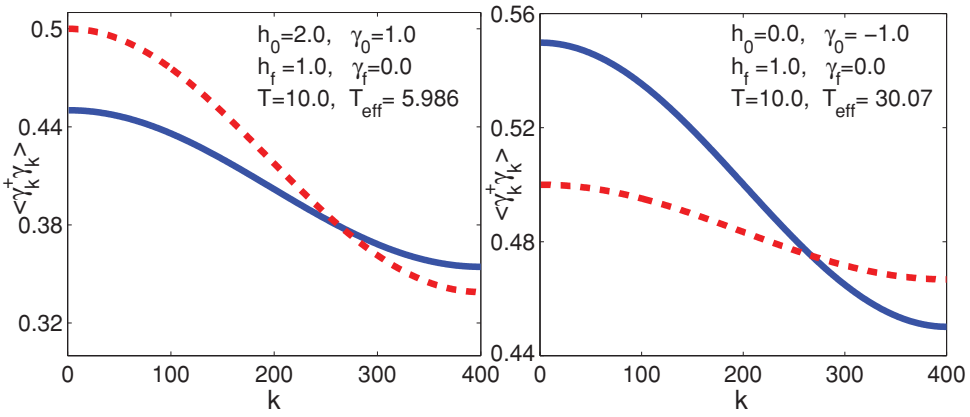

FIG. 13. (Color online) Comparison between the long-time quasiparticle excitation following a sudden quench $h_0 \mapsto h_f = h_c = 1, \gamma_0 \mapsto \gamma_f = \gamma_c = 0$ toward the MCP B (blue solid line) and the equilibrium value predicted by a fictitious thermal ensemble at $T_{\rm eff}$ (red dashed line). The system is initially in a thermal state with temperature $T = 10$. Left: Initial state is the thermal state at $h_0 = 2.0, \gamma_0 = 1.0$ (inside the PM phase). Right: Initial state is the thermal state at $h_0 = 0.0, \gamma_0 = -1.0$ (inside the FM phase). Notice that due to the fact that the excitation probability of low-energy modes exceeds $1/2$, $T_{\rm eff}$ is much higher than in any other situation with the same initial T, cf. Figs. 11(b), 11(d), 11(f), and Fig. 13(a).

regular QCP A [Fig. 11(b)], *no* thermal behavior emerges, the observed expectation value $\langle \gamma_k^\dagger \gamma_k \rangle$ for modes close to k_c being significantly smaller or larger than the thermal equilibrium prediction, respectively.

This anomalous long-time behavior can be traced back to the asymmetry of the impulse region along the control path, as sketched in Fig. 1 (bottom). Following Ref. 23, the location of the minimum gap for each mode k along the path $h = 1 + \gamma$ is determined by requiring $\partial \Delta_k(\gamma, 1+\gamma)/\partial \gamma = 0$, that is,

$$\tilde{\gamma}(k) = (\cos k - 1)/(1 + \sin k^2) < 0,$$

which indicates that the center of the impulse region is largely shifted into the FM phase for each k. As a result, after a sudden quench to the MCP B from the FM phase, the excitation probability of low-energy modes tends to be enhanced above $1/2$, whereas for a sudden quench to MCP B from the PM phase, the excitation probability of low-energy modes tends to be suppressed below $1/2$. Since the thermal equilibrium value is close to $1/2$ in the high-temperature limit for low-energy modes, thermal behavior is not realized in either quench process.

Based on the above results, we conjecture that *quenching toward the center of the impulse region* is a necessary requirement for $\gamma_k^\dagger \gamma_k$ or $1/N \sum_k \gamma_k^\dagger \gamma_k$ to thermalize following a sudden quench. While typically this is the case in a quench to a regular QCP (for instance, a sudden quench of h to QCP A at fixed $\gamma = 1$), for a sudden quench to MCP B along the path $h = 1 + \gamma$, the location of the minimum gap (hence the center of the impulse region) is different for each mode k, preventing thermalization to be possible along this path irrespective of the final values h_f, γ_f. More generally, we expect the above requirement to be *necessary* for local observables other than those examined here. While this goes beyond our current scope, it would be interesting to verify, for instance, whether the transverse magnetization or the density of kinks would still effectively thermalize in a multicritical quench to QCP B from the ground state.

We also remark that in a recent work,[41] general conclusions have been reached for the equilibrium distribution after a sudden quench, predicting, in particular, effective thermal behavior for generic observables when the quench is performed around a noncritical point, and poor equilibration otherwise. While at first these results seem to contradict both our present conclusions for critical quenches toward QCP A in the appropriate temperature regime as well as earlier results for zero temperature,[39,40] a crucial assumption in Ref. 41 is a small quench amplitude, causing only a small number of excited states to effectively contribute around a QCP. The opposite condition is implied throughout our discussion, the sudden quench amplitude being in fact large enough for the number of excited states involved in a critical quench to outweigh those involved in a noncritical one (cf. Fig. 8). In light of that, we also conjecture that having a sufficiently large number of states involved in the excitation process is a general necessary condition for effective thermalization after a sudden quench.

V. CONCLUSIONS

In summary, we have addressed how different aspects of many-body nonequilibrium dynamics depend upon initialization in a state other than the ground state for a class of one-dimensional exactly solvable XY models. Our main findings may be itemized as follows:

Dynamical scaling: Initial pure excited states. Provided that the nonequilibrium response of the system is characterized in terms of suitable *relative* indicators (such as the relative excitation density), adiabatic quench dynamics can still encode the ground-state equilibrium critical exponents for a large class of initial energy eigenstates as well as for pure excited states prepared by a sudden parameter quench. A crucial role is played by how the initial excitation is distributed over the set of *relevant* quasiparticle modes that effectively evolve in an adiabatic quench. In particular, a unifying criterion that ensures the emergence of KZS in both of the above scenarios

in the thermodynamic limit is obtained by requiring that the *majority of the relevant modes share a common initial excitation pattern*, as expressed by Eq. (22).

Our results recover ground-state scaling when no excitation is initially present, but they also allow for the critical exponents of the ground-state QPT to be encoded in the scaling behavior for highly energetic initial configurations, where most of the relevant modes are fully or half excited. While this makes contact with similar conclusions on critical entanglement scaling in excited energy eigenstates recently obtained for *static* QPTs,[53] it confirms that only the set of relevant modes is important in dynamical scenarios, as opposed to the full static mode set. Besides being supported by exact numerical methods and analytical derivations in limiting regimes, a justification of the proposed criterion has also been obtained for the case of excited-eigenstate initialization by suitably extending the perturbative (first-order) AR approach we previously employed for ground-state continuous QPTs.

Dynamical scaling: Initial mixed states. In general, more restrictive conditions on the distribution of the initial excitation over relevant modes must be obeyed for universal dynamical scaling to emerge in adiabatic quench dynamics that originates from a statistical (incoherent) mixture as compared to a (coherently prepared) pure state. In particular, two distinct scaling regimes have been identified for an initial thermal ensemble at a finite temperature T, depending on whether the latter is very low or very high relative to the relevant quasiparticle energy scale, and leading to KZS $\tau^{-1/2}$ vs τ^{-1} for a standard QCP, respectively. Since in both cases *all* the relevant modes must share a common excitation pattern if the initial thermal state is prepared *at criticality*, this implies that KZS is fragile against thermal fluctuations in this case, the scaling exponent deviating from the KZ prediction as soon as $T \neq 0$. From a practical standpoint, it is, however, important to note that a finite range of temperatures can still support KZS if the system is initially at thermal equilibrium sufficiently far from criticality. General predictions for scaling behavior in adiabatic thermal quenches involving a MCP have also been obtained [cf. Eq. (31)], and verified to be consistent with exact numerical results.

Effective thermalization. Effective thermal behavior may emerge in the relaxation dynamics of the quasiparticle density following a sudden quench from a thermal state under appropriate conditions. Specifically, the long-time expectation value of this observable is determined by a *fictitious* thermal equilibrium ensemble at temperature T_{eff} provided that (i) the system is quenched toward the *center of the impulse region*, and (ii) the initial temperature is *sufficiently high* with respect to all the relevant gaps. For a standard QCP, the first requirement is met by a sudden quench *toward criticality*, which has been found sufficient for local observables such as the transverse magnetization per site and the kink density to thermalize starting from the ground state.[39,40] Our results indicate that, in general, condition (i) alone need *not* suffice for arbitrary local observables. While requirement (ii) may be taken to be in line with what expected for a free (integrable) theory,[36,43] it remains an interesting open question to precisely characterize what subclass of local observables may exhibit effective thermal behavior under the sole condition (i).[60]

Our results additionally show that for certain observables (such as the quasiparticle density), effective thermalization may fail to occur altogether (or possibly require yet more stringent requirements) for sudden quenches to a *multicritical* QCP. Physically, we have traced this behavior back to the existence of quasicritical (path-dependent) energy states and the corresponding shift of the impulse region, which also underlies the emergence of anomalous scaling exponents.[23] In this context, an interesting next step would be to examine the thermalization behavior of other local observables as considered in Refs. 40 and 39.

While the above analysis provides a more complete picture of nonequilibrium dynamics in a paradigmatic class of spin chains than available thus far, it remains a main open question to understand how crucially our results rely on the XY chain being an exactly solvable noninteracting model. From this point of view, it would be worthwhile to explore, for instance, whether dynamical critical scaling may still exist for finite-energy initial states in nonintegrable models, or even in more complex but still integrable systems such as a Bethe-ansatz solvable one-dimensional Heisenberg XXZ chain[53] or an infinitely coordinated Lipkin-Meshkov-Glick model.[30]

ACKNOWLEDGMENT

S.D. gratefully acknowledges partial support from a Hull Graduate Fellowship.

[1] S. Sachdev, *Quantum Phase Transitions* (Cambridge University Press, Cambridge, England, 1999).
[2] M. Vojta, Rep. Prog. Phys. **66**, 2069 (2003).
[3] T. Kadowaki and H. Nishimori, Phys. Rev. E **58**, 5355 (1998).
[4] E. Farhi *et al.*, Science **292**, 472 (2001); G. E. Santoro and E. Tosatti, J. Phys. A **39**, R393 (2006).
[5] E. Barouch and M. Dresden, Phys. Rev. Lett. **23**, 114 (1969).
[6] E. Barouch, B. M. McCoy, and M. Dresden, Phys. Rev. A **2**, 1075 (1970).
[7] E. Barouch and B. M. McCoy, Phys. Rev. A **3**, 2137 (1971).
[8] M. Greiner, O. Mandel, T. Esslinger, T. W. Hänsch, and I. Bloch, Nature (London) **415**, 39 (2002); A. Micheli, G. K. Brennen, and P. Zoller, Nat. Phys. **2**, 341 (2006); L. E. Sadler, J. M. Higbie, S. R. Leslie, M. Vengalattore, and D. M. Stamper-Kurn, Nature (London) **443**, 312 (2006); C. N. Weiler *et al.*, *ibid.* **455**, 948 (2008).
[9] T. Kinoshita, T. Wenger, and D. Weiss, Nature (London) **440**, 900 (2006); S. Hofferberth, I. Lesanovsky, B. Fisher, T. Schumm, and J. Schmiedmayer, *ibid.* **449**, 324 (2007).
[10] W. H. Zurek, U. Dorner, and P. Zoller, Phys. Rev. Lett. **95**, 105701 (2005).
[11] A. Polkovnikov, Phys. Rev. B **72**, 161201 (2005).
[12] J. Dziarmaga, Adv. Phys. **59**, 1063 (2010).
[13] T. Kibble, Phys. Today **60**, 47 (2007).

[14]J. Dziarmaga, Phys. Rev. Lett. **95**, 245701 (2005); B. Damski, *ibid.* **95**, 035701 (2005); B. Damski and W. H. Zurek, Phys. Rev. A **73**, 063405 (2006); R. W. Cherng and L. S. Levitov, *ibid.* **73**, 043614 (2006); F. M. Cucchietti, B. Damski, J. Dziarmaga, and W. H. Zurek, *ibid.* **75**, 023603 (2007); A. Fubini, G. Falci, and A. Osterloh, New J. Phys. **9**, 134 (2007).

[15]A. Polkovnikov and V. Gritsev, Nat. Phys. **4**, 477 (2008).

[16]V. Mukherjee, U. Divakaran, A. Dutta, and D. Sen, Phys. Rev. B **76**, 174303 (2007).

[17]S. Deng, L. Viola, and G. Ortiz, *Recent Progress in Many-Body Theories* (World Scientific, Singapore, 2008), Vol. 11, p. 387.

[18]D. Sen and S. Vishveshwara, Europhys. Lett. **91**, 66009 (2010).

[19]V. Mukherjee, A. Dutta, and D. Sen, Phys. Rev. B **77**, 214427 (2008).

[20]S. Mondal, K. Sengupta, and D. Sen, Phys. Rev. B **79**, 045128 (2009).

[21]R. Barankov and A. Polkovnikov, Phys. Rev. Lett. **101**, 076801 (2008).

[22]U. Divakaran, V. Mukherjee, A. Dutta, and D. Sen, J. Stat. Mech. (2009) P02007.

[23]S. Deng, G. Ortiz, and L. Viola, Phys. Rev. B **80**, 241109(R) (2009).

[24]V. Mukherjee and A. Dutta, Europhys. Lett. **92**, 37004 (2010).

[25]V. Mukherjee, A. Polkovnikov, and A. Dutta, Phys. Rev. B **83**, 075118 (2011).

[26]F. Pellegrini, S. Montangero, G. E. Santoro, and R. Fazio, Phys. Rev. B **77**, 140404 (2008).

[27]S. Mondal, D. Sen, and K. Sengupta, Phys. Rev. B **78**, 045101 (2008); D. Sen, K. Sengupta, and S. Mondal, Phys. Rev. Lett. **101**, 016806 (2008).

[28]S. Deng, G. Ortiz, and L. Viola, Europhys. Lett. **84**, 67008 (2008).

[29]D. Chowdhury, U. Divakaran, and A. Dutta, Phys. Rev. E **81**, 012101 (2010).

[30]T. Caneva, R. Fazio, and G. E. Santoro, Phys. Rev. B **78**, 104426 (2008).

[31]J. Dziarmaga, Phys. Rev. B **74**, 064416 (2006); T. Caneva, R. Fazio, and G. E. Santoro, *ibid.* **76**, 144427 (2007).

[32]B. Damski and W. H. Zurek, New J. Phys. **11**, 063014 (2009); G. Schaller, Phys. Rev. A **78**, 032328 (2008); M. Collura, D. Karevski, and L. Turban, J. Stat. Mech. (2009) P08007; J. Dziarmaga and M. M. Kus, New J. Phys. **12**, 103002 (2010).

[33]A. Das, K. Sengupta, D. Sen, and B. K. Chakrabarti, Phys. Rev. B **74**, 144423 (2006).

[34]Y. Li, M. X. Huo, and Z. Song, Phys. Rev. B **80**, 054404 (2009); H. Guo, Z. Liu, H. Fan, and S. Chen, e-print arXiv:1001.0909 (to be published).

[35]C. De Grandi, V. Gritsev, and A. Polkovnikov, Phys. Rev. B **81**, 012303 (2010).

[36]S. Sotiriadis, P. Calabrese, and J. Cardy, Europhys. Lett. **87**, 20002 (2009).

[37]D. Patané, A. Silva, F. Sols, and L. Amico, Phys. Rev. Lett. **102**, 245701 (2009); M. Rigol, V. Dunjko, and M. Olshanii, Nature (London) **452**, 854 (2008); M. Rigol, Phys. Rev. Lett. **103**, 100403 (2009); M. Cramer, C. M. Dawson, J. Eisert, and T. J. Osborne, *ibid.* **100**, 030602 (2008); M. Kollar and M. Eckstein, Phys. Rev. A **78**, 013626 (2008).

[38]D. Rossini, A. Silva, G. Mussardo, and G. E. Santoro, Phys. Rev. Lett. **102**, 127204 (2009).

[39]S. Suzuki, D. Rossini, and G. E. Santoro, e-print arXiv:0910.4055 (to be published).

[40]D. Rossini, S. Suzuki, G. Mussardo, G. E. Santoro, and A. Silva, Phys. Rev. B **82**, 144302 (2010).

[41]L. Campos Venuti and P. Zanardi, Phys. Rev. A **81**, 032113 (2010).

[42]E. Canovi, D. Rossini, R. Fazio, G. E. Santoro, and A. Silva, e-print arXiv:1006.1634 (to be published).

[43]M. A. Cazalilla and M. Rigol, New J. Phys. **12**, 055006 (2010).

[44]V. Gritsev and A. Polkovnikov, in *Understanding Quantum Phase Transitions* (Taylor & Francis, Boca Raton, 2010); e-print arXiv:0910.3692 (to be published).

[45]D. Patané, A. Silva, L. Amico, R. Fazio, and G. E. Santoro, Phys. Rev. Lett. **101**, 175701 (2008); D. Patané, L. Amico, A. Silva, R. Fazio, and G. E. Santoro, Phys. Rev. B **80**, 024302 (2009).

[46]G. Ortiz, J. E. Gubernatis, E. Knill, and R. Laflamme, Phys. Rev. A **64**, 22319 (2001); R. Somma, G. Ortiz, J. E. Gubernatis, E. Knill, and R. Laflamme, *ibid.* **65**, 42323 (2002).

[47]D. Poulin and P. Wocjan, Phys. Rev. Lett. **102**, 130503 (2009).

[48]P. Zanardi, H. T. Quan, X. Wang, and C. P. Sun, Phys. Rev. A **75**, 032109 (2009).

[49]C. Negrevergne, R. Somma, G. Ortiz, E. Knill, and R. Laflamme, Phys. Rev. A **71**, 032344 (2005).

[50]X. Peng, J. Zhang, J. Du, and D. Suter, Phys. Rev. Lett. **103**, 140501 (2009); J. Zhang, F. M. Cucchietti, C. M. Chandrashekar, M. Laforest, C. A. Ryan, M. Ditty, A. Hubbard, J. K. Gamble, and R. Laflamme, Phys. Rev. A **79**, 012305 (2009).

[51]E. Lieb, T. Schultz, and D. Mattis, Ann. Phys. (NY) **16**, 407 (1961); P. Pfeuty, *ibid.* **57**, 79 (1970).

[52]R. Somma, G. Ortiz, H. Barnum, E. Knill, and L. Viola, Phys. Rev. A **70**, 042311 (2004).

[53]V. Alba, M. Fagotti, and P. Calabrese, J. Stat. Mech. (2009) P10020.

[54]A. Messiah, *Quantum Mechanics* (North-Holland, Amsterdam, 1962), Chap. XVII.

[55]In a recent work by B. Damski, H. T. Quan, and W. H. Zurek, e-print arXiv:0911.5729 (to be published), the behavior of the *decoherence factor* has been advocated as a dynamical indicator of the QPT in an Ising environment. Formally, the required procedure of first turning on the system-environment coupling at the initial time, followed by adiabatic evolution of the Ising chain across the QCP A, can be interpreted in terms of a combined sudden adiabatic quench scheme on the joint system-plus-environment Hamiltonian. Interestingly, KZS is found to occur in the exponent of the decoherence factor as well.

[56]N. V. Vitanov and B. M. Garraway, Phys. Rev. A **53**, 4288 (1996).

[57]S. Sachdev, Nucl. Phys. B **464**, 576 (1996); S. Sachdev and A. P. Young, Phys. Rev. Lett. **78**, 2220 (1997).

[58]P. Gegenwart, Q. Si, and F. Steglich, Nat. Phys. **4**, 186 (2008).

[59]We note that our prediction differs from the one recently established in Ref. 24, where a linearization procedure around the QCP is invoked in order to use the Landau-Zener formula.

[60]From this point of view, it is interesting to note that both the transverse magnetization per site and the density of kinks are closely related to the final quenched Hamiltonian [cf. in particular Eq. (35) in Ref. 40].

Bibliography

[1] S. Sachdev, *Quantum Phase Transitions* (Cambridge University Press, Cambridge, 1999).

[2] S. Sachdev, B. Keimer, Phys. Today **64**, 29 (2011).

[3] M. Uhlarz, C. Pfleiderer, and S. M. Hayden, Phys. Rev. Lett. **93**, 256404 (2004).

[4] M. A. Nielsen, and I. L. Chuang, *Quantum Computation and Quantum Information* (Cambridge University Press, Cambridge, 2000)

[5] H. Eugene Stanley, Rev. Mod. Phys. 71, S358 (1999).

[6] N. Goldenfeld, *Lectures on Phase Transitions and the Renormalization Group* (Perseus Publishing, 1992).

[7] M. Greiner, O. Mandel, T. Esslinger, T. W. Hänsch, and I. Bloch, Nature **415**, 39 (2002).

[8] V. Kalmeyer, and R. B. Laughlin, Phys. Rev. Lett. **59**, 2095 (1987).

[9] L. E. Sadler, J. M. Higbie, S. R. Leslie, M. Vengalattore, and D. M. Stamper-Kurn, Nature **443**, 312 (2006).

[10] A. Micheli, G. K. Brennen, and P. Zoller, Nat. Phys., **2**, 341 (2006) 341.

[11] P. C. Hohenberg, B. I. Halperin, Rev. Mod. Phys. **49**, 435 (1977).

[12] E. Barouch, B. M. McCoy, and M. Dresden, Phys. Rev. A, **2**, 1075 (1970).

[13] J. B. Vallespir, eprint arXiv:quant-ph/0603124.

[14] A. Sen(De), U. Sen, and M. Lewenstein, Phys. Rev. A, **70**, 060304 (R) (2004).

[15] A. Osterloh, L. Amico, G.Falci, and R. Fazio, Nature (London) **416**, 608 (2002).

[16] G. Vidal, J. I. Latorre, E.Rico and A. Kitaev, Phys. Rev. Lett. **90**, 227902 (2003).

[17] M. E. Fisher in *Multicritical Phenomena*, edited by R. Pynn, and A. Skjeltorp (Plenum Press, New York, 1984).

[18] W. Wootters, Phys. Rev. Lett. **80**, 2245 (1998).

[19] A. Ekert and P. L. Knight, Am. J. Phys. **63**, 415 (1995).

[20] T.W. B. Kibble, J. Phys. A **9**, 1387 (1976); Phys. Rep. **67**, 183 (1980).

[21] T.W.B. Kibble, Phys. Today **60**, 47 (2007).

[22] W. H. Zurek, Nature (London) **317**, 505 (1985).

[23] W. H. Zurek, Acta Phys. Pol. B **24**, 1301 (1993).

[24] I. L. Chuang, R. Durrer, N. Turok, and B. Yurke, Science **251**, 1336 (1991).

[25] M. I. Bowick, L. Chandar, E. A. Schiff, and A. M. Srivastava, Science **263**, 943 (1994).

[26] P. C. Hendry, N. S. Lawson, R. A. M. Lee, P. V. E. McClintock, and C. D. H. Willams, Nature (London) **368**, 315 (1994).

[27] C. Bäuerle, Y. M. Bunkov, S. N. Fisher, H. Godfrin, and G. R. Pickett, Nature (London) **382**, 334 (1996).

[28] P. Laguna, and W. H. Zurek, Phys. Rev. Lett. **78**, 2519 (1997).

[29] P. Laguna, and W. H. Zurek, Phys. Rev. D 58, 85 021 (1998).

[30] A. Yates, and W. H. Zurek, Phys. Rev. Lett. 80, 5477 (1998).

[31] M. E. Dodd, P. C. Hendry, N. S. Lawson, P. V. E. McClintock, and C. D. H. Williams, Phys. Rev. Lett. **81**, 3703 (1998).

[32] R. Carmi, E. Polturak, and G. Koren , Phys. Rev. Lett. **84**, 4966 (2000).

[33] R. Monaco, J. Mygind, and R. J. Rivers, Phys. Rev. Lett. **89**, 080603 (2002).

[34] R. Monaco, J. Mygind, and R. J. Rivers, Phys. Rev. B **67**, 104506 (2003).

[35] L. Amico, R. Fazio, A. Osterloh, and V. Vedral, Rev. Mod. Phys. **80**, 517 (2008).

[36] R. Horodecki, P. Horodecki, M. Horodecki, and K. Horodecki, Rev. Mod. Phys. **81**, 865 (2009).

[37] E. Lieb, T. Schultz, and D. Mattis, Ann. Phys. **16**, 407 (1961).

[38] D. C. Johnston, J. W. Johnson, D. P. Goshorn, and A. J. Jacobson, Phys. Rev. B **35**, 219222 (1987).

[39] M. Hase, I. Terasaki, and K. Uchinokura, Phys. Rev. Lett. **70**, 3651 (1993).

[40] S. Kobayashi, S. Mitsuda, M. Ishikawa, K. Miyatani, and K. Kohn Phys. Rev. B **60**, 3331 (1999).

[41] O. Derzhko, J. Richter, T. Krokhmalskii, O. Zaburannyi, Phys. Rev. E **69**, 066112 (2004).

[42] K. Okamoto, and K. Yasumura, J. Phys. Soc. Jpn. **59**, 993 (1990).

[43] P. Pfeuty, Ann. Phys. **57**, 79 (1970).

[44] E. Schrödinger, "Die gegenwärtige Situation in der Quanten-mechanik", Naturwissenshaften **23**, 807 (1935).

[45] H. Barnum, E. Knill, G. Ortiz, and L. Viola, Phys. Rev. A **68**, 032308 (2003).

[46] H. Barnum, E. Knill, G. Ortiz, R. Somma, and L. Viola, Phys. Rev. Lett. **92**, 107902 (2004).

[47] I. Peschel, J. Stat. Mech. P12005 (2004).

[48] N. D. Mermin and H. Wagner, Phys. Rev. Lett. **17**, 1133 (1966).

[49] A. Acín, A. Andrianov, L. Costa, E. Jané, J. I. Latorre, and R. Tarrach, Phys. Rev. Lett. **85**, 1560 (2000).

[50] R. Somma, G. Ortiz, H. Barnum, E. Knill, L. Viola, Phys. Rev. A **70**, 042311 (2004);

[51] R. Somma, H. Barnum, E. Knill, G. Ortiz, and L. Viola, Int. J. Mod. Phys. B **20**, 2760 (2006).

[52] M. Kindermann, Phys. Rev. Lett. **96**, 240403 (2006).

[53] L. Viola and H. Barnum, arXiv:quant-ph/0701124 (2007), and references therein. Published in "Philosophy of Quantum Information and Entanglement", edited by A. Bokulich and G. Jaegez (Cambridge Univ. Press, Cambridge, 1999).

[54] S. J. Gu, S. Deng, Y. Q. Li, and H. Q. Lin, Phys. Rev. Lett. **93**, 086402 (2004).

[55] S. Deng, S. J. Gu, and H. Q. Lin, Phys. Rev. B **74**, 045103 (2006).

[56] S. Deng, L. Viola and G. Ortiz, *Recent Progress in Many-Body Theories*, Vol. **11** (World Scientific, Singapore, 2008), p. 387, arXiv:0802.3941.

[57] W. H. Zurek, U. Dorner, and P. Zoller, Phys. Rev. Lett. **95**, 105701 (2005);

[58] J. Dziarmaga, Phys. Rev. Lett. **95**, 245701 (2005).

[59] B. Damski, Phys. Rev. Lett. **95**, 035701 (2005).

[60] B. Damski and W. H. Zurek, Phys. Rev. A **73**, 063405 (2006).

[61] F. M. Cucchietti, B. Damski, J. Dziarmaga, and W. H. Zurek, Phys. Rev. A **75**, 023603 (2007).

[62] A. Polkovnikov, Phys. Rev. B **72**, 161201 (2005).

[63] A. Polkovnikov, and V. Gritsev, Nat. Phys. **4**, 477 (2008).

[64] A. Messiah, *Quantum Mechanics* (North-Holland, Amsterdam, 1962), Chapt. XVII.

[65] R. W. Cherng and L. S. Levitov, Phys. Rev. A **73**, 043614 (2006).

[66] A. Fubini, G. Falci, and A. Osterloh, New J. Phys. **9**, 134 (2007).

[67] V. Mukherjee, A. Dutta, and D. Sen, Phys. Rev. B **77**, 214427 (2008).

[68] S. Mondal, D. Sen, and K. Sengupta, Phys. Rev. B **78**, 045101 (2008).

[69] D. Sen, K. Sengupta, and S. Mondal, Phys. Rev. Lett. **101**, 016806 (2008).

[70] R. Barankov, and A. Polkovnikov, Phys. Rev. Lett. **101**, 076801 (2008).

[71] J. Dziarmaga, Phys. Rev. B **74**, 064416 (2006).

[72] T. Caneva, R. Fazio, and G. E. Santoro, Phys. Rev. B **76**, 144427 (2007).

[73] T. Caneva, R. Fazio, and G. E. Santoro, Phys. Rev. B **78**, 104426 (2008).

[74] F. Pellegrini, S. Montangero, G. E. Santoro, and R. Fazio, Phys. Rev. B **77**, 140404 (2008).

[75] K. Sengupta, D. Sen, and S. Mondal, Phys. Rev. Lett. **100**, 077204 (2008).

[76] U. Divakaran, A. Dutta, and D. Sen Phys. Rev. B **78**, 144301 (2008).

[77] S. Deng, G. Ortiz, and L. Viola, Europhys. Lett. **84**, 67008 (2008).

[78] D. Chowdhury, U. Divakaran, and A. Dutta, Phys. Rev. E **81**, 012101 (2010).

[79] V. Mukherjee, U. Divakaran, A. Dutta, and D. Sen, Phys. Rev. B **76**, 174303 (2007)

[80] U. Divakaran, V. Mukherjee, A. Dutta, and D. Sen, J. Stat. Mech. P02007 (2009).

[81] S. Mondal, K. Sengupta, and D. Sen, Phys. Rev. B **79**, 045128 (2009).

[82] C. Zener, Proc. R. Soc. London A **137**, 696 (1932).

[83] N. V. Vitanov, Phys. Rev. A **59**, 988 (1999).

[84] A. Das, K. Sengupta, D. Sen, and B. K. Chakrabarti, Phys. Rev. B **74**, 144423 (2006).

[85] S. Sotiriadis, P. Calabrese, and J. Cardy, Europhys. Lett. **87**, 20002 (2009).

[86] Y. Li, M. Huo, and Z. Song, Phys. Rev. B **80**, 054404 (2009).

[87] H. Guo, Z. Liu, H. Fan, and S. Chen, arXiv:1001.0909.

[88] C. De Grandi, V. Gritsev, and A. Polkovnikov, Phys. Rev. B **81**, 012303 (2010).

[89] D. Patané, A. Silva, F. Sols, and L. Amico, Phys. Rev. Lett. **102**, 245701 (2009);

[90] M. Rigol, V. Dunjko, and M. Olshanii, Nature (London) **452**, 854 (2008);

[91] M. Rigol, Phys. Rev. Lett. **103**, 100403 (2009);

[92] M. Cramer, C. M. Dawson, J. Eisert, and T. J. Osborne,Phys. Rev. Lett. **100**, 030602 (2008);

[93] M. Kollar and M. Eckstein, Phys. Rev. A **78**, 013626 (2008).

[94] D. Rossini, A. Silva, G. Mussardo, and G. E. Santoro, Phys. Rev. Lett. **102**, 127204 (2009).

[95] S. Suzuki, D. Rossini, and G. E. Santoro, arXiv:0910.4055.

[96] D. Rossini, A. Silva, G. Mussardo, G. E. Santoro, and A. Silva, Phys. Rev. B **82**, 144302 (2010).

[97] L. C. Venuti and P. Zanardi, Phys. Rev. A **81**, 032113 (2010).

[98] E. Canovi, D. Rossini, R. Fazio, G. E. Santoro, and A. Silva, Phys. Rev. B **83**, 094431 (2011).

[99] M. A. Cazalilla and M. Rigol, New J. Phys. **12**, 055006 (2010).

[100] V. Gritsev and A. Polkovnikov, in: *Understanding Quantum Phase Transitions*, (Taylor & Francis, Boca Raton, 2010); arXiv:0910.3692.

[101] D. Patané, A. Silva, L. Amico, R. Fazio, and G. E. Santoro, Phys. Rev. Lett. **101**, 175701 (2008)

[102] D. Patané, L. Amico, A. Silva, R. Fazio, and G. E. Santoro, Phys. Rev. B **80**, 024302 (2009).

[103] G. Ortiz, J. E. Gubernatis, R. Laflamme, and E. Knill, Phys. Rev. A **64**, 22319 (2001);

[104] R. Somma, G. Ortiz, J. E. Gubernatis, R. Laflamme, and E. Knill, Phys. Rev. A **65**, 42323 (2002).

[105] D. Poulin and P. Wocjan, Phys. Rev. Lett. **102**, 130503 (2009).

[106] C. N. Weiler, T. W. Neely, D. R. Scherer, A. S. Bradley, M. J. Davis, and B. P. Anderson, Nature **455**, 948 (2008).

[107] C. Negrevergne, R. Somma, G. Ortiz, E. Knill, and R. Laflamme, Phys. Rev. A **71**, 032344 (2005).

[108] X. Peng, J. Zhang, J. Du, and D. Suter, Phys. Rev. Lett. **103**, 140501 (2009);

[109] J. Zhang, F. M. Cucchietti, C. M. Chandrashekar, M. Laforest, C. A. Ryan, M. Ditty, A. Hubbard, J. K. Gamble, and R. Laflamme, Phys. Rev. A **79**, 012305 (2009).

[110] V. Alba, M. Fagotti, and P. Calabrese, J. Stat. Mech. P10020 (2009).

[111] V. Mukherjee and A. Dutta, Europhys. Lett. **92**, 37004 (2010).

[112] S. Deng, G. Ortiz, and L. Viola, Phys. Rev. B **80**, 241109(R) (2009).

[113] S. Deng, G. Ortiz, and L. Viola, Phys. Rev. B **83**, 094304 (2011).

[114] N. V. Vitanov and B. M. Garraway, Phys. Rev. A **53**, 4288 (1996).

[115] M. Vojta, Rep. Progr. Phys. **66**, 2069 (2003).

[116] S. Sachdev, Nuclear Phys. B **464**, 576 (1996);

[117] S. Sachdev and A. P. Young, Phys. Rev. Lett. **78**, 2220 (1997).

[118] P. Gegenwart, Q. Si, and F. Steglich, Nature Phys. **4**, 186 (2008).

[119] V. Scarani, M. Ziman, P. Štelmachovič, N. Gisin, and V. Bužek, Phys. Rev. Lett. **88**, 097905 (2002).

[120] W. H. Zurek, Rev. Mod. Phys. **75**, 715 (2003).

[121] B. Damski, H. T. Quan, and W. H. Zurek, Phys. Rev. A **83**, 062104 (2011).

[122] H. T. Quan, Z. Song, X. F. Liu, P. Zanardi, and C. P. Sun, Phys. Rev. Lett. **96**, 140604 (2006).

[123] P. Zanardi, H. T. Quan, X. Wang, C. P. Sun, Phys. Rev. A **75**, 032109 (2007).

[124] P. R. Levstein, G. Usaj, and H. M. Pastawski, J. Chem. Phys. **108**, 2718 (1998).

[125] R. A. Jalabert, and H. M. Pastawski, Phys. Rev. Lett. **86**, 2490 (2001).

[126] W. H. Zurek, Phys. Rev. D **24**, 1516 (1981).

[127] R. Coldea, D. A. Tennant, E. M. Wheeler, E. Wawrzynska, D. Prabhakaran, M. Telling, K. Habicht, P. Smeibidl, and K. Kiefer, Science **327**, 177 (2010).